AN EFFICIENT METHODOLOGY FOR WARM-FORMING PROCESS DESIGN OF BIMETALLIC COMPONENTS USING REVERSE SIMULATION APPROACH

KONG TING-FAI

PhD

The Hong Kong Polytechnic University

2012

The Hong Kong Polytechnic University

Department of Industrial and Systems Engineering

An Efficient Methodology for Warm-Forming Process Design of Bimetallic Components Using Reverse Simulation Approach

KONG TING-FAI

A thesis submitted in partial fulfilment of the

requirements for the degree of Doctor of Philosophy

June 2012

CERTIFICATE OF ORIGINALITY

I hereby declare that this thesis is my own work and that, to the best of my knowledge and belief, it reproduces no material previously published or written, nor material that has been accepted for the award of any other degree or diploma, except where due acknowledgement has been made in the text.

_____ (signed)

KONG Ting-Fai (Name of student)

Abstract

The success of warm forming process is identified by a complete filling of die cavity without occurrence of defects. Outcomes are highly influenced by the shape of the initial billet or workpiece. The traditional design of billet shapes, which is based on either practical experience or a trial-and-error approach by forward simulation, is inefficient and costly. Therefore, this study aims to develop an efficient methodology for a warm-forming process design of bimetallic components using a reverse simulation approach. This approach is able to directly predict the shape of billet by starting from the final shape of formed bimetallic component.

The significance of this study is to develop an integrated algorithm that can be used effectively for reverse simulation. The weld interface of the bimetallic component was assumed to be a sticking condition at the beginning of the reverse simulation. When such simulation was being performed, the two metals had to be separated gradually, and their mating surfaces then restored to a sliding condition. The reverse shape could be determined by the proposed algorithm, which was established with a significant modification based on the “backward tracing method”, proposed by Part et al. in 1983 as well as reasonable assumptions about the constancy of volume and convex expansion of lateral deformation surfaces. An original idea of billet-height minimization routine was incorporated into the finite-element package for tracing the hollow cylindrical shape as the desired shape of original billet. The straight-line-repair (SLR), boundary-edge-mirror (BEM), nearest-die-profile-repair (NDPR), and profile-offset (PO) methods were developed to reconstruct the reverse shapes, while at the

same time, avoiding the concave-shape problem and compensating for both excessive and insufficient volume. These procedures were adopted sequentially under specified conditions in order to maintain the desired volume of the suitable reverse shape.

Three axisymmetric components were taken as examples to evaluate the effectiveness of the developed approach. Two such shapes were made of aluminium alloy 6063 (AA6063), while the third was a bimetallic component composed of AA6063 and stainless steel AISI 316L (SS316L). The flow stress data of these two specimen materials were obtained by uniaxial compression tests, which were conducted at elevated temperatures ranging from 20 to 900 °C with intervals of 100 °C, except for the larger interval between 20 and 200 °C. These material data, as well as the friction factors acquired by the ring compression tests were identified as significant information for process modelling. The bimetallic joint was achieved successfully by solid-state welding. The strength of the joint was an average more than 10% greater than that of AA6063. The thickness of the diffusion zone was 4 μm, which was extremely small compared to the height of the base metals. The deformation behaviour of the bonding interface had practically no effect on the flow stress of the bimetallic component. In other words, the materials behaved in accordance with their own properties except at their joint. Therefore, at the start of modelling the reverse simulation for warm-forming bimetallic components, the key step was to identify a large shear-friction factor as a nearly sticking condition at the weld interface. During the procedures of reverse simulation, the value of this shear-friction factor could be

reduced in stages, dependent upon the forming load obtained from the increment of forward simulation.

The cylindrical billets predicted by the reverse simulation approach in the three case studies were verified by forward simulation and practical experiments under compatible process conditions. The results confirmed that the proposed methodology was capable of predicting the billet shapes for warm forming not only axisymmetric components, but also bimetallic components. It is believed that the developed approach can be applied for actual production with substantial savings of raw materials and a reduction of numerous uncertain and iterative trials during the process design.

Publication List (Journal Papers)

1. Kong, T.F., Chan, L.C., and Lee, T.C. (2004) Prediction of a billet shape for axisymmetric warm forming using variational analysis, *Key Engineering Materials*, 274-276, 733-738.

2. Kong, T.F., Chan, L.C., and Lee, T.C. (2005) Numerical determination of blank shapes for warm forming of non-axisymmetric components, *Journal of Materials Processing Technology*, 167, 472-479.

3. Kong, T.F., and Chan, L.C. (2008) Numerical and experimental investigation of preform design in non-axisymmetric warm forming, *International Journal of Advanced Manufacturing Technology*, 37(9-10), 908-919.

4. Kong, T.F., Chan, L.C., and Lee, T.C. (2008) Qualitative study of bimetallic joints produced by solid-state welding processes, *Science and Technology of Welding and Joining*, 13(8), 679-682.

5. Kong, T.F., Chan, L.C., and Lee, T.C. (2009) Weld diffusion analysis of forming bimetallic components using statistical experimental methods, *Materials and Manufacturing Processes*, 24(4), 422-430.

6. Kong, T.F., Chan, L.C., and Lee, T.C. (2009) Experimental study on effects of process parameters in forge-welding bimetallic materials: AISI 316l stainless steel and 6063 aluminium alloy, *Strain*, 45(4), 373-379.

Publication List (Conference Papers)

1. Kong, T.F., Chan, L.C., and Lee, T.C. (2007) Computer simulation of material flow in warm-forming bimetallic components, *AIP Conference Proceeding of Numiform 2007*, 1029-1034.

2. Kong, T.F., Chan, L.C., and Lee, T.C. (2007) Experimental study of optimal process parameters for deformation welding of dissimilar metals, *Experimental Analysis of Nano and Engineering Materials and Structures, Proceedings of the 13th International Conference on Experimental Mechanics*, 461-462.

3. Kong, T.F., Chan, L.C., and Lee, T.C. (2011) Flow stress experimental determination for warm-forming process, *Proceedings of the 6th ASME 2011 International Manufacturing Science and Engineering Conference*.

Acknowledgments

I wish to acknowledge the encouragement and the financial support for this study received from the Hong Kong Industrial Support Fund (UIT/054; Project No. ZY42), the Central Fund of The Hong Kong Polytechnic University (Project No. ZW88), and Giant Metal Manufactory Ltd.

I would like to take this opportunity to express my sincere appreciation to my chief project supervisor, Dr. Luen-chow Chan, for his guidance and encouragement throughout the research period. His enthusiasm, constructive criticism, and valuable supports have been an inspiration. Gratitude is also extended to my co-supervisor, Prof. Tai-chiu Lee, for his strong technical support and for providing me with many contributive suggestions and considerable useful advice to support my research work.

Thanks are also due to my present colleagues in Giant Metal Manufactory Ltd. as well as all teachers in The Hong Kong Polytechnic University for their kind supports and useful discussions during the course of my studies.

Needless to say, my parents deserve my greatest gratitude because of their endless encouragement, full support to my growth, and unlimited patience. Finally, I wish to thank all of my good friends for supporting me during my study and for sharing my happiness in the most delightful moment of submitting this dissertation.

Table of Contents

List of Figures

Chapter 1

Chapter 2

Chapter 3

Chapter 4

Chapter 5

Chapter 6

List of Tables

Chapter 5

Chapter 6

Nomenclature

A	Instantaneous cross-sectional area of tensile-test specimen
A_0	Initial cross-sectional area of tensile-test specimen
A_2	Multiplying factor
A_b	Constant
A_c	Cross-sectional area of reverse shape
A_s	Cross-sectional area of cylinder
A_t	Atom content
$\mathbf{B}$	Strain-rate matrix
C	Stiffness factor (relationship between stress and strain rate)
c	Yield locus
c_1	Material constant of Power law
c_2	Material constant of constitutive equation for aluminium alloys
D	Outer diameter of reverse shape
D_0	Initial diameter of compression-test specimen
D_3	Multiplying factor
D_4	Multiplying factor
D_c	Diameter of compression-test specimen
D_r	Ideal outer diameter of reverse shape
d	Inner diameter of reverse shape
d_r	Ideal inner diameter of reverse shape
$d\varepsilon$	Infinitesimal strain

$d\varepsilon_{ij}$	Strain increment tensor
E_{11}	Lagrangian strain component
$\dot{E}_{11}$	Lagrangian strain-rate component
e	Engineering strain
$\dot{e}$	Engineering strain rate
e_e	Convergence error limit of velocity for Newton-Raphson method
e_l	Limit of the difference between to shapes
F	Yield function
F_c	Uniaxial compressive force
F_f	Friction force
F_i	Non-linear equations
F_l	Forming load
F_n	Normal force
F_w	Depth of deformation
$\mathbf{F}$	Entire vector of functions F_i
f_s	Friction stress
$f\left(\sigma_{ij}\right)$	Yield function
G	Plastic potential function
H	Stain-hardening constant
h	Height of reverse shape
h_0	Initial height of compression-test specimen
h_c	Instantaneous height of compression-test specimen
h_r	Ideal height of reverse shape

I_1	First (linear) invariant
I_2	Second (quadratic) invariant
I_3	Third (cubic) invariant
J_2	Second (quadratic) invariant
J_3	Third deviatoric stress invariant
$\mathbf{J}$	Jacobian of transformation (Jacobian matrix)
j	Element number
k	Shear yield stress (parameter regulating the stress scale)
k_r	Difference between the ideal shape and reverse shape
LCL_R	Lower control limits of the R chart
$\mathrm{LCL}_{\bar{\bar{X}}}$	Lower control limits of the *X*-bar chart
$\mathbf{L}$	Lower triangular matrix
l	Instantaneous length of tensile-test specimen
l_0	Initial length of tensile-test specimen
M	Total number of elements
m	Shear-friction factor
m_{sub}	Number of subgroups (number of trials)
$\mathbf{N}$	Shape function
n_1	Strain exponent
n_2	Strain-rate exponent
n_j	Unit normal to the corresponding surface
n_{sub}	Subgroup size (samples taken for each trial)
P	Uniaxial force in tensile test

$\mathbf{P}$	Point of the first reverse shape
p	Positive scalar factor
$\mathbf{Q}$	Point of the final shape
q_n	Transformation function of iso-parametric element
R	Range
R_g	Gas constant of constitutive equation for aluminium alloys
R_i	Data point of the R chart
$\bar{R}$	Average range
r	One of cylindrical coordinates
S	Boundary surface
S_F	Part of the boundary surface
S_f	Contact surface
S_r	Ram speed
S_u	Part of the boundary surface
s_{11}	Stress measure corresponding to the Lagrangian strain rate
T	Temperature
T_{abs}	Absolute temperature
T_{av}	Average temperature of two dissimilar metals
T_{di}	Temperature discrepancy between two dissimilar metals
T_f	Forming temperature of stainless steel AISI 316L
T_w	Welding temperature
t	Time
t_i	Surface tractions

UCL_R	Upper control limits of the R chart
$\mathrm{UCL}_{\bar{\bar{X}}}$	Upper control limits of the *X*-bar chart
$\mathbf{U}$	Upper triangular matrix
u_i	Velocity components
$\dot{u}_i^{\tau}$	Relative velocity vector
$\mathbf{u}$	Velocity field
V	Volume
V_x	Volume of a cylindrical shape about the x-axis
V_y	Volume of a cylindrical shape about the y-axis
v_i	Velocity
$\mathbf{v}$	Velocity vector at nodal point
W_0	Rate of work per unit volume
X	Coordinates in the reference (or undeformed) state or position
$\bar{X}$	Mean (average)
$\bar{\bar{X}}$	Average of $\bar{X}$
x	Coordinates in the deformed state or position
x_c	x coordinate of centre of gravity
$\mathbf{x}_0$	Geometrical configuration of final shape
$\mathbf{x}_{0-1}$	First reverse shape
Y	Yield strength of material
y_c	y coordinate of centre of gravity
z	Cylindrical coordinate z
α	Incompressibility penalty (volume penalty) factor

β	Normal penalty (interface penalty) factor
δ_{ij}	Kronecker delta
$\delta\mathbf{v}$	Newton step
ε	True strain (natural strain)
$\dot{\varepsilon}$	True strain rate
$\dot{\varepsilon}_{ij}$	Strain-rate tensor
$\dot{\varepsilon}_V$	Volumetric strain rate
$\bar{\varepsilon}$	Effective strain
$\dot{\bar{\varepsilon}}$	Effective strain rate
λ	Lagrange multiplier
λ_s	Step length of Newton-Raphson method
ΔH	Active energy
Δt	Time increment
ξ	One natural of coordinates
η	One natural of coordinates
θ	One of cylindrical coordinates
μ	Friction coefficient
π	Ratio of circumference to diameter
	Plane of zero mean stress in stress space
σ	True stress
σ_1	Principal stress along the 1st direction
σ_2	Principal stress along the 2nd direction
σ_3	Principal stress along the 3rd direction

σ_{11}	Engineering stress component
σ_i	Tensile strength of bimetallic weld of subgroup
$\sigma_{i\max}$	Maximum tensile strength of bimetallic weld
$\sigma_{i\min}$	Minimum tensile strength of bimetallic weld
σ_{ij}	Cauchy stress tensor
σ_n	Normal stress
σ_m	Mean stress
σ_p	Hydrostatic component of the stress
σ_V	Volumetric stress
$\bar{\sigma}$	Effective stress (Flow stress)
σ_1'	Principal component of deviatoric stress tensor along the 1st direction
σ_2'	Principal component of deviatoric stress tensor along the 2nd direction
σ_3'	Principal component of deviatoric stress tensor along the 3rd direction
σ_{ij}'	Deviatoric stress tensor
σ_t	Tensile strength of bimetallic weld
τ_{ij}	Shear stress components
τ_i^f	Shear friction stress
Ω	Domain of integration
ω	Number of variables
$\overrightarrow{OP}$	Vector representing $(\sigma_1', \sigma_2', \sigma_3')$
$\overrightarrow{OS}$	Vector representing $(\sigma_1, \sigma_2, \sigma_3)$
$\overrightarrow{PS}$	Vector representing $(\sigma_m, \sigma_m, \sigma_m)$

1. Introduction

1.1 Warm forming

In a typical manufacturing process, a raw material starts either shapeless or has a simple geometry which is subsequently transformed into a useful part through various operations in the process. The finished products usually have a more complex shape with a well-defined profile/appearance, dimensional accuracy, surface finish, and mechanical properties. Metal forming is one among many kinds of manufacturing processes. It aims to transform metal into a desired final shape without damage from applied forces. The formed components can also achieve the above requirements by plastic deformation. Unlike elastic deformation, the plastic deformation is not recoverable, and the change of component shape is permanent.

An initially simple shape of a workpiece such as a solid billet or sheet blank is plastically deformed by tools (or called forming dies) to obtain the final profile of the component or product. Based on the geometry of the workpiece, metal-forming processes are usually classified into two major groups. They are:

- Massive or bulk forming – Typical deformation processes include forging, rolling, extrusion, and wire drawing. A deforming material or workpiece is mostly in either a solid blank, bar, or billet form so that a considerable change in its thickness, height, width, length, and/or diameter occurs during its deformation. The workpiece undergoes a large permanent (plastic) deformation, leading to a significant change in its raw thickness and shape of cross-section. It

is also worth noting that the magnitude of the workpiece undergoing elastic deformation is relatively small, and thus elastic strain recovery after deformation is insignificant in the forming analysis.

- Sheet-metal forming – Typical processes include blanking, piercing, bending, stretch forming, deep drawing, and roll bending. A sheet blank as a workpiece is permanently deformed into a desired three-dimensional shape without appreciable changes in its thickness and surface characteristics. The recoverable portion of elastic deformation is particularly considerable against the permanent change of plastic deformation. Thus, the elastic-strain recovery and spring-back effect should also be concerned.

Temperature is one crucial factor in determining the formability and properties of formed components because most materials behave differently under various temperature conditions. Mostly, the yield stress (i.e., a threshold value of stress required for starting plastic deformation) of a metal increases with the increasing strain (or deformation) at ambient temperature and with increasing strain rate (or deformation rate) in high-temperature environments. This general principle governing the forming of metals at various temperatures is basically the same. Thus, another common way of classifying metal forming is according to workpiece pre-heat temperature, namely cold forming, warm forming, and hot forming. This classification can contribute a great deal to the understanding and improvement of the processes.

Cold forming refers to the plastic deformation, which is usually carried out below the recrystallization temperature of the forming material, generally at room

temperature (i.e., no heating is involved). Even though the formability of most metals room temperature is poor, no oxidisation on surfaces and high dimensional accuracy of cold-formed components are the main benefits that can save subsequent machining and processing costs. The cold-formed materials can also obtain stronger mechanical properties such as higher yield and tensile strengths compared to those of the raw materials due to the strain-hardening behaviour. The process is often applied mainly to make axis-symmetric or nearly axis-symmetric parts in large volumes by the extrusion process. Under these circumstances, using cold forming to manufacture the metal parts or components may involve a large number of dies and multi-stage operations. Therefore, its efficiency is very low. Figure 1.1 shows a stainless-steel watch case produced by a multi-stage cold-forming process. On the other hand, when the deformation is carried out above the recrystallization temperature of the forming material, it is called hot forming. Although the process requires smaller forming loads, drawbacks of low dimensional accuracy and poor surface finish of products cannot be avoided because of thermal expansion and heavy oxidization (or contamination), respectively. Normally, hot-forming ferrous materials like stainless steel should be undertaken at around 1100 °C. To have a compromise between cold forming and hot forming concerning economic production and quality products, warm forming is proposed. As the name implies, the warm forming is carried out at the temperature range that is higher cold-forming temperature but well below hot-forming temperature (i.e., the room and material recrystallization temperatures) [1]. Under suitable conditions, warm forming is feasible for forming the preheated metal efficiently into the final shape within a single-stage operation. Typically, the warm-forming

temperature ranges for plain steel, low-alloy steel, or stainless steel and aluminium alloy are from 550 to 900 °C [2] and 200 to 300 °C [3], respectively.

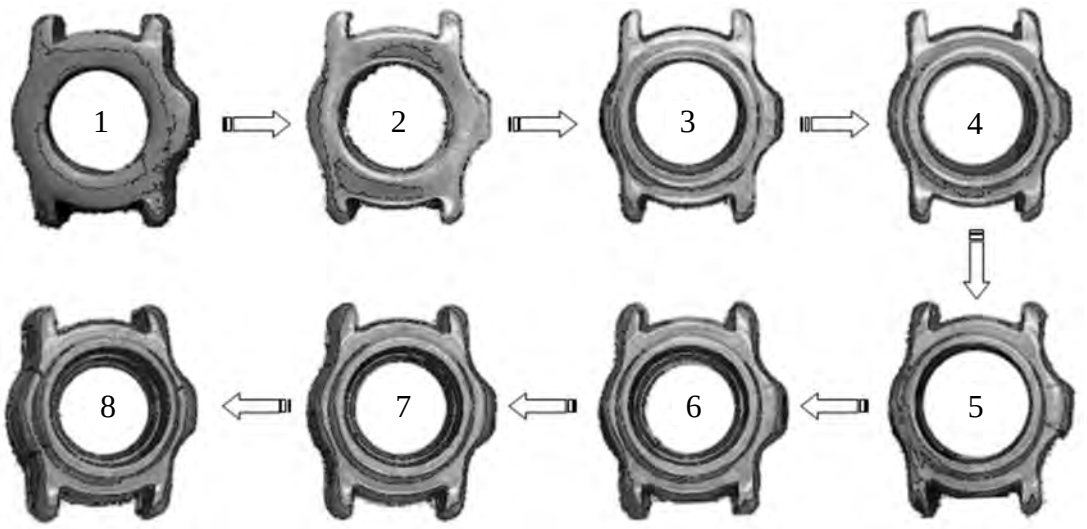

Fig. 1.1 The conventional cold-forming sequence of a stainless-steel watch case.

Most investigations and reports indicate that warm forming is widely used in the automotive industry for mass-producing complicated parts and critical mechanical components such as turbine disks, differential gears, shafts, hubs, connecting rods, and joints. Figure 1.2 shows various automotive components that are manufactured by warm forming [4].

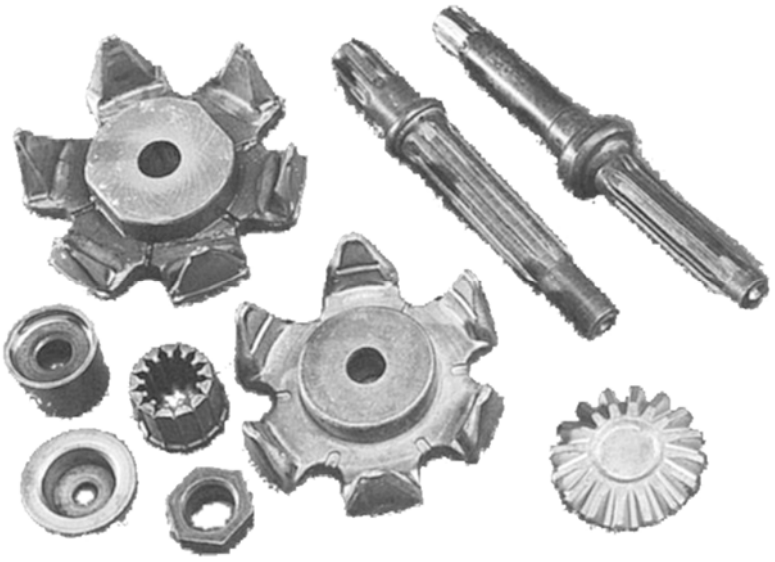

Fig. 1.2 A wide range of automotive components can be made by warm forming [4].

The warm forming described in this thesis is basically the warm bulk-forming process. It is well-known that bulk forming (or forging) requires a larger force and energy to process the plastic deformation. By increasing forming temperature to a point above room temperature, the stress required for the same amount of deformation can be greatly reduced. If the workpiece is a bulk metal, the benefits are provided by raising the temperature. This is the reason why bulk forming was selected as the particular warm forming focus in this study.

Warm forming makes use of sequential dies with the die cavities or impressions that are designed based on the profile of the finished component (i.e., closed-die forming) to form the workpiece or preform into the desired shape without the excessive flash formation and underfill [5,6]. Normally, as a near-net-shape process, the warm-formed component still needs to be undergone some subsequent fabrication processes

such as welding, machining, and polishing to reach the ultimate profile and dimensions of the final product [7]. To fulfil the mechanical requirements such as strength and toughness for load-bearing applications, the material flow of the warm-formed components can also be optimised to obtain the desired grain structures. Therefore, warm forming is nowadays increasing its presence in the automotive, aviation, and timepiece industries for the production of complex components as those are concerning the cost-effectiveness as well as quality and reliability [8]. A typical warm-forming process for manufacturing a watch bezel is shown in Fig. 1.3.

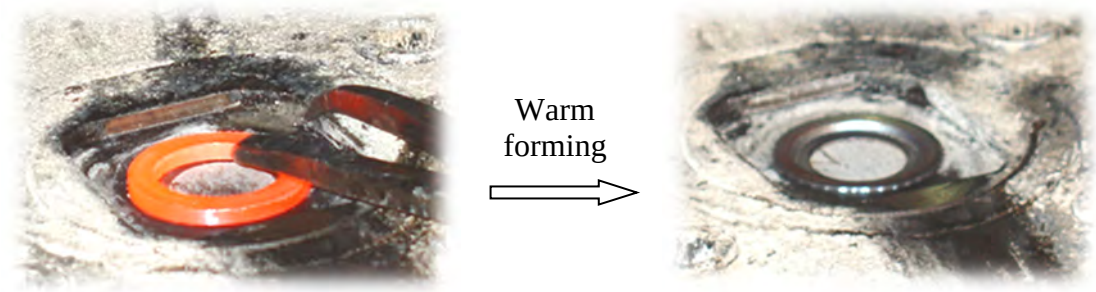

Fig 1.3 A stainless-steel watch bezel is produced by warm forming.

1.2 Bimetallic components

The metal-forming industry is facing a situation where the market trend is towards greater demand for light, strong, and economical products. In fact, each material has its unique properties and characteristics, and hence no single metal or alloy can perfectly satisfy all these requirements. For example, titanium alloys and aluminium alloys are lighter than alloy steel for making the armours of weaponry.

However, the titanium alloys are costly whilst the aluminium alloys do not have sufficient strength and wear resistance. An alternative solution is the use of bimetal, in which two different metals or alloys are joined together. This takes advantage of their strengths, usefulness, and cost-effectiveness. Therefore, the functions of bimetallic components can be optimised to target specific requirements such as applicable performance, weight, and cost [9-14]. Figure 1.4 presents various bimetallic tools, products, and components that can provide increased performance and additional functionality.

Fig. 1.4 The bimetallic tools, products, and components used in various aspects.

1.3 Significance of warm-forming process design

Warm forming is able to change the workpiece from simple geometry to complicated one as the finished component. In this process, a heated workpiece is compressed between opposing dies so that the material is forced into the die cavity. The material flow and stress distribution regarding the acting force on the workpiece are highly influenced by the areas between the contacting die and workpiece surfaces. In other words, the geometry of the dies becomes a critical design factor in the warm-forming process. For a single-stage forming operation, the die geometry, particularly the die cavity is usually governed by the shape of the formed component. On the other hand, the design of the billet (i.e., workpiece) shape and selection of the suitable forming process conditions to fulfil overall goals of quality, time, and cost reduction is actually the most primary task in this case. Nevertheless, in certain cases, the finished component is not simple, which is not expected to be formed by a single-stage operation. Transition shapes (i.e., preforms) are thus required to modify the trajectory of metal flow that changes the shape of the workpiece to form the finished component. Consequently, most forming requirements such as no crack, no internal and external defect, limited flash, minimum strain variation, and complete die filling are highly related to the shapes of workpieces or preforms and could be achieved by their proper design.

The main concern of warm-forming process design is to understand the material flow during operation. There are multi-variables correlated with each other that can greatly affect the success of the warm-forming process such as raw material properties,

forming temperatures, punch speeds, as well as lubrication and heat transfer between the die and workpiece interfaces [15]. For instance, the increasing temperature can help to reduce the flow stress of formed material resulting in a lower applied load and better formability, but against this may be difficult to control the dimensional stability of the product after thermal expansion. According to a study of the forming processes for 6061 aluminium-alloy wheels, it was found that the temperature of the workpiece increased when the punch speed was changed from 0.1 to 0.2 m/s. The lower punch speed caused a larger chilling near the contact region between the die and the workpiece. On the other hand, the die-chilling effect was less extensive at higher punch speed since it took less time to complete the forming operation. A high ratio of contact area at the tool-workpiece interface in the forming of a wheel also affected the friction and the heat transfer, and hence the workpiece temperature [16]. Another study focusing on tool-workpiece friction indicated that the selection of forming lubricants and die coatings for warm forming needed to be considered together because interactive effects were found in their different combinations. Concerning the environmental protection and extension of tool life, the oil-graphite-free lubricant and graphite-based coating were the suggested choice when forming temperature was 650 to 900 °C. [17]. The correlations among various process variables associated with the die geometry result in complicated problem formulations of forming analysis. It is extremely difficult to determine a workpiece from the infinite range of transition shapes possible in the deformation sequence of the forming process.

Traditional process design relies largely on experience and intuition. However, the empirical guidelines found in design handbooks may be insufficient or not suitable for complicated formed components. In order to properly make use of the typical experience-based process-design approach, computer-aided engineering (CAE) technology such as the finite-element method (FEM) and finite-element analysis (FEA) are employed effectively to simulate the metal flow and predict the defect formation during forming operations. This also provides a virtual forming platform to evaluate the feasibility of the process, and hence the number of physical trial runs can be reduced. Commercial finite-element (FE) simulation packages such as DEFORM [18], QForm [19], and MSC.SuperForge [20] are able to provide such information on the analysis of the bulk-forming design process. The FE simulation can provide certain valuable information regarding the warm-forming process in terms of metal flow velocity, required forming load, stress and strain distributions, and thermal gradient. However, demanding computational hardware (mainly the microprocessors and memory) and time, as well as significant expertise in forming analysis and process improvement, are required also. Although the simulation results associated with iterative optimization methods as well as design knowledge and experiences are very supportive and beneficial for workpiece design improvement or modification, the workpiece design and modification procedures are basically a process of the trial-and-error scheme, which may be time-consuming for some difficult cases, but is more cost-effective than through the physical problem solving and trials. Clearly, the more efficient method is to build a knowledge-based or expert system, which captures the heuristic knowledge and expertise in forming-process design from academic research

and/or other industrial experiences and scientific work. Certain techniques and analytical methods such as expert systems and genetic algorithms are developed and used for various forming processes and their workpiece or preform designs. More extensive reviews and discussions on the limitations and weaknesses of current workpiece-design methods are given in the next chapter.

1.4 Reverse simulation for bulk-forming process

Regarding the aforementioned current techniques for process design of warm forming, a more efficient and systematic approach has to be developed that can assist in determining an acceptable workpiece shape directly so that the work is undertaken at a faster pace and further helps to reduce the lead-time for producing new-formed components. Consequently, a proposed reverse simulation approach implements the core concept of reversing the metal flow and velocities in the conventional forward FE simulation, which starts from the final shape of a workpiece (i.e., the final formed component) with its reverse (i.e., negative) node velocities [21-26]. When the die is moving backward and the contact boundary nodes are being released during a number of reverse steps, the simulation can gradually predict an initial workpiece shape. In other words, the workpiece shape predicted by the reverse simulation can be more acceptable rather than various uncertain trial-shapes need to be verified with the forward simulation as discussed above. Figure 1.5 illustrates the fundamental concepts of forward simulation and reverse simulation used for the workpiece design of the bulk-forming process.

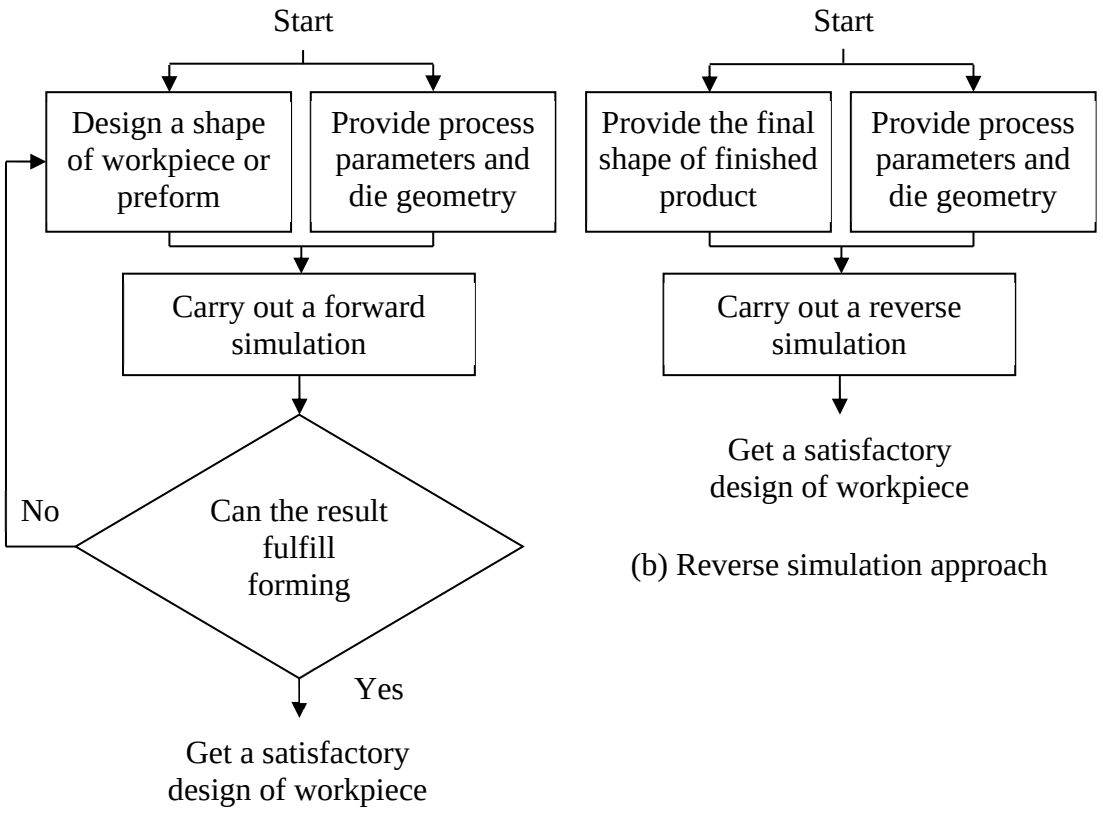

Fig. 1.5 The forward simulation approach and reverse simulation approach used for workpiece design of bulk-forming process.

Since the study of the reverse simulation of warm-forming bimetallic components is unique, there is a significant gap in the literature addressing this issue of using the reverse simulation approach. In addition, the demand for and consumption of bimetals is rapidly increasing and will provide a very wide range of applications of bimetallic components used in automotive, marine, aerospace, and military industries. Therefore, intensive study in this area is certainly an urgent need in such process modelling.

1.5 Objective of study

The primary objective of this study is to develop an efficient methodology for the warm-forming process design of bimetallic components using the reverse simulation approach, which is based on several empirical and physical rules with the finite element procedure. The study aims to demonstrate the implementation of the proposed idea to control the material flow and distribution as well as the methods of shape reconstruction in the reverse simulation to predict the workpiece or billet shape in the axisymmetric bulk-forming applications, especially warm-forming bimetallic components. The predicted workpiece should have a minimum height and should be able to fill up the die cavity completely with a controlled amount of flash in a manner that avoids the occurrence of forming defects such as folds or overlaps. The reverse simulation certainly predicts the shape of a workpiece without a trial initial geometry of the workpiece and should prove to an efficient methodology. This research work also attempted to investigate and improve the process modelling of warm-forming bimetallic components. In order to achieve the objective of this study, the tasks were carried out as follows:

- To design and manufacture the special tooling for performing the isothermal uniaxial compression test, ring-compression test, welding experiments of dissimilar metals, and warm-forming experiments.
- To obtain flow stress data at elevated temperatures of the specimen materials as well as the values of friction factors at the interface between workpiece and die, to be used for process modelling and numerical simulation.

- To study the mechanical properties of different base metals and even their bimetals, especially the tensile strengths of the bimetallic joints and interfaces (i.e., the joint efficiency).
- To investigate the intermetallic bond of diffusion zone found in the bimetallic joint that may significantly influence the modelling of warm-forming bimetallic components.
- To establish an algorithm for determining the reverse shape of the workpiece or preform based on the backward tracking method and finite element formulation of rigid-plastic materials.
- To develop a procedure for defining the desired shape and contact boundary conditions, shape reconstruction, and determination of the condition of the bimetallic interface in the reverse simulation.
- To implement the reverse simulation for the warm-forming axisymmetric component and a bimetallic component with various final shapes of finished products.
- To verify the predicted results of reverse simulation by forward simulation and physical experiments.

1.6 Layout of dissertation

Chapter 1 – Introduction provides background information about warm forming, bimetallic components, and reverse simulation including their definitions, advantages,

and applications. The main objectives of the study, as well as the sequence of the research work are outlined.

Chapter 2 – Literature Review presents the relevant information on the workpiece or preform design from industry, handbooks, and research work. This reviews the fundamentals of bulk forming as well as the previous studies of workpiece and preform-design in order to realise their principles, assumptions, advantages, limitations, etc. The difficulties and complications related to their applications are addressed, especially in the reverse simulation approach.

Chapter 3 – Theoretical Background gives the theory and equations governing the bulk-forming process. It includes the yield criteria, general assumption, constitutive equations, modelling method, boundary conditions, etc. which are related to the FE simulation performed in this study.

Chapter 4 – Reverse Simulation Approach proposes the idea of a workpiece-design approach using reverse simulation involving the concept of controlling the material flow and distribution. The key concepts of the backward tracking method and determination of contact boundary conditions to be used in this study are described. The methods are then incorporated into various empirical and physical rules governing the typical bulk-forming process for reconstruction of reverse shape. The specific considerations on the development of warm-forming bimetallic components and determination of the condition of the bimetallic interface are mentioned.

Chapter 5 – Research Methodology explains the information on the experimental work including the specimen materials and preparation, tooling set up, and test procedures. This chapter also discusses how to consolidate the useful findings and achievements used in process modelling. The finite-element formulation for the two-dimensional axisymmetric bulk-forming process and the numerical treatment for reverse simulation are described in detail.

Chapter 6 – Results and Discussions presents and discusses the results of computer simulation by DEFORM-2D using the proposed workpiece-design approach. Physical experimental verification is presented as the findings include flow stress data, friction factors, joint efficiency of bimetal, suitable process conditions of warm-forming bimetallic components, and the prediction of the billet shapes for warm forming the base metal as well as bimetals.

Chapter 7 – Conclusions summarises the results from this study and makes some suggestions for the further investigation of warm-forming process design of bimetallic components using the reverse simulation approach.

2. Literature Review

2.1 Forming-process design

The manufacturing industry was always concerned about a low cost, high quality, and short lead-time to remain competitive strength as components and products were being developed. For the components produced by bulk forming, the characteristics were determined in terms of structural integrity, dimensional accuracy, free of internal and external imperfections, mechanical properties, and surface finishing. In order to achieve the required quality of bulk-forming, potential candidates for material and the appropriate operations must be studied. In addition, the production cost including material, tooling, and operation costs had to be reduced. To find the optimal solution quickly, it was indeed a difficult task due to the many design and process variables involved in a bulk-forming process [8].

Many design and process variables were involved in the forming system that included raw material properties, shapes of workpieces and finished components, friction conditions, punch speeds, forming temperatures, tool design, etc. Figure 2.1 presents a closed-die forming process considered as a system [8]. The effects of these variables on various operations and shapes of finished components might be different. For example, the influence of workpiece temperature on the forming process using a hydraulic press was greater than using a drop hammer process due to ram speed, operation time, die chilling, and heat transfer. Also, due to the absence of recrystallisation of microstructure, cold and warm formed components can attain better

mechanical properties, which were beneficial from the strain or work hardening effects against hot-formed components with recovered grain structures. In consequence, understanding the effects of these variables on material flow was very important to design a successful forming process that yielded higher product quality at a lower cost.

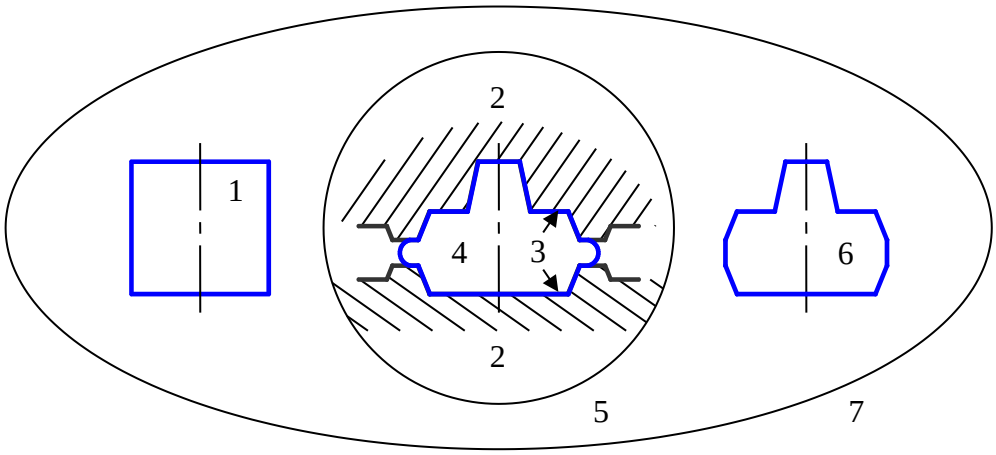

1 Billet/workpiece
2 Tooling/die
3 Material/tool interface
4 Deformation zone
5 Forming equipment/press
6 Formed product/component
7 Production environment

Fig. 2.1 The closed-die forming process considered as a system [8].

Suitable but not optimal process parameters, as well as suggested tool and workpiece design could be determined or selected based on previous practices, empirical rules or design guidelines, and/or expert systems [27]. For instance, the suggested forming temperature for automotive-grade aluminium alloy type 5754 was in the range of 300 to 350 °C [28]. The graphite-based lubricant was mostly recommended for aluminium alloy [29]. The die material could be the hot-working

tool steel AISI H13 [30], and the manufacturing method for the dies could also be based on existing techniques, such as electrical discharge machining (EDM), computer numerical control (CNC) machining, EDM wire cutting, and high-speed machining. Therefore, the approaches to determining effective shapes of workpieces or preforms and die configurations would become more significant for new forming product design.

The die geometry, particularly the shapes of the die cavities involved in the final stage of the bulk-forming process was highly dependent on the shape of the finished component. The design of the dies could be helped by the suggestions from the guidelines, handbooks, or experience. However, the design of workpiece or preform (i.e., transition shapes of the formed components) shape was definitely a challenging task for engineers and researchers because of numerous interactions among different forming factors and process variables towards affecting the results of shape prediction. The interactions among significant process variables in closed-die forming are shown in Fig. 2.2 [8].

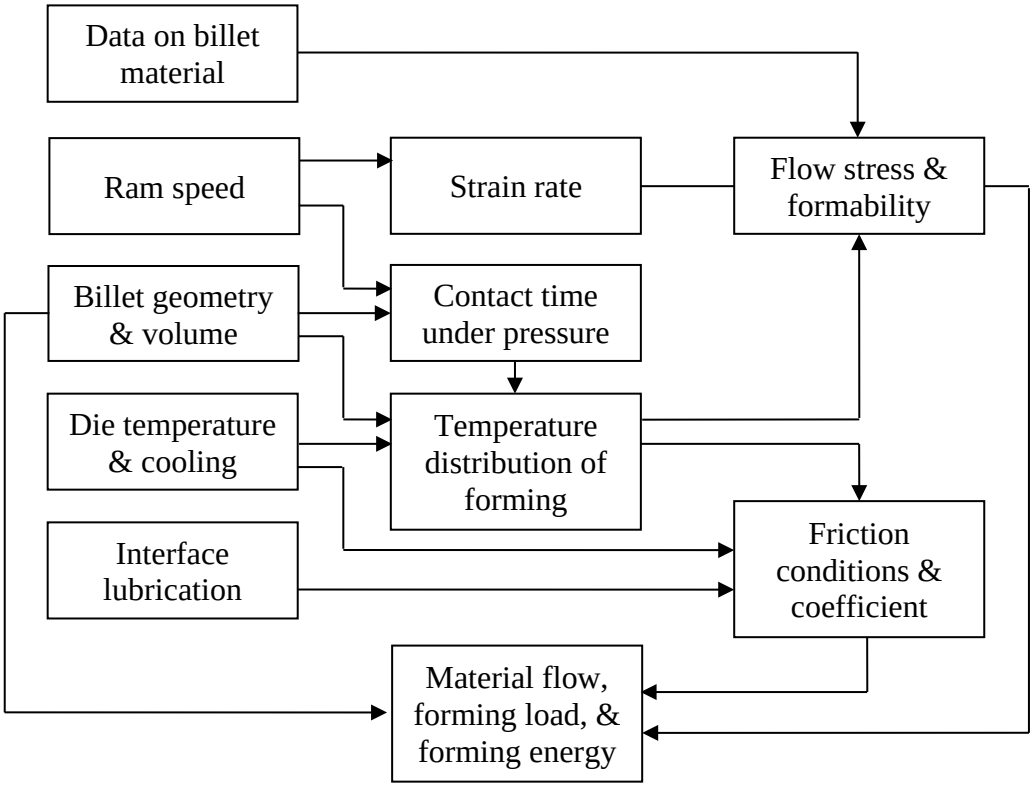

Fig. 2.2 The interactions among significant process variables in the closed-die forming [8].

The experiences on workpiece design of researchers or from industry provided useful suggestions and recommendations but might not be applicable or suitable, especially for a new type of components or products. Although velocity fields of material flow, as well as different forming information such as temperature, stress, and strain distributions used to evaluate the success of the bulk-forming process, could be acquired and analysed with the aid of computer simulation, the workpiece shapes and die configurations had to be determined at the beginning and could be further improved based on the results of simulation trials. The combination of experience and computer-simulation-aided approach was still essentially a process of trial and error and usually required demanding and expensive computer workstation environments in terms of

microprocessor and memory hardware, computational time, and expertise. Therefore, an automatic and efficient workpiece-design system was highly desirable in the metal-forming industry; one that was able to determine the shape of the workpiece directly to improve component quality, minimise costs and reduce production lead time.

2.2 Workpiece design by empirical methods

Extensive knowledge and thorough understanding of workpiece design were the keys to success in producing good components and remaining competitive. They were accumulated from years of work experience and industry practices, which were usually the invisible assets owned by a metal-forming industry or enterprise. Existing strategic approaches to the design of workpieces or preforms were limited at the research level. Systematic methods for the applications in industrial sectors should be developed. Thus, this section mainly focused on the fundamental principle of workpiece-design procedures. It was conceivable to consolidate and compile the information as the guidelines facilitating the die design at single-stage forming since the die cavity or impression was usually close to the profile of the finished component. The general procedure of bulk-forming die design is shown in Fig. 2.3. It normally started from studying the technical and geometrical requirements of the formed component to selecting appropriate process parameters [31,32].

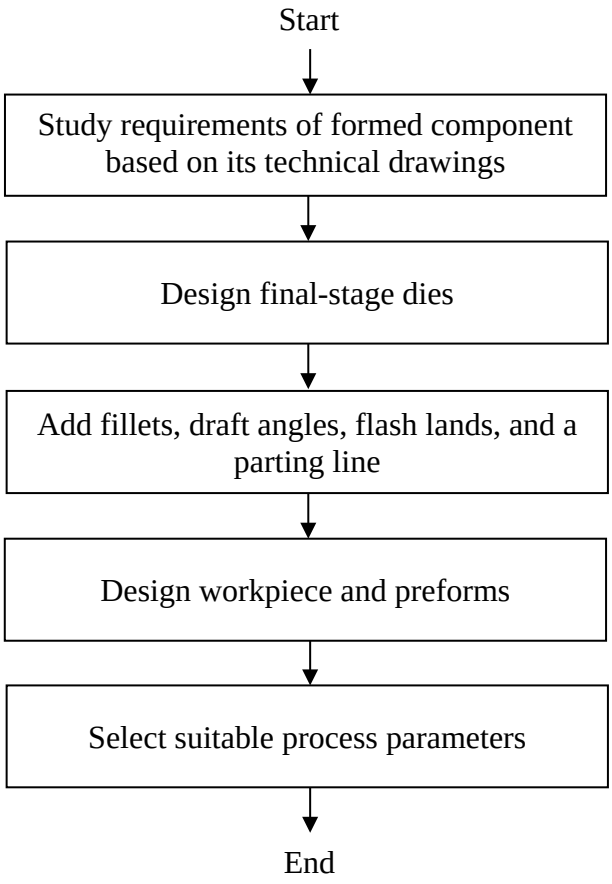

Fig. 2.3 The sequence of designing forming dies.

As mentioned in Chapter 1, most formed components needed subsequent machining and polishing processes to become the ultimate products because of high-precision dimensional control and/or shaping undercuts and re-entrant angles. It was therefore necessary to give additional dimensional allowances towards machining and tool wear in designing the formed component. The mating allowances should be sufficient and usually added on external surfaces required for machining. Tool wear allowances were provided as the tolerances dependent upon the size of die cavities being enlarged after wear. Thermal expansion allowances might also be included

because the warm or hot forming processes lead to shrinkage after die chilling of the workpiece.

2.2.1 Design of forming die

Empirical methods had evolved from extensive past experience in metal forming to aid the design of final-stage dies. Some applicable geometrical features within the die cavities were proposed for general grain structure and direction controls of material flow from a workpiece to the finished component. These features and terminology of the dies used in closed-die forming are shown in Fig. 2.4 and their details are described as follows [33-37].

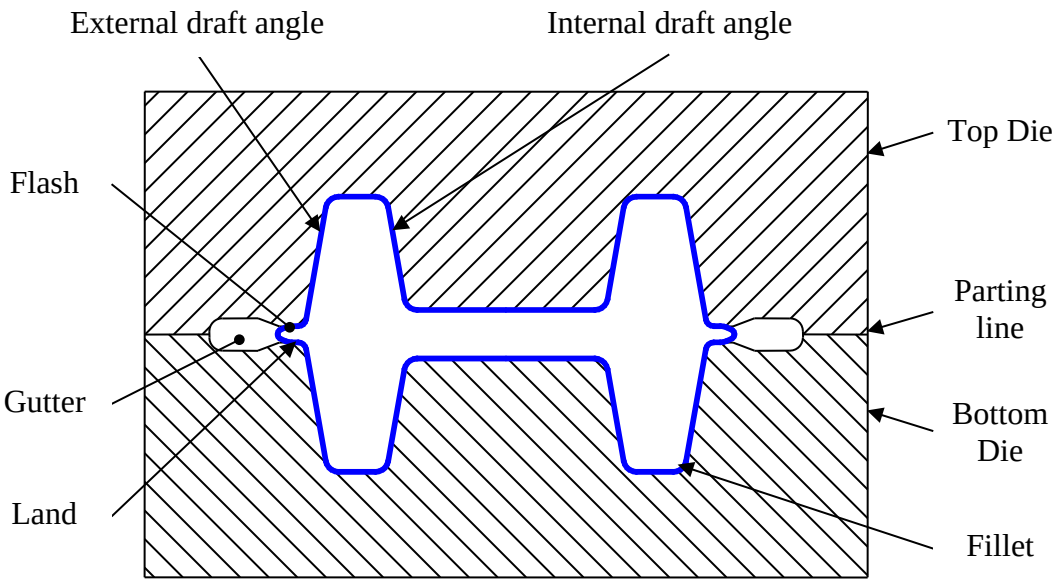

Fig. 2.4 Various die features in typical closed-die forming.

Parting line (or parting surface) – during the bulk-forming process, material flows towards cavities, and the parting line, which was on the plane of separation where the two halves of (i.e., top and bottom) die met. The design of the parting line could affect the flow pattern and hence influenced forming properties. The parting line was typically located around the cross-section with the greatest dimensions of the formed component. In the simplest case, the straight or single-plane part line was located at the middle of the simple symmetric or axisymmetric components. On the other hand, the irregular curved surface might be applied to complicated shapes. Also, an unbalanced load resulting in misalignment of the die set during the forming process must be avoided when designing the parting line.

Flash, land, and gutter – Some excessive flow of material (i.e., the flash material) was required, in which the material was restricted to flow into a gutter. Such a proper flash design could not only relieve the unnecessary forming load but also pushed the material into the intricate sections of the die cavity to achieve complete die filling. However, the flash was surplus, which should be trimmed after the bulk-forming operation. Typically, extra volume (about 2 to 5% of formed-component volume) was sufficient to flow across the flash land and provided an allowance for filling the die cavity. The length of flash land was around twofold larger than the flash clearance, which was 3% of the maximum thickness of the formed component. The functions of the gutter were to store the excess flash and relieve flow pressure. Its width and depth should be adequate to reduce excessive forming load produced by the sliding friction between the surfaces of flash and gutter.

Draft angles – The draft angles were necessary for forming dies so as to remove the workpiece from the dies easily. Because of the thermal shrinkage that occurred during cooling in non-isothermal forming processes, internal draft angles were usually made larger than external draft angles. Generally, the external and internal draft angles were about 3 to 5 degrees and 7 to 10 degrees, respectively.

Fillets – The fillets smoothly connect surfaces, which provided the essential function in ensuring the smooth flow of material in die cavities as well as other regions (e.g., flash land). As a general rule, if it was permitted subject to the geometrical constraints and requirements of formed components, large fillet radii were preferred to obtain satisfactory material flows and prevent stress concentrations at the corners, which could easily reduce the tool or die life.

2.2.2 Transition stages of workpieces

In most cases, a complicated shape could not necessarily be formed without defects and excessive die wear in one operation from the initial billet to the finished component or product. In other words, transition stages (i.e., preforming stages) became necessary, so as to control the material flow and distribution. Principally, the material of the workpiece had to flow in the direction toward the least resistance according to the minimum work-rate criterion. To control the material flow in an optimal situation, the material should be distributed gradually and evenly throughout filling up the die cavity. The detailed design considerations are presented below [31].

(i) Number of transition stages/steps

Locating the workpiece – particular workpieces or preforms had to be placed in corresponding die cavities of different stages stably without slippage and rotation so as to avoid inconsistent and uneven die filling. Normally outer profiles of the workpiece, preform or blank were approximately equal to these of the finished component with an offset-width around 0.1 to 0.2 mm depending on the materials of the workpiece and die. This ensured that the workpiece could be placed inside the impression of the bottom die without shifting. Either blanking or fine-blanking was able to produce such workpieces or blanks with identical cross-sectional profiles efficiently.

Friction and tool wear – tool or die wear could be caused by overstressing, cyclic contact pressure, and/or usually sliding friction between the workpiece and tool surfaces during the material flow. An appropriate workpiece design was able to reduce the friction and material flow over the die surface and hence reduce the tool wear. In other words, sharp corners on the workpiece or preform should be removed.

Tool fracture – the tool profiles with insufficient die-closing contact surface might cause the tool fracture because the impact load was generated in high-speed deformation, especially in drop forging (one type of bulk-forming processes). The rate of the deformation influenced by the ram speed of the forming press must be considered to prevent tool fracture.

Mechanical properties – the plastic strain (i.e., amount of the permanent plastic deformation) as well as the strain rate were the major magnitudes to reflect the best measure of the mechanical properties of formed components. Since the strain rate could affect the heat generation during the material deformation, the change of internal grain structures would be varied, when the material temperature was elevated to the threshold level. Increasing the number of transition stages could be a strategy in this manner to control the strain and strain rate achieving the desired mechanical properties.

(ii) Forming volume and stock size

Basically, a volume of material from most metallic workpieces (except porous metals) was nearly constant throughout the forming process. This was a very convenient assumption frequently applied for forming process and workpiece design. The volume was calculated from the full forming envelope (e.g., a block or a cylinder) including the flash draft and fillet radii from the ideal forming shape. Computer-aided design (CAD) systems could help process designers or toolmakers to acquire this value. For the simplest shape of the workpiece that could be fabricated easily, like cylindrical billets or round blanks, their cross-sections should be consistent (i.e., round shape or same cross-sectional profiles). Thus, the critical stock size standards of a bar (for making a billet) and a plate (for making a blank) were their diameter, height, and thickness/gauge, respectively. For instance, the ratio of diameter to height was always used to represent the shape of the cylindrical billet, in which this ratio was concerned to prevent buckling and barrelling effects.

Traditional workpiece design methods used in bulk-forming industry were mostly based on existing guidelines and procedures derived from practical experience. These might be unable to deliver sufficient information used for analysing the overall process operations, especially for the material-flow prediction. The problem cases of forming new materials such as bimetals as well as unusual component shapes would be more difficult and limited to propose design recommendations. On the other hand, computer technology was widely used in the manufacturing industry. Computer modelling or simulation was obviously an indispensable tool that assisted in bulk-forming analysis and process improvement before the actual operation. Therefore, the computer-aided simulation approach incorporated with some techniques and experience might be more applicable for workpiece or preform design.

2.3 Computer FE simulation

In the early 1990's, computers were still expensive and not popular in the consumer market. Thus, physical models, which were made of other affordable and cost-effective materials such as clay and plasticine as the substitute material of metal were used to simulate and predict the material flow. An actual material was then employed to carry out an experiment for verification of the feasibility of the process. This method could provide sufficient information such as material flow and die filling for bulk-forming analysis. However, in order to obtain more reliable and reasonable results, the substitute material should possess mechanical properties similar to those of the original material at a specific temperature. For instance, a strain rate sensitive

material, plasticine at room temperature was selected to model, alloy steel AISI 4130 at 1200 °C for the analysis of axisymmetrical heavy forging with the theory of similarity. The friction model was formulated using ring compression tests, in which the tissue paper was acted as the lubricant with a specific friction coefficient of 0.3. The verification was implemented eventually that a dome-shaped heavy component was formed successfully as similar to the prediction [38].

Compared to the virtual forming platform established by computer simulation, the physical modelling method was costly, infeasible, and inefficient because the specimens and equipment had to be prepared carefully for each trial. It might not be realistic if suitable substitute materials could not be found. In spite of that, this method was a direct alternative for workpiece-design verification under the practical forming environment.

Computer simulation considered all the significant process variables involved to model real bulk-forming processes starting from a billet or workpiece to the finished component. The FEM based simulations had the capacity to predict detailed information about material flow, and hence the die filling and occurrences of defects. A computer with the simulation software thus acted as a virtual forming machine for engineers or researchers to try out their billet, workpiece, or preform designs before a practical tooling trial run was processed. For example, the thermo-mechanical coupled FEM simulation was used to improve the preform design in gear blanking forming. The quality component was formed by the modified preform successfully. The results

showed that improved fill characteristics, decreases of forming load and pressure as well as prolonged tool life were achieved [39].

By making use of a commercial FEM code, DEFORM-2D and DEFORM-3D, a study of the flashless forging of connecting rods at both isothermal and non-isothermal conditions was carried out. Different workpiece design configurations, which were divided into crank-end, pin-end, and I-beam sections were optimised independently with multi-shape parameters. The numerical modeling and computer simulation were helpful in the design practices for the bulk-forming process, in which the simulation provided more information about the process such as load requirements and material flow at different stages of the process. This resulted in effective material savings of such flashless forging when the volume of the preform could be controlled strictly. Besides, the non-isothermal analysis was significant and necessary in warm and hot forging design [40]. The FE simulation approach was widely used to assist in the workpiece or preform design and process optimisation through the investigation of process variable data provided and extracted from the software. Examples of industrial applications included the modification of Tee-shaped preform design in forming a solid spur gear and cylindrical cup features [41], and the determination of optimal preform shape for forming aerofoil section with benefits of minimin material removal, production-cost reduction, and dimensional-accuracy improvement [42].

The FE simulation was definitely an effective approach to evaluate the workpiece or preform design. Unfortunately, it still needed a trial workpiece even it

was a virtual computer model or a CAD file as well as the corresponding knowledge and experiences on modifying the trial workpiece after the simulation analysis.

2.4 Expert systems for workpiece design

Building a database system to capture practical expertise and know-how from academic research outcomes and various experiences in the industry could provide a foundation for workpiece design in bulk forming. An expert system was established in this way [27,43,44]. It was usually an artificial intelligence program composed of a quantity of design rules and guidelines gathered from numerous sources to solve the related problems. The system was typically divided into two sub-systems, which were the knowledge base and inference engine. The knowledge base represented the workpiece design rules in terms of major geometrical and process parameters in different forming stages. The inference engine or called inference mechanism would apply these data and information from the knowledge base to provide the solution of suggested workpiece shapes. There also was a user interface that allowed the operators to control and interact with the system in natural text or graphical representation. An additional knowledge acquisition tool could be used to modify or update the information to the knowledge base. The mechanism of the inference engine was built using the “if-then” rules approach that searched the data set from the knowledge base and provided information on designing a specific workpiece with an explanation based on the input requirements [45-47].

To facilitate the knowledge base of an expert system for tool design, existing technical knowledge and expertise in related aspects from industry experience and research outputs were required. Based on this concept, an intelligent knowledge-based system used for forging process and corresponding tool design was developed [48], in which this system could make the comparison between the target forged component and reference forged components recorded in the data library to evaluate the weighting of different process parameters and geometrical factors in affecting the process success significantly. The subsequent experimental work was carried out to verify the weighting effects on upsetting and forward extrusion.

Another intelligent forming workpiece design system entitled “blocker initial-guess design”, was developed using the expert system approach also. This system was established by historical data sets of design criteria and guidelines, which were extracted from the industry literature and many researchers [49].

An expert-system-based computer-integrated manufacturing system for cold forming was established. It captured the empirical process design guidelines and computer simulation results to provide useful information to support the forming die design. A strategy for cold-forming process planning was also implemented into the system to assist the operations of the overall shop floor, and hence all design work from component design to actual production process could be undertaken simultaneously [50,51].

The expert systems might be limited for assisting in the workpiece design that the finished shapes of the formed components were relatively simple and could be

categorised easily such as cylindrical shapes, H-shapes, and axisymmetric shapes. On the other hand, the systematic and rigorous scientific knowledge of workpiece design could not be collected and managed in a timely and efficient manner due to the complexity of interactions among the design variables in the bulk-forming process.

2.5 Artificial neural networks for workpiece design

The human brain contains neurons, which were only used for recognition, but also for processing new information and learning from experiences to generate concept and internal representations. They were able to interpret information from different conditions. Researchers and scientists had been investigating the behaviours and functions of the training processes and attempting to imitate them by using artificial neural networks, in which the neural networks were typically composed of inter-connected units acting as the models like real neurons. Figure 2.5 presents the architecture of an artificial neural network, which was determined based on the imaginary artificial neuron units as illustrated in Fig. 2.6. The training rules governed how each connection (i.e., the weight) was modified. This weight represented the influence between the units so that the goal (output pattern) was reached efficiently. Activation of each input unit multiplied by the weight on its connectors and each of these products added together to obtain a total input. The total input was then converted into the final output by applying the specified activation function. In other words, the computational mechanism was dependent on both the weights of the connection and activation function used [52,53].

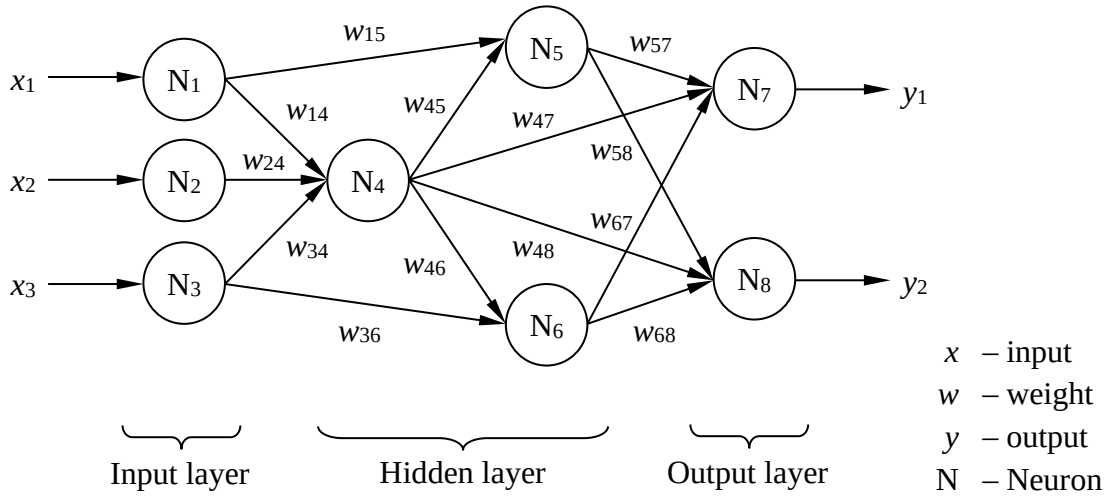

Fig. 2.5 Basic artificial neural network.

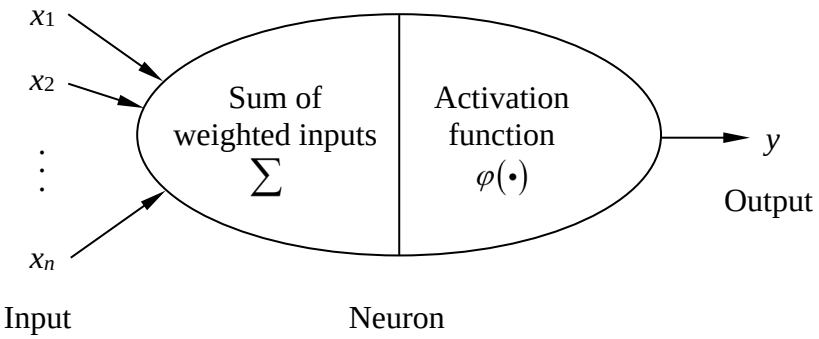

Fig. 2.6 Schematic representation of an artificial neuron.

In order to obtain the neural network that could achieve the objectives, the weights of connections needed to be determined properly. In the training process, an algorithm, such as the back-propagation algorithm was employed to repeatedly adjust the weight values, which could minimise the variation between the target and actual output activation. The weights indeed represented the strength of connections among

the units and involved in gaining the knowledge to make informed decisions for the determination of billet geometry [54].

Using the back-propagation algorithm, empirical and/or scientific design knowledge of workpiece design in bulk-forming coming from the results of physical work and FE simulation could be acquired for training the neural networks, in which this trained network could interpolate the predicted workpiece (or blocker) shapes within the category of forging plane-strain symmetrical H-shaped components. This would greatly reduce the number of FE simulations and physical modelling for the process design [55].

The artificial neural network combined with the Taguchi method was implemented for minimising objective functions of proper combinations of design parameters in multi-stage upsetting, which also considered the workability limited by ductile fracture integrated with the FE simulation. Both orthogonal array and simulation results were employed to train the networks, and thus the finished component was formed successfully without any fracture from the design of optimal preform. This presented an effective and analytical approach for such kind of workpiece design [56].

A multi-stage cold forging process design system was established based on the induction of a knowledge-acquisition procedure, in which the multi-layer neural network model and the back-propagation algorithm were applied to learn the training examples acquired from FE simulation results. The geometry of the desired T-type

component and pre-defined process condition were the input parameters when the output was to predict the shape of the axisymmetric workpiece [57].

It was evident from the above examples that the neural networks could be applied for the workpiece or preform design of bulk forming, whereas the following elements were essential in enabling this function. (i) The design parameters as the inputs of the neural networks had to include a series of pre-defined geometrical variables, which could be correlated to the shapes of both workpiece and final formed component; (ii) The neural networks had to be trained by the presented information and existing knowledge such as the empirical design guidelines as well as the results from bulk-forming experiments and simulation trials; (iii) The connection weights of the neurons had to be determined by suitable mathematical models or algorithms.

Artificial neural networks might provide useful design information for a specific task, in which the shape of components could be classified such as forming plane strain symmetrical H-shaped components, and axisymmetric cold forging. On the other hand, for complicated shapes or newly designed components, it was extremely difficult both to constrain the number of variables used to describe the geometry and to identify the key variables or parameters. The existing information and knowledge for the inputs might not cover wide ranges of metal (e.g. the bimetal in this study), component shapes, and/or forming operations. The unexcepted or abnormal results would be obtained in some situations when excessive or redundancy layers of the neural network were applied, even though this could provide additional training to the system reaching more accurate solutions [58]. These major drawbacks of artificial neural networks needed to

be considered carefully before they were applied to general-purpose workpiece design in bulk-forming.

2.6 Genetic algorithms for workpiece design

Nowadays the mechanisms driving the natural behaviours could not be fully recognised, whereas certain features and characteristics were well-known. In biology, one of the key elements in natural evolution was chromosomes, which were the organic molecules as the tools to encode the configuration of living human beings. The chromosomes carried genes, which defined the specific properties of an organism. A researcher, Holland, and his co-workers investigated the secrets and features of the natural evolution in the early 1970's. They believed that the structure of natural evolution could be a scientific technique for problem-solving or idea generation when it was properly incorporated with computer algorithms. In this way, nature had been done through a progressive evolution employing two critical processes: natural selection and sexual reproduction. Then Holland and his co-workers carried on the algorithms that decoded and operated on strings of binary digits which were called "chromosomes". Since the root was based on the genetics research and study, this methodology was called as the genetic algorithms [54,55].

When the genetic algorithms were used for workpiece design in bulk forming, the design or geometrical parameters were the possible solutions of the problem, which were represented by chromosomes. The target chromosomes were chosen by an evaluation of the fitness of each chromosome so that those chromosomes with good

evaluations led to reproduce more frequently than those with bad evaluations. Eventually, the desired chromosomes with high fitness were selected in the population after several evolutionary consequences, and the required workpiece design could be obtained.

A workpiece-design method using genetic algorithms was proposed. It was able to predict the optimal preform shapes for several axisymmetric examples with isothermal flow formulation. Continuous and discrete design variables such as the ratio of the external radius to the internal radius as well as the friction coefficient were considered. The objective function was associated with the quality of the formed component, in which the barrelling effect in upsetting a cylinder was reduced greatly and the total deformation energy in a single-stage upsetting process was minimised by using the prescribed preform shapes. This study concluded that the genetic algorithm approach provided promising results and information that could be devoted to solving practical industrial problems related to multi-stage bulk forming processes [59].

Another example of using genetic algorithms was to determine an optimal model block (i.e., the billet) for the hot non-symmetric profile extrusion with aluminium alloy 6062. Two dimensions of the die-hole layout were selected as the design variables, which were used to form the chromosomes. The study showed that the approach was able to predict the billet, in which the objective function was to balance the velocity of material flow in the process. It indicated that the construction of the optimal design model with genetic algorithms for technological variables and parameters was effective and feasible [60].

As a consequence, the following strategies were required when genetic algorithms were applied to the bulk-forming preform design. (i) The chromosomes were represented as a binary string of 0's and 1's containing the design variables, which usually included the preform dimensions and the number of deformation stages; (ii) The desired chromosomes were found in the population by the fitness function, which was essentially an objective function. To formulate the objective functions, some quantitive forming requirements such as minimum deformation energy, complete die filling, and minimum variation of effective plastic strain could be taken into account in the evaluation; (iii) A probability function could be used to generate new chromosomes. Thus, the computation time and cost could be reduced when the population size was controlled by this sub-function.

Likewise, for the complicated shapes of formed components, the problem of defining the workpiece in terms of geometrical parameters was the same as that encountered in the design approach based on the artificial neural networks. High computing time and cost was also a major problem because the evaluation of genetic strings required a great deal of FE analysis.

2.7 Forward simulation approach for workpiece design

This referred to the fact that the bulk-forming process was not only influenced by the tool geometry, but also by the shape of the initial billet or workpiece as well as other process parameters such as forming temperatures, friction conditions, and punch speeds. A desired or optimal shape of workpiece could be found through a lot of

physical experiments, which were performed based on the existing knowledge and information as well as the findings or outcomes accumulated from the iterative trials within a range of modification of geometrical parameters and process conditions. This kind of practical trial-and-error process was obviously inefficient, expensive, and time-consuming. A traditional forward simulation approach of the bulk-forming process started from the billet, workpiece or preform, and then arrived at the final shape of the formed component. The simulation could serve as a virtual press and could be combined with an iterative optimisation subject to specific criteria or technical requirements, for example, more uniform stress, strain, and temperature distributions. It was possible to search for and determine the most suitable workpiece design. The following describes the optimisation of workpiece design with respect to different but reasonable forming objectives.

(i) Complete filling of die cavity

The most important requirement of the successful bulk-forming process was certainly that the workpiece material could fill up the die cavity completely without the occurrence of forming defects like fold, crack, and damage on the workpiece. This primary requirement could be converted into an objective function required by the iterative algorithm for workpiece design through the FE simulation. A shape-optimisation method that minimised the objective function regarding the gap distance between the shapes obtained in the simulation and desired final shape of the finished component was proposed. The die profiles were adequately modelled by spline

functions when the displacements of the defined knot vertices on the spline in normal direction were selected as the design variables [61,62].

Another example also made use of the optimisation method, in which each optimisation iteration required both the preforming stage and final stage of one completed upsetting simulation to compare and minimise the difference between the desired and actually achieved final shapes of the formed component. The model could obtain the acceptable workpiece design after taking several iterations [63-65].

These two examples of workpiece-design approaches also indicated that the shape optimisation regarding the achievement of complete die filling as the objective function could be used with the forward simulation. This was able to provide a suitable workpiece design with minimum variation between the simulated and required shapes of the formed component.

(ii) Uniform stress and strain distributions

The mechanical properties of the formed components could be affected by stress and strain distribution or homogeneity of the microstructure. This was also a criterion for evaluating the quality of a workpiece design. In addition, the reduction of friction between the material and tool surface as well as stress concentration could be contributing to the tool-life improvement because localised stress increase and energy dissipation were avoided [37]. This should be taken under consideration in the both workpiece and tool design.

A commercial bulk-forming simulation package, FORGE2, which was associated with an optimisation technique was employed to determine the tool profile in a polynomial expression. This was able to obtain an axisymmetric hot-forged component with the most homogeneous recrystallised grain sizes, which was defined as a function of component strain and working temperature [66].

A systematic and practical procedure was applied to design the workpiece for a complex rib-web type forging, in which the sensitivity analysis was used to achieve the optimal workpiece shape through the iteration of FE simulation with the Fourier-transform filtering method. The objective function was to minimise the variation of strain distribution within the formed component that the forming defects such as under-filling and folding eliminated. This study demonstrated the overall methodology used for both two-dimensional and three-dimensional workpiece design problems [67].

A study made use of commercially available software DEFORM-3D to design the optimal billet in forging a front axle beam. The optimisation approach was implemented to minimise the billet mass, length of flash land, and flash radius through a set of FE simulations. In other words, the minimisation of volumes of flash and billet helped to reduce the overall forming load resulting in tool-life improvement [68].

A method that involved the minimisation of damage accumulation on the forming die was proposed for the workpiece design in hot forging gear annulus. A high local stress concentration found at the corner of the die cavity was selected as the damage accumulation, which was calculated in each simulation. The optimal workpiece design was modelled by different geometrical parameters, which were

combined with the specific damage mechanics approach to tool fracture as well as the analysis of the ductility of tool material. Consequently, the die life was prolonged significantly more than ten times [69].

As a summary, optimisation techniques associated with FE simulation had been used to design the billets, workpieces, and preforms subject to different process requirements. Nevertheless, the approach required iterative calculations of the forward simulation, and the resulting high computing time and cost constitutes. This might hinder their applications in engineering practices contributing to various bulk-forming problems request by the manufacturing industry such as warm-forming bimetallic components. Since the possible shapes of workpieces or preforms had to be predefined based on the limited configurations, which could be expressed by the restricted geometrical parameters or variables, the optimal workpiece shape could only be selected from among all simulation results after evaluation of forming quality and performance. The general procedures with optimisation approach for workpiece design are briefly outlined below. (i) The major geometrical variables or parameters were selected to define the workpiece shape or the die profile; (ii) The objective function (i.e., minimisation or maximisation) was properly formulated to evaluate the performance of optimisation; (iii) The shape of the trial workpiece was predefined based on the know geometrical constraints and/or preliminary results of FE simulation. Some criteria and iterative algorithms were necessary to ensure the new trial workpiece, which could converge to the optimal solution; (iv) Computer FE simulation software such as commercial software package or self-developed code was used to simulate

bulk-forming processes under the specified work conditions; (v) These steps were repeated to evaluate the quality of trial workpiece in each iteration until the desired workpiece shape, which could achieve the objective function was obtained.

2.8 Reverse simulation approach for workpiece design

The concept of the reverse simulation was derived from the idea of patently reversing the simulation flow by starting from the final shape of a formed component with the die moved inversely negative velocities. The corresponding boundary nodes between the workpiece elements and die surfaces were detached from the die gradually based on some reasonable rules or design criteria derived from natural deformation behaviours. After a number of iterated steps, the simulations predict an original billet or an initial preform while the component was unable to be formed in a single-stage forming process [24-26].

The plastic deformation normally caused by grain-boundary sliding or dislocation that was dependent on the previous stress-strain history, and thus the bulk forming was a load path-dependent process highly influenced by the stress-strain behaviour of formed materials. In other words, the bulk-forming process was not considered as strictly reversible in action. Appropriate treatments for modelling a reverse process, which should be close to the realistic forming practices and deformation behaviours, were therefore important for using the reverse simulation to predict the workpiece shapes. The studies in this area using different methodologies and approaches are discussed as follows.

2.8.1 Backward tracing method

The early reverse simulation approach used in bulk-forming process was the backward tracing method proposed in 1983. The first study was performed with the FEM to determine the preform shape of shell nosing [21,70]. The backward tracing method was an approach for resolving the geometry of the workpiece at individual backward increments from the final shape of the finished component. The design criteria of the searching algorithm gathered from the basis of deformation behaviours as well as empirical knowledge was imposed for controlling the boundary conditions and determining the trial perform for each step of the backward tracing process. The FE simulation was conducted repetitively dependent upon the perceived similarity between the shapes of the target formed component and the current component obtained by the traced trial preform was reached. This method was able to predict workpieces or their initial geometry if the boundary conditions could be specified at each time increment in the backward tracing method. Similar approaches were applied to several industrial applications or processes such as improvement of uniformity of strain distribution in a peripheral region of disk forging [71], determination of initial temperature distribution in thermo-viscoplastic deformation problem [72], optimal preform design in flashless forging two-dimensional airfoil section blade [73], flat front shape design in axisymmetric extrusion [74], and preform modification in net-shape forming of shell nosing products [75]. Extended development of the backward tracing method applied for a three-dimensional problem in the upsetting process was conducted [76]. These studies had shown that the backward tracing method was an

efficient preform design approach for the case of upsetting a rectangular block. Further investigation of this method should focus on the following aspects. (i) Reducing the computational time and cost due to numerous iterative FE simulations; (ii) Developing a more effective algorithm to identify the boundary conditions; (iii) Diversifying the application fields such as warm-forming bimetallic products or components.

2.8.2 Optimisations of target process variables

Optimisations of target process variables such as minimisation of strain rate difference aimed to predict the optimal shape of the workpiece that can improve the deformation uniformity and other technical or process requirements of the formed components by the reverse simulation approach. For example, the process criterion, which minimised the effective strain rate variation of the H-shaped plane strain and axisymmetric formed component was selected to formulate the algorithm for releasing the contact boundary areas from the inversely-moved die in the backward tracing procedures. The node with the lowest velocity among the workpiece elements was leading to the minimum influence on the material flow. It could be detached from the die surface in the increment of each reverse step [77]. Another study presented a similar application for the closed-die forging of a disk and a ball-joint socket. The modified algorithm of backward deformation optimisation was employed to search the reverse path between the initial and final shapes of the workpiece based on the minimum variation in accumulation plastic strain during the deformation of the workpiece in FE simulation [78]. The backward tracing method and the optimisation

approach for releasing the node of contact boundary were the core mechanisms to process the reverse simulation. However, the validity and accuracy of the predicted shapes of workpieces should be taken into consideration with the experimental verification, particularly for dealing with new materials or bimetals and complicated forming processes.

2.8.3 Fuzzy logic

Fuzzy logic was a cognitive problem-solving methodology, in which many electronic devices and software applications with embedded information processing, decision making, and fuzzy control were developed. This rule-based technology was able to represent knowledge and systematically process uncertainty and imprecision information by using the rules with approximate or subjective reasoning. The early study of fuzzy logic was conducted in the middle 1960s [79,80]. In traditional simple logic, an event such as “the student goes to school by bus”, must have the answer of true (yes) or false (no) only. However, most information and problems regarding the decision making might deal with uncertainties having different degrees regardless of precision and accuracy such as long, heavy, and bulky for describing a cargo. In this situation, the membership functions were required to model these dominant uncertainties of the input information, in which the degrees of goodness and correctness were evaluated like probability. For example, a simple membership function based on the weight of the cargo in tonnage to measure the degree of heaviness could be formulated as:

$$\text{Degrees of heaviness (weight)} = \begin{cases} 0 & : \quad \text{Weight} < 20 \\ \dfrac{\text{Weight} - 20}{10} & : \quad 20 \le \text{Weight} \le 40 \\ 1 & : \quad \text{Weight} > 40 \end{cases}$$

Another membership functions could be defined to measure the degree of other similar information such as length and capacity. Such a number of membership functions were then generated to evaluate the correctness of the different input information, in which the fuzzy rules and membership functions were generally established by the existing knowledge and expertise captured from literature, practical experiences, experimental and simulation results, etc.

The shape of a steel billet for the multi-stage axisymmetric H-section disk forging was optimised using fuzzy logic in conjunction with the backward tracing method. The input variables including the effective plastic strain deviation of the formed component as well as the distance of a boundary node from the symmetry plane, axisymmetric axis, or separation line, in which these variables were formulated the membership functions to determine the billet shape based on the fuzzy decision-making rules. These rules were also used to measure the node releasing priority to identify the updated contact boundary conditions at each step of backward increment. The presented billet-design method was able to deliver the formed component with a more uniform plastic strain distribution [81].

The fuzzy logic was an alternative method used with reverse simulation for searching the optimal workpiece shapes in the bulk-forming process. The process variables and the geometrical parameters expressing the degree of complexity

associate with the component shape were evaluated by the membership functions. The applicable fuzzy rules constructed according to the related design information and knowledge also played key roles in determining the output (i.e., the workpiece shape).

2.8.4 Change of contact time

In the forward simulation of bulk forming, the boundary condition was defined where a specific surface of the die would contact the workpiece, in which the contact time was identified and could be further modified based on the target process variables for the reverse simulation. This traced the inverse deformation path to achieve a more desirable shape of the initial billet or workpiece. By making use of this concept, the specific rules and guidelines were established based on the material flow attributes and different situations of die filling to change the contact time and sequence of the boundary conditions from forming a trial workpiece in the forward simulation. The new boundary conditions were found subsequently by applying this updated sequence in the reverse simulation [82,83]. It was significant that the trial workpiece design was needed in this procedure for recording the change in boundary conditions during the forward simulation, and it was also necessary to develop a scientific model for changing the recorded sequence of boundary conditions.

2.8.5 Reduction of shape complexity

The fulfilment of the geometrical requirements was one criterion of workpiece design and generally understood that the complete die filling or avoiding the under-filling problem would occur at the final step of the simulation (i.e., the end of the bulk-forming process). The function of shape complexity of the workpiece was basically related to the geometrical difference between the initial billet or workpiece and the final shape of the formed component, a smaller value of this function meant that the workpiece shape was simple and not like the finished component. In the forward simulation operation of most practical bulk-forming processes, the value would be increased after the material deformation. On the other hand, in the reverse simulation operation, the value would be decreased or minimised as the workpiece was being returned to the simple shape.

A workpiece design method applied this concept was proposed to carry out the FE simulation with the backward tracing method that defined a shape complexity factor of the workpiece design. Obviously, the cylindrical billet was the simplest shape having the smallest value of this factor. When the billet was deformed during the forward simulation, the value was increased accordingly. The specific technique for releasing die contact nodes in the sequence was employed, in which the detached node resulting in the minimum shape complexity factor would be released for each reverse step, this algorithm was repeated until a few nodes remained in contact. The workpieces predicted by this method were properly employed for forging an integrated blade and rotor turbine disk blank [23]. In addition, positive benefits in forming load

and deformation uniformity were realised. The reverse simulation approach using the concept of minimising shape complexity had great potential for further study and development. Likewise, high computational time and cost were again the shortcomings, which needed to be overcome for more industrial bulk-forming applications.

2.8.6 Upper bound element technique

The upper bound elemental technique (UBET) was proposed in the 1970's [84-87]. It mainly obtained upper bound solutions by dividing a workpiece into elementary and mostly regular regions for two-dimensional plane strain and axisymmetric forming problems. This technique provided a more efficient simulation for predicting an approximate material flow and required forming loads. The intensive application of UBET was associated with the reverse simulation approach to resolve design problems in axisymmetric forging. It was able to predict the forging loads, material flow, workpiece shape, and local die pressure. The surface profile of the workpiece was attained by the reverse of velocity vectors with the material flow toward the objective function as minimising the overall energy-dissipation rate. Unfortunately, there was no attempt to control the contact boundary conditions [88].

On the other hand, certain prescribed rules for controlling contact regions were used to define the boundary conditions for the UBET reverse simulation. The backward tracing method was also employed in the FE simulation to determine the inverse loading path in forging a connecting rod. This workpiece design procedure was

reliable could be used as a practical design technique, in which the predicted workpiece shapes were successfully verified by both forward simulations as well as physcial experiments [89].

The UBET-based reverse simulation could be used to predict workpiece in an early design stage due to its relatively high efficiency in terms of reduction of approximation. The validity of the predicted shapes of the workpiece at different forming stages could be examined by the forward simulation quickly and the physical work under the same process conditions eventually. The updated contact boundary conditions were defined for each particular trial of UBET-based during the reverse simulation process. Like the previously mentioned reverse simulation approach, this procedure needed to be repeated until the desired workpiece shape was achieved. An axisymmetric gear blank with the minimum flash was forged from a cylindrical billet, in which its shape was optimised using the FEM-UBET method [90].

A concept of simple comparison factor was proposed. It was used to quantify the shape complexities of the deformed workpieces, which were obtained from different contact boundary conditions by detecting nodes from the reverse die surface among all contact nodes. The smallest complexity factor representing the simplest workpiece shape (i.e. close to the billet shape) was selected as the deformed shape for the next step of reverse increment. The velocity field at the nodes was considered in this study with the tetrahedral elemental upper bound analysis, which was different from that on the element boundaries in the UBET [91]. Nevertheless, such a reverse simulation

approach was still time-consuming with limited computation resources because a large number of FE contact nodes were involved in the calculation.

The UBET based reverse simulation approach was relatively fast as it could provide an approximate shape of a workpiece for bulk forming design. The predicted shape could be verified by the forward simulation and experiment, and further modifications were made according to the results. The extensive study making use of the tetrahedral elemental upper-bound analysis was able to deal with the problems with more complex geometries with comparatively short computational time. On the other hand, as similar to the abovementioned reverse simulation approaches, a mathematical model, algorithm, or method was required to control the contact boundary conditions during the node detaching process.

2.8.7 Summary of reverse simulation approach

In a practical bulk-forming process or forward simulation, the deformation occurred after dies contacting with the workpiece and moving forward (or downwards). The determination of contact boundary conditions for the forward simulation operation could be performed directly according to the relative positions of the workpiece and die geometries. Nevertheless, this situation did not occur during the reverse simulations. Consequently, one of the major research directions of the reverse simulation was to establish an algorithm, which could define a desired reverse shape back to the simplest geometry of the initial billet or workpiece. The reduction of shape complexity was usually used in the algorithm to specify the detached nodes and

regions of the workpiece. Hence, the appropriate contact boundary conditions could be properly defined in the reverse simulation. In previous studies [23,77,82,83], the optimisation approach was consistently demonstrated to be applied in such an algorithm but high computing time was required by the large number of numerical iterations involved. In this situation, a more efficient workpiece-design system using the reverse simulation approach had to be developed. The following points should be considered. (i) An optimisation algorithm was used to iteratively modify or update the reversed shape that the variation between results in the reserve deformation and forward deformation at specific time steps could be minimised; (ii) The reverse simulation should enable to deal with more complicated formed components that were widely applied to general and industrial forming applications. (iii) The desired shape of workpiece needed to be determineded because it influenced the deformation in terms of design requirements such as a low shape complexity and reasonable shapes; (iv) A more effective strategy for defining contact boundary conditions at each reverse increment through the reverse procedures should be developed.

2.9 Problem identification

In the bulk-forming industry, the conventional billet or workpiece design was mainly based on the existing design experience and relevant knowledge from guidelines, literature, and handbooks. Such industrial approaches might be time-consuming or unsuitable when a new type of design or forming problem was encountered as there was no existing design knowledge.

The expert systems capturing the existing industry experience and valuable knowledge were capable of helping designers judge or design forming workpieces or preforms as well as process conditions. Unfortunately, these systems might only be effective in some typical or tailor-designed cases that the formed components could be classified by different types of predefined features.

The FEM based computer forward simulation could substitute the physical experimental trials to predict the deformation process and behaviours with different variables from the initial workpiece to the final shape of finished components. The simulation validated an existing empirical design, and the results provided guidelines for the modification of the design if the required forming quality was not achieved. The drawback was noticeably the expensive trial and error procedures yet better than practical experiments.

The optimal workpiece could be determined subject to specific requirements such as complete die filling and consistency of mechanical properties. Optimisation techniques could be combined with FE simulation to establish systematic design systems. The shape of the trial workpiece was modified gradually through the iterative optimisation process. The methods based on artificial intelligence techniques such as genetic algorithms and neural networks could be combined with the FE simulation for the workpiece design. The previous studies showed that these approaches were successful to assist in designing forming tools, and workpieces or preforms subject to some technical requirements such as complete die filling, and uniform stress and strain distributions. However, the lack of effective methods for representing geometrical

features of the formed components as well as spending a lot of time and cost on iterating the optimal results in FE simulation might not be an efficient approach for bulk-forming process design.

To conclude the literature review, the ordinary bulk-forming process design approach was based on the forward simulation. It might be inefficient and time-consuming, but they could provide analytical information on material flow and forming variables, which were beneficial for the process improvement. On the other hand, the reverse simulation approach had the potential to provide an even more efficient and effective way, in which the process started from the final shape of the finished component and ends with an initial workpiece. Comparing to the iterative optimisation used in the forward simulation, this design apporach did not require an initial geometry as the trial workpiece. Therefore, both time and cost for bulk-forming process design were reduced, if appropriate algorithms or modelling techniques could be implemented. In previous studies, the reverse simulation approach mainly made use of the backward tracing method associated with different techniques such as UBET, and fuzzy logic to control the contact boundary conditions during the node detaching process. It would be capable of dealing with the more complicated bulk-forming problems. As a consequence, it was believed that the reverse simulation approach after some modification had great potential toward the application for warm-forming process design of bimetallic components.

3. Theoretical Background

3.1 Fundamental of plasticity

The mechanics principles of plastic deformation mainly applied to metals and alloys are described by the plasticity, which is deduced from experimental studies of the stress and strain response under simple loading conditions. This theory assumes that the material is an ideal plastic body by ignoring the Bauschinger effect and the size effect. Also, it is valid only at temperatures where recovery, creep, and thermal effect can be neglected. The basic theory of classical plasticity is described by Hill [92], and also by some researchers [93-97]. In this chapter, determinations of stress and strain are introduced. The governing equations for plastic deformation and principles that are the foundations for the analysis are described. Finally, the process modelling of bulk-forming is outlined which involves the yield criterion, flow rule, incompressibility, and frictional boundary conditions.

The stress σ , strain ε, and strain-rate $\dot{\varepsilon}$ are the fundamental magnitudes that are employed to describe the deformation mechanics of a solid body that deforms from one shape/configuration to another under an external force. Although it is very difficult to describe the one-dimensional deformation with complete mathematical formulations, their determinations can be made on the case of a simple uniaxial tensile test. In the test, a dog-bone-shaped specimen has an initial length l_0 and an initial cross-sectional area A_0. This specimen is stretched in the axial direction by the force P to the length l and the cross-sectional area A at time t . The response of the material is

recorded as the load-displacement curve, and converted to the stress-strain curve. It is assumed that the deformation is homogeneous until necking occurs.

In the infinitesimal deformation theory, the stresses and strain-rates (or infinitesimal strains) are stated with respect to a fixed coordinate system in the material configuration at a time under consideration [70,98-100]. They are defined by:

$$\text{stress } \sigma = \frac{P}{A} \tag{3.1}$$

$$\text{strain rate } \dot{\varepsilon} = \frac{\dot{l}}{l} \tag{3.2}$$

$$\text{infinitesimal strain } d\varepsilon = \frac{dl}{l} \tag{3.3}$$

where the dot represents the time derivative. The stress defined in equation (3.1) is called true stress or Cauchy stress. The total amount of deformation is measured by integrating infinitesimal strain as:

$$\varepsilon = \int_{l_0}^{l} d\varepsilon = \ln\left(\frac{l}{l_0}\right) \tag{3.4}$$

and is called true, logarithmic, or natural strain [96].

In the Lagrangian description of finite deformation, the measures of stress, strain, and strain-rate are expressed as follows. Let the position of a mass point in the deformed configuration x at time be designated by:

$$x = \chi(X, t) \tag{3.5}$$

where X and t are the reference position of a mass point and time respectively. In the uniaxial tensile test, let X be directed along the longitudinal axis of the specimen. Then:

$$x = X + \left(\frac{l - l_0}{l_0} \right) X \tag{3.6}$$

Extension is defined as the displacement gradient relative to the reference position and is expressed by:

$$\frac{\partial \left(x - X \right)}{\partial X} = \frac{l - l_0}{l_0} = e \tag{3.7}$$

This is the engineering strain [7].

The Lagrangian strain component E_{11} is defined by:

$$E_{11} = \frac{1}{2}\left(\frac{\partial x}{\partial X}\frac{\partial x}{\partial X} - 1 \right) = \frac{1}{2}\left[\left(1 + e \right)^2 - 1 \right] = e + \frac{1}{2}e^2 \tag{3.8}$$

The strain-rate components are the time derivatives of strain components given by equations (3.7) and (3.8). They are:

$$\dot{e} = \frac{\dot{l}}{l_0} \tag{3.9}$$

and

$$\dot{E}_{11} = \frac{\partial x}{\partial X}\frac{\partial \dot{x}}{\partial X} = \left(1 + e \right)\dot{e} \tag{3.10}$$

since

$$\dot{x} = \left. \frac{\partial \chi}{\partial t} \right|_{X = \text{constant}} \tag{3.11}$$

The Piola-Kirchhoff stress tensor is defined as force intensity acting in the deformed configuration that measured per unit area of the reference configuration, while the Cauchy stress is defined as force per unit area in the deformed state. In the uniaxial tensile test, the engineering stress:

$$\sigma_{11} = \frac{P}{A_0} \tag{3.12}$$

corresponds to a component of the non-symmetric (or first) Piola-Kirchhoff stress tensor. Correspondence between stress and strain-rate measures is established such that the work rate per unit volume, W_0 in the reference configuration is the product of stress and strain rate. From equations (3.11) and (3.12),

$$\dot{W}_0 = \frac{P\dot{l}}{A_0 l_0} = \sigma_{11}\frac{\partial \dot{x}}{\partial X} = \frac{\sigma_{11}}{1+e}\dot{E}_{11} \tag{3.13}$$

Therefore, the stress measure corresponding to the Lagrangian strain rate $\dot{E}_{11}$ is:

$$s_{11} = \frac{\sigma_{11}}{1+e} \tag{3.14}$$

The stress given by equation (3.14) corresponds to a component of the symmetric (or second) Piola-Kirchhoff stress tensor [70,96,97].

Regarding the analysis of metal-forming processes, flow formulation complies with infinitesimal deformation theory, while solid formulation considers finite deformation.The strain-rate tensor [$\dot{\varepsilon}_{ij}$], where $i, j = x, y, z$ is symmetric and the tensor components are given as:

$$\dot{\varepsilon}_x = \frac{\partial u_x}{\partial x} \tag{3.15}$$

$$\dot{\varepsilon}_y = \frac{\partial u_y}{\partial y} \tag{3.16}$$

$$\dot{\varepsilon}_z = \frac{\partial u_z}{\partial z} \tag{3.17}$$

$$\dot{\varepsilon}_{xy} = \frac{1}{2}\left(\frac{\partial u_x}{\partial y} + \frac{\partial u_y}{\partial x}\right) = \frac{\dot{\gamma}_{xy}}{2} \tag{3.18}$$

$$\dot{\varepsilon}_{yz} = \frac{1}{2}\left(\frac{\partial u_y}{\partial z} + \frac{\partial u_z}{\partial y}\right) = \frac{\dot{\gamma}_{yz}}{2} \tag{3.19}$$

$$\dot{\varepsilon}_{zx} = \frac{1}{2}\left(\frac{\partial u_z}{\partial x} + \frac{\partial u_x}{\partial z}\right) = \frac{\dot{\gamma}_{zx}}{2} \tag{3.20}$$

where u_i and $\dot{\gamma}_{ij}$ are velocity and shear strain rate components respectively. Using suffix notation, equations (3.15) to (3.20) can be expressed as:

$$\dot{\varepsilon}_{ij} = \frac{1}{2}\left(u_{i,j} + u_{j,i}\right) \tag{3.21}$$

where a comma denotes differentiation with respect to the subsequent coordinates.

The Cauchy stress tensor [σ_{ij}], where i, j = 1, 2, 3 or x, y, z is also symmetric and is defined by the nine components as:

$$[\sigma_{ij}] = \begin{bmatrix} \sigma_{11} & \sigma_{21} & \sigma_{31} \\ \sigma_{12} & \sigma_{22} & \sigma_{32} \\ \sigma_{13} & \sigma_{23} & \sigma_{33} \end{bmatrix} = \begin{bmatrix} \sigma_x & \tau_{yx} & \tau_{zx} \\ \tau_{xy} & \sigma_y & \tau_{zy} \\ \tau_{xz} & \tau_{yz} & \sigma_z \end{bmatrix} \tag{3.22}$$

The stress may also be specified by the three principal components, or by the three tensor invariants. The principal stresses σ_1, σ_2, σ_3 are the roots of the cubic equation:

$$\sigma^3 - I_1\sigma^2 - I_2\sigma - I_3 = 0 \tag{3.23}$$

where I_1, I_2, and I_3 are quantities independent of the direction of the coordinate axes and called the three invariants of stress tensor σ_{ij}. They are given by the relations:

$$I_1 = \sigma_x + \sigma_y + \sigma_z = \sigma_1 + \sigma_2 + \sigma_3 \tag{3.24}$$

$$I_2 = -\left(\sigma_x\sigma_y + \sigma_y\sigma_z + \sigma_z\sigma_x\right) + \tau_{xy}^{\,2} + \tau_{yz}^{\,2} + \tau_{zx}^{\,2} = -\left(\sigma_1\sigma_2 + \sigma_2\sigma_3 + \sigma_3\sigma_1\right) \tag{3.25}$$

$$I_3 = \sigma_x\sigma_y\sigma_z + 2\tau_{xy}\tau_{yz}\tau_{zx} - \sigma_x\tau_{yz}^{\,2} - \sigma_y\tau_{zx}^{\,2} - \sigma_y\tau_{xy}^{\,2} = \sigma_1\sigma_2\sigma_3 \tag{3.26}$$

The first (linear) and second (quadratic) invariants have particular physical meanings for the theory of plasticity [70].

3.2 Yield criteria

The yield criterion represents the limit of elasticity under any possible combinations of stresses. It is expressed by:

$$f\left(\sigma_{ij}\right) = F \text{ (constant)} \tag{3.27}$$

A function of stresses $f\left(\sigma_{ij}\right)$ is called yield condition. Any proposed yield criterion must be verified by experiment to check its suitability.

For isotropic materials, plastic yield is only related to the magnitude of the three principal stresses and not their directions. Then any yield criterion can be expressed in the following form:

$$f\left(I_1, I_2, I_3\right) = F \tag{3.28}$$

This the experimental fact that the yielding of a material is to a first approximation, not affected by a moderate hydrostatic pressure, or tension, it follows that yielding depends on the principal components σ_1', σ_2', σ_3' of the deviatoric stress tensor:

$$\sigma_{ij}' = \sigma_{ij} - \delta_{ij}\sigma_p \tag{3.29}$$

where

$$\sigma_p = \frac{1}{3}\left(\sigma_1 + \sigma_2 + \sigma_3\right) \tag{3.30}$$

is the hydrostatic component of the stress, and $\delta_{ij} = 1$ for $i = j$ and $\delta_{ij} = 0$ for $i \neq j$ is the Kronecker delta. The principal components of the deviatoric stress tensor are dependent, since $\sigma_1' + \sigma_2' + \sigma_3'$ is identically zero.

The yield criterion then reduces to the form:

$$f\left(J_2, J_3\right) = F \tag{3.31}$$

where

$$J_2 = -\left(\sigma_1'\sigma_2' + \sigma_2'\sigma_3' + \sigma_3'\sigma_1'\right) \tag{3.32}$$

$$J_3 = \sigma_1'\sigma_2'\sigma_3 \tag{3.33}$$

Two simple criteria have been in extensive use for the analysis of metal deformation. Tresca criterion (shear stress criterion) given in 1864 is:

$$\sigma_1 - \sigma_3 = \text{constant} \tag{3.34}$$

with $\sigma_1 \geq \sigma_2 \geq \sigma_3$. It may alternatively be written in the form of equation (3.31) in terms of J_2 and J_3, but the results are complicated and not useful.

Another criterion was proposed by Huber in 1904 [95], by von Mises in 1913 [96], and by Maxwell in a letter to his friend Thomson (or called Kelvin) in 1856 [97]. It has been traditionally called the von Mises criterion or the Huber-Mises criterion. This is also the yield criterion mainly used in this study. The criterion states that yielding occurs when J_2 reaches a critical value. In other words, the yield function of equation (3.31) does not involve J_3. It can be written in the alternative forms:

$$J_2 = \frac{1}{2}\left(\sigma_1'^2 + \sigma_2'^2 + \sigma_3'^2\right) = \frac{1}{2}\sigma_{ij}'\sigma_{ij}' = k^2 \tag{3.35}$$

or

$$\left(\sigma_1 - \sigma_2\right)^2 + \left(\sigma_2 - \sigma_3\right)^2 + \left(\sigma_3 - \sigma_1\right)^2 = 6k^2 \tag{3.36}$$

or

$$\left(\sigma_x - \sigma_y\right)^2 + \left(\sigma_y - \sigma_z\right)^2 + \left(\sigma_z - \sigma_x\right)^2 + 6\left(\tau_{xy}^2 + \tau_{yz}^2 + \tau_{zx}^2\right) = 6k^2 \tag{3.37}$$

where k is a parameter regulating the stress scale and depending on the material property. In the suffix notation used in equation (3.35), a recurring letter suffix indicates that the sum must be formed of all terms obtainable by assigning to the suffix the values x, y, z (or 1, 2, 3).

The constant in both yield criteria may be determined from simple states, such as in uniaxial tensile test. At yielding in simple tension, $\sigma_1 = Y$ (yield strength of

material) and $\sigma_2 = \sigma_3 = 0$. As a consequence, equations (3.34) and (3.36) may be written as:

$$\sigma_1 - \sigma_3 = Y \tag{3.38}$$

and

$$(\sigma_1 - \sigma_2)^2 + (\sigma_2 - \sigma_3)^2 + (\sigma_3 - \sigma_1)^2 = 2Y^2 \tag{3.39}$$

respectively. Parameter k in equations (3.35) to (3.37) can be identified as the shear yield stress by considering yielding in simple shear:

$$k = \frac{Y}{\sqrt{3}} \tag{3.40}$$

according to the von Mises criterion.

It should be noted that the yield criteria defined by equation (3.39) must depend on the previous process of plastic deformation (i.e., strain hardening). If it is assumed that the hardening occurs, only plastic work is done. Then it assumes yield criterion is independent of the hydrostatic component implies that there is no volume change during plastic deformation.

The stress state is completely determined by the values of the three principal components. Then any stress state may be represented by a vector in a three-dimensional stress space, where the principal stresses are taken as Cartesian coordinates. Figure 3.1 is a geometrical representation of a plastic state of stress in $(\sigma_1, \sigma_2, \sigma_3)$ space. $\overrightarrow{OS}$ is the vector $(\sigma_1, \sigma_2, \sigma_3)$ and its component $\overrightarrow{OP}$ is the vector representing the deviatoric stress $(\sigma_1', \sigma_2', \sigma_3')$. $\overrightarrow{OP}$ always lies in the plane π whose

equation is $\sigma_1+\sigma_2+\sigma_3=0$. The hydrostatic component $(\sigma_m,\sigma_m,\sigma_m)$ of the stress is represented by $\overrightarrow{PS}$, which is perpendicular to the plane π. A yield criterion, which is independent of the hydrostatic component of stress, is represented by a locus c in the plane π. The yield locus corresponding to the shear stress criterion is a regular hexagon, while it is obvious from the relation in equation (3.35) that the locus of the distortion energy criterion is a circle of radius $\sqrt{2}k$ or $\sqrt{2/3}Y$. By selecting the values of the constant in equation (3.34) and k in equation (3.36), according to equation (3.39), the two criteria can be made to agree with each other and with experiments of uniaxial tensile test. Their loci are illustrated in Fig. 3.2.

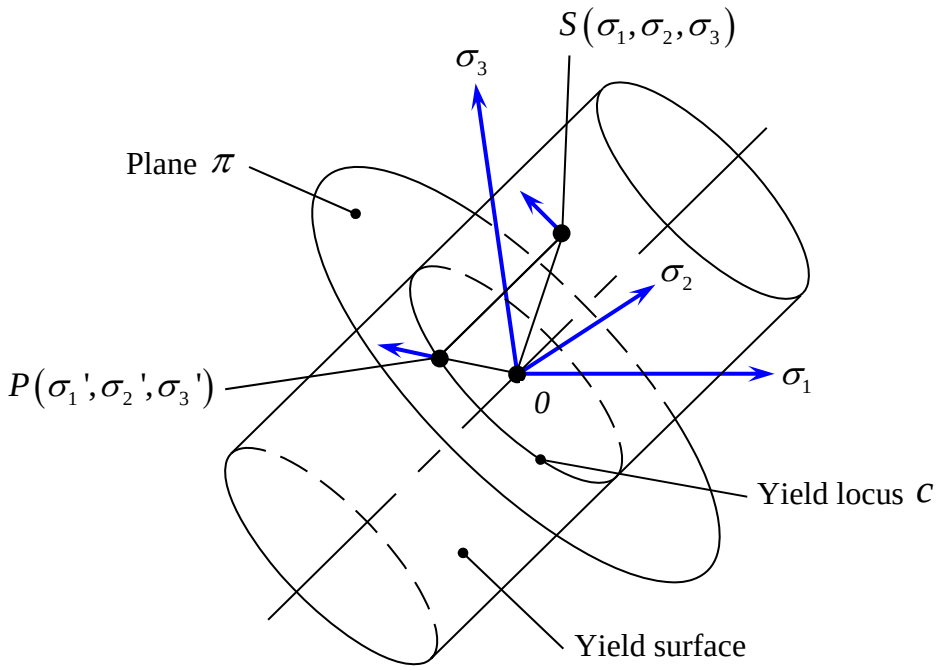

Fig. 3.1 A geometrical representation of a plastic state of stress in $(\sigma_1,\sigma_2,\sigma_3)$ space.

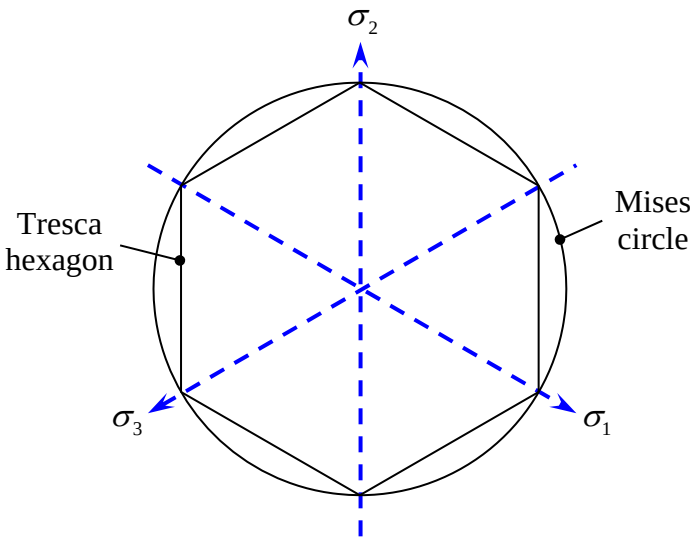

Fig. 3.2 Yield loci on the plane π for distortion energy criterion and maximum shear stress criterion.

3.3 Plastic deformation in bulk forming

The process modelling of bulk forming requires analytical knowledge regarding material flow, heat transfer as well as process details related to friction, heating and cooling of material, and characteristics of forming equipment. The purpose of modelling a bulk-forming process is to investigate the mechanics of plastic deformation processes without spending on costly experiments. Besides, the following major objectives are taken into account.

- The kinematic relationships such as the shape, velocities, strain-rates, and strains between the undeformed stage (i.e., billet, blank, or preform) and the deformed stage (i.e., final product) should be established so that the material flow during the forming process can be predicted. This objective includes the temperatures

and heat transfer prediction, since these variables greatly influence local metal-flow states.

- The formability or workability determines whether the shape of workpiece is possible to be deformed without causing any surface or internal defects (i.e., cracks or folds) during the forming operation.
- The stresses, the forces, and the energy required to achieve the forming operation should be predicted. This information is necessary for tool design and for suitable equipment selection, with adequate forming force and energy capabilities, to perform the forming operation.

Therefore the process modelling of bulk forming provides the means for determining how the material flows, how the desired geometry can be obtained by plastic deformation, and what the expected mechanical properties of the formed components are.

For understanding the variables of a bulk-forming process, it should consider the process as a system, as illustrated in Fig. 2.1 as well as the interaction of significant variables in bulk forming are shown in Fig. 2.2 in Chapter 2. Obviously, for a given billet or preform material and part geometry, the deformation speed influences strain-rate and flow stress. Deformation speed, die temperature , and part geometry influence the temperature distribution in the formed component. Finally, flow stress, friction, and workpiece geometry determine material flow, forming load, and forming energy.

3.3.1 General assumption of process conditions

This is the fact that the real process of bulk-forming is very complicated. In order to achieve a meaningful mathematical description of material deformation, several simplified but reasonable assumptions of process conditions should be made. The bulk-forming operation is designed to achieve the desired process conditions which control the material behaviour of workpiece. The process variables include the geometry of both workpiece and tools, the speed of tools, the lubrication conditions between the workpiece and tools, and the temperature of both workpiece and tools. With the intention of making appropriate assumptions for modelling a bulk-forming process, it is important to understand which variables are significant to influence the process critically.

The tool velocity can affect the strain rate, operating time and heat transfer. A bulk-forming operation under different strain-rate conditions, which may result from using different forming machines (or presses), and hence different forming loads and energy are required. For instance, the maximum load in a drop hammer process, which is a high strain rate process, may be lower than that of a hydraulic press. The phenomenon is different from the result of material tests (i.e., compression tests or tensile tests), which show that a higher load is required at a higher strain-rate condition. This is caused by different heat transfer conditions in these two cases. In the hydraulic press operation, the ram speed is slow and the flash area cools more obviously. On the other hand, the temperature of workpiece remains nearly no changes in the drop hammer process because the operation time as well as the contact time are very short

[5,8,70]. Therefore, while the deformed workpiece has been removed from the dies, the tool temperature can decrease for a considerable period of time until the next operation is performed.

The temperature involves the operation temperature and heat generation of deformed material. The initial temperatures of the workpiece and tools may be established according to the process design. Besides plastic deformation generates heat which remains in the deformed material or flows into dies, atmosphere or un-deformed material. The temperature may increase several hundred degrees in some forming stages, such as drawing and extrusion, which are processed at a high speed (i.e., a higher strain rate). This generated temperature modifies the constitutive relation (relationship between stress and strain) for the workpiece. Therefore it should be a significant factor in determining the maximum deformation speed that can be used to produce good-quality formed components without excessive tool damage. It also affects the lubrication condition and hence tool life [70]. The main factors influencing the magnitude and distribution of the temperature include the workpiece and tool temperatures, the heat generation due to the plastic deformation, the friction and the heat transfer between the workpiece, tools and environment.

The lubrication is highly related to the friction effects between the workpiece and die interface. In the bulk-forming process, the applied force is transferred from the dies to the workpiece. Therefore, the friction conditions at the workpiece-die interface influence the formation of surface stresses acting on the interface and hence the material flow. Additionally friction can generate heat that changes the distributions of

temperature and conclusively affect the material behaviour as well as forming load and energy. Indeed appropriate lubricants for particular forming applications should be used that can control the frictional conditions. In general the lubricant is applied simply to prevent sticking and reduce the sliding friction and thus prolong the tool life.

It is noticeable from above. The appropriate assumptions of the bulk-forming process conditions are important and should be taken into account according to the characteristics of the process. In this study, the assumptions are made as follows:

- The elastic deformation is neglected since its amount is extremely small compared with the plastic deformation in bulk-forming process.
- The deforming material is regarded as a continuum (i.e., the bimetal is two continua). Metallurgical aspects such as grains, grain boundaries, and dislocations are not considered.
- Uniaxial compression test data are correlated with flow stress in multi-axial deformation conditions.
- Anisotropy and Bauschinger effects are disregard.
- The volume of material remains constant.
- The temperature effects are not taken into account (i.e., isothermal warm-forming conditions) in which the temperature is well controlled and its effects are small on the specimen materials.
- The velocity of die is constant that mean the process is mainly applied with using the hydraulic press.

- The tools are rigid body since the deformation of tools compared with that of workpiece is negligible.
- Friction exists at tool-workpiece interface.

3.3.2 Flow formulation for modelling material behaviour

The bulk forming is a large plastic deformation problem which can commonly be solved by two kinds of formulation, i.e., solid formulation and flow formulation [70]. The solid formulation considers the behaviour of the material as a classical elastic-plastic solid [101,102]. The formulation can predict a complete stress-strain history which is thus useful for the analysis of residual stress. Nevertheless, this formulation has the limitation to the magnitude of strain and rotation increments, which may make the method rather expensive in computation. When analysing warm-forming process, elastic strain of a workpiece is negligible since it is usually very small compared to plastic strain. By neglecting elastic strain, a deforming material can be treated as a nearly fluid to simplify the formulation. It is then possible to relate the stress σ to the strain rate $\dot{\varepsilon}$ in the following general form.

$$\sigma = C\dot{\varepsilon} \tag{3.41}$$

where the quantity C may be dependent on the effective strain $\bar{\varepsilon}$, the strain rate $\dot{\varepsilon}$ and temperature T. That means:

$$C = f\left(\bar{\varepsilon}, \dot{\varepsilon}, T\right) \tag{3.42}$$

The formulation based on the above simplification is known as a flow formulation [103]. It can provide useful information with lower computing costs than the solid formulation. However, the stress distribution of flow formulation is only determined by current strain-rate distribution at identical time increment. The solution is not affected by the previous stress state. Therefore, it is not able predict the complete stress-strain history for the analysis of residual stress. Fortunately some improvements have been made to flow formulation to deal with residual stress [104] whereas the solid formulation has also been improved so that it can deal with large strain increments [102].

Theoretically, the plastic deformation can be defined as follows:

a. Constitutive equations – these equations describe the relationship between stress and strain during plastic deformation.

$$\dot{\varepsilon}_{ij} = \frac{3}{2}\frac{\dot{\bar{\varepsilon}}}{\bar{\sigma}}\sigma_{ij}' \tag{3.43}$$

b. Yield criterion – the criterion is a function of the stress tensor, which predicts a stress state required for plastic deformation. The von Mises criterion is used in this study.

c. Equilibrium equations – the stress along the boundary surface S is in equilibrium, if the body force is negligible.

$$\sigma_{ij,i} = 0 \tag{3.44}$$

d. Compatibility equations – these equations, which are relationships between displacements and strains, maintain the continuum requirement without fracture or crack formation.

$$\dot{\varepsilon}_{ij} = \frac{1}{2}\left(u_{i,j} + u_{j,i}\right) \tag{3.45}$$

e. Boundary conditions – surface tractions, displacements (or velocities) and temperature distribution are the main boundary conditions in the bulk-forming.

$$\sigma_{ij} n_j = t_i \text{ on } S_F \tag{3.46}$$

$$v_i = v_i^0 \text{ on } S_u \tag{3.47}$$

where $\dot{\varepsilon}_{ij}$ and σ_{ij} are the components of the strain-rate tensor and deviatoric stress tensor, respectively. $\bar{\dot{\varepsilon}}$ and $\bar{\sigma}$ are the effective strain rate and effective stress, respectively. n_j is the unit normal to the corresponding surface, $\dot{\varepsilon}_V$ is the volumetric strain rate, and a comma means partial differentiation. It is supposed that a body of volume V is bounded by a surface S with the traction t_i prescribed on a part of the surface S_F and the velocity v_i prescribed on a part of the surface S_u. The body is composed of a rigid-plastic material which obeys the von Mises yield criterion and its associated flow rule. If the inertia effects and body forces area assumed to be absent, then the actual stress σ_{ij}, and velocity field $\mathbf{v}$ satisfy the above conditions.

In flow formulation, the relationship between stress and strain (or strain rate) is represented by a flow rule which is associated with a yield criterion. These definitions

and the virtual work principle are used to construct the weak form formulation, which describes the system in terms of energy, for modelling the bulk-forming process.

3.4 Flow rule associated with von Mises yield criterion

As mentioned in previous section, to analyze the bulk-forming process, it is necessary to develop a yield criterion and a flow rule. The yield criterion in terms of mathematical relationships predicts when the plastic deformation (i.e., the yield occurs). The flow rule a relationship of stress and strain during plastic deformation, describes how and where the material will flow.

Two criteria that are commonly used for the yielding prediction are Tresca (maximum shear stress) criterion and von Mises criterion. In flow formulation, it is assumed that the normality principle is fulfilled. Some singularity points may be encountered by using Tresca criterion, and hence require special treatment in any generalised formulation. On the other hand, von Mises criterion can be easily applied to the analysis and prediction of yielding for most engineering metals with sufficient accuracy [105]. Therefore, the von Mises criterion is commonly used in flow formulation for modelling the bulk-forming process. The derivation of equations can be found in Section 3.2.

The flow rule is a kinematic assumption for plastic deformation/flow. It gives the ratio or relative magnitude of the components of the plastic strain increment tensor $d\varepsilon_{ij}$. An alternative expression of plastic strain increment is in terms of strain rates

$\dot{\varepsilon}_{ij}$. The increment $\dot{\varepsilon}_{ij}$ may be represented by a vector with nine components in a strain space. The flow rule therefore also defines the direction of the plastic strain increment vector $\dot{\varepsilon}_{ij}$ in the strain space. The plastic flow equations representing increments of strain related to stress are written in the form:

$$\varepsilon_{ij} = p\frac{\partial G}{\partial \sigma_{ij}} \tag{3.48}$$

where

$$G = G\left(\sigma_{ij}, \varepsilon_{ij}\right) \tag{3.49}$$

is a plastic potential function and p is a proportional positive scalar factor, which is nonzero only when plastic deformation occurs. The simplest case of defining the plastic potential function assumes that the plastic potential and the yield function F coincide (i.e., $G = F$). Therefore,

$$\varepsilon_{ij} = p\frac{\partial F}{\partial \sigma_{ij}} \tag{3.50}$$

Equation (3.50) is called the correlation flow rule because the plastic flow is related to the yield criterion.

For an isotropic material, the yield function F in equation (3.50) can be defined by von Mines yield criterion.

$$F = J_2 - k^2 \tag{3.51}$$

Evaluating the derivative in equation (3.50) gives:

$$\frac{\partial F}{\partial \sigma_{ij}} = \frac{\partial}{\partial \sigma_{ij}} J_2 = \frac{\partial}{\sigma_{ij}}\left(\frac{1}{2}\sigma_{ij}'\sigma_{ij}'\right) = \sigma_{ij}' \tag{3.52}$$

Using equations (3.50) and (3.52), the flow rule is written as:

$$\dot{\varepsilon}_{ij} = p\sigma_{ij}' \tag{3.53}$$

For a von Mises material model, the effective stress $\bar{\sigma}$ is shown as:

$$\bar{\sigma} = \sqrt{3J_2} = \sqrt{\frac{3}{2}\sigma_{ij}'\sigma_{ij}'} \tag{3.54}$$

and the effective strain rate $\dot{\bar{\varepsilon}}$ is expressed as:

$$\dot{\bar{\varepsilon}} = \sqrt{\frac{2}{3}\dot{\varepsilon}_{ij}\dot{\varepsilon}_{ij}} \tag{3.55}$$

Using equations (3.53), (3.54) and (3.55) obtains the scalar p:

$$p = \frac{3}{2}\frac{\dot{\bar{\varepsilon}}}{\bar{\sigma}} \tag{3.56}$$

Thus,

$$\sigma_{ij}' = \frac{2}{3}\frac{\bar{\sigma}}{\dot{\bar{\varepsilon}}}\dot{\varepsilon}_{ij} \tag{3.57}$$

which is the Levy-Mises equation, and it is similar to equation (3.43).

For a rigid-perfectly plastic material, the elective stress is expressed in the form:

$$\bar{\sigma} = Y = \text{constant} \tag{3.58}$$

Consequently, the flow rule associated with von Mises yield criterion defines the relationship between the deviatoric stress and strain rate for the rigid perfectly plastic material as:

$$\sigma_{ij}' = \frac{2}{3}\frac{Y}{\dot{\bar{\varepsilon}}}\dot{\varepsilon}_{ij} \tag{3.59}$$

In this study, the workpiece is assumed to be a rigid-perfectly plastic material (i.e., there is no elasticity and no work hardening or softening). This is a reasonable approximation for most formable materials at warm and high temperatures [106]. In terms of the deviatoric stress σ_{ij}', the power of plastic deformation is written as

$$\int_V \left(\sigma_{ij}' + \delta_{ij}\sigma_V\right)\dot{\varepsilon}_{ij}\,dV \tag{3.60}$$

and due to the incompressibility $\dot{\varepsilon}_{ii} = 0$,

$$\delta_{ij}\sigma_V\dot{\varepsilon}_{ij} = \sigma_V\dot{\varepsilon}_{ii} = 0 \tag{3.61}$$

Using the equation (3.59), flow rule associated with von Mises yield criterion, the power of plastic deformation for rigid-perfectly plastic material becomes:

$$\int_V \frac{2}{3}\frac{Y}{\dot{\bar{\varepsilon}}}\dot{\varepsilon}_{ij}\dot{\varepsilon}_{ij}\,dV \tag{3.62}$$

Substituting the effective strain rate, equation (3.55) into the power of plastic deformation gives:

$$\int_V \sqrt{\frac{2}{3}}Y\sqrt{\dot{\varepsilon}_{ij}\dot{\varepsilon}_{ij}}\,dV \tag{3.63}$$

Therefore, the problem of modelling plastic deformation is written as follows:

$$\text{minimise} \qquad \int_V \sqrt{\frac{2}{3}}Y\sqrt{\dot{\varepsilon}_{ij}\dot{\varepsilon}_{ij}}\,dV \tag{3.64}$$

subject to: incompressibility, and

boundary conditions of velocity

3.5 Incompressibility

A kinematically admissible velocity field that satisfies the compatibility equations should also meet the incompressibility requirement (i.e., the volumetric strain rate equals zero, $\dot{\varepsilon}_V = 0$). This requirement has been added into the model as a constraint which ensures that the minimum energy dissipation is only dependent on internal shear deformation if friction effects are not taken into account. Two methods, the Lagrange multiplier, and the penalty method, are most frequently used to deal with the incompressibility constraint in minimization problems.

3.5.1 Lagrange multiplier

Consider a function $\int_\Omega f(x)dx$ that is to be minimised subject to a constraint condition, $g(x) = 0$, which is differential in domain Ω. The Lagrange multiplier method defines a function M to be $M(x) = \int_\Omega \left[f(x) + \lambda g(x) \right] dx$, where λ is a new variable called the Lagrange multiplier. The variables, x and λ, are then solved by equations, $\partial M / \partial x = 0$, and $\partial M / \partial \lambda = 0$, to find the minimum value. It can be seen that the total number of unknowns has increased when using the Lagrange multiplier [103,107].

3.5.2 Penalty method

For the same example of minimization problem, $\int_\Omega f(x)dx$ and the constraint $g(x) = 0$. The penalty method defines a function $I(x) = \int_\Omega \left\{ f(x) + \alpha \left[g(x) \right]^2 \right\} dx$,

where α is a large positive real number [103,108]. In order to minimise the function $I(x)$, it is necessary to ensure $\int_{\Omega}\left[g(x)\right]^2 dx$ is close to zero as a is a large positive number. This can only be true if $g(x)=0$ is close to zero everywhere in the domain II, this almost satisfies the constraint g(z) = 0. However, if α is small, the constraint cannot be satisfied. On the other hand, if α is too large, numerical errors may increase. Therefore, it is necessary to use an appropriate α value. The value is determined by experience.

Due to the drawback of increasing unknown variables by using the Lagrange multiplier method, the penalty method is used to deal with the incompressibility requirement in this study. The penalty method is then transferred into:

$$\text{minimise } \int_V \sqrt{\frac{2}{3}} Y \sqrt{\dot{\varepsilon}_{ij}\dot{\varepsilon}_{ij}}\, dV + \int_V \alpha\left(\dot{\varepsilon}_{kk}\right)^2 dV \tag{3.65}$$

subject to: boundary conditions of velocity

where the penalty constant a may be interpreted as a constant to the bulk modulus [94] because the mean stress σ_m is related to the volumetric strain rate $\dot{\varepsilon}_V$ by:

$$\sigma_p \cong \alpha \dot{\varepsilon}_V \tag{3.66}$$

3.6 Frictional boundary conditions

The material flow, surface of the formed component, internal defects, pressure applied on the dies, as well as the load and energy requirements are greatly affected by the friction between the workpiece and dies. Therefore it is necessary to take the

friction effects into consideration in the analysis model in terms of a quantitative friction factor. Work done by friction may then be expressed by a rate form:

$$\int_{S_f} \tau_i^f \dot{u}_i^\tau dS \tag{3.67}$$

where $\dot{u}_i^\tau$ is the relative velocity vector used to reflect that the shear friction stress τ_i^f should be in the opposite direction to the relative motion between the workpiece and dies. S_f is expressed as the contact surface.

The most common form of friction law is known as Coulomb's law, $F_f = \mu F_n$, where F_f is the friction force and F_n is the normal force. The form may be expressed in a stress field by $f_s = \mu\sigma_n$ in which f_s and σ_n are friction stress and the normal stress, respectively. μ is called the friction coefficient. This law is generally found applicable at low contact pressures compared to material strength before a great deal of deformation occurs. However, in the bulk-forming process contact pressures are generally high. The Coulomb's law may drastically overestimate the friction [109]. Due to the yielding process, the tangential stress required to induce slip which causes deformations is dependent on the shear strength of the material. Moreover, the friction at the interface cannot exceed the shear strength, and velocities are the variables used to model plastic deformation. A model, Tresca friction model (or shear friction model) [104 in terms of the yield shear stress k and the relative velocity vector $\dot{u}_i^\tau$; is used to reflect the shear friction stress τ_i^f in the form:

$$\tau_i^f = mk \frac{\dot{u}_i^r}{\left\| \dot{u}_i^r \right\|} \tag{3.68}$$

Where m is a friction factor between 0 and 1 to represent a fraction of the yield shear stress, and $k = Y/\sqrt{3}$ (equation 3.40) since Tresca yield stress is involved. In order to obtain the m, a ring compression test should be used.

Finally, the problem of modelling plastic deformation involving friction effects can be stated as:

$$\text{minimise } \int_V \sqrt{\frac{2}{3}} Y \sqrt{\dot{\varepsilon}_{ij}\dot{\varepsilon}_{ij}}\, dV + \int_V \alpha \left(\dot{\varepsilon}_{kk}\right)^2 dV + \int_{S_f} \tau_i^f \dot{u}_i^\tau dS \qquad (3.69)$$

subject to: boundary conditions of velocity, and constraints of shear contact friction

where the constraints of shear contact friction enforce the relative velocity vector $\dot{u}_i^\tau$, in the tangential direction at the frictional interfaces.

4. Reverse Simulation Approach

4.1 Overall review

During the past fifteen years, many researchers had implemented innovative ideas about reverse simulation for various bulk-forming applications [24,25,110-113], especially for the prediction of the original shapes of workpieces and preforms. Although their results clearly demonstrated that the predicted shapes could be tested in a forward simulation and the trend of the deformation and the estimated forming loads were similar to those of the reverse simulation, most approaches were limited in their abilities to incorporate domain knowledge for specific bulk-forming problems. For example, Chang et al. [24,25] made use of reverse simulation to predict an initial rectangular billet section for a two-dimensional plane-strain forging problem. Its approach could find a deformation path, which always led towards a simple distribution from the final forging geometry to an initial billet, such that a rectangle was set as the target shape of the initial billet, and the main focus was to determine the difference between the deformed shape and a rectangle using the second moments of the area about the x-axis, and y-axis, which was the criterion for measuring how the material spread over the orthogonal axes of the shape from its centroid. In other words, the nearly rectangular billet could be obtained with the closest value of the second moments of the area to the value of the deformed workpiece. This work was sound and ingenious, but only applicable for particular simple plane-strain forging problems. Some versatile, but relatively complicated component geometry such as hollow shapes

(i.e., the component with a center hole) might create difficulty in applying this method to trace the natural and reasonable deformation path, since independent deformation occurred near the center region. Also, the concave-shape problem of reverse shape, as shown in Fig. 4.1, was not taken into account, which would cause the defects of internal folding or/and buckling. In this case, significant improvement or modification would be beneficial for further development.

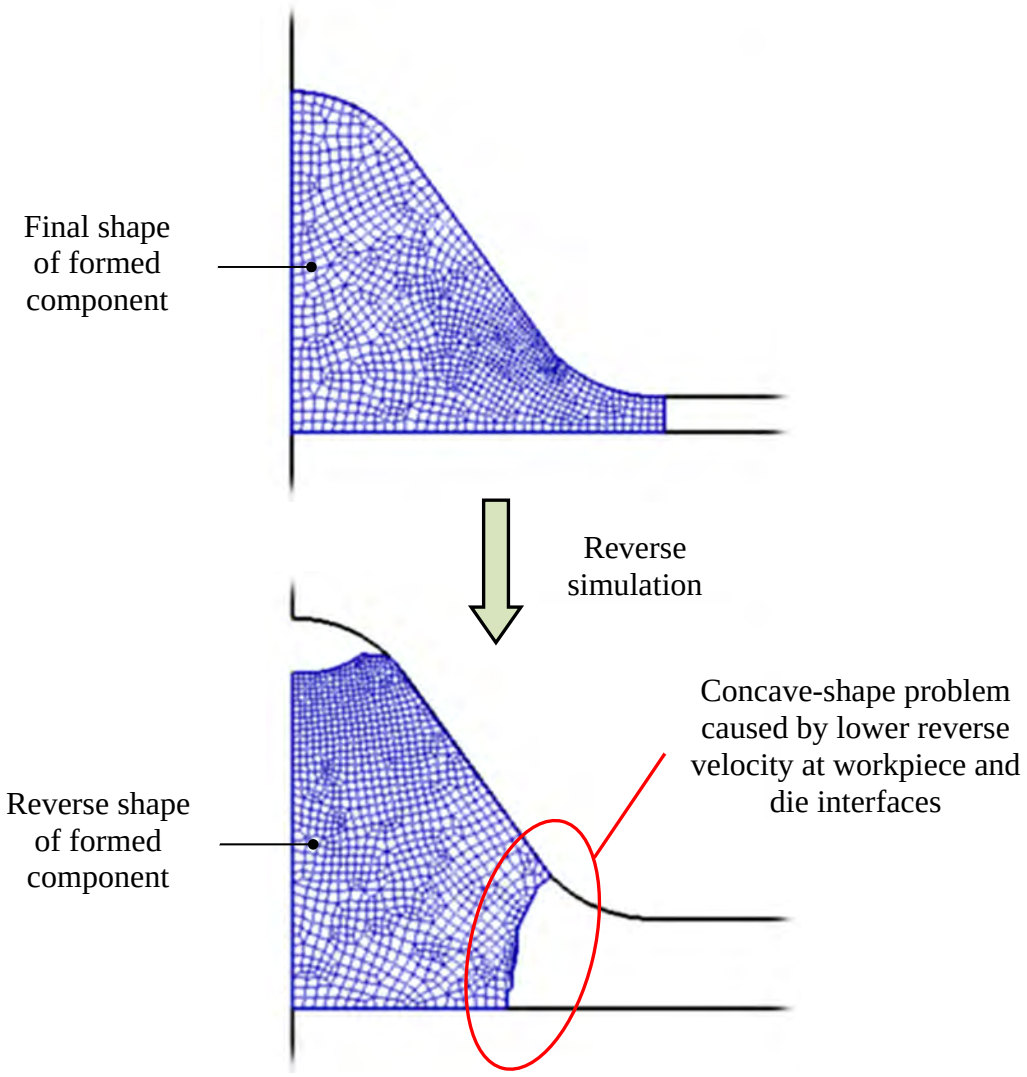

Fig. 4.1 The concave-shape problem was found in former reverse simulation.

Zhao et al. [112] used the inverse die contact tracking method to design the preform shapes for a representative plane-strain cross section of the track link blocker forging, in order to reduce the scrap material lost as flash. A candidate preform was employed to establish a record of the boundary-condition time sequence through forward simulation into the final forge shape. This recorded time sequence was then modified according to the material flow characteristics and the state of die filling that satisfied the requirement of material utilization and forging quality. The modified boundary condition sequence was applied to control die node separation during the reverse deformation, and therefore the blocker preform shape from the buster dies could be obtained by the section analysis. There was a great improvement in terms of die filling, flash size, strain variance, frictional power, and die load. Perhaps the proposed techniques were only able to improve the preform shape in the specific forging problem, as the candidate preform was required. Therefore, a more effective and direct approach should be developed to enhance the industrial viability and reliability of reverse simulation.

The overall reverse simulation approach of this study is shown in Fig. 4.2. This emerged from a number of physical rules and practical experiences regarding the bulk-forming process, which are incorporated into the backward tracing method introduced by Part et al. [21] for starting the reverse deformation step, and several adaptive strategies proposed by Chang et al. [24,25] for determining contact boundary conditions. In deducing the methods and techniques for significantly modifying the former reverse simulation, the following empirical and physical rules are applied:

- Nearly same outer profiles or cross sections of workpiece and final component.
- Compensation of material for incomplete die filling.
- Elimination for excessive material flowing into improper regions of die cavity.
- Assumption of constant volume of non-porous solid metal.
- Convex expansion of lateral deformation surface.
- Material flowing with a higher velocity at the lowest resistant region of die cavity.

By combining both the former reverse simulation procedures [21,24,25] and original developed methods and techniques throughout the workpiece and preform design of bulk forming, the improved reverse simulation approach should be able:

- To predict the initial hollow billet or workpiece shapes with minimal height for bulk-forming hollow axisymmetric components.
- To reconstruct the abnormal reverse shape, with such concave and inwards deformation surfaces.
- To further extend for the applications of warm forming bimetallic components, in which a new method regarding the interface frictions for determining the sliding and sticking conditions between two dissimilar metals will be conceived.

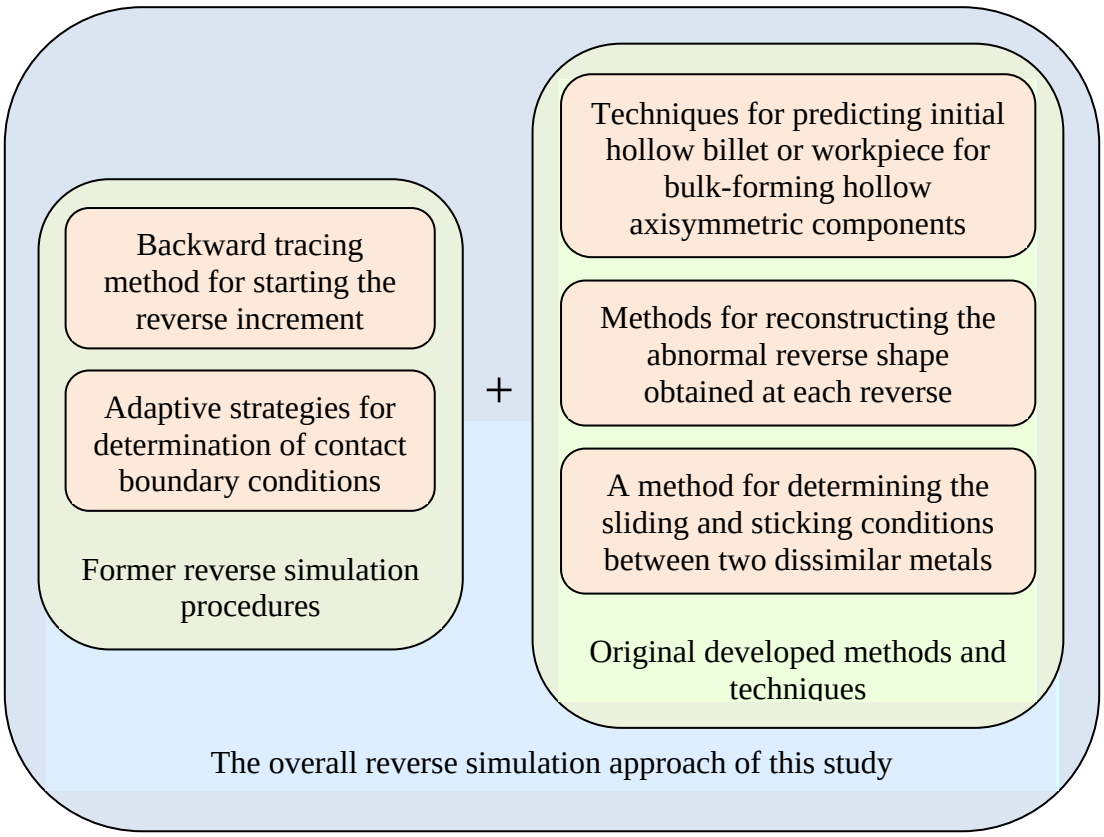

Fig. 4.2 The overall reverse simulation approach of this study.

4.2 Basic concept of reverse simulation

Reverse simulation is made use of as an effective approach to predict workpiece (i.e., billet or preform) shapes in the bulk-forming process [21-26,110-113]. It arises from the idea of simply reversing flow simulation by starting from the final shape of the formed component with the die velocity reversed. Once the boundary contact surfaces are being released as the die is moved backwards, the formed component reverts its original shape. Figure 4.3 illustrates the idea for predicting billet and preform shapes using the reverse simulation approach. If the component cannot be formed by one single stage, the predicted shape will act as the preform of the previous

stage, which is then used to predict further preform or billet shapes. It is important to remark that this idea can also be applied for the warm-forming process design of bimetallic components.

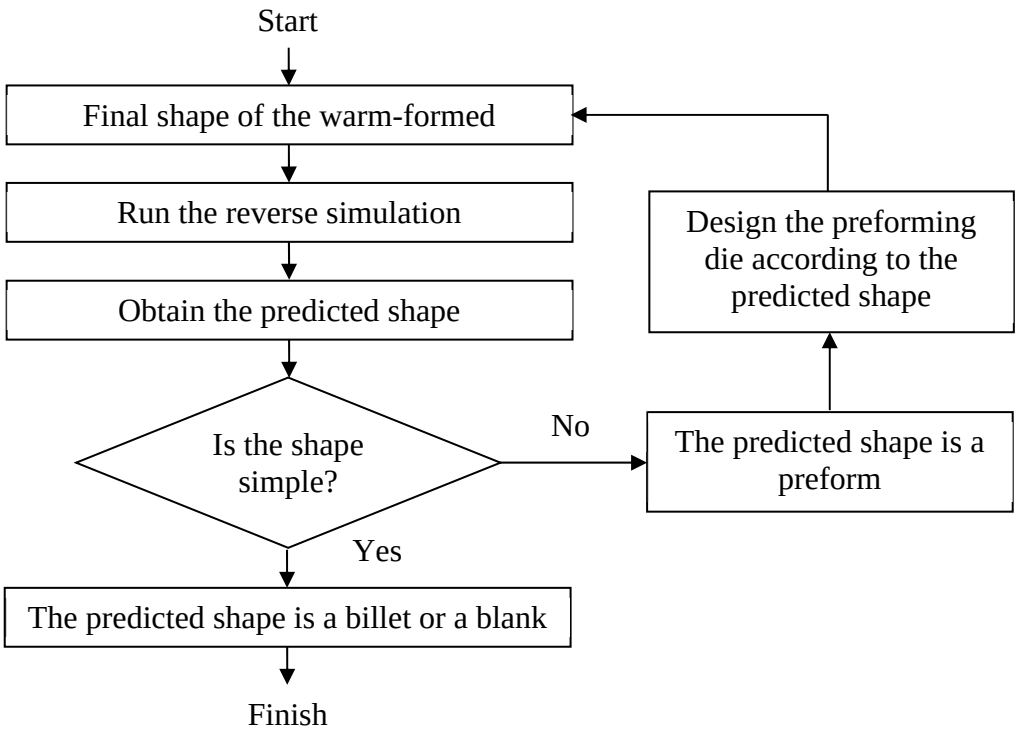

Fig. 4.3 The workflow of the reverse simulation approach in predicting the shapes of billets and preforms.

In accordance with the generally accepted behaviour of the material flow in the bulk-forming process, the deformation of the workpiece depends on the previous loading history due to the strain-hardening effect. This means that the process may not be reversible strictly. This is because the actual distributions of stress and strain of the finished product, as well as the field of temperature, are not able to be identified readily. Therefore, it is necessary to model the reversible bulk-forming process, which should

be as close as possible to the realistic behaviour of deformation, even for bimetals, by reasonably assuming the operation conditions and material characteristics as follows:

- The die velocity remains constant during the bulk-forming process whether it is upwards or downwards. This can be expressed as the die moves along the axial motion of the conventional hydraulic press.
- The bulk-forming process is performed under isothermal conditions so that the effects of temperature change on the workpiece and the heat transfer between the die and formed material are not taken into account. This assumption can be applied to most bulk-forming operations in which the working temperature is well controlled, like warm-forming bimetallic components, or the die velocity is fast enough to overcome the die-chilling effects, especially for warm forming small and intricate parts such as watch cases and buckles.
- The die is defined as a rigid body and not deformable. In the real situation, the deformation of the tool, generally elastic deformation compared with the plastic deformation of the workpiece, is extremely small or negligible. This is physically reasonable for most bulk-forming processes.
- The near-net shape forming process is worked as the closed-die forming process with less flash against the flashless forming. A few surplus materials have to be extruded into the flash gap at the end of the forming stroke. In other words, the flow of material can start from the flash regions at the beginning of the reverse simulation.

- The specimen material is rigid-perfectly plastic and thus the elastic recovery does not take place after the deformation. This means that the material has no elastic deformation but suddenly begins to deform plastically when the yield criterion is satisfied. Both strain hardening and softening are disregarded also. This is appropriate for most metals and alloys such as stainless steel and aluminium alloy worked at their warm or hot conditions.
- The specimen material is isotropic, homogeneous, and incompressible. This simplification of material conditions is easily justified since there is no effective way to verify such identity attributes and their effects are not significant in the bulk-forming processes.
- The extrinsic lateral surface of deformed specimen material is convex. This phenomenon is often regarded as the friction, which exists between the contact surfaces of the workpiece and die.

In traditional forward simulation, the conditions of contact vary continuously according to the deforming workpiece as well as the die profiles. They are used to determine the boundary conditions, which are able to provide a desired shape in the bulk-forming process. Nevertheless, this situation does not occur in the reverse simulation, in which the contact surfaces of the workpiece are being detached from the die during the process. Thus, a methodology of defining the desired shape for reverse simulation is necessary and then the contact boundary conditions can be determined. In this study, the primary aim is to find the simplest shape of the billet (e.g., a block, or a cylindrical bar) or the preform (e.g., a flat blank with identical cross-section over

its entire height) as the original workpiece by using the reverse simulation. An approach of controlling the material flow and distribution is proposed that can determine the reverse shape effectively at each time incremental step. Based on a number of empirical and physical rules governing the typical bulk-forming process, it is required to set a desired shape and to reduce the shape complexity of the workpiece for the ongoing process. The desired shape is then used to identify a contact region to be released from a die surface and therefore the boundary conditions can be established.

In order to assess and demonstrate the feasibility of the proposed idea for the warm-forming process design, several empirical and physical rules will be employed to control the material flow and volumetric distribution in three two-dimensional axisymmetric forming case studies, warm forming bimetallic component being one among them. The solid and hollow cylindrical billets with the closest volumetric distribution to the workpiece geometry are selected as the desired shape in the reverse simulation for each incremental change. Possible boundary conditions are then determined by releasing the contact regions, which are finite-element nodes detached from the die surfaces according to the desired shape (i.e., the cylindrical billet). The procedure is iterated until all contact regions are released from the die surfaces. If the predicted shape is very close to a cylindrical billet, the dimensions of the initial workpiece (i.e., diameter and height) can be identified readily. When the predicted shape is still complicated, a preform is required, which is treated as the starting shape to run another stage of reverse simulation until a simple shape close to a cylindrical billet is obtained, as shown in Fig. 4.4.

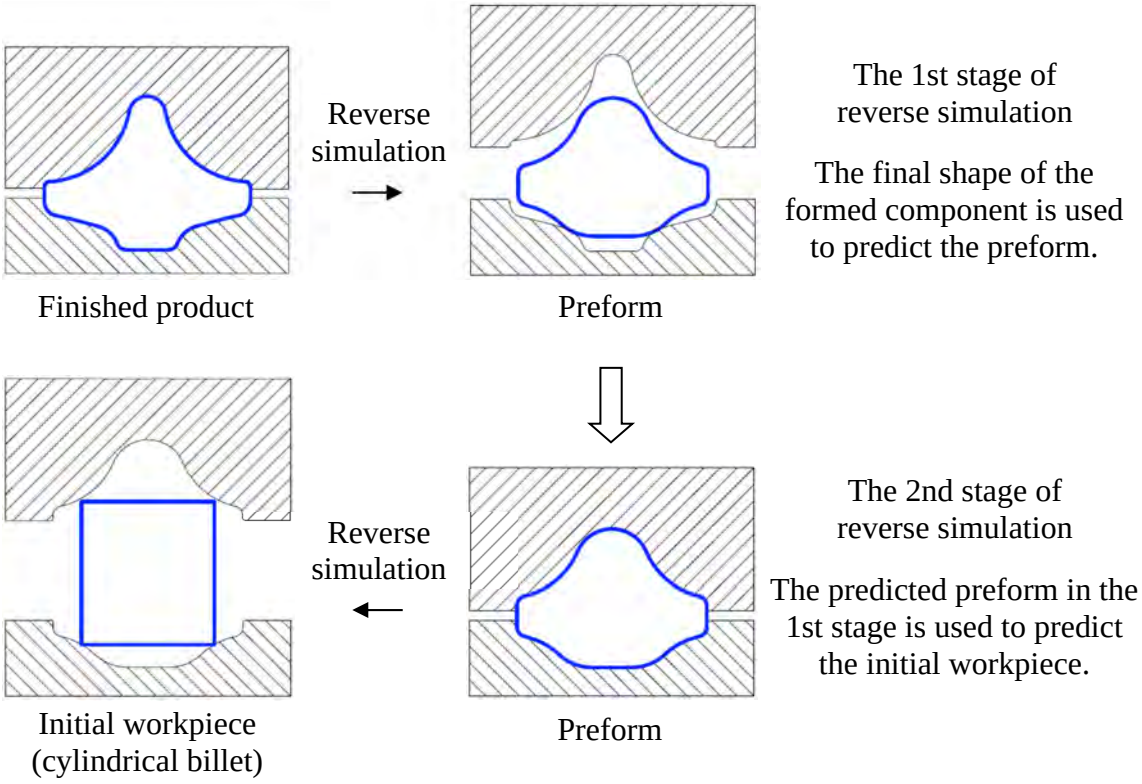

Fig. 4.4 The reverse simulation is carried on provided that the predicted shape is not as simple as a cylindrical billet [24,25].

4.3 Backward tracing method

In the real case, excluding the geometric designs, the deformation of the workpiece in bulk-forming process is highly dependent on its loading (or stress and strain) history, material properties, and working conditions which can influence the contact boundary to the die and further determine the material flow. However these three factors may interact with each other and they cannot be fully considered before the finished product is formed. In other words, the stress, strain, and temperature distributions on the workpiece cannot be identified properly at the last stage of the forming process. Only the final shape of the formed component can be defined.

Therefore, the modelling of the bulk-forming process in reverse construction needs some assumptions that treat the process as the loading independent (i.e., the material is rigid-perfectly plastic without strain hardening or softening) under the isothermal conditions. The finite-element simulation and the backward tracing method can then be used as a solution for reversing the bulk-forming process.

The rigid-perfectly plastic model is taken up to describe the workpiece material in the finite-element simulation. Both strain hardening and softening effects are neglected in the model. Also, all deformed regions of the workpiece have the same stress value, which is a constant obtained by physical experiments. The solution is not being affected by the magnitude of the flow stress. Thus, the process is independent of stress and strain state which defines loading history. This is nearly compatible as most hot or warm forming processes for particular materials such as stainless steel and aluminium alloy in real situations.

The reverse simulation incorporated with finite-element techniques can be considered for the situation of deformation including the coordinates, velocity fields, and displacements of nodes at each particular time incremental step. However, the geometrical configuration of the workpiece and the contact-boundary conditions vary during the entire forming process. As a consequence, the process is still influenced by these factors and loading. The backward tracing method can be implemented to overcome this problem since it allows tracing back the deformed shape step by step as a route followed by the velocity fields of nodes and forward loading. This method was proposed by Part et al. [21] in 1983 and it refers to the prediction of the workpiece

configuration at any stage in a deformation process, while the final shape of the formed component and process conditions (e.g., die velocity, working temperature, and friction factor) are given. The principal concept of the method is illustrated in Fig. 4.5.

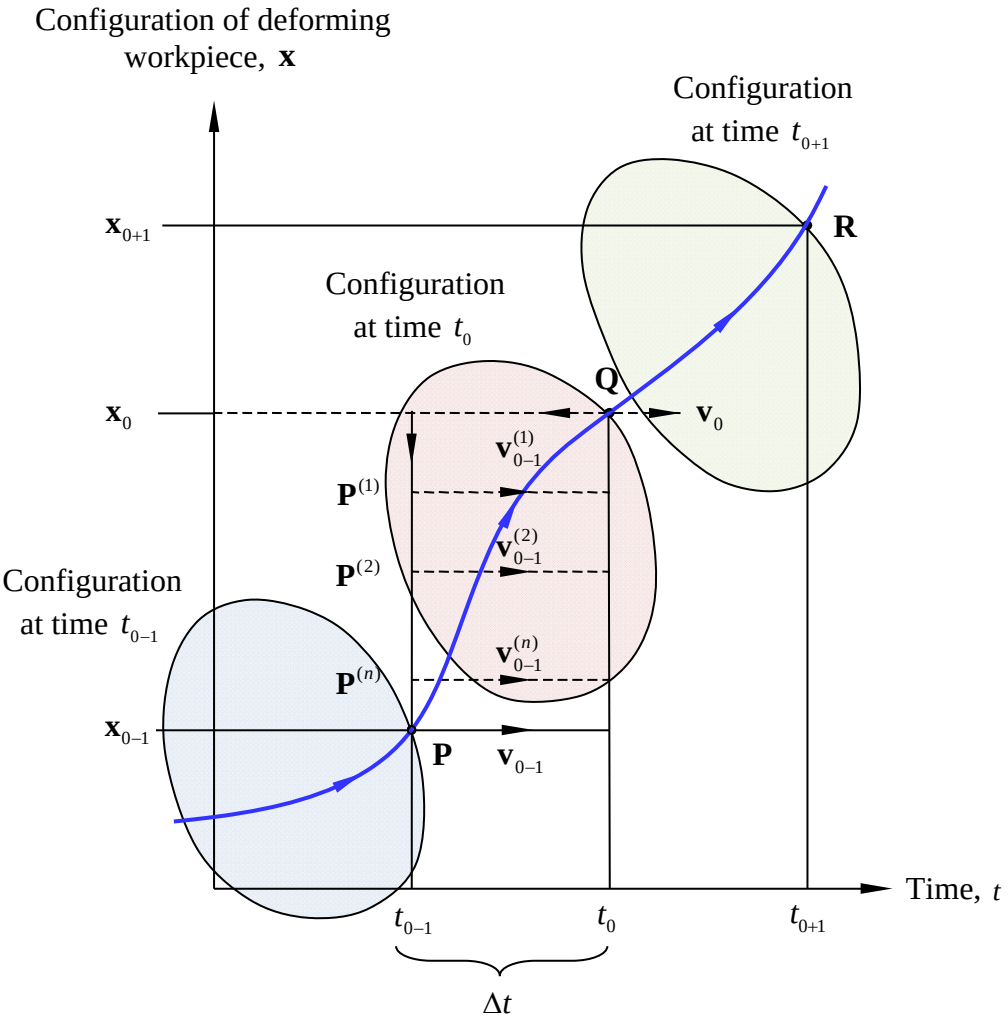

Fig. 4.5 The concept of backward tracing method and update of the geometrical configuration during forward loading and backward tracing [21].

At the time $t = t_0$, the geometrical configuration $\mathbf{x}_0$ of a deforming workpiece is represented by a point **Q**. During the forward simulation, the point **Q** is arrived by moving from point **P**, whose configuration is given as $\mathbf{x}_{0-1}$ at time $t = t_{0-1}$ through

the velocity field $\mathbf{v}_{0-1}$ during a time increment $\Delta t = t_0 - t_{0-1}$, and thus the expression of the configuration $\mathbf{x}_0$ at time $t = t_0$ is:

$$\mathbf{x}_0 = \mathbf{x}_{0-1} + \mathbf{v}_{0-1}\Delta t \tag{4.1}$$

Therefore the problem of the reverse simulation is to determine the velocity field $\mathbf{v}_{0-1}$ based on the known information on $\mathbf{x}_0$ at point **Q**. The essentiality of the backward tracing method is to take the forward simulation at point **Q** so that the velocity filed $\mathbf{v}_0$ is obtained. The first estimate of $\mathbf{P}^{(1)}$ can be made according to:

$$\mathbf{P}^{(1)} = \mathbf{x}_0 - \mathbf{v}_0\Delta t \tag{4.2}$$

This reverses the configuration of **Q** by using the negative velocity field $-\mathbf{v}_0$. Then the next velocity field $\mathbf{v}_{0-1}^{(1)}$ can be calculated by the forward simulation based on the $\mathbf{P}^{(1)}$ and used to form $\mathbf{Q}^{(1)}$ by:

$$\mathbf{Q}^{(1)} = \mathbf{P}^{(1)} + \mathbf{v}_{0-1}^{(1)}\Delta t \tag{4.3}$$

If the $\mathbf{Q}^{(1)}$ is not sufficiently close to the original $\mathbf{Q}$, then $\mathbf{P}^{(2)}$ can be estimated by:

$$\mathbf{P}^{(2)} = \mathbf{x}_0 + \mathbf{v}_{0-1}^{(1)}\Delta t \tag{4.4}$$

The solution for velocity field at $\mathbf{P}^{(2)}$ is then $\mathbf{v}_{0-1}^{(2)}$ and the second estimate of configuration $\mathbf{Q}^{(2)}$ can be obtained by:

$$\mathbf{Q}^{(2)} = \mathbf{P}^{(2)} + \mathbf{v}_{0-1}^{(2)}\Delta t \tag{4.5}$$

The iteration is carried on till:

$$\mathbf{Q}^{(n)} = \mathbf{P}^{(n)} + \mathbf{v}_{0-1}^{(n)}\Delta t \tag{4.6}$$

Becomes sufficiently closed to the original $\mathbf{Q}$. The criterion for terminating the iteration can be made by:

$$\left|\mathbf{x}_0 - \mathbf{x}_0^{(n)}\right| \leq e_l \tag{4.7}$$

Where e_l is the limit of the difference and is generally set to 5 x 10^{-3}, and $\mathbf{x}_0^{(n)}$, which represents the geometrical configuration of $\mathbf{Q}^{(n)}$. Finally, the configuration of reverse deformation can be defined by the point $\mathbf{P}^{(n)}$. Figure 4.6 is a flow chart that describes the backward tracing procedure systematically. If the boundary conditions can be defined at time t_{0-1}, the $\mathbf{v}_{0-1}^{(n)}$ will be acquired based on equation (4.6). Repeated calculations of the solutions for times t_{0-2}, t_{0-3}, … will lead to a backward tracing of the entire deformation process.

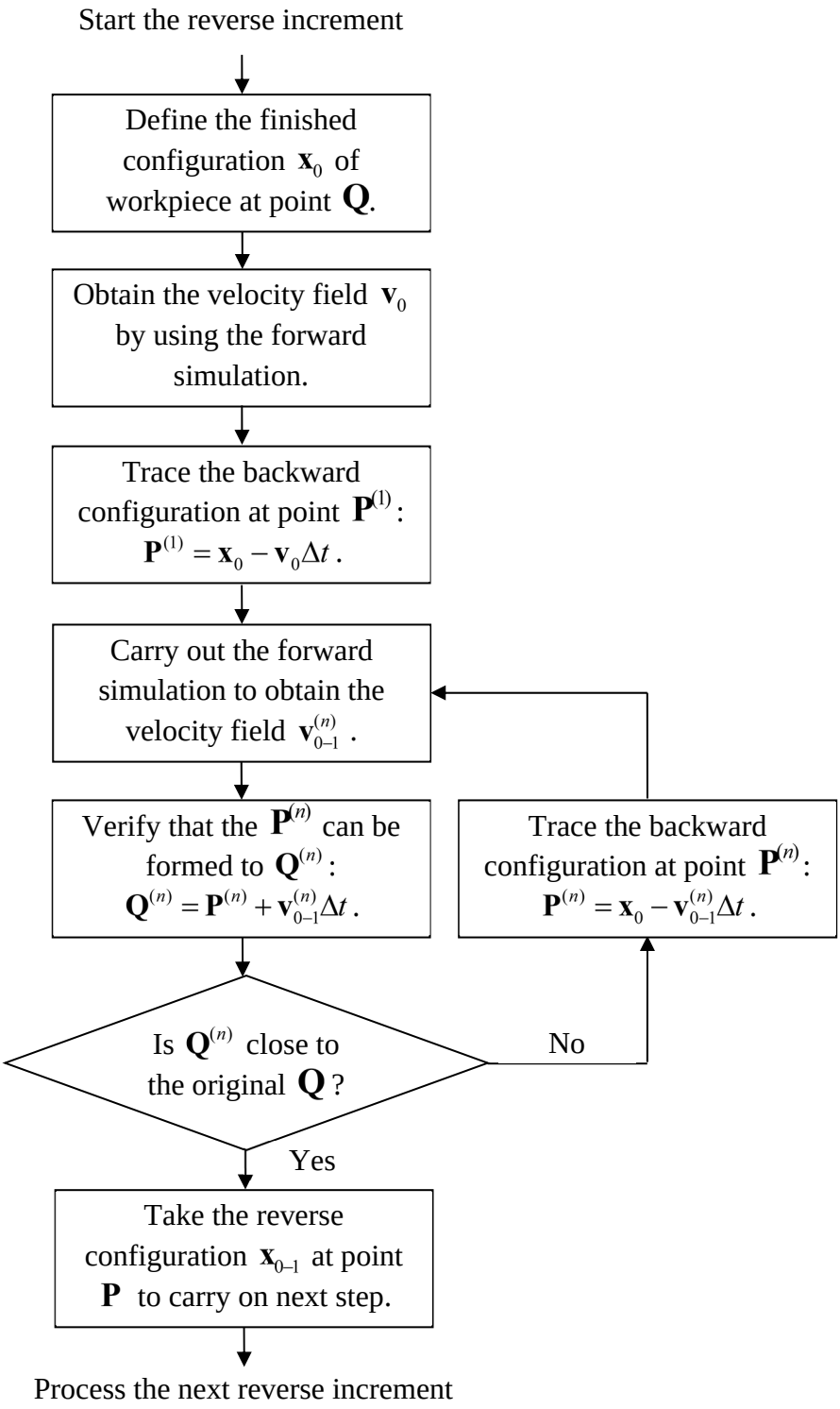

Fig. 4.6 The flow chart for the backward tracing procedure implemented into the finite-element deformation analysis [21].

The formulation of the above backward tracing concept will be incorporated further with the techniques to determine contact boundary conditions. It should be noted that the boundary conditions affect the solutions of the velocity field $\mathbf{v}_{0-1}^{(n)}$ greatly and subsequently to the point $\mathbf{P}^{(n)}$. This is due to the fact that there are infinite numbers of deformation paths from the points $\mathbf{P}$ to $\mathbf{Q}$, which broadly represent the bulk-forming process from a simple shape to its final shape. Figure 4.7 illustrates that two different shapes of preforms with various contact boundary conditions can also be transformed into the same final shape through the complete die filling. It is noted that the application of forward simulation and the backward tracing method become straightforward if the change of the boundary conditions during the process can be determined. In many cases, the change of the boundary conditions during loading depends upon the preform shape itself. Therefore, the method to determine the contact boundary conditions is so important to control a backward deformation that aims towards a simple geometrical configuration of the workpiece in the reverse simulation.

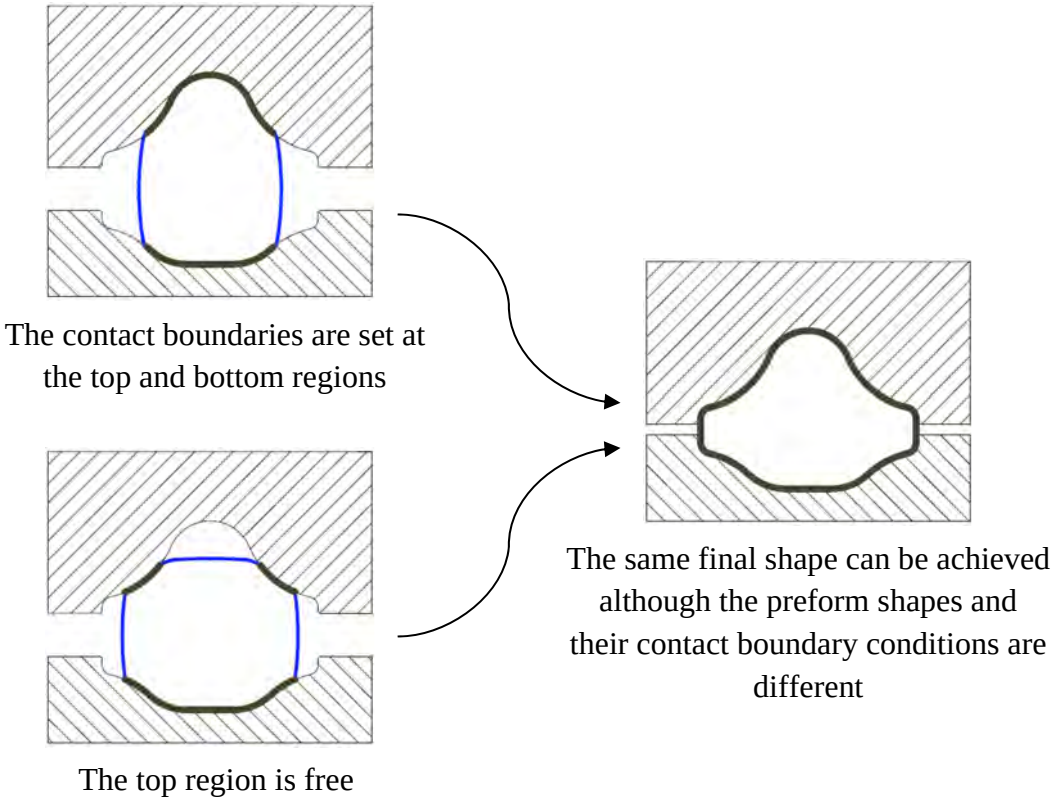

Fig. 4.7 Two different shapes of workpiece with various contact boundary conditions can form the same geometrical configuration of finished product.

In this study, some of the ideas proposed by Chang et al. [24,25] and several sets of empirical and physical rules governing the bulk-forming process were used to determine the contact boundary conditions as the most rational solution, so as to control the reverse geometry of the deformed workpiece. The effects of metallurgical response and phenomena such as strain hardening, strain-rate sensitivity, dynamic recovery, and temperature softening were disregarded. With the implementation of the backward tracing method, it is possible to predict the deformation path of the workpiece in a reverse direction effectively if the boundary conditions are all known.

The location of the dies and the geometrical configuration of the workpiece during the forward simulation can be used to determine the contact boundary conditions. In other words, the die profiles have to construct a preferred preform shape for bounding the material flow to form a final shape of the finished product. The following section gives the basis for defining this desired shape in the reverse simulation in order to determine the contact boundary conditions rationally. Therefore, the material flow and strain distribution of deforming workpiece are able to be controlled in the reverse condition to revert the original simple shape which is an initial cylindrical billet or a preform.

4.4 Determination of contact boundary conditions

The desired shape can be defined as the final destination of the deformation in both forward and reverse simulations. In forward simulation the desired shape is exactly the geometrical configuration of the finished product (i.e., the final shape), which should be used to examine whether a selected billet or a designed preform achieves the requirement or not for complete die filling without any forming defects. In the contrast, the reverse simulation process starts from a complete die filling condition to predict possible preforms or a billet without knowing the desired shape. It is thus necessary to develop strategies for defining the desired shape in the reverse simulation. Since the performs, especially the billet, should have the universal geometrical characteristics of simple material distribution as well as shape such as a block or a cylindrical bar compared to the final shape of the product, the desired shape

defined can be based on reducing the complexity of the material distribution. This interpretation is reasonable as previous mentioned in the primary aim of reverse the simulation, which is to find the simplest billet or preform shapes for being the workpiece.

An axisymmetric closed-die forming process, shown in Fig. 4.8, has been used to illustrate how a desired shape is defined for reverse simulation. In this figure, the deformed shape “C” is the preform of the final shape “D”, and it also represents a reverse deformation. Figure 4.9 compares these two interrelated shapes by overlapping them together. Some contact regions of the final shape “D” have been located at the outside profile of desired preform shape “C”. If these outside regions of the shape “D” (i.e., regions “a”, “b”, and “c”) are released to determine new contact boundary conditions for a reverse increment of the simulation, it should result in a shape which is close to shape “C”. Thus, the reverse simulation is able to achieve the goal that the workpiece reverts towards a simple shape (i.e., to reduce the complexity of shape “D”). On the other hand, releasing the inside regions “d” and “e” tends to increase the complexity of shape “D”. This should be improper to predict a shape close to the exact reverse shape “C”.

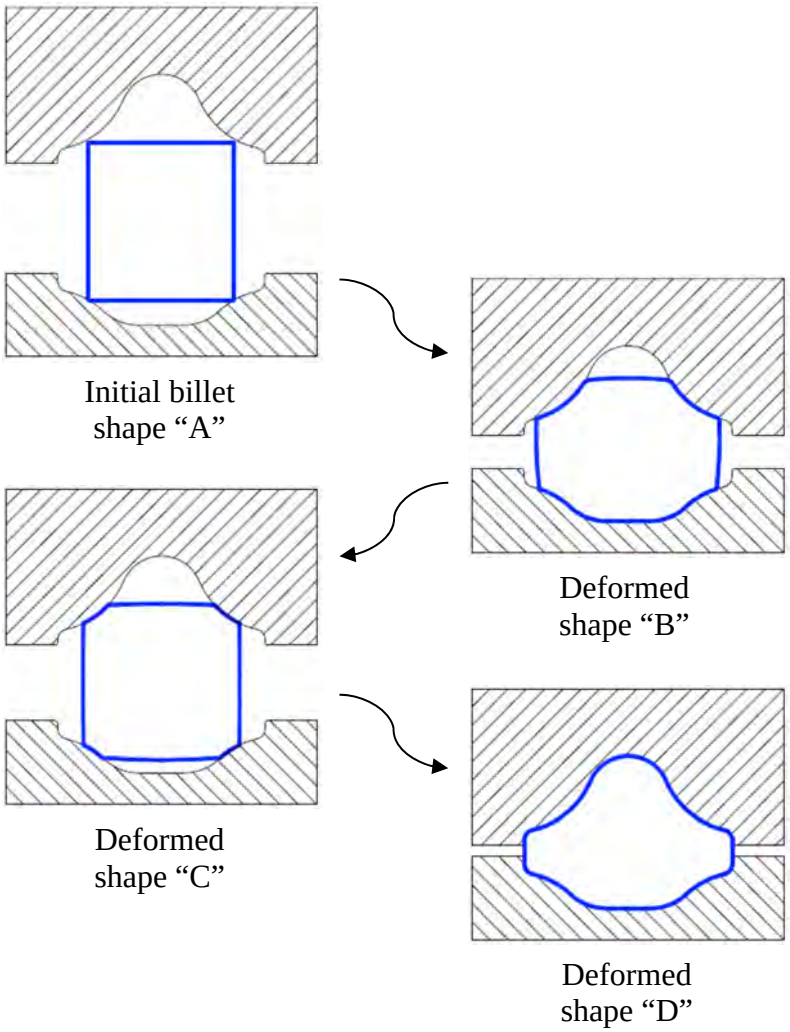

Fig. 4.8 A general deformation sequence of workpiece material in an axisymmetric closed-die forming.

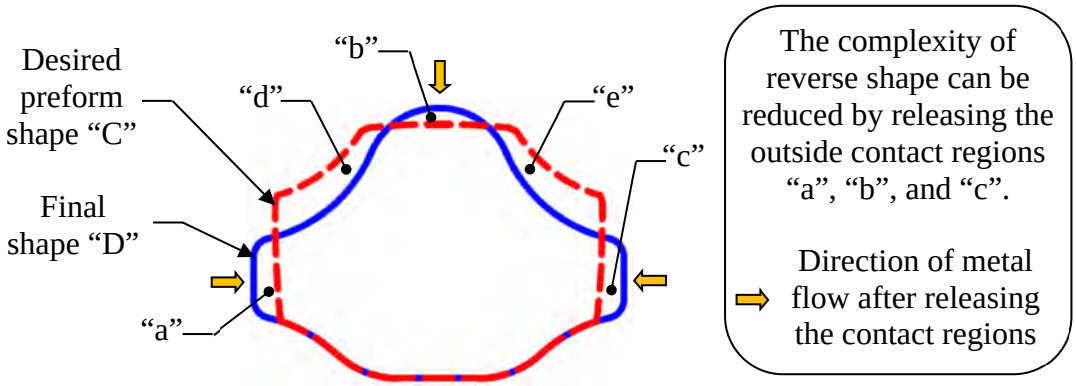

Fig. 4.9 The reverse shape should trend to the desired preform shape “C” once the outside contact regions, “a”, “b”, and “c” are released after a reverse increment.

As mentioned in the previous sections, the determination of contact boundary conditions applies not only to the die profiles, but also to the locations of the deformation workpiece. In the example of Fig. 4.10, different locations of the desired shape (i.e., the profile of shape “C”) influence outside contact regions, and hence the contact boundary conditions are varied. From the point of view for normal material distribution, the simplest shape, which is the initial billet shape “A”, will be changed to the most complex of the final shape “D” after the process. The shape “C” can be stated as one among the intermediate complex shapes between the shapes “A” and “D” in the deformation sequence. This means that the development of defining the unspecified shape “C” as the representation of the desired shape in the reverse simulation can be based on the reduction of complexity of the final shape “D”.

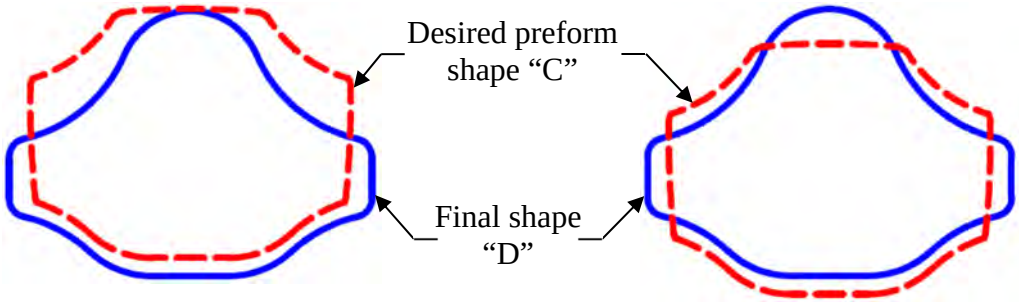

Fig. 4.10 Different locations of the profiles of desired preform shape “C” can result different outside contact regions, and hence different reverse shapes.

In addition, it is necessary to consider when and which contact regions should be released since these influence the shape of reverse preform critically. Figure 4.11 shows examples of different reverse shapes obtained by releasing different contact

regions. The shape with the lowest complexity among them is the most effective solution. This is consistent with the primary purpose of workpiece design.

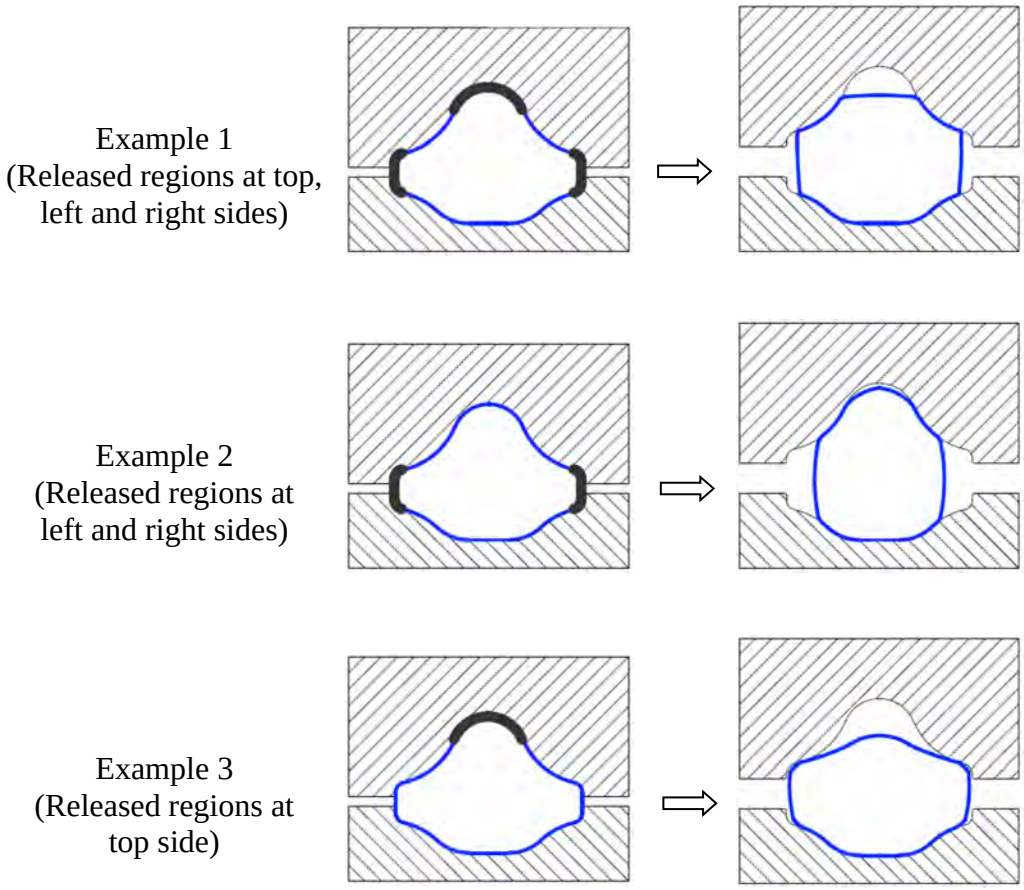

Fig. 4.11 Different contact boundary conditions can result different reverse shapes.

The most suitable contact boundary condition should be able to reduce the shape complexity effectively. It may be achieved by searching for all possible combinations of reverse shapes. Nevertheless, this may be very time consuming, especially for the complex shape analyzed by the finite-element simulation. For a relatively large time increment, several nodes or regions may need to be released in order to reduce the complexity of the workpiece after a reverse step. On the other hand, to consider the

use of a relatively small time increment and releasing only one region per increment, the same regions or nearby regions are possibly released within the same time step. The exact time at which the region should be released is uncertain. Thus, some physical rules or guidelines still have to be established for solving this specific problem in the meanwhile that the releasing node procedure may not necessarily be required for each small increment. The determination of either the node or region releasing operation has been taken into account as described in later sections. Since a smaller time increment can increase the prediction accuracy of the simulation, the difference between the shapes resulting from the most suitable combination for a larger time increment and that following one-region-released condition in the small increment can be smaller and acceptable. Therefore, a more practical solution is to assume that only one region is released at each reverse increment. Figure 4.12 illustrates this concept is implemented to the reverse simulation approach. The determination of the region with a potential to reduce the shape complexity depends on the desired shape. This concept can also be extended for the application of the reverse simulation of the material flow in warm-forming bimetallic components, once the interface condition between two materials has been identified.

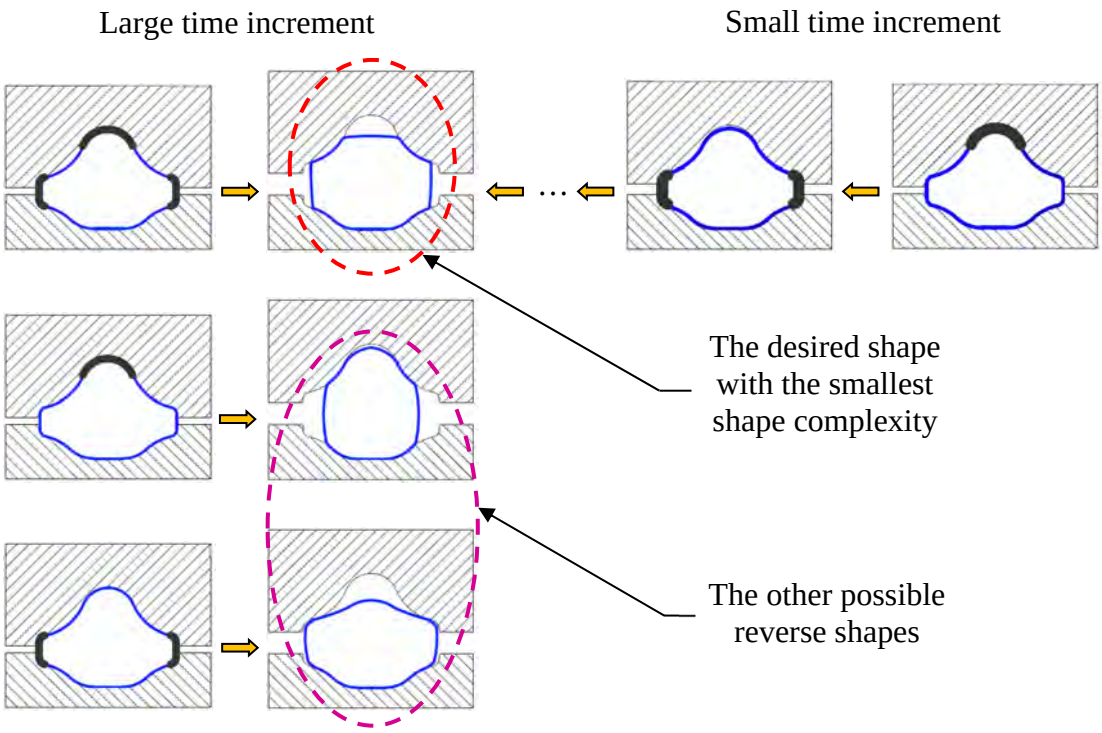

Fig. 4.12 Using one-region-released conditions in many small time increments is more efficient than searching for possible reverse shapes in a large time increment.

It is normally understood that the contact region furthest from the boundary of the desired shape is regarded as the most complex region. This region should be released in advance so as to reduce the shape complexity, and hence the reverse shape will then become closer to the desired shape (i.e., the simple shape). In most closed-die forming processes, the billets or preforms are formed in the dies such that the bulk of the material flows towards the die cavity. The excessive material is extruded through a restrictive narrow gap (i.e., the flash land) and appears as a flash around the formed component at the parting line of the die. In other words, the amount of the contact region increases along the cavities and the material eventually reaches the deepest area. Once the material fills up the cavities completely, the flash is produced by the surplus

material. This contacting sequence is inverted in the reverse simulation. The contact regions are detached from the flash and subsequently along the cavities from the deepest area. According to the above concepts, the contact region with the furthest distance to the boundary side of the desired shape is released to form a new boundary condition and then to obtain a new reverse shape. Figure 4.13 shows various desired shapes identifying different contact regions with the furthest distances to their profiles in each case.

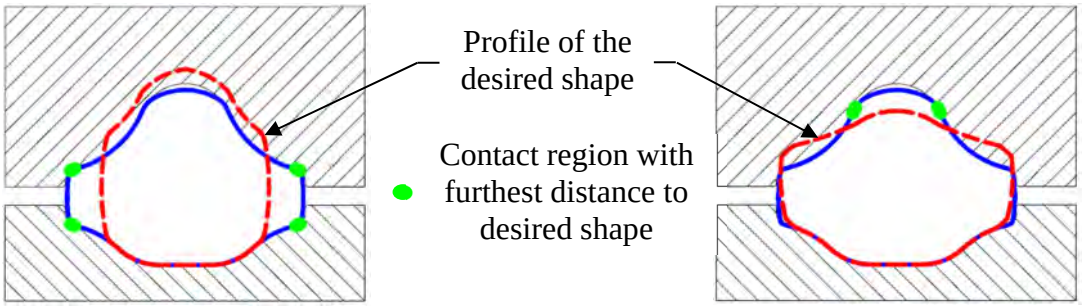

Fig. 4.13 Various desired shape can indentify different contact regions with the furthest distance to their profiles.

If the situation is that all contact regions are located inside the desired shape, the region-releasing procedure cannot be performed. If this assumption is made, there are only two possible contact boundary conditions, one-region-released and keeping the same contact condition as previously (i.e., the no region-released condition), which is taken into account since the exact time to release a region is unknown and cannot be defined in advance. Thus, a measure of the shape complexity is necessary and used to select a simple reverse shape for the next time increment.

The desired shape in the axisymmetric bulk-forming is usually a cylindrical billet which is the ideal material distribution shape and the most convenience for ease of manufacture. Therefore, two major geometric variables, height and diameter are involved to describe the billet. Indeed the difference between the desired shape and the deformed workpiece is one of the methods used to measure the complexity of the shape. It is understood that different contact boundary conditions result in different reverse shapes, and hence the desired shapes for the next time increment are different in such a case. Each desired shape also varies from the previous one in the last time increment. Figure 4.14 shows the outside regions used to determine the shape complexity. This requires measuring the total volumetric distribution and surface areas of the outside regions of the axisymmetric deformed component.

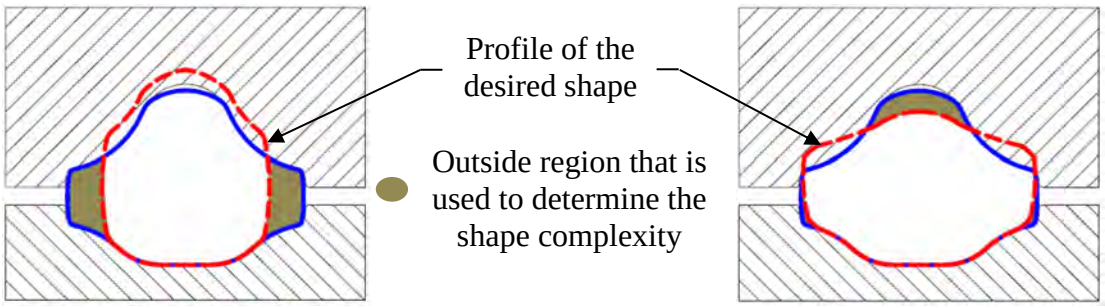

Fig. 4.14 The outside regions are used to determine the shape complexity.

Based on the above, Part et al. [21] and Chang et al. [24,25] proposed concepts for determining contact boundary conditions and controlling the reverse geometry of the deformed workpiece, the reverse simulation approach for the prediction of billet and preform shapes in the bulk-forming process can be developed, in which the noticeable tasks listed as follows have to be achieved.

- To devise a method for defining the desired shape at each time increment, the development of this method should be based on reducing the shape complexity according to the rational material flow and distribution. Generally, the workpiece with a cylindrical shape is the simplest and most primitive for the axisymmetric forming.
- To develop a method for locating the defined desired shape, this method should be linked to the minimum shape complexity such that the difference between the desired shape and the deformed or reverse shape can be diminished after the appropriate location of the desired shape has been determined. Therefore, the reverse shape can be close to the desired shape.
- Likewise, to select the most suitable reverse shape among various possible shapes after reverse increments, the measurement of shape complexity should be involved in this selection process to ensure that the predicted billet is sufficient to consider the simplest shape.

The contact boundary conditions can be determined for the reverse simulation once the methods or techniques used to deal with the above tasks are established firmly. Figure 4.15 gives a flowchart of the reverse increment. Indeed, this proposed concept is general and can be applied universally for various bulk-forming processes. Although the demonstrated examples presented in the next chapter are axisymmetric components, the methodology described in this thesis should also be sufficiently rigorous to meet the needs of three dimensional bulk-forming billet and preform design problems. The following sections will describe methods based on the empirical and

physical rules to achieve the requirements of using the proposed idea in the reverse simulation approach for axisymmetric bulk-forming problems.

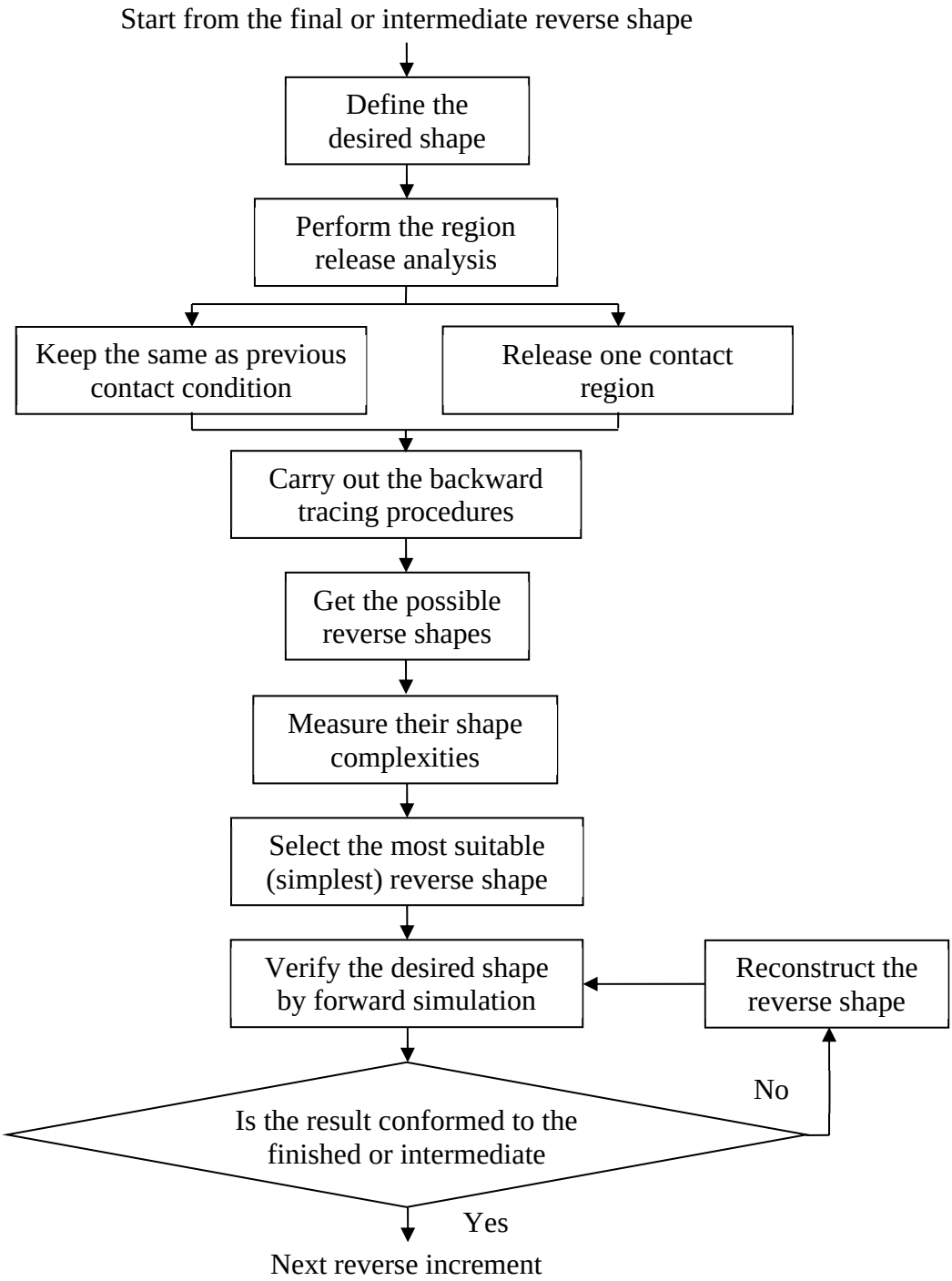

Fig. 4.15 A reverse increment with control of contact boundary conditions.

4.5 Control of material flow and distribution

The material flow and distribution of the workpiece vary during bulk-forming. As a general empirical rule, the initial shape of the workpiece (i.e., the initial billet) or the desired shape needs to be a simple geometry, such as a cylindrical bar (for axisymmetric forming), a circular or rectangular block (for two-dimensional plane strain forming), or a preformed blank with an identical cross section (for three-dimensional forming of an arbitrary shape), as shown in Fig. 4.16. The reverse simulation should be able to find a deformation path which will always lead towards a simple geometrical distribution from the shape with a simple material flow and distribution to determine the contact boundary conditions in the backward tracing process. In this study, the demonstrated examples are presented for axisymmetric bulk forming. A circular cross section or a ring cross section (i.e., a hollow circular cross section with a center hole) is supposed to be the cross section of the billet that is the desired shape to be reverted ultimately. In the simplest way, the cross-sectional area and volume of the cylindrical or hollow cylindrical geometry are shown as follows:

$$A_c = \left(\frac{D^2 - d^2}{4} \right) \pi \tag{4.8}$$

$$V = A_c h \tag{4.9}$$

Where A_c is the cross-sectional area, D is the outer diameter, d is the inner diameter, V is the volume, and h is the height. Figure 4.17 shows the configurations of desired shapes for both solid and hollow axisymmetric formed components.

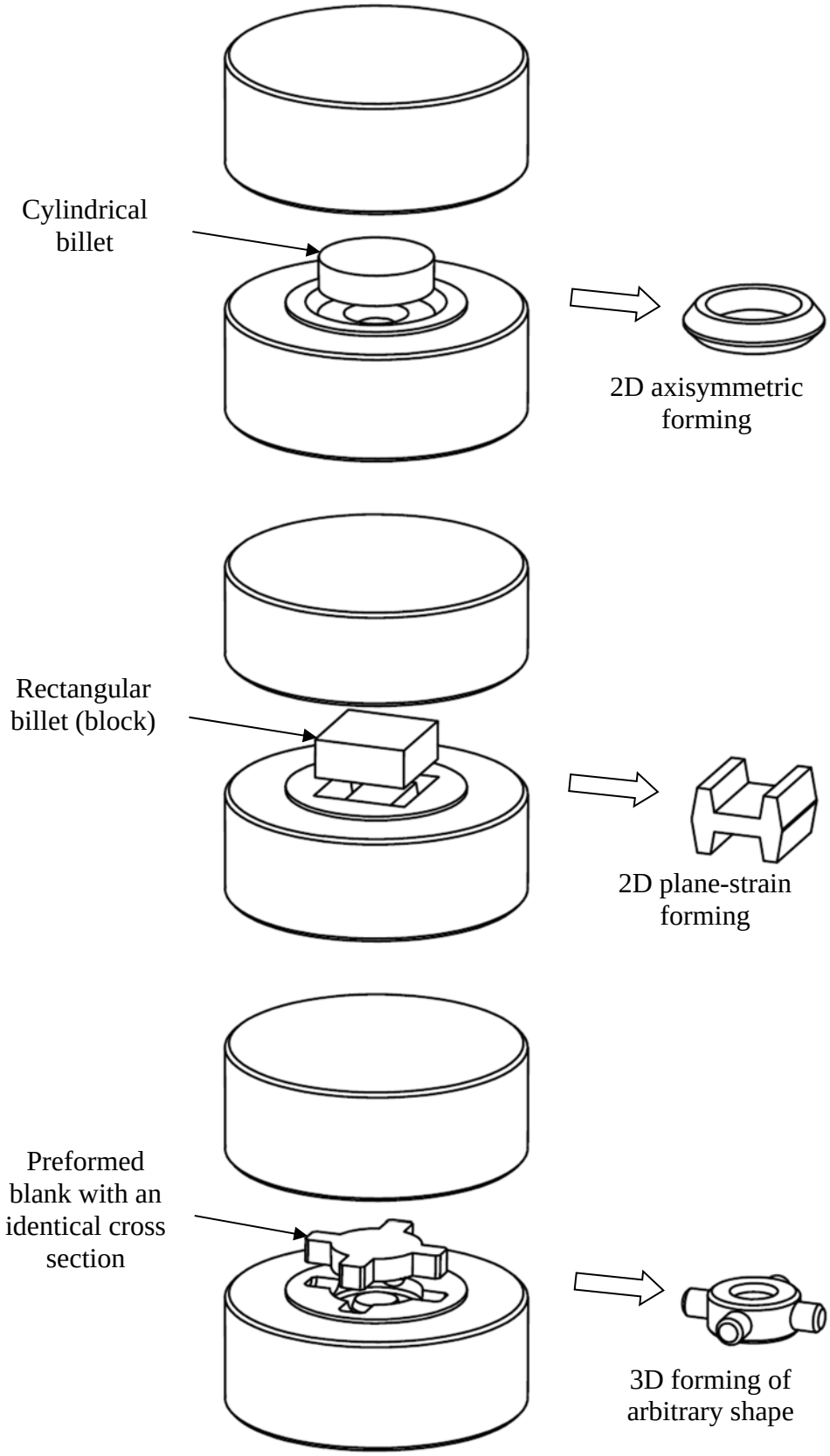

Fig. 4.16 Different kinds of billets and blanks used in different types of bulk forming processes.

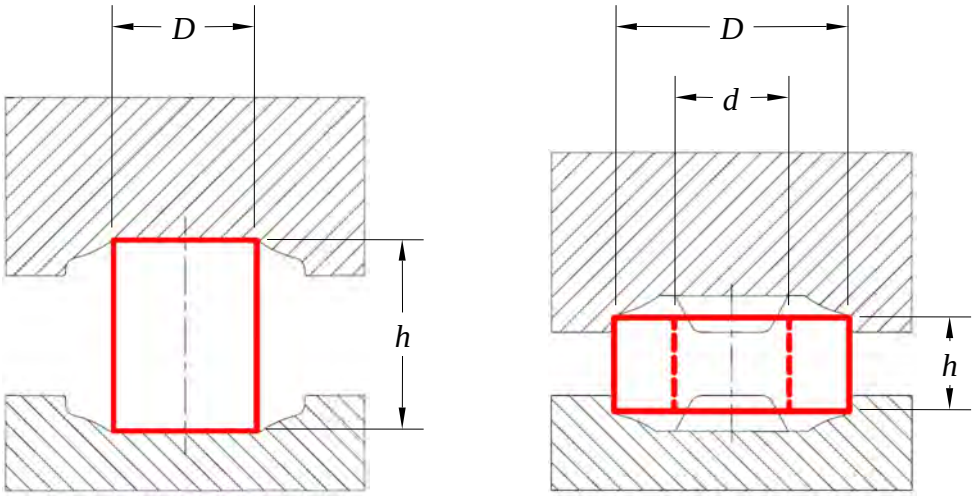

The desired shape (cylindrical billet) for forming axisymmetric component

The desired shape (hollow cylindrical billet) for forming hollow axisymmetric component

Fig. 4.17 The configurations of desired shapes for both solid and hollow axisymmetric formed components.

As a matter of fact, the height of the billet (or the workpiece) should always be minimised because this is able to reduce the amount of deformation greatly, and hence decrease the forming load and energy consumption. Besides, if the shape of the raw material or stock is a plate, a blanking or fine-blanking process can be used to produce the initial workpiece. In this case, using thinner plate or material is more efficient and economical from a mass production point of view, since the total volume of scraps can be reduced remarkably. In order to evaluate the volume in a continuous domain, its integration form may be required. In this study, a concept based on the assumption of constant volume is essential to control the material flow and distribution by minimizing the h of the billet, when the values of D and d are defined in the reverse increment.

The volume of a cylindrical shape (or volume of a solid revolution) in the integration form about the x-axis, V_x and the y-axis, V_y at the centre of gravity (x_c, y_c) are expressed as:

$$V_x = \pi \int_{x_c - h/2}^{x_c + h/2} \left[\left(y_2 \right)^2 - \left(y_1 \right)^2 \right] dx \tag{4.10}$$

$$V_y = \pi \int_{y_c - h/2}^{y_c + h/2} \left[\left(x_2 \right)^2 - \left(x_1 \right)^2 \right] dy \tag{4.11}$$

Where $x_1 = d/2$, $x_2 = D/2$ at the y-axis direction, and $y_1 = d/2$, $y_2 = D/2$ at the x-axis direction. The values V_x and V_y of a shape can be calculated by means of Gaussian quadrature from the finite element model or computer aided design (CAD) software. In practice, only the value of V_y (i.e., the shape is created by the revolution along the y-axis) is considered since the x-axis and y-axis are supposed to be the horizontal axis and vertical axis respectively in most two-dimensional finite element software packages.

In accordance with the assumption of constant volume, the material is incompressible in the bulk-forming process. Then the main purpose is to minimise the value of h, subject to the limits of D and d, while the volume is a constant and the centre of gravity is able to be acquired from a finite element model. Indeed, the limits of D and d are bounded by the shapes of previous reverse increments excluding the flash regions. This means the D and d cannot be larger or smaller respectively than their limits. Figure 4.18 shows an approach using the reverse shapes to define the limits of D and d. The largest D and the smallest d within the range of permissible limits are usually chosen. Therefore, it is only necessary to reduce the height of the billet (or

the workpiece) along the y-axis during the simulation so that the requirement of the simplest shape for the reverse simulation can be satisfied. Therefore, an appropriate approach can be used to search for the desired shape, such as a cylindrical shape (a rectangle in two-dimensional representation), based on the consideration of the simple material flow and distribution.

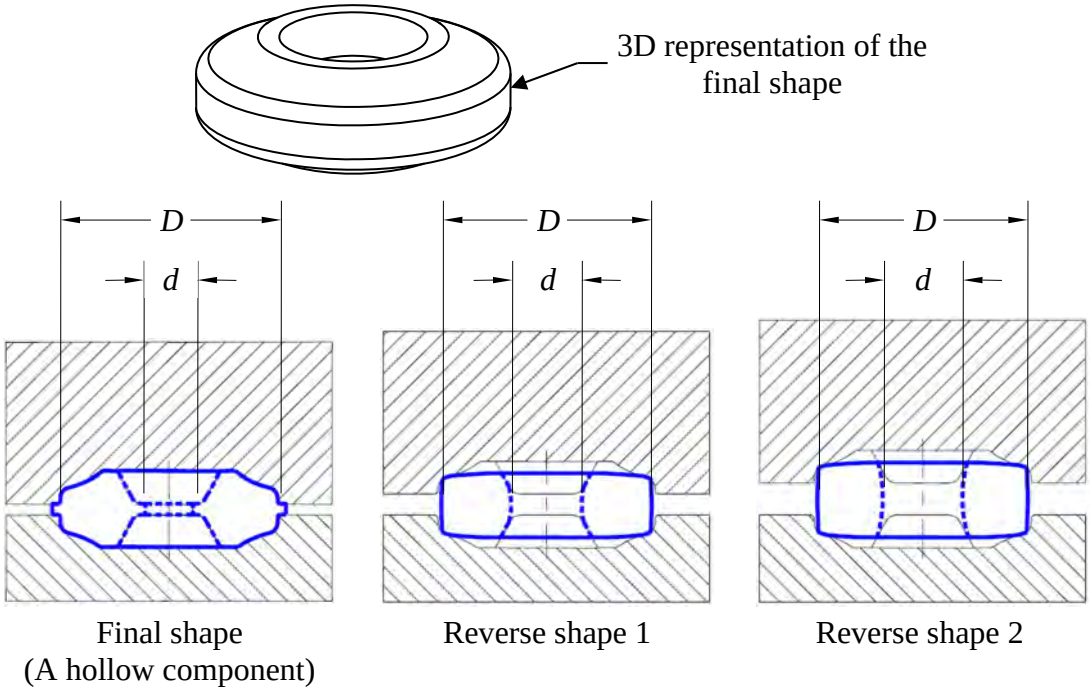

Fig. 4.18 The limits of D and d can be defined by various reverse shapes.

The reverse simulation aims to predict an ideal cylindrical shape (i.e., a rectangle in two-dimensional representation) with an ideal outer diameter D_r and ideal inner diameter d_r about the y-axis incorporated into the constant volume of the formed component. In order to ensure the acquisition of minimum difference of material spreading between the ideal and deforming shapes, the values of h and k_r need to be minimised. Their equations are as follows:

$$h = \frac{4V_y}{\pi\left(D^2 - d^2\right)} \tag{4.12}$$

$$k_r = \sqrt{\left[\left(D_r^{\,2} - d_r^{\,2}\right) - h_r^{\,2}\right] - \left[\left(D^2 - d^2\right) - h^2\right]} \tag{4.13}$$

Where h_r is the ideal height of the billet. For a cylindrical shape (or a hollow cylindrical shape), the value of $D_r^{\,2} - d_r^{\,2}$ is a function of A_c . That is:

$$D_r^{\,2} - d_r^{\,2} = \frac{4A_c}{\pi} \tag{4.14}$$

The equations (4.12), (4.13), and (4.14) can be used to construct all possible ideal cylindrical shapes as the desired shape with the constant volume of the deformation workpiece. An ideal desired shape can be defined based on reducing the value of h to represent the material flow and distribution. In Fig. 4.19, the point **P** ($D^2 - d^2$, h), representing the material distribution of the deformed workpiece, has the closest point **Q** on the h versus $D^2 - d^2$ curve. The desired shape is then defined by the $D_r^{\,2} - d_r^{\,2}$ and h_r at point **Q**. During the reverse simulation, the h and d should increase, and the D should decrease physically.

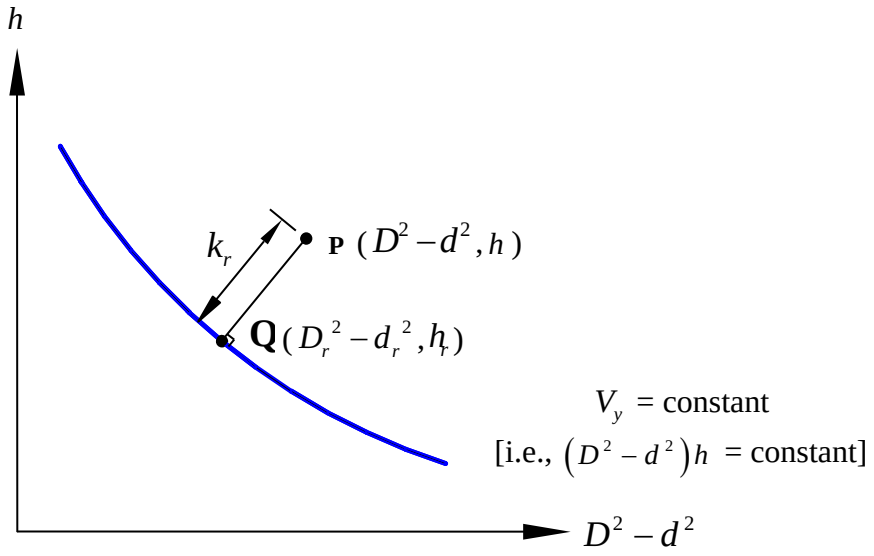

Fig. 4.19 The h versus D^2-d^2 curve for hollow cylindrical shape with the constant volume V_y.

It is necessary to locate the defined desired shape for determining the contact boundary conditions in the reverse simulation. The minimization of h of the billet (or the workpiece) is also required to reduce the shape complexity. In fact, the mid-point of the minimum h should be the centre of gravity (i.e., the centroid) of the shape. Therefore, the centroid can be used to locate the desired shape for specifying the outside contact regions for releasing the contact regions, as mentioned in the previous section. Figure 4.20 shows an example of two desired shapes with the mid-points of their h are set on the centroids of corresponding reverse shapes in different reverse stages.

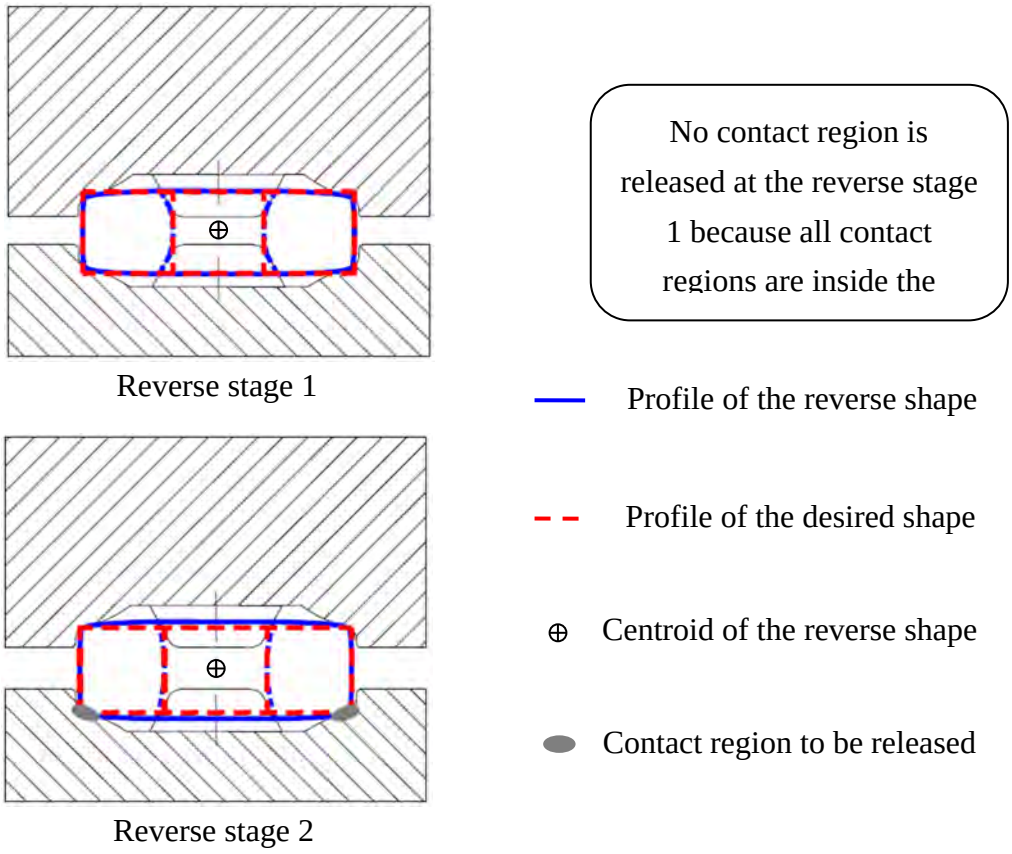

Fig. 4.20 The centroid is used to locate the desired shape.

Once the desired shape and its location are defined, the determination of the contact boundary conditions and shape complexity can be performed. The new contact boundary conditions are determined by releasing a contact region which is furthest from the desired shape. In fact, the contact region is released by detaching the node(s) from the die surface in the finite element model. Possible contact boundary conditions can be obtained and several reverse shapes are predicted. The selection of the most suitable predicted shape for next reverse increment involves measuring the shape complexity. The shape complexity is defined by the magnitude of the volume and the surface area outside the desired shape, which has to be located in the die properly, as described in the preceding section. The shape with the smallest magnitude (i.e., the

simplest shape) is then selected for carrying out the verification of reverse shape in which a forward simulation starts from the selected shape to perform the deformation process. If the result conforms to the final or intermediate shape, this selected shape can be forwarded to the next reverse increment. Otherwise, the shape has to be reconstructed by various methods, which are described in the next section. They are originally developed upon a number of empirical and physical rules governing the typical bulk-forming process.

The proposed method based on the assumption of constant volume and minimization of the workpiece height is used to set the desired shape for controlling the material flow and distribution. This method minimises the height with respect to the outer diameter and inner diameter of the hollow cylindrical shape, and hence reduces the shape complexity of the workpiece during the reverse simulation.

4.6 Empirical and physical rules for reconstruction of reverse shape

The empirical and physical rules are deduced from general bulk-forming practices in terms of the deformation behaviour of material, billet, and preform design, and the nature of boundary conditions at the interface between the workpiece and die surface by making specific assumptions. These can establish various methods to reconstruct the reverse shape in order to ensure that the reverse shape can be fully deformed into the finished or intermediate shape at the particular forward increment. In this study, the following empirical and physical rules were employed strategically to prevent occurring the abnormal reverse geometry of the workpiece.

- Empirical rules

  (i) Nearly same cross sections of workpiece and final component – The area of each cross section (or outer profile) along the height of the workpiece or billet should be nearly the same as that of the finished product augmented by the few areas necessary for flash.

  (ii) Compensation of material for incomplete die filling – An adequate volume of material should be added to a certain region of the workpiece, where the material is insufficient to flow into the particular zone of the die cavity and causes the incomplete die filling.

  (iii) Elimination for excessive material flowing into improper regions of die cavity – This is in contrast to the compensation of material. The excessive volume of the workpiece material, which flows into the improper regions of the die cavity, especially the flash regions, should be eliminated. Also, the volume of material at those regions is related directly to the amount of waste material, and the flash is subsequently removed by a trimming die. Therefore, the excessive material should be removed from an economic point of view.

- Physical rules

  (i) Assumption of constant volume – This reasonably assumes that the deformed material is non-porous and incompressible, and thus the mass and volume of the workpiece remain constant during the plastic deformation. This assumption is practically realistic for many bar-type and

plate-type metals to be used in bulk forming such as stainless steel and aluminium alloy.

(ii) Convex expansion of lateral deformation surface – The interfacial friction existing between the contact surfaces of the workpiece and die retards the flow or radial displacement of the die-contact material. As a consequence, the materials at the other non-contact regions, particularly the middle region of the workpiece, expand more rapidly, thereby forming a convex lateral surface outwards.

(iii) Material flowing with a higher velocity at the lowest resistant region of die cavity – Likewise, due to the frictional effect acting on the interface between the workpiece and die, the material first fills up the die cavities or regions that have the lowest resistance and friction rather than the high-resistant regions (e.g., flash land). In other words, the material flows with a high velocity at those lower resistant regions.

As mentioned above, the material should be compressed convexly (i.e., in a barrel shape) along the vertical die action in the bulk-forming process, due to the existence of friction between the contact surfaces of the workpiece and die. According to the backward tracing procedures, the $\mathbf{v}_0$ and Δt are taken for calculating the backward configuration or the reverse shape of $\mathbf{x}_{0-1}$ at time $t = t_{0-1}$. After the calculation, a concave-shape problem of the profile of $\mathbf{x}_{0-1}$ may occur, as illustrated in the example given by Fig. 4.21.

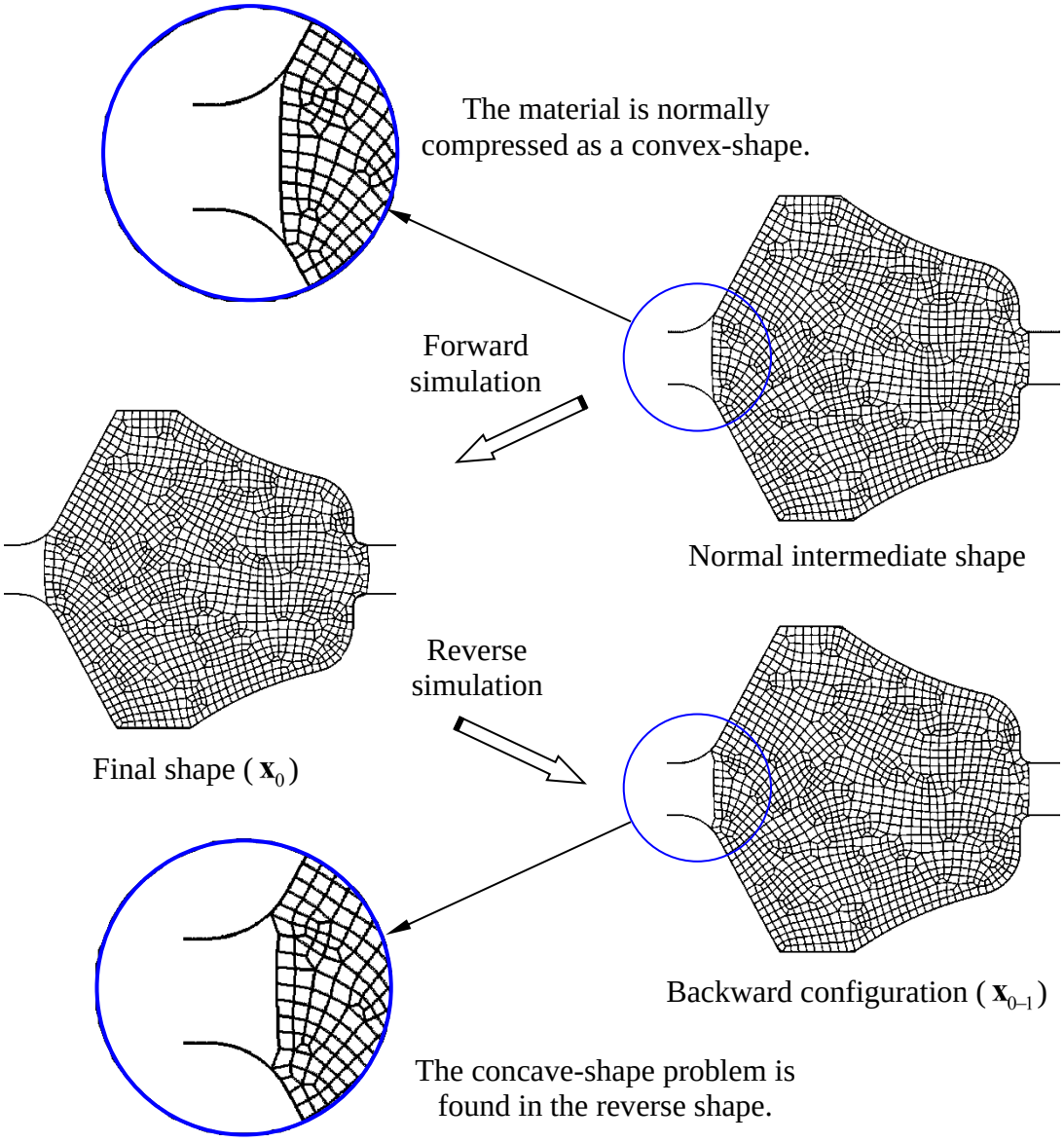

Fig. 4.21 The concave-shape problem occurred in the reverse shape.

Although the previous study by Chang et al. [24,25] did not address this problem, such a situation is not realistic and has to be solved together with other problems involving abnormal reverse shapes. There are two possible methods for reconstructing these concave-shape problems arising in the reverse simulation.

- Straight-line-repair (SLR) method – The concave boundary edge (i.e., the concave boundary surface in three-dimensional representation) is replaced by a

straight line (i.e., a flat surface in three-dimensional representation), which links up the two governing nodal points with a minimum distance.

- Boundary-edge-mirror (BEM) method – The concave boundary edge (i.e., the concave boundary surface in three-dimensional representation) is mirrored along a virtual straight line (i.e., a virtual plane in three-dimensional representation). This straight line (or plane) is the same as that of the SLR method, which imaginably connects the two governing nodal points with a minimum distance.

In Fig. 4.22 the identical concave-shape problem (which presents in Fig. 4.21) is resolved by the SLR and BEM methods respectively. This is the fact that using the BEM method should be more reasonable and realistic as the material is compressed convexly in practice. Nevertheless, it is necessary to consider the final volume of the reconstructed reverse shape in choosing these two methods. The method with the volume that is much closer to that of the final shape (i.e., the finished product) should be preferable. In other words, for the example given in Fig. 4.22, the reverse shape restored by the SLR method should be opted. Its accuracy and reliability are then examined by a forward simulation. It is so important to be aware that only the concave-shape problems encountered along the x-axis (i.e., the horizontal axis) need to be resolved. If the concave shapes occur at the top or bottom regions of the workpiece that are oriented substantially the same direction of the y-axis (i.e., the vertical axis), these can be ignored because the concave shapes at those regions are possibly attained in the actual closed-die forming process.

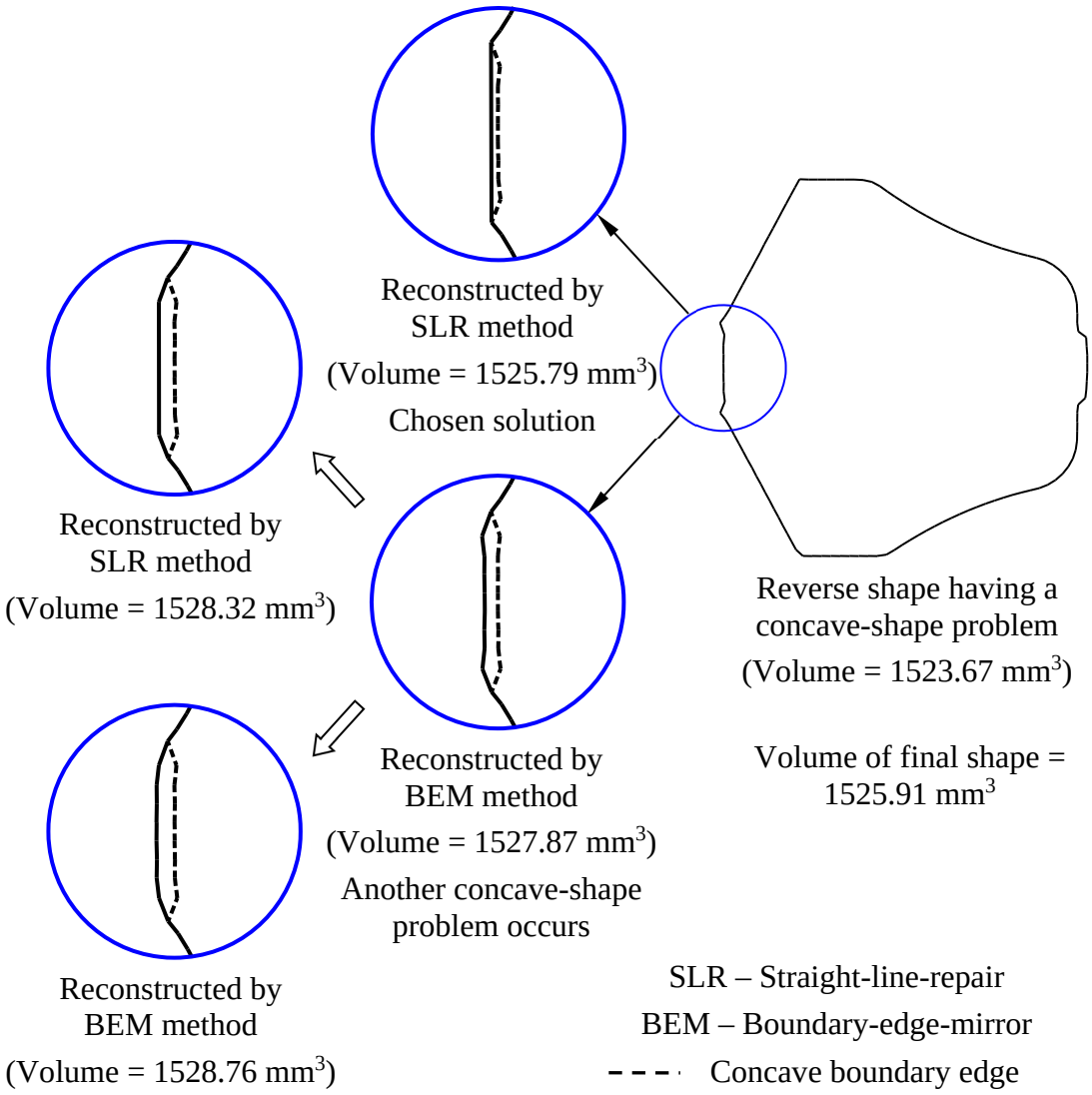

Fig. 4.22 Straight-line-repair (SLR) method and Boundary-edge-mirror (BEM) method used for resolving the concave-shape problem of reverse shape.

The physical rule for the convex expansion of lateral the deformation surface follows the consistent material flow and distribution along the vertical forming direction. This rule implies that the reverse shapes cannot be concave or have inwards surfaces. Both the SLR and BEM methods are useful to resolve the concave-shape problem. However, it is noted that some concave boundaries may be quite complicated and require more than one shape reconstruction, as in Fig. 4.22. The cycle of shape

reconstruction for an identical region should be limited so that the process of reverse simulation can be carried out without obstruction. The suggested number of cycles in this study is five. If the shape updated by the SLR or BEM method still remains the concave-shape problem after five cycles of shape reconstruction, the time increment of the current reverse step should be halved for the iteration to converge.

The reconstructed reverse shape is subsequently taken to process the forward simulation with a downward stroke of the die, its displacement being properly opposite in a sense to that reverse of stroke so that the reliability of the reverse shape can be verified. The verification method to be used in this study is totally different from that used in the original backward tracing method [21-25]. The traditional method calculates the difference between the $\mathbf{x}_0$ and $\mathbf{x}_0^{(n)}$, which may involve the comparison of the coordinates of each node. If $\left|\mathbf{x}_0 - \mathbf{x}_0^{(n)}\right| > e_l$ (where e_l is the limit of the difference and is normally set to 5×10^{-3}), which means the reverse shape is not so close to the final shape, and further iterations of the reverse simulation at that increment and die position are required until the value of e_l is smaller than the limit. This original scheme will be very time consuming, particularly for the complicated shapes and finite element models with numerous nodes. On the other hand, the proposed verification method based on the empirical rules for compensation and elimination of material should be more straightforward and efficient. It supposes the $\mathbf{x}_0$ and $\mathbf{x}_0^{(n)}$ are overlapped, and hence protrusions (i.e., excess of material) and indentations (i.e., lack of material) can be found by the Boolean operation in the finite element model or CAD model in terms of the volume and surface area. Figure 4.23

illustrates this method for the shape comparison and verification. The preselected allowances of the protrusion and indentation are 0.5% and 0.25% of the volume of final shape, respectively. These values of percentage should be good enough to control the material flow and distribution. While the $\mathbf{x}_0^{(n)}$ is verified with the accepted amounts of protrusion and indentation while the next reverse increment can go ahead. Otherwise, the time increment of the current reverse step needs to be halved for the iteration and reiteration. Certainly, the value setting of the allowance for protrusion and indentation affects the accuracy and efficiency of the reverse simulation.

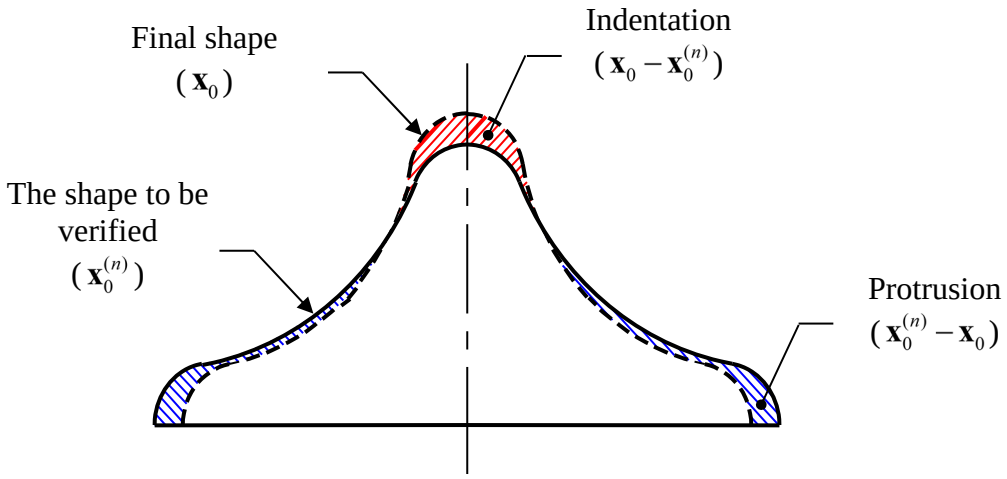

Fig. 4.23 An example of shape comparison between $\mathbf{x}_0$ and $\mathbf{x}_0^{(n)}$.

The volume of the final shape in the example presented in Fig. 4.22 is 1525.91 mm^3, and thus the volumes of allowances of protrusion and indentation are 7.63 and 3.81 mm^3, respectively. Figure 4.24 illustrates the same example of Fig. 4.22 for the shape comparison, which demonstrates how the protrusion and indentation can represent the difference between two similar shapes.

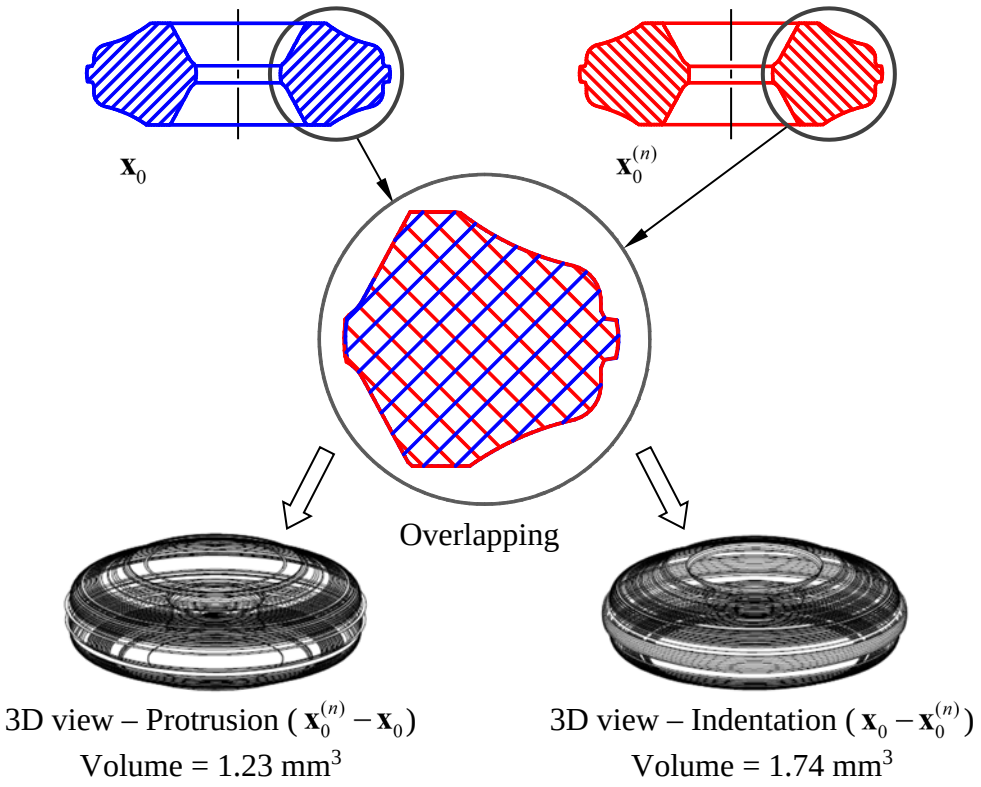

Fig. 4.24 The protrusion and indentation used in shape comparison.

In certain cases, reverse shapes probably have more than one concave-shape problem at various regions by the side of x-axis. Both SLR method and BEM method should be used to restore such abnormal regions. However, it is essential to be certain that the reconstructed revere shape cannot be penetrated into the die. Under situations of both these applied methods usually cause the inevitable die-penetration problem such that, another method, the nearest-die-profile-repair (NDPR) method can be employed. Figure 4.25 demonstrates how this suggested method can be applied to resolve the die-penetration problem.

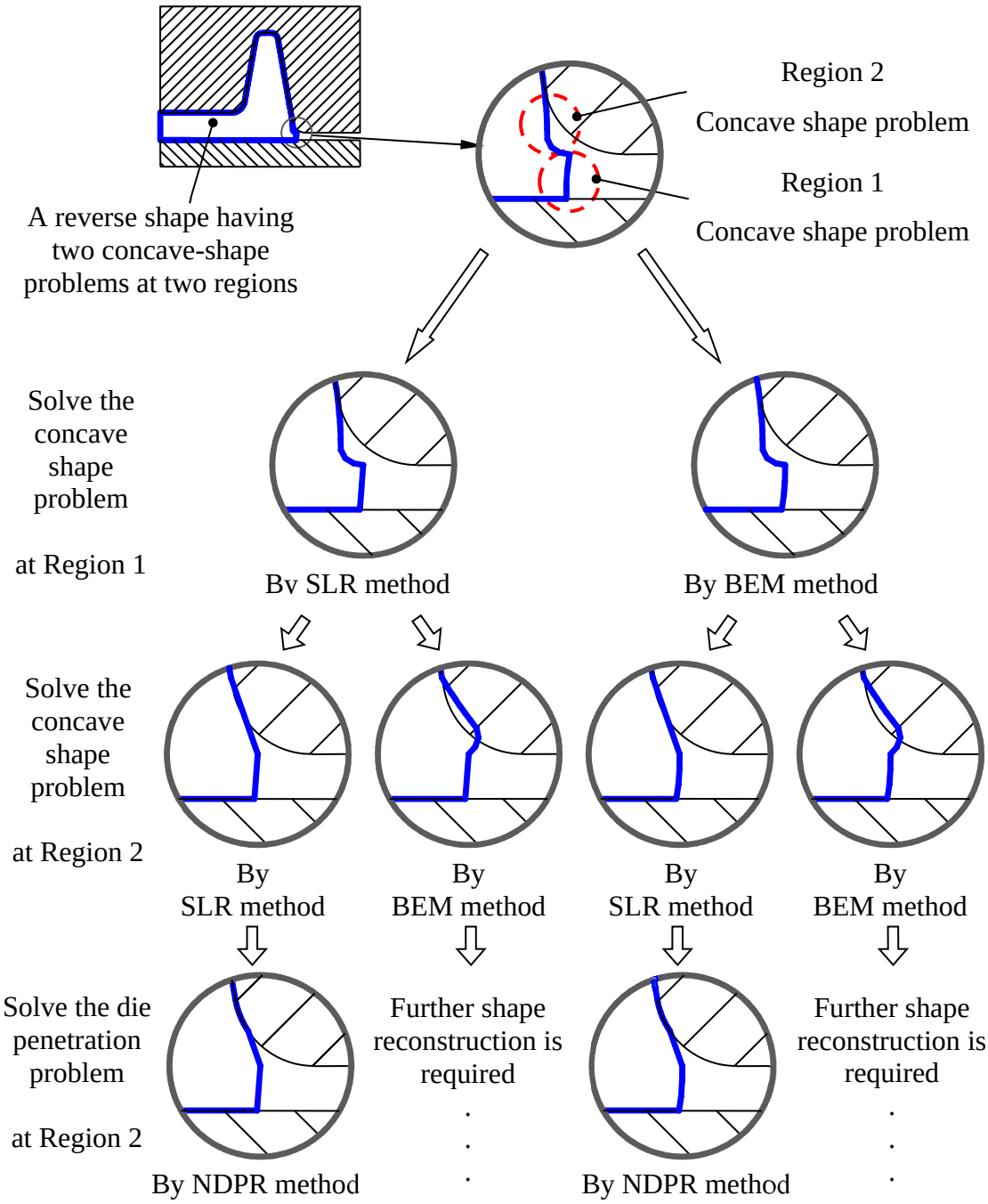

Fig. 4.25 The nearest-die-profile-repair (NDPR) method can be used if the reconstructed shapes have the die-penetration problem.

The verification of the reverse shape has to be performed at each reverse increment in order to ensure that the predicted reverse shape or its reconstructed shape

is able to be formed as the intermediate shape or the final shape of the product. This requires volumes of the protrusions and indentations that are lower than the preselected allowance. If this fails with a number of excessive and lacking material regions, the profile-offset (PO) method can be used to compensate the lacking volume and to eliminate the excessive volume, as illustrated in Fig. 4.26. This method directly adds and subtracts the exact volumes of materials at particular regions of the workpiece by offsetting its boundary profiles under the assumption of constant volume. If the reconstructed shape updated by the PO method is still not able to satisfy the requirement, an acceptable volume of protrusions and indentations, the time increment of the current reverse step should be halved for the iteration and reiteration to converge. As a consequence, the overall algorithm of reverse simulation with the procedures of reverse-shape reconstruction can be established as shown in Fig. 4.27.

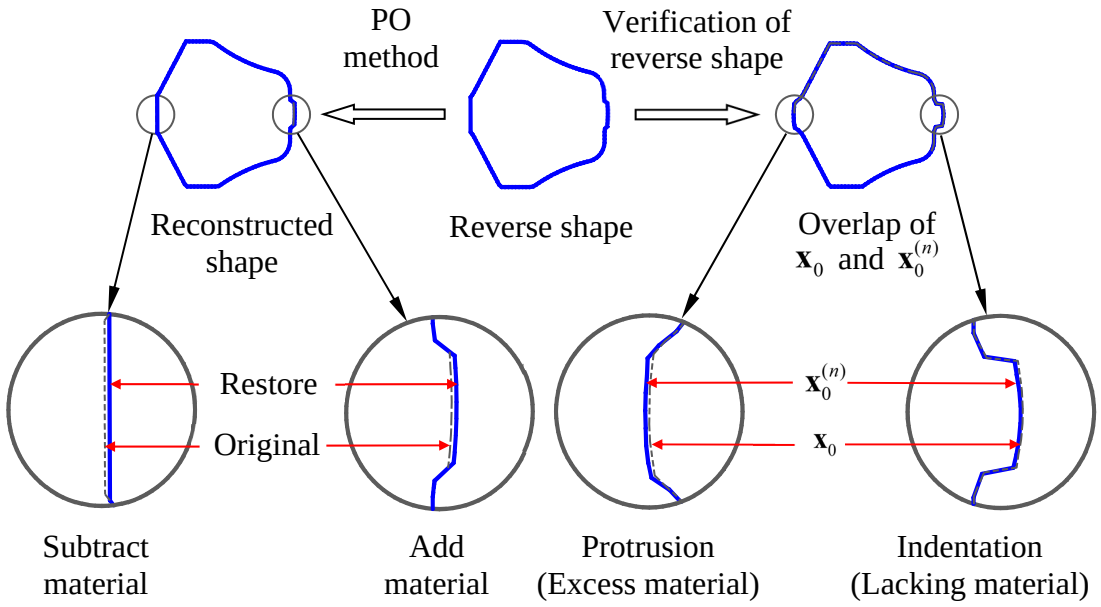

Fig. 4.26 The operation of profile-offset (PO) method.

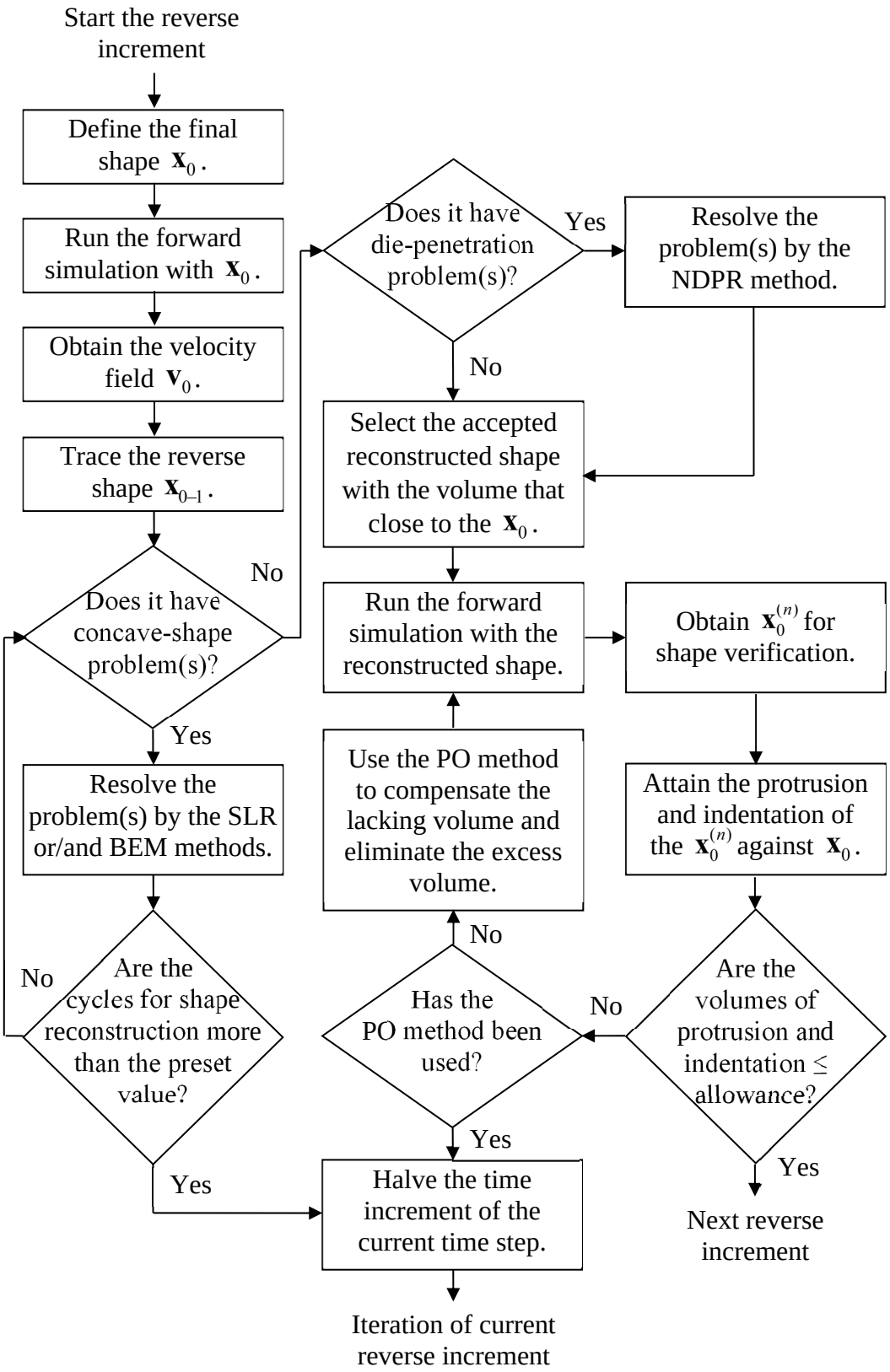

Fig. 4.27 The flowchart of reverse simulation with the procedures of reverse-shape reconstruction.

The initial step of the reverse simulation is straightforward. The process may only involves reversing the material flow at flash regions because the flash should be formed finally in an usual bulk-forming process. After that, the further steps of reverse simulation have to take into account of the detachment of the nodes as the material may flow or reverse from other regions and cavities rather than the flash land. In the actual forming process, according to the minimum work-rate principle, the material should always flow in the path of least resistance. This means the material first fills up the die cavities or regions that have the lowest resistance and friction rather than the high-resistant regions (e.g., flash land). It is a fact that the material flows with high velocities at those lower resistant regions. Therefore, the velocity of the material flow can be used to determine such resistance of die cavities and regions, as well as the sequence of detachment of nodes. Based on this physical rule, the material at the cavities or regions with the highest resistance (i.e., the lowest velocity) should be released in the beginning of the reverse simulation. In this situation, a prolonged-cavity die (i.e., the cavities of die are prolonged) is applied to determine the appropriate detachment of the boundary nodes. The detachment criterion is to compare the velocities of material flowing to various regions and the flash land. Figure 4.28 is an example, which shows the velocity fields of the material after a forward simulation. If the velocity of the material flow at particular regions is equal or slower than that at the flash land, the nodes at that region and the flash land will be detached. Otherwise, only the nodes at the flash land are detached. In other words, the lowest-velocity nodes are detached. Once the node of specific regions has been detached, the material at that region keeps flowing in a reverse direction continuously. This node-detachment

process triggers while the reverse increment cannot perform the automatic node detachment under the backward tracing process and one-region-release process. If there is more than one cavity, the nodes with the lowest velocity of materiel flow are detached.

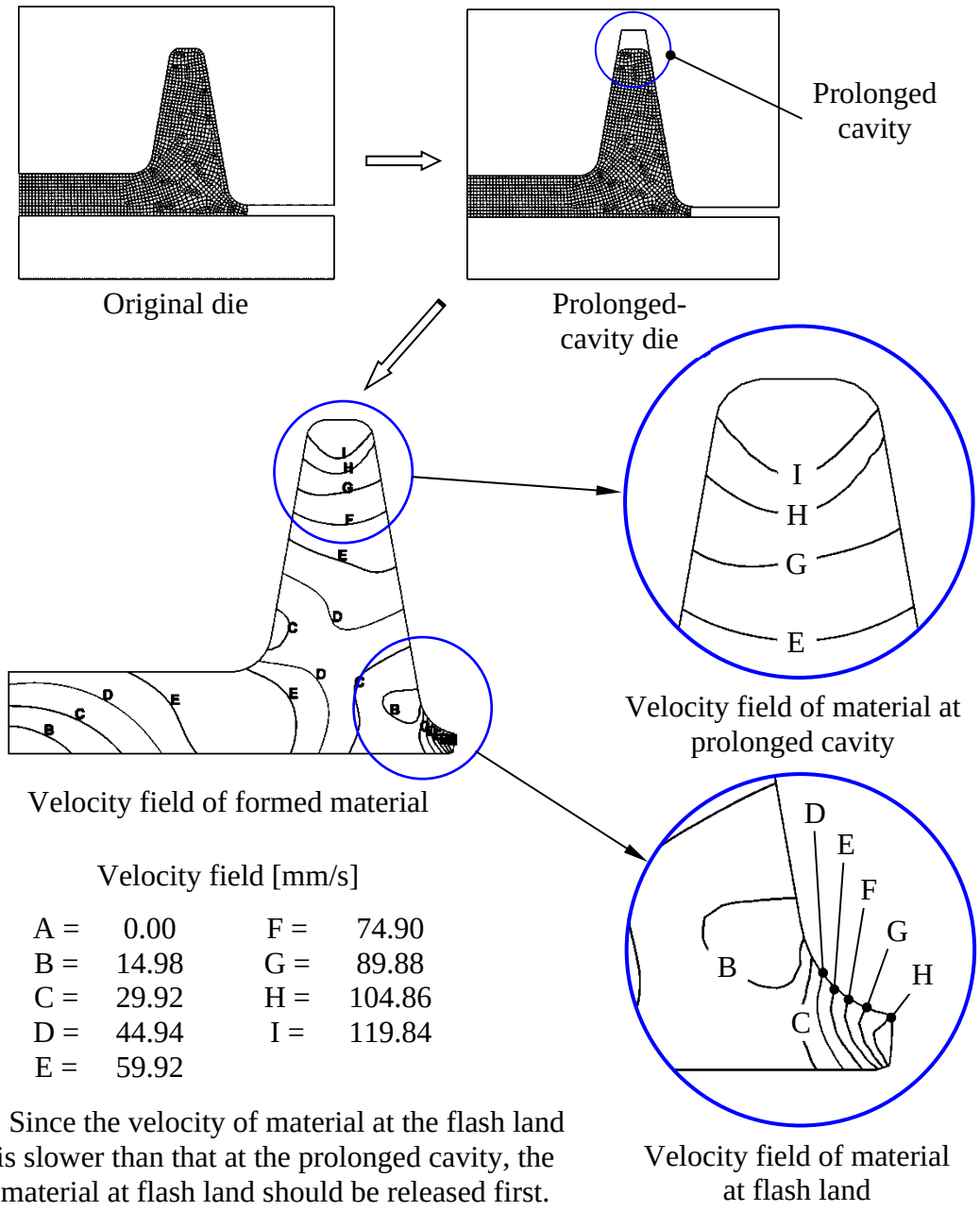

Fig. 4.28 A comparison of the velocity of materiel at the flash land and the prolonged cavity with using the prolonged-cavity die.

4.7 Warm-forming bimetallic components

The process of warm-forming bimetallic components involves two major activities: (i) welding, and (ii) shaping two dissimilar metals together. These two activities must be carried out concurrently within the process over a short duration of time. As far as the success of the process is concerned, both heat and pressure are very important factors. The sufficient heat energy and plastic deformation are not only used for shaping the components, but are also necessary to generate the intermetallic bond between the dissimilar metals as known as solid-state welding [10-12] (e.g., hot-pressure welding and forge welding). It is noted that sufficient plastic deformation absolutely exists at the mating surfaces of two dissimilar metals, while in the warm-forming process. In other words, the temperatures of materials during welding and forming become the most significant and have to be determined carefully by physical experiments.

Additional preparation and consideration for reverse simulation of warm-forming bimetallic components are required such as determination of material temperatures and the evolution of the condition of bimetallic interface (i.e., a sticking condition returning to a sliding condition), because the flow properties and mechanical behaviour of each metal are totally different.

In this study, in order to simplify the process modelling, it was assumed that the bulk-forming process would be carried out under the isothermal conditions. This also corresponds to the warm-forming bimetallic component, in which a compact sample component (i.e., smaller than Ø50 × 10 mm) is formed with a faster die velocity (i.e.,

equal or faster than 40 mm/s). Since the cycle time of the process is less than 0.25 seconds, the effects of the die chilling as well as the drop of temperature are disregarded. Although the heat transfer is not taken into account, the discrepancy of flow stress of the two dissimilar metals causes the heterogeneous material flow, which have to be minimised by appropriate selection of the forming temperatures. In this way, different forming temperatures have to be chosen for each metal in both the forward and reverse simulation. The welding temperature of the quality-weld threshold determined by the experiments is recognised as the forming temperature of the softer metal (e.g., aluminium alloy), which has a smaller overall flow stress in comparison with another end configured to the bimetallic component. Accordingly, the suitable forming temperature of the stronger metal (e.g., stainless steel) has to be selected consistently with the experimental flow stress data of those dissimilar metals so that the couple can flow together with parallel velocity fields.

At the beginning of warm-forming the bimetallic component, two dissimilar metals are separated as their contact interface is under a dry sliding condition. When a pressure is applied on them, their cohesion appears to be as strong as an intermetallic bond that is like a sticking condition. Therefore, at the start of the modelling of the reverse simulation for warm-forming bimetallic components, the key step is to identify a larger shear-friction factor m (e.g., 0.9) as a nearly sticking condition at the weld interface of the final shape of the finished product (i.e., $\mathbf{x}_0$). During the procedures of reverse simulation, this m is reduced to the sliding condition in stages, which depends

on the forming load F_l to be obtained from the increment of forward simulation. The shear-friction factor m_n of the reverse shape is expressed as follows:

$$m_{0-1} = m_0 \left(\frac{F_{l(0)}}{F_{l(0+1)}} \right)$$

$$m_n = m_{n+1} \left(\frac{F_{l(n+1)}}{F_{l(n+2)}} \right) \tag{4.15}$$

Where m_{0-1} is the shear-friction factor of the first reverse shape $\mathbf{x}_{0-1}$, m_0 is the shear-friction factor of the final shape $\mathbf{x}_0$, $F_{l(0)}$ is the forming load required for forming $\mathbf{x}_{0-1}$ into $\mathbf{x}_0$ by forward simulation, and $F_{l(0+1)}$ is the forming load required for forming $\mathbf{x}_0$ into $\mathbf{x}_{0+1}$ by forward simulation. The equation (4.15) should be subject to $F_{l(n+1)} \leq F_{l(n+2)}$. Also, the initial shear-friction factor m_i should be determined by the experiment such as a ring compression test, and hence the reduction of m can be stopped, whenever the value of m_n reaches to m_i. The process of changing the interface conditions (from the nearly sticking condition of the weld interface to the sliding condition of the two separated dissimilar metals) is illustrated in Fig. 4.29. The remaining procedures and algorithm for tracing the reverse shape are almost the same as those used for bulk-forming the single metal.

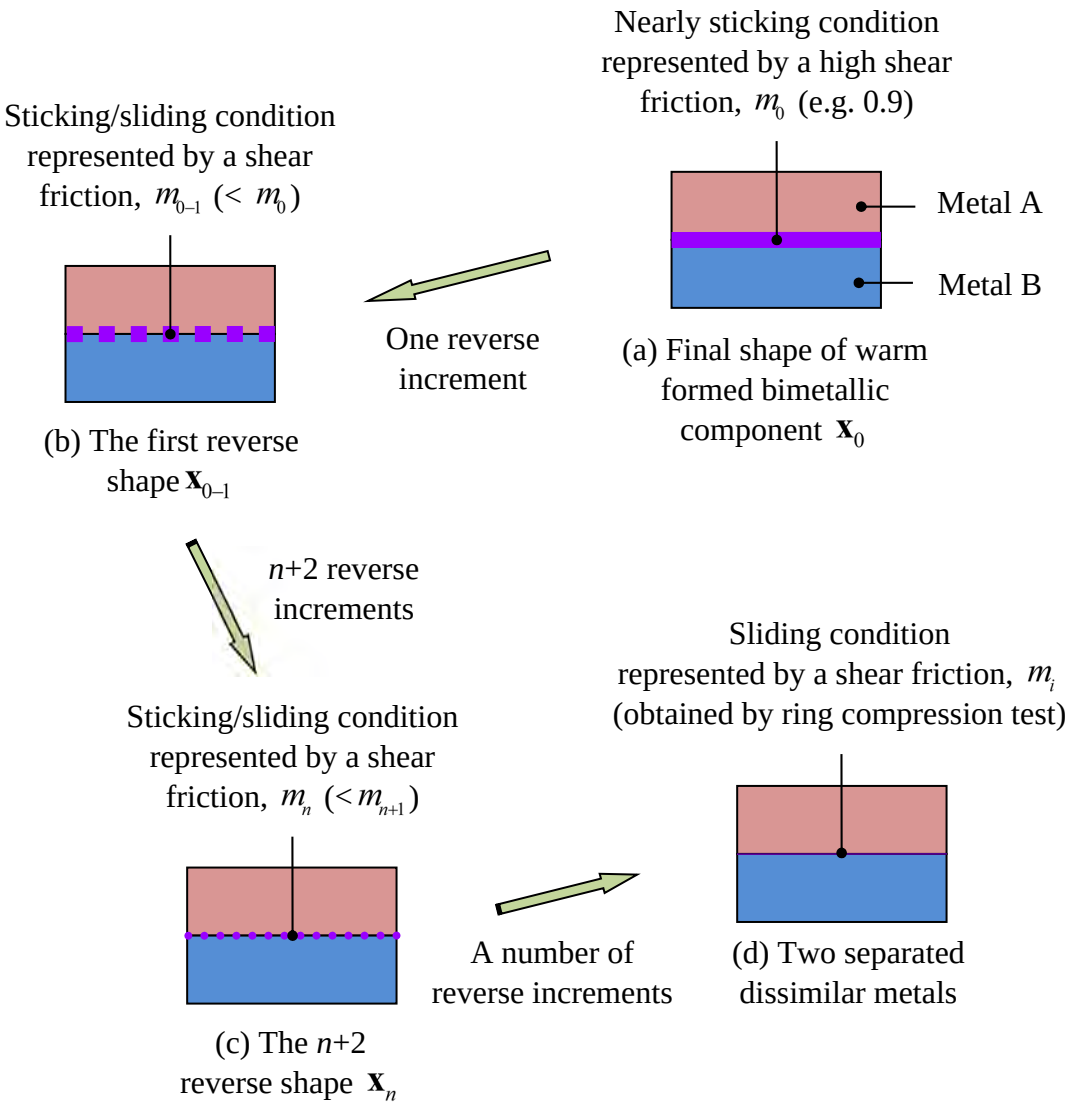

Fig. 4.29 The process of changing the interface conditions during the reverse simulation of warm forming bimetallic component.

4.8 Summary of reverse simulation approach

The methodology for the workpiece design makes use of the reverse simulation approach to predict a reverse path of the deformation as well as the initial positioning of the model. This approach is based on the concept that both the material flow and distribution are used to determine a desired shape which is the simplest hollow cylindrical shape with diameters (i.e., inner and outer diameters) and a height for axisymmetric or hollow axisymmetric bulk forming in this study. After defining the desired shape and its location, the new contact boundary conditions for a reverse increment can subsequently be determined by using appropriate strategies and methods. Since the time to release the contact region and area is unknown and cannot be defined in advance, the keeping the same as previous contact condition is also taken into account. Therefore, several possible reverse shapes may be obtained in each reverse increment. A measure of the shape complexity is then used to select the simplest shape. By repeating the above procedure until all nodes are separated from the dies, a reverse shape with a simple material flow and distribution can be predicted. If the reverse shape is not cylindrical, it acts as a preform and further reverse simulation is required. The die profile of the secondary reverse simulation is determined by the reverse shape which is found in the previous reverse simulation. The procedure is repeated until a simple geometry (i.e., a cylindrical billet) is obtained.

The reverse simulation approach adopted for the workpiece design provides an efficient and effective procedure that is able to control the material flow and distribution and contact boundary conditions because using the assumption of constant

volume of cylindrical shapes and minimum height of billet as a control criterion depends on the centre of gravity as well as the coordinates of the shape. The method seeks a reverse path which achieves the reduction of the shape complexity from the final shape of finished product according to the selection of the material flow and distribution close to a simple geometry at each reverse increment. The approach is finally incorporated with several shape reconstruction methods including SLR, BEM, NDPR, and PO methods established by the empirical and physical rules governing the bulk-forming process. These methods can help to reconstruct the reverse shape exhaustively and to ensure that the predicted shape is able to be formed into the final shape. With the additional procedures including the determination of material temperatures, as well as the evolution of the condition of the bimetallic interface, the reverse simulation approach can also be implemented to warm-forming bimetallic components without problems.

5. Research Methodology

5.1 Background

In this study, various mechanical tests and physical experiments were required to process and verify the proposed reverse simulation approach. The acquired material data and the determined processing conditions can be utilised for modelling the bulk-forming process, particularly warm-forming bimetallic components regardless of whether the forward simulation or reverse simulation is desired. The tests and experiments performed are listed as follows:

- Uniaxial compression test – The uniaxial compression test is generally used to obtain the flow stress data of the specimen materials at different strain rates and elevated temperatures. In order to avoid the necking correction during the tensile test, compression test was adopted in this study for the data acquisition, and hence it can be conducted with large strains that are comparable to those found in bulk forming process.
- Ring compression test – The ring compression test is a common test used to evaluate the friction condition at the interface between the specimen materials and die. The ring-shape (i.e., hollow cylindrical) specimens are upset to different reductions with a lubricant or under a dry condition. An increase of the inner diameter of ring means the friction is small, whereas the friction becomes higher as the inner diameter of the ring decreases.

- Welding experiment of dissimilar metals – The investigation of welding dissimilar metals is necessary to know about how to produce good-quality bimetallic welds or components as well as the selection of more appropriate process conditions for process modelling. Two types of solid-state welding processes, hot-pressure welding and forge welding were used for joining dissimilar metals (i.e. bimetals) in this study. The reason for selecting solid-state welding rather than fusion welding (e.g., electrical arc welding and laser welding) is that the diffusion occurs without any melting of the parent metals, and metallurgical changes of the joints are minimised [10-12,114-118].
- Experiment of warm forming bimetallic components – This experiment aimed to study the effects of the process parameters in bulk-forming bimetallic components at elevated temperatures. This helps to determine the suitable forming temperature and ram speed (i.e., the die velocity) for attaining the complete die filling of the bimetals.
- Physical experiments for verification of reverse simulation result – The physical experiments were conducted to verify the results obtained by reverse simulation. The process conditions of the experiments, such as the geometries of the workpiece and die, die velocity, forming temperature, and lubrication (i.e., friction factor) should be the same as or equivalent to those of the simulation. This demonstrates the success of the proposed reverse simulation approach, which is able to be applied to the real situation.

5.1.1 Specimen materials, specifications, and preparation

This study focused on forming aluminium alloy 6063 and stainless steel AISI 316L axisymmetric bimetallic components. The chemical compositions and mechanical properties of the two specimen materials are given in Tables 5.1 and 5.2, respectively. Aluminium alloy 6063 is used widely in the transport, architectural, and construction industries for items such as connecting rods, irrigation tubing, window frames, and doors because of its light weight. Stainless steel AISI 316L is a durable structural material which provides high mechanical strength and excellent corrosion resistance for engineering applications. Such a combination with different thickness/length variations is also good for making non-axisymmetric or irregular-shape components, such as watch cases, gears and shields, having higher strength, lighter weight, and a better ability to withstand corrosive environments.

Tables 5.1 Chemical composition of the specimen materials.

Specimen material	Chemical composition [weight %]													
	Si	Mn	Cr	Fe	C	S	P	Mo	Ni	Al	Cu	Mg	Ti	W
Aluminium alloy 6063	0.4	0.1	0.1	0.3	–	–	–	–	–	98.3	0.08	0.5	0.08	0.1
Stainless steel AISI 316L	0.5	1.7	16	69.6	0.02	0.02	0.03	2.1	10	–	–	–	–	–

Table 5.2 Mechanical properties at 20 °C of the specimen materials after annealing.

Specimen material	Yield strength [MPa]	Tensile strength [MPa]	Vickers hardness [HV]
Aluminium alloy 6063	48	90	46
Stainless steel AISI 316L	230	521	221

Annealing conditions of aluminium alloy 6063

Temperature: 420 °C; Annealing time: 2 hours; Cooling rate: 7 °C/min.

Annealing conditions of stainless steel AISI 316L

Temperature: 1050 °C; Annealing time: 15 mins; Cooling rate: 35 °C/min.

(i) For uniaxial compression test

In the uniaxial compression test, the specimens were made with a diameter-to-height ratio of 1.5 according to the recommendation of the American Society for Testing and Materials (ASTM) [119-121]. The specimen configurations and appearances are shown in Figs. 5.1 and 5.2, respectively. For each specimen material, thirty specimens were tested but some were invalid due to the barrelling and non-uniform deformation. They were made from large 12 mm thick metal plates by EDM (electrode discharge machining) wire cutting. The final shape of the specimen was constructed by turning because this minimised the residual stresses and only changed the local microstructure close to the end-faces. Chamfered edges were required to avoid fold-over in the compression. In order to reduce the barrelling effect of the specimen profile caused by friction, the top and bottom faces of the specimen were machined with parallel groove of 0.3 mm depth to retain graphite-based lubricant. After machining, dimensions were measured within a tolerance of ±0.02 mm.

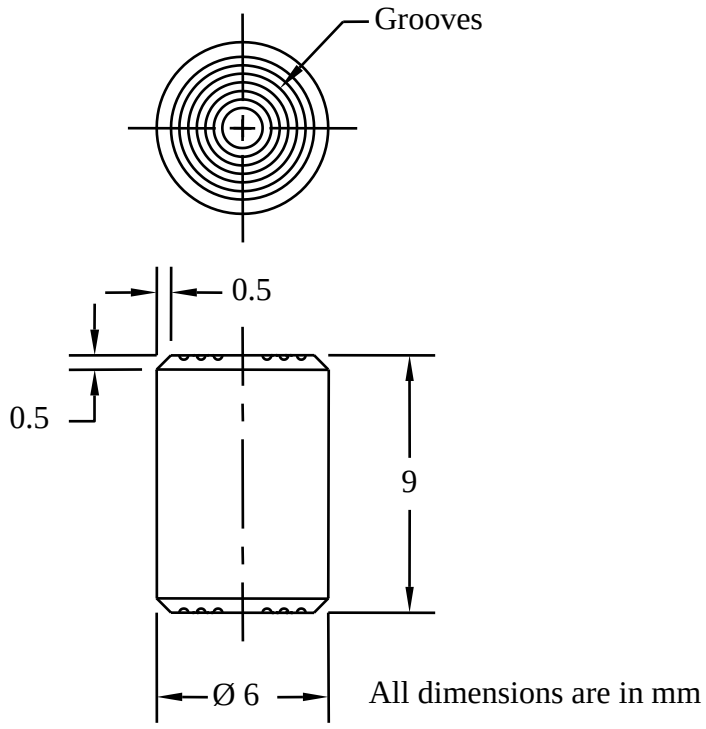

Fig. 5.1 The configurations of the specimen for the uniaxial compression test.

Fig. 5.2 The specimen fabricated for the uniaxial compression test.

(ii) For ring compression test

The ring compression test was carried out on the aluminium alloy 6063 only. This aimed to evaluate the friction under a dry condition and a lubrication condition at

warm forming temperature (i.e. 300 °C for aluminium alloy). Twenty ring specimens were made in the ratio 3:2:1 of outer diameter (i.e., 18 mm), inner diameter (i.e., 12 mm), and thickness (i.e., 6 mm) respectively. Figure 5.3 shows the geometry of the specimen used in the ring compression test.

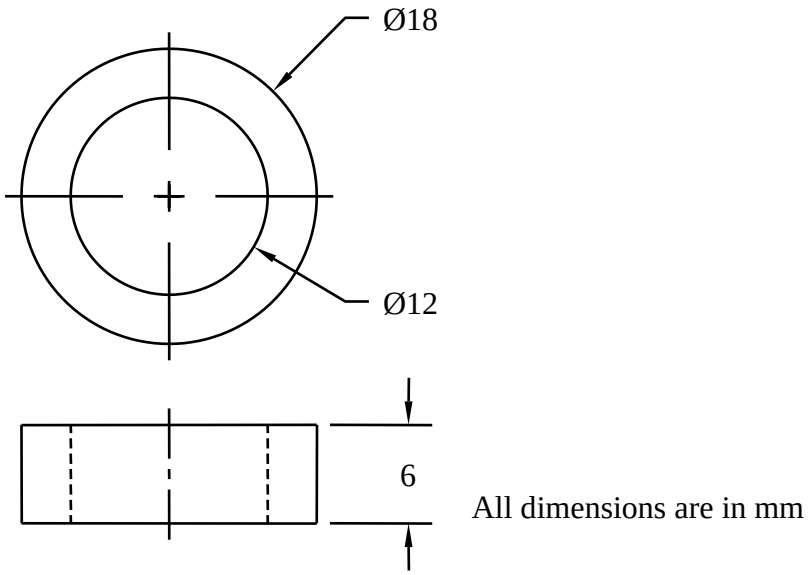

Fig. 5.3 The geometry of the specimen used in the ring compression test.

(iii) For welding experiment

In the experiment of welding dissimilar metals, the specimens of both aluminium alloy 6063 and stainless steel AISI 316L were cylindrical with a diameter of 6 mm, which was appropriate to be held in the grips of the MTS machine for the evaluation of joint efficiency. However, it is worth noting that the findings of this experiment can also be used as references for irregular shapes of workpieces as well as non-axisymmetric bimetallic components. During the welding processes, the plastic

deformation took place essentially in the softer aluminium alloy 6063. Thus, the lengths of the aluminium alloy 6063 specimens were 22 mm while the stainless steel AISI 316L rods were cut into 10 mm lengths as shown in Fig. 5.4. The faying surfaces of specimens were dry-turned, their roughness (Ra) being around 5 μm. Pre-forming with 2 mm length reduction of aluminium alloy 6063 was carried out in order to make a tight-fitting contact between the two materials and to avoid contamination at the weld interface. The time interval between the turning and pre-forming was kept to within 10 minutes. The preformed bimetallic specimen was then inserted in a specimen holder that restricted the formation of upset made near the weld interface.

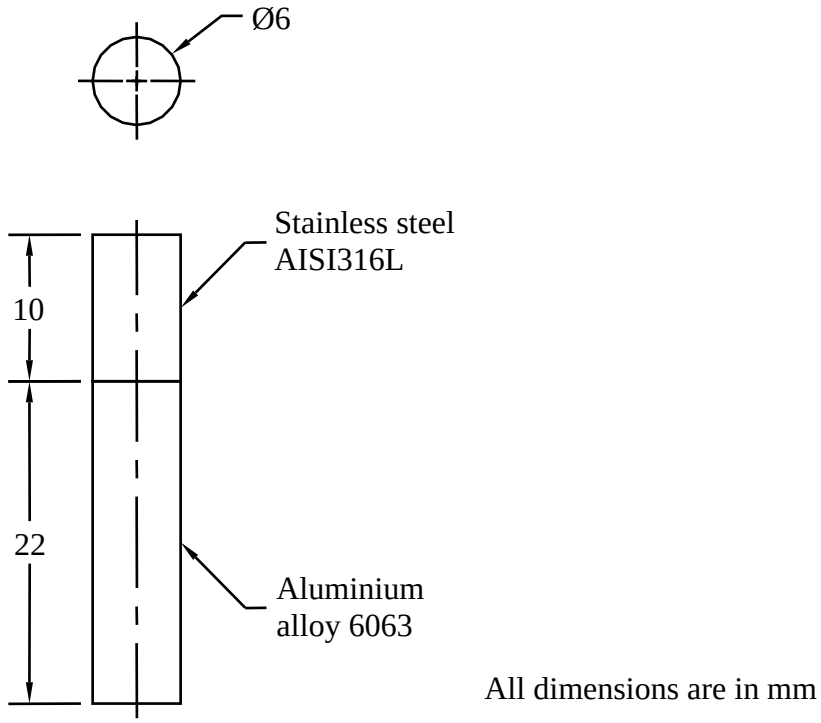

Fig. 5.4 The configurations of the specimens for the welding experiment.

(iv) For warm forming bimetallic components

A non-axisymmetric watch-case-like component was used as an example in the experiment, which demonstrates how to determinate the suitable process conditions of warm-forming bimetallic components. Figure 5.5 shows its configurations and detailed dimensions. Compared with most conventional axisymmetric formed components such as automotive break discs, valve heads, and wheel hubs, and other non-axisymmetric components, the shape complexity of this component was much greater (surface-to-volume ratio = 0.53) that increased the difficulty in manufacture as well as the determination of process parameters. Therefore, it was especially preferable as a typical example, which would provide useful information about the bulk-forming of such intricate bimetallic components. The scientific conclusion drawn through the analysis of both simulations and experimental results can also be generalised and applied to the forming of other bimetallic circular, axisymmetric, or hollow axisymmetric components.

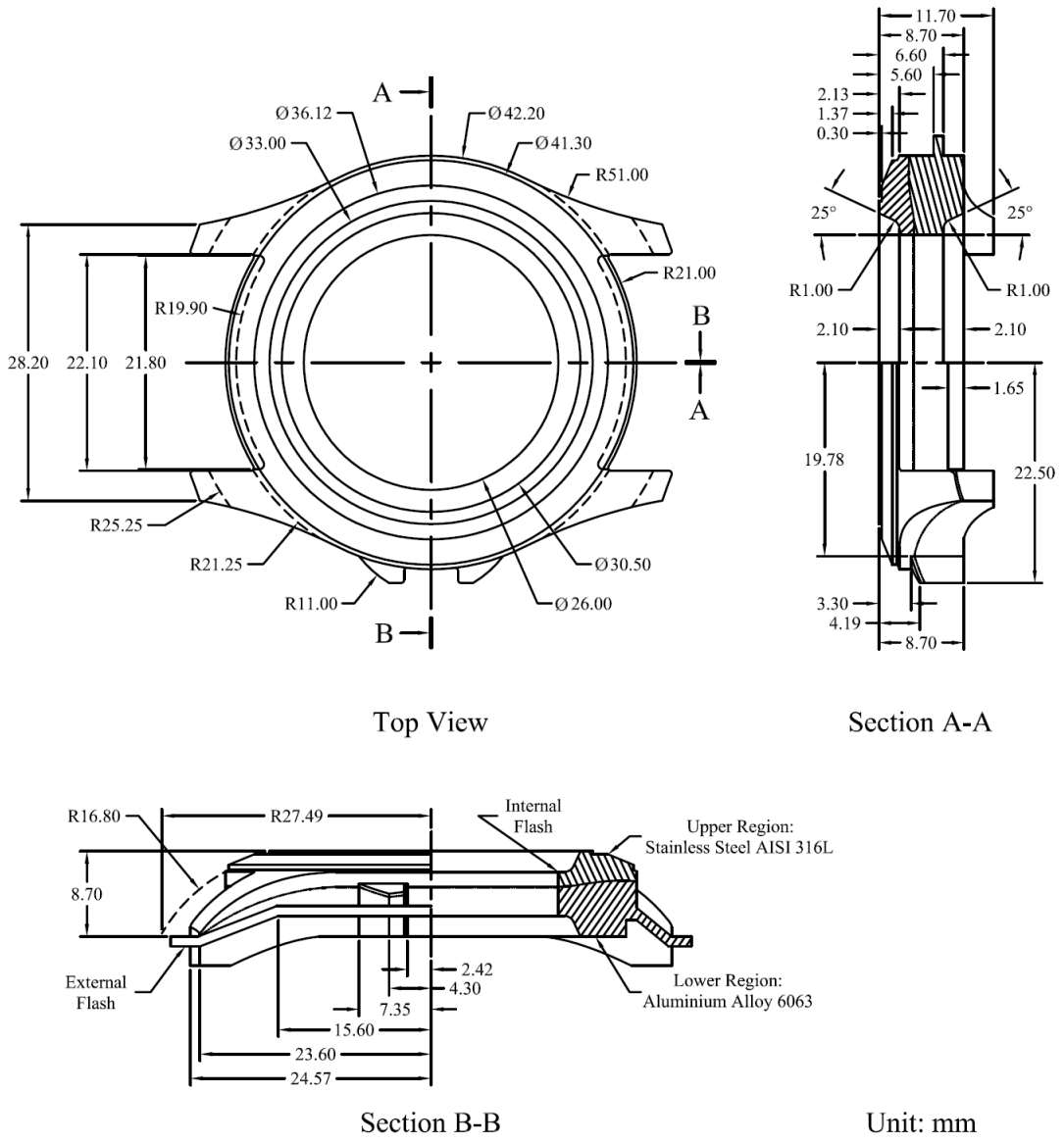

Fig. 5.5 The final shape of bimetallic non-axisymmetric component.

This component can be produced by the closed-die forging process in one single stroke. Parting lines of the die were placed at the area with the largest cross-section, center-hole, and around the entire perimeters that was based partially on the gain-flow considerations [8,32-37,122]. Flashes were extruded accordingly at the parting lines after the die cavity had been filled completely. In order to reduce the scrap rate, the external flash thickness was minimised as 1.0 mm. Indeed, the flash thickness is an

important factor influencing the die filling and forming load. The flash land on the die becomes smaller by decreasing the flash thickness that leads the restriction of metal flow and increases the frictional forces. Since metal always flows along the path with the least resistance, the die cavity should be filled before the excess material is extruded to the smaller flash land. A larger forming load is also required to compress the metal into the thinner flash. The detailed information about the flash design can be found in references [8,32-37,122]. The influence of flash thickness is expected and understood reasonably well from a qualitative viewpoint, hence the analysis of flash thickness on the die filling and forming load has been excluded from this experimental study.

The upper region and the lower region of the component were made of 3 mm thick stainless steel AISI 316L and 6 mm thickness aluminium alloy 6063 respectively. In other words, the lower preform was the stainless steel AISI 316L and the upper preform was the aluminium alloy 6063. Figure 5.6 is the design of the hollow bimetallic preforms. The component was hollow having a center hole. The preforms were constructed accordingly as the hollow shapes in order to reduce the forming load greatly [32]. An identical outer profile along the thickness of the preforms was shrunk by 0.2 mm from the outer profile of the component. This led the preforms that could be fitted properly inside the cavity of lower die as shown in Fig. 5.7. The volume of the component with expected flashes was approximately 8380 mm^3. While the whole component was made of stainless steel AISI 316L, the weight was around 66.2 grams. In this example, nearly 66.3 % of volume of the component was made of aluminium

alloy 6063. The weight of the component could be reduced to 37.3 grams with around 43.6 % of weight reduction, whilst the stainless steel AISI 316L upper region could provide better wear resistance as well. This was a good applicable instance to reveal the benefits and advantages of using bimetals in metalwork. The trial performs were produced by EDM wire cutting. Their faying surfaces were machined and ground by sand paper and then cleaned in acetone and alcohol prior to forge welding.

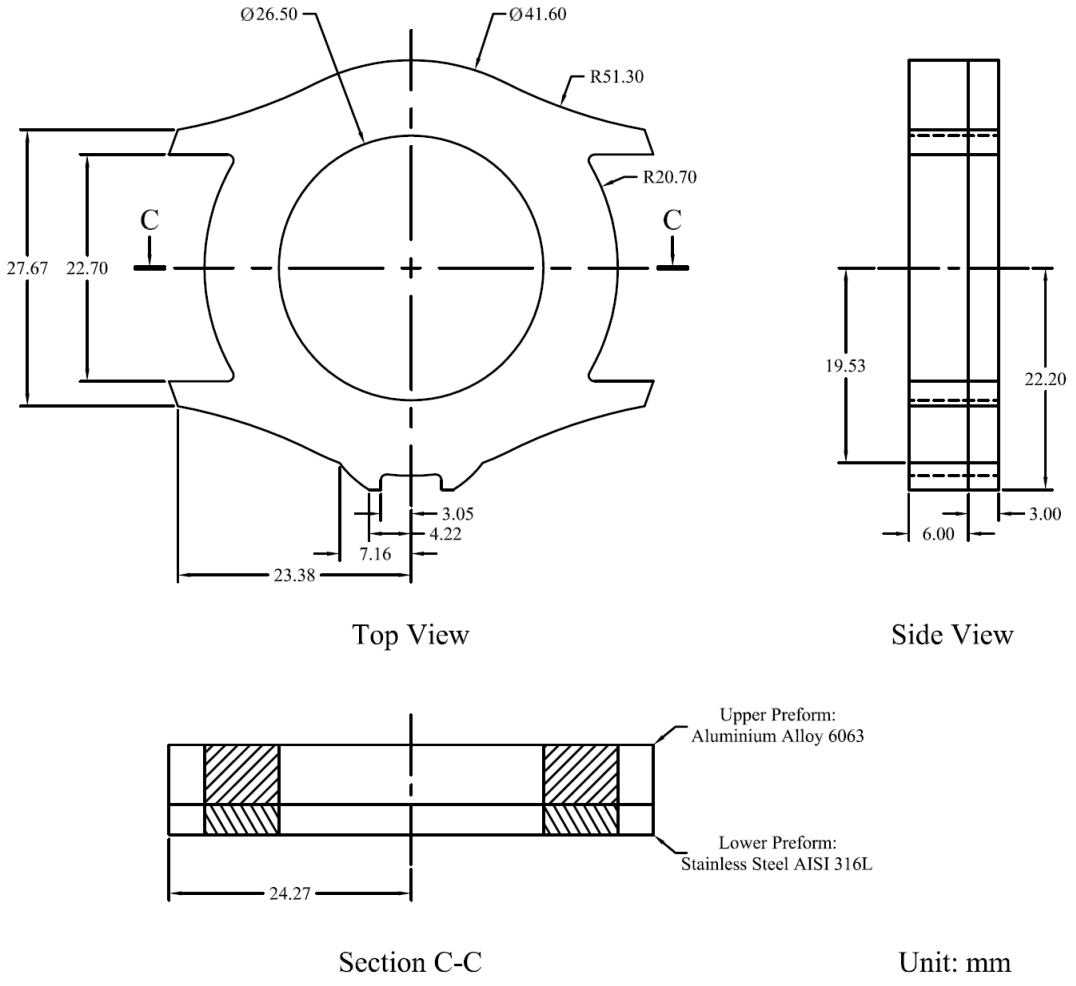

Fig. 5.6 The proposed design of the hollow bimetallic preforms.

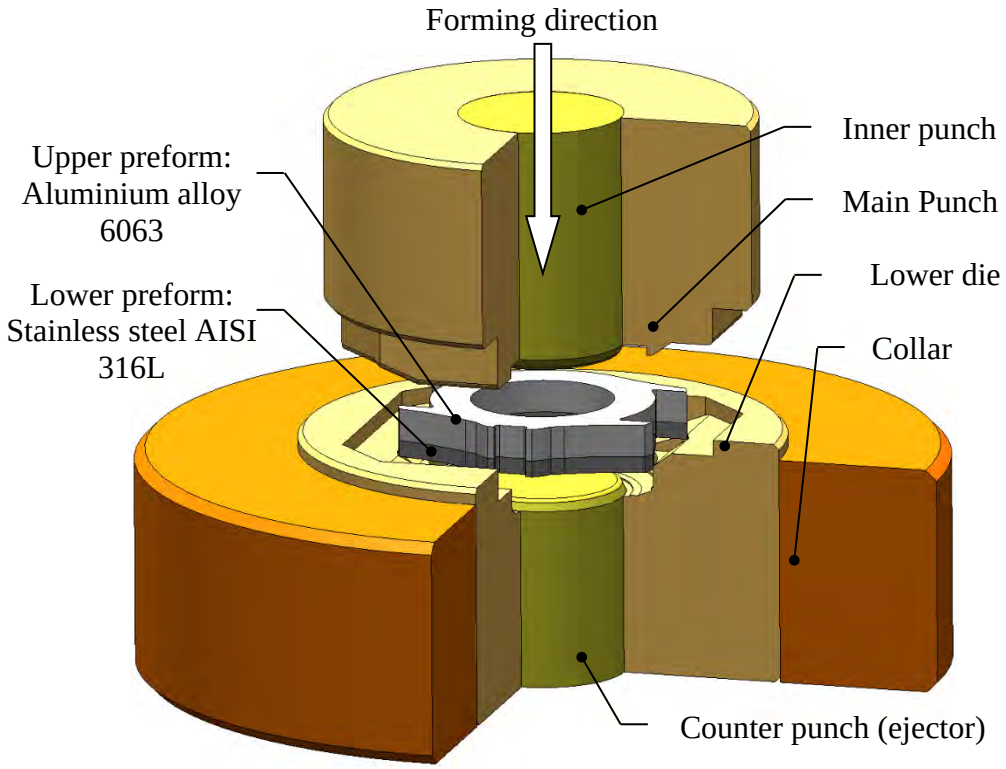

Fig. 5.7 The preforms should be fitted properly inside the cavity of lower die.

(v) Specimen shapes for reverse simulation and its experimental verification

Three case studies were carried out to evaluate the reverse simulation approach. The configurations of the final shapes of the finished components are shown in Fig. 5.8. The components of the case studies 1 and 2 were similar. Their main difference was the existence of a center hole that could influence the design of the billet as a non-hollow shape (i.e., a cylinder) or hollow shape (i.e., a ring). Aluminium alloy 6063 was used as the specimen material in these two cases. The dimensions of the component of the case study 3 were the same as those of the case study 2. However, the case study 3 aimed to form a bimetallic component which was made of aluminium alloy 6063 and stainless steel AISI 316L.

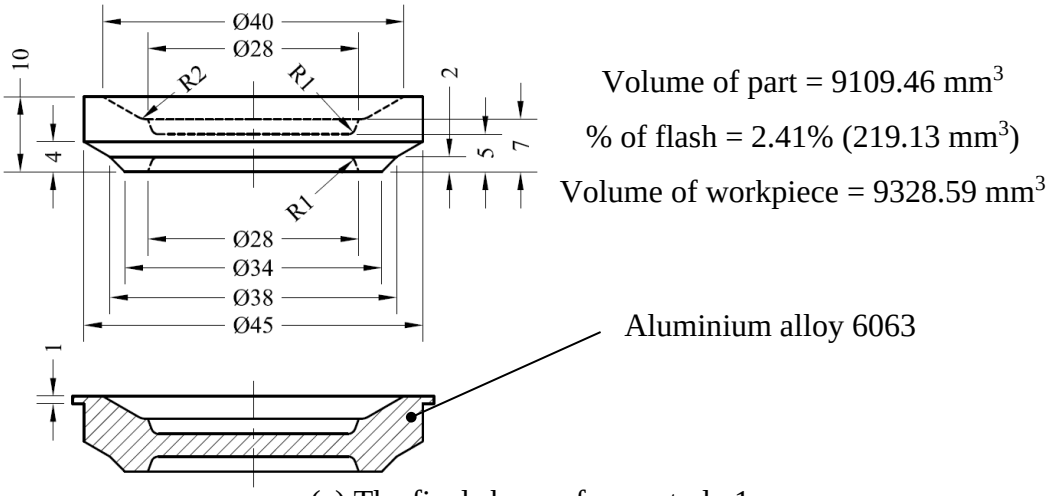

(a) The final shape of case study 1

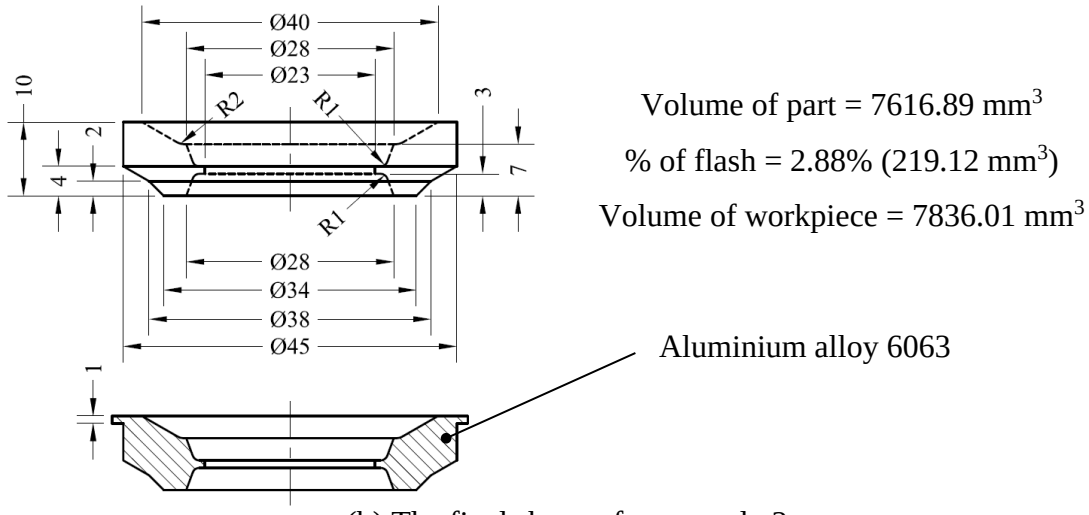

(b) The final shape of case study 2

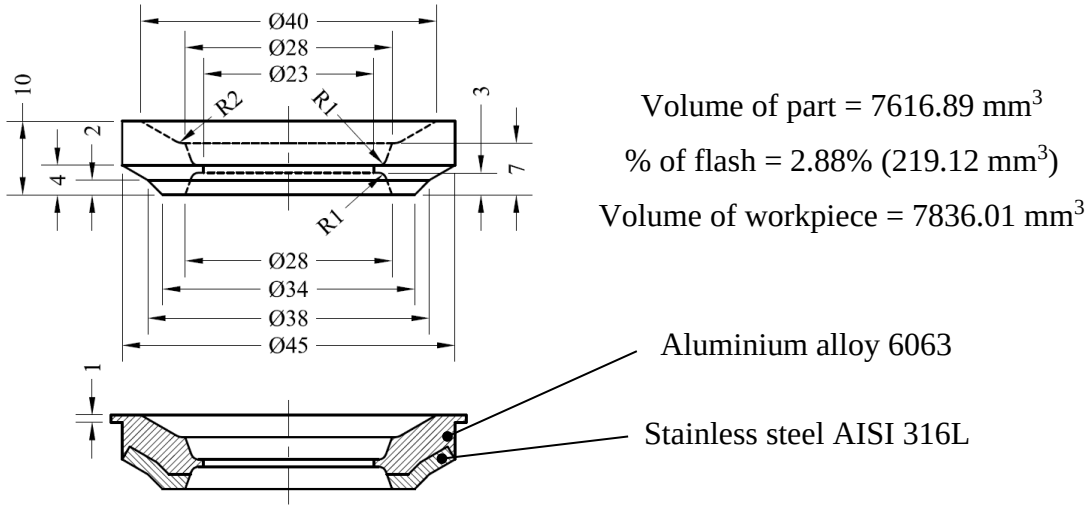

(c) The final shape of case study 3

Fig. 5.8 The final shapes of axisymmetric components used in the case studies for evaluation of the reverse simulation approach.

Those geometry were simplified from a watch-case-like component (a three-dimensional non-axisymmetric component) as illustrated in Fig. 5.9, so that the results could serve as valuable reference for the future study on such three-dimensional forming problems. Indeed those formed components with simple geometry could be made by one-stage forming with appropriate process conditions. The case studies concentrated on predicting the billet for a one-stage forming and understanding differences between the theoretical reverse and forward simulations and the practical work. The study had been regarded as a formed component produced with a minimal flash by determining a suitable billet size to form the final shape, although in practice flash might be required to permit variations in billet volume.

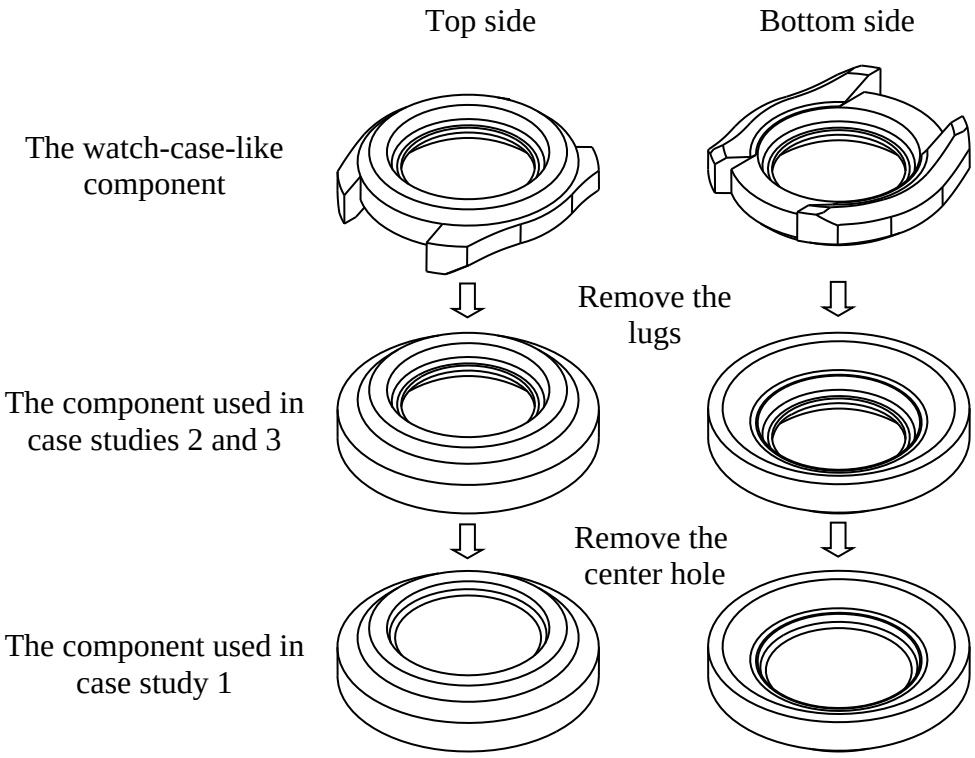

Fig. 5.9 The final shapes of components used in case studies of reverse simulation were simplified from a watch-case-like component.

5.1.2 Tooling setup

(i) For uniaxial compression test

The setup of equipment for the uniaxial compression test is shown in Fig. 5.10. An Instron material testing machine and a MTS machine were selected for testing the aluminium alloys 6063 and stainless steel AISI 316L respectively. These two instruments were capable of monotonic loading at servo-controlled cross-head speeds of 0.002 to 15 mm/s. This is good enough to compress the specimens with acceptable strain and strain rate values. The heating methods of the uniaxial compression tests for the two materials were different. The aluminium alloy 6063 and stainless steel AISI 316L were heated by a furnace and induction heating respectively. This is because the effect of magnetic fields generated by induction on aluminium alloy is weak (i.e. low efficiency). On the other hand, the furnace cannot be operated at the test temperatures for stainless steel. In the test of stainless steel AISI 316L, The specimen, placed inside an induction coil, was heated up to the testing temperature and it was kept constant throughout the test period. The circular induction coil had five turns of copper tube of 6 mm diameter. The inner diameter of the coil was 32 mm. Pitch between each turn was 1 mm. This gap allowed an infra-red non-contact thermometer, IR-FA series fibre, to point to the specimen inside the coil and monitor its temperature. The setup used three infra-red type thermometers. Accuracy was within ±5 °C as validated by a thermocouple thermometer. One infra-red thermometer was used to measure the temperature of the specimen while the other two used to measure temperatures of the

two ceramic insulators linking the specimen and the punches. The ceramic insulators were both made of high-purity (94.5 %) alumina (i.e., aluminium oxide, Al_2O_3) which is an extremely hard material and is generally used for grinding and polishing of hard materials. It was able to withstand high compressive strength of up to 1200 MPa. Alumina was non-metallic and could not be heated by the induction. The contact surfaces of insulator had been polished that ensured the geometric conformance of the alignment between the specimens and the loading axis. One end face of the ceramic insulator acted as a platen that allowed the specimen to be placed on it. Another end face made contact with the punch. A lower punch and an upper punch were screwed on the cross-head and the top mount of the MTS machine. They were made of hot-working tool steel AISI H13. Comparing to the stainless steel AISI 316L, tool steel AISI H13 was relatively strong in both cold and hot working conditions. In order to avoid the loss of accuracy when the load cell and other instruments were overheated, some holes were drilled on the punches to let water flow through within them. Since the alumina could not be easily machined, two mild steel holders were made for connecting the ceramic insulators and the punches.

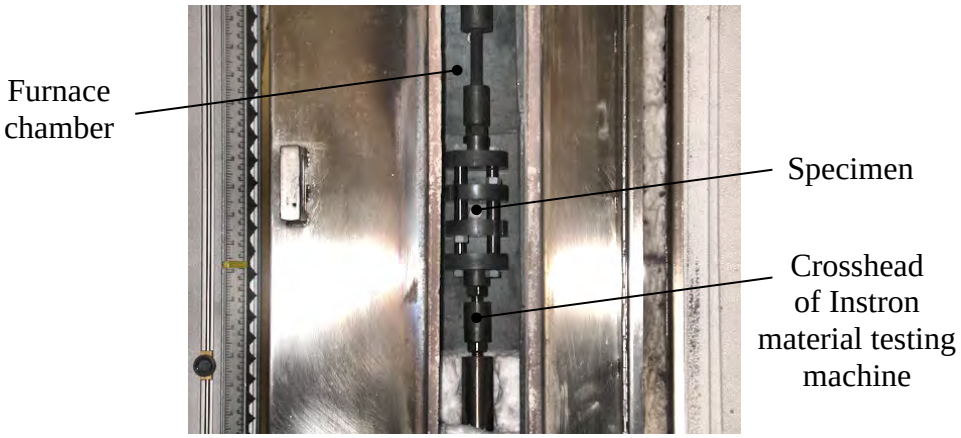

(a) The aluminium alloy 6063 is compressed in the furnace

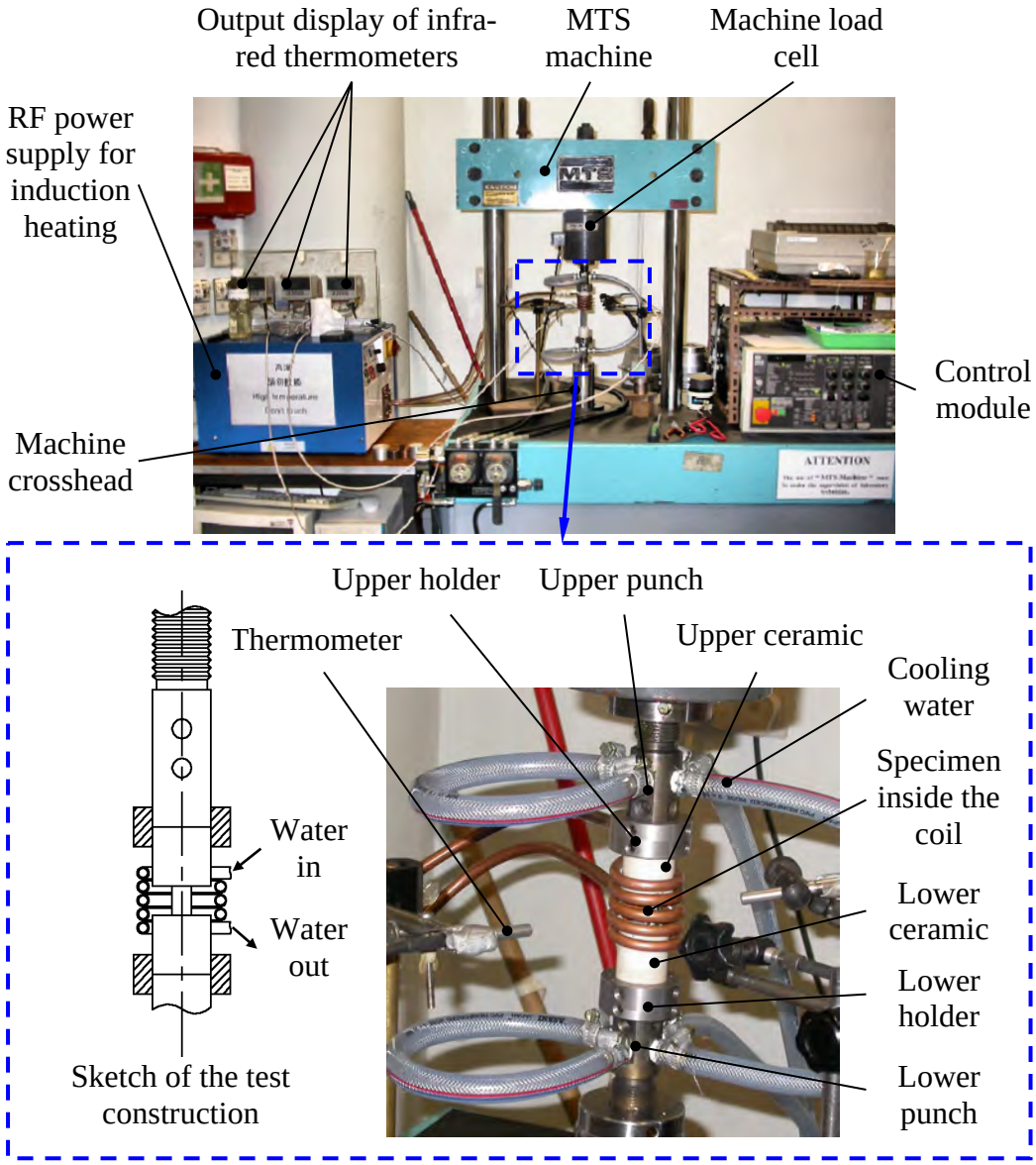

(b) The stainless steel AISI 36L is compressed under induction heating

Fig. 5.10 Experimental setup of uniaxial compression tests.

(ii) For ring compression test

The equipment and tooling used in the ring compression test were the same as those used in the uniaxial compression test for aluminium alloy. The fixture shown in Fig. 5.11 was made of hot-working tool steel AISI H13. It was connected to the crosshead of the Instron material testing machine to transform the tensile load into a compressive load. Likewise, the operation was performed inside the closed furnace chamber as an isothermal condition.

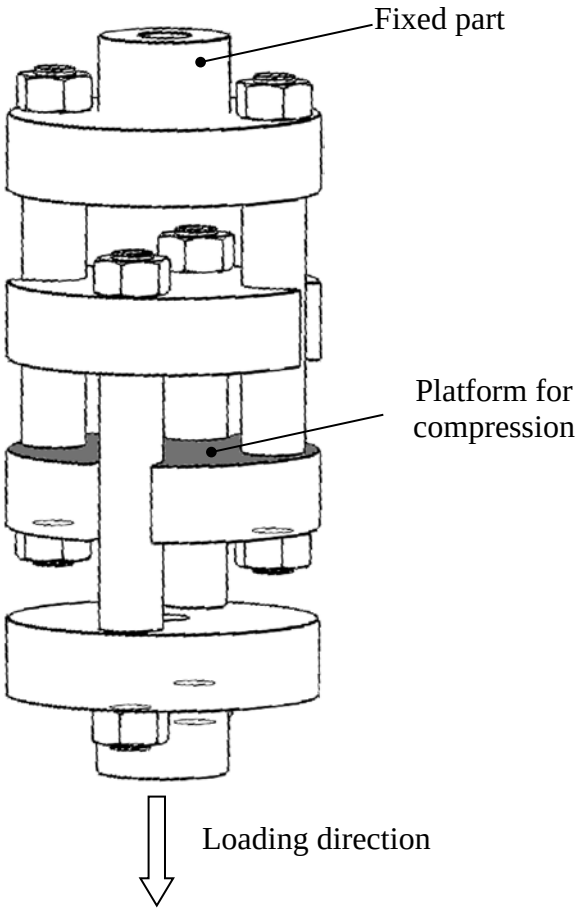

Fig. 5.11 The fixture used in the compression tests

(iii) For welding experiment

It is complicated to use fusion-welding processes such as manual-arc welding and metal inert gas welding to coalesce dissimilar metals (i.e., aluminium alloy and stainless steel in the case of this study) together because of their different melting temperatures and material microstructures. Certain metallurgical aspects have to be taken into consideration, including different fusion boundary regions and heat-affected zone (HAZ) effects [10]. Solid-state welding is another group of welding processes which use heat and pressure (or deformation) to weld either similar or dissimilar metals. Diffusion of elements occurs without melting of the parent metals so that effects on the heat-affected zone and metallurgical changes of the welds are minimised. These processes are particularly suitable for welding dissimilar metals rather than fusion welding [10,114-118].

Diffusion welding (or diffusion bonding) is one kind of solid-state welding process. It has been developed over many years to weld dissimilar metals. However, since this process has the limitations of a long processing time (from half an hour to several hours) and specific work environments such as vacuum and shielding gases, it is not used commonly on an industrial scale requiring high production rates [123,124]. According to the British standards: BS499-1:1991, hot-pressure welding, forge welding, and friction welding are other solid-state welding processes at the same technological level. In these the metals are heated to the welding temperature and then a force or pressure is applied to cause plastic deformation at the joining surfaces. An intermetallic bond is created by diffusion to coalesce the dissimilar metals. The heating

method used in hot pressure welding and forge welding is either induction heating or flame; it is likely the heat applied in friction welding is generated by the rotational friction between the workpieces pressed together. Compared to diffusion welding, their processing times are relatively short (within two minutes) and work environments are less stringent [125-127]. Nevertheless, the applications of friction welding are limited due to its poor adaptability to the shapes of the workpiece. Table 5.3 compares different solid-state welding processes, in which the comparative advantages of hot pressure welding and forge welding are identified. If a large amount of deformation of the workpiece is permitted, these two processes are more efficient than others such as friction welding and diffusion welding for making arbitrary shapes of bimetals. According to this point of view, two metals can be welded and formed simultaneously, as warm-forming bimetallic components.

Table 5.3 A comparison between different solid-state welding processes.

Criterion	Hot-pressure welding	Forge welding	Friction welding	Diffusion welding
Joint configuration	Butt, lap, and tee joints	Butt, lap, and tee joints	Butt and tee joints	Butt, lap, and tee joints
Geometry of workpiece	Regular /irregular	Regular /irregular	Axisymmetric	Regular/ irregular
Processing time	Short (< 2 minutes)	Short (< 1 minute)	Short (< 1 minute)	Long (> 45 minutes)
Diffusion rate	High	High	High	Low
Deformation of workpiece	Large	Large	Moderate	Very small
Specific work environment	No	No	No	Yes

The operations and principles of hot pressure welding and forge welding are similar. Their main difference is that the welds of hot pressure welding are produced by isostatic pressures while forge welding makes use of hammering or other impulsive forces. Presses (i.e., forming machines) are used in hot pressure welding and forge welding in addition to the heating devices. Hydraulic presses and mechanical presses are the most common facilities for providing isostatic pressures (for hot pressure welding) and impulsive forces (for forge welding) [114-118].

The presses employed in the hot pressure welding and forge welding experiments were a mechanical press and a hydraulic press respectively. These could both provide a maximum 160-ton load capacity. The ram speed of the hydraulic press was around 10 mm/s and that of the mechanical press was variable by the cycle rate of

35 strokes per minute (spm), so that the average punch speed was 30 mm/s approximately within the forming stroke. Figure 5.12 shows the experimental setup of different welding processes.

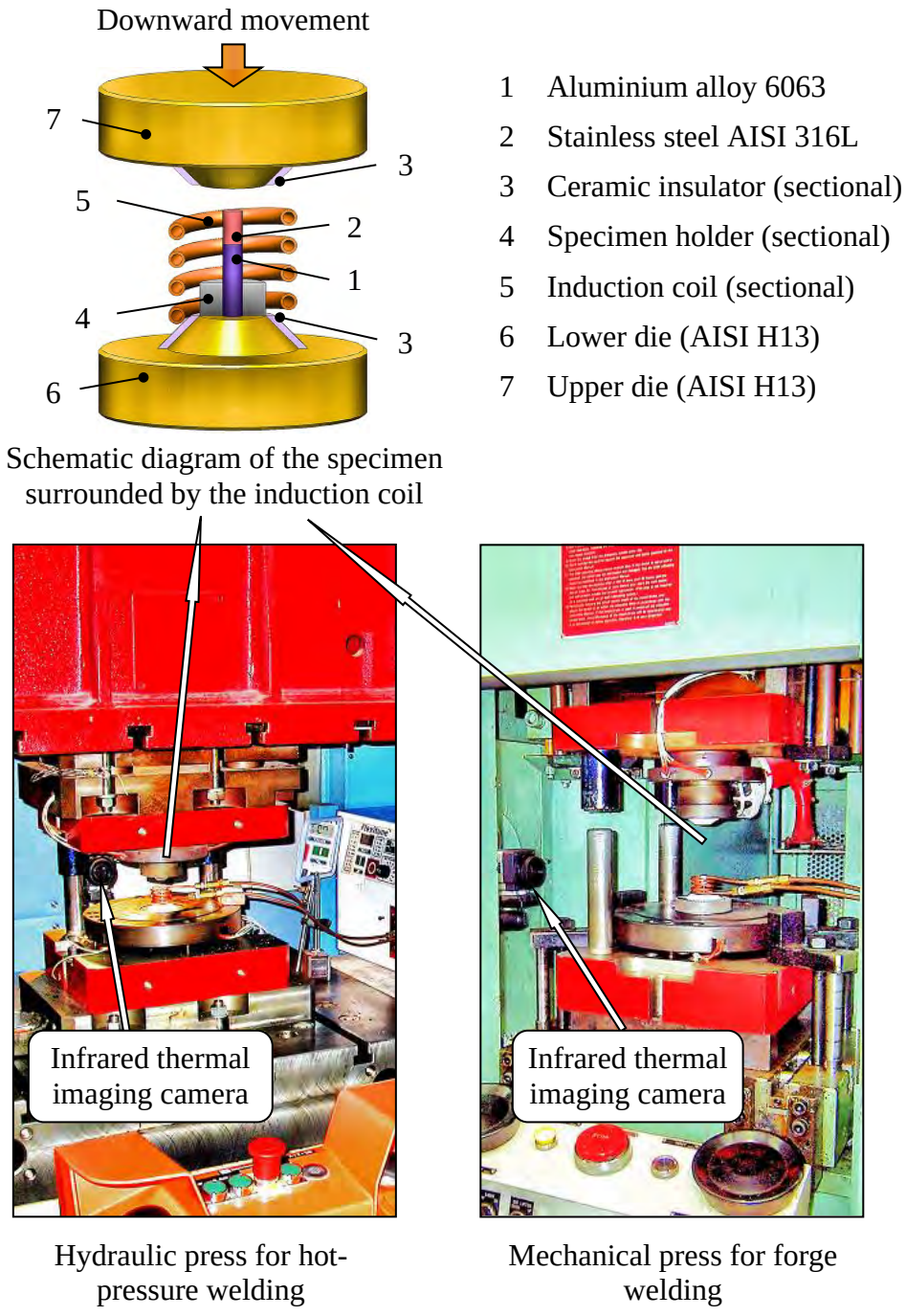

Fig. 5.12 Experimental setup for hot-pressure welding and forge welding.

(iv) For warm forming bimetallic components

The experiment of warm forming bimetallic components was carried out using a 300-ton mechanical press. The ram speeds of average 20, 40, and 60 mm/s could be achieved (these are the average values within the effective forming stroke) by interchanging the belt and pulley system that were connected to the motor and flywheel of the machine. A radio-frequency power supply and an induction coil were used to heat the stainless steel AISI 316L preforms up to the test temperatures. The temperature was then monitored by an infra-red thermal imaging camera during the first instant of the forming operation. The exact-focus images were target-captured for the heated specimens in order to ensure the achievement of more accurate and reliable results. A load cell consisted of four strain gauges in a Wheatstone bridge configuration that was installed above the upper-die assembly to record the peak of the forming load. Figure 5.13 shows the overall setup of the equipment. Heat-treated hot work tool steel W302 (equivalent to AISI-H13) was used as the tooling material since this can provide good temper resistance and superior strength under warm-forming conditions. A lubricant was spread over the surfaces of the lower die. After the forming process, the dimensions of the formed components were measured by a digital vernier calliper and a height gauge. Some joint interfaces were taken from the selected components, which were inspected by the optical microscope in order to evaluate the diffusion zone between two dissimilar metals.

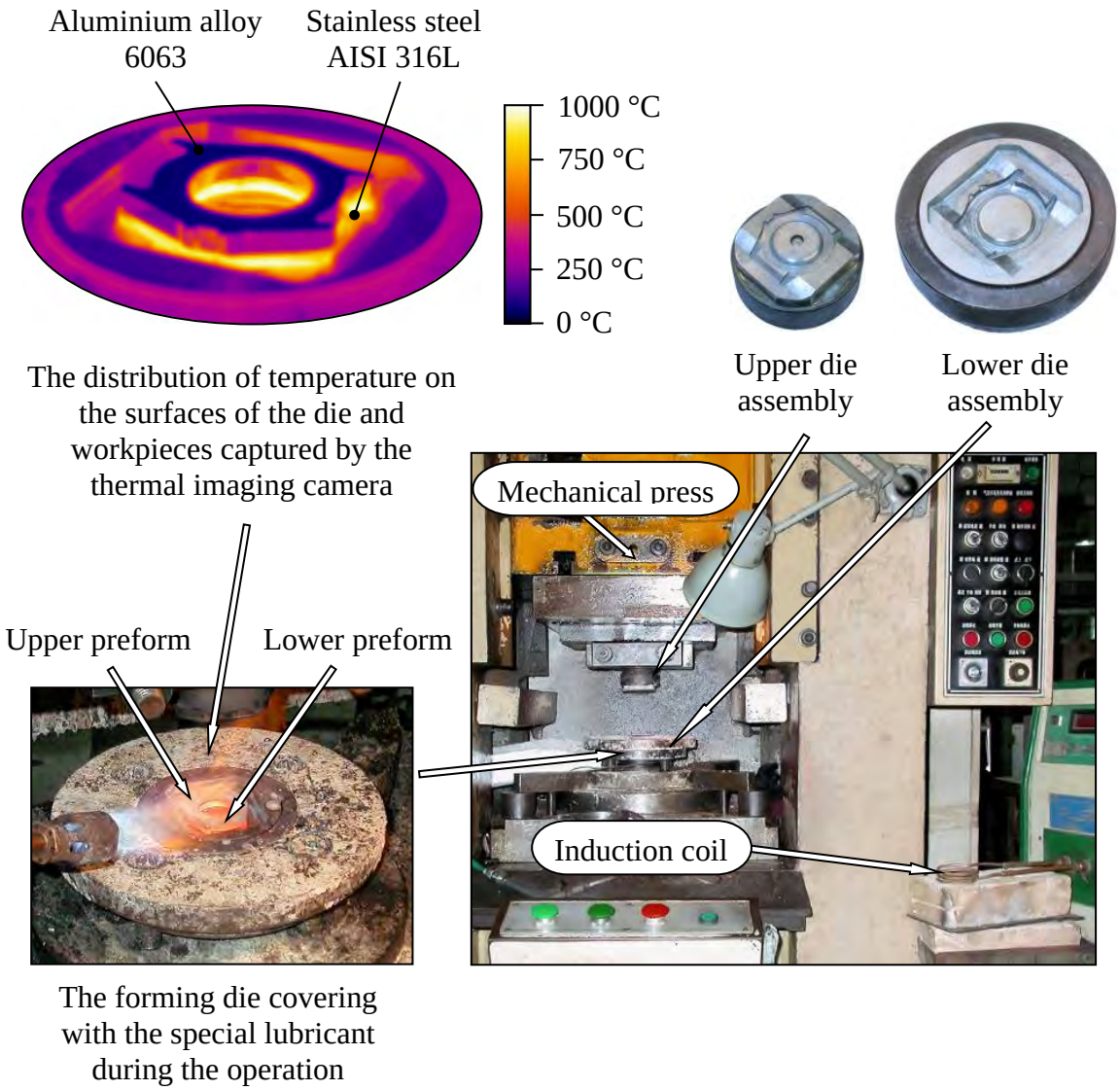

Fig. 5.13 The experimental setup for warm forming bimetallic components.

(v) For experimental verification of reverse simulation

A computer-controlled hydraulic press and a data acquisition system were used for another practical warm-forming experiment. The press is capable of a forming force of 160 tons and a constant ram speed of 40 mm/second. A load cell (with a strain gauge) was fixed between the ram and the top die, and connected to a computer with an interface to record the forming load. Calibration of the load cell was carried out by

the MTS machine. The displacement of the top die was measured by a low voltage displacement transducer (LVDT) during the process. Figure 5.14 shows the hydraulic press and the temperature control system which were used to carry out the warm-forming experiments in this study.

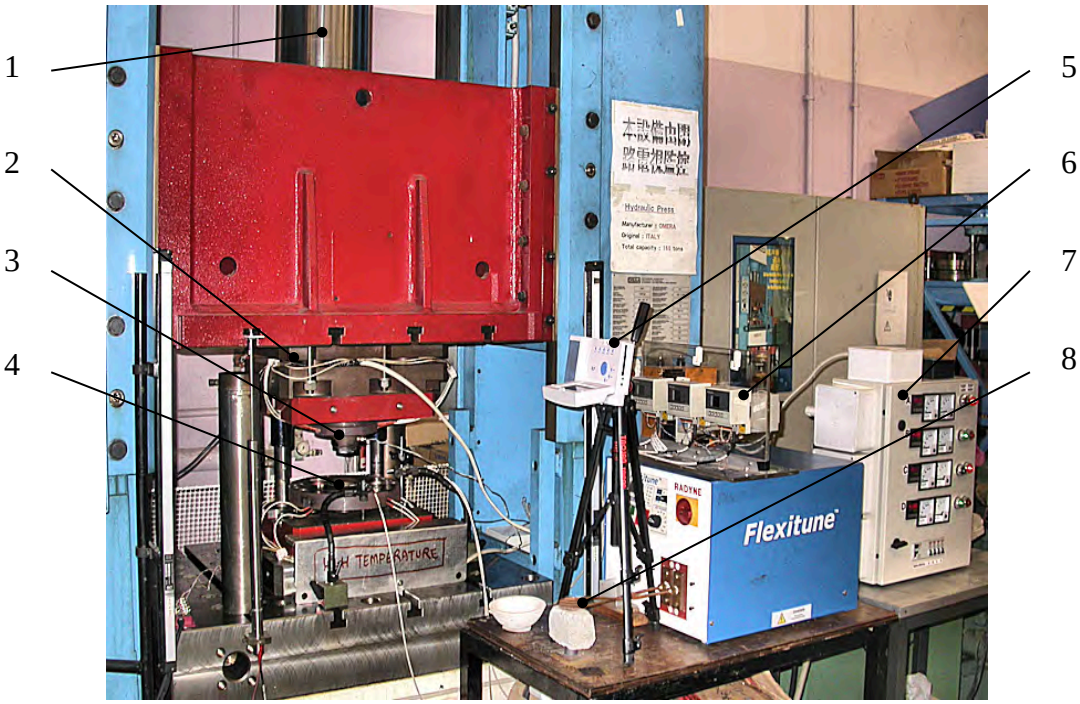

1	Ram of hydraulic press	5	Infra-red thermal camera
2	Load cell	6	Infra-red thermometer
3	Top die (with heaters)	7	Power supply for heaters
4	Bottom die (with heaters)	8	Induction coil

Fig. 5.14 Hydraulic press and temperature control system.

Heat-treated hot work tool steel W321 (equivalent to AISI-H13) was used as the tooling material. Like the tool steel W302, it can provide good temper resistance and superior strength under warm-forming conditions. Figure 5.15 shows the actual die set.

In order to maintain the isothermal condition, both the top die and bottom die were inserted into four cartridge heaters (i.e., eight heaters totally) that were connected with the power supply constructed by the temperature regulator circuits. Two Infra-red-FA series fibres were used as the temperature detectors to check the specimen and die temperatures. The temperature of the material is one of the key factors in the success of isothermal warm forming as it influences the flow stress of the material greatly. Consequently, it must be calibrated regularly and monitored frequently.

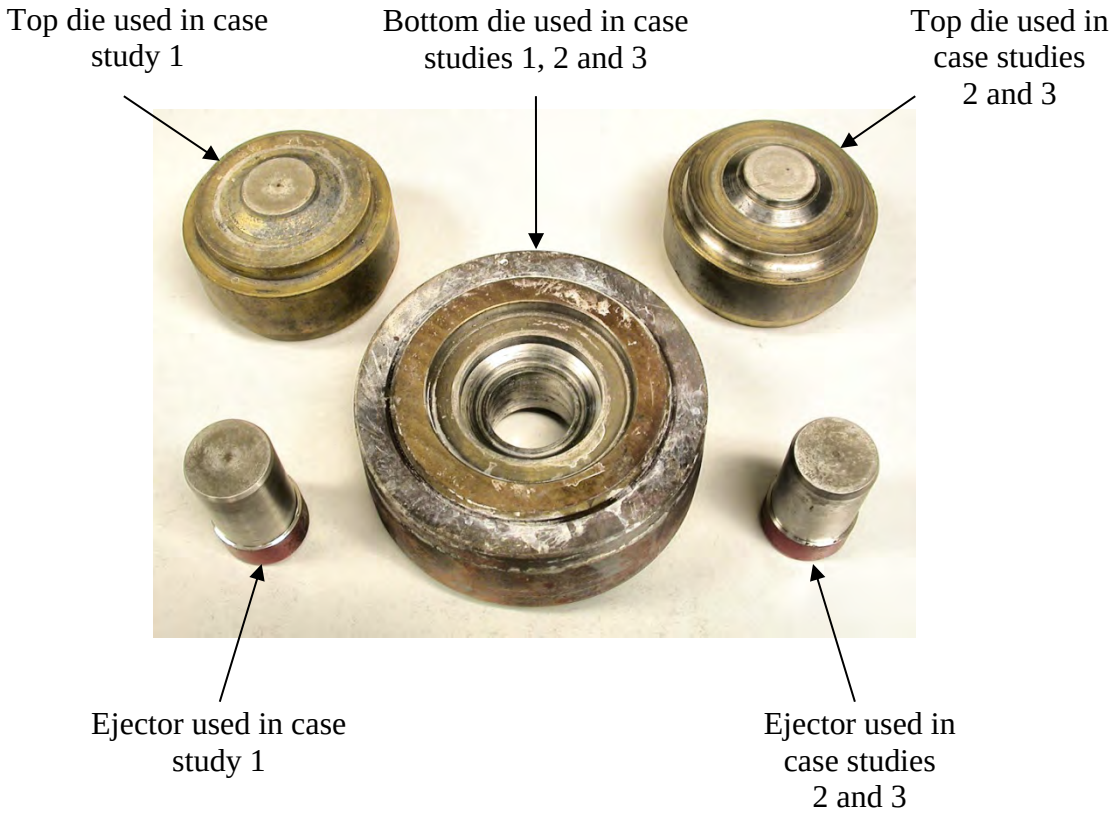

Fig. 5.15 The warm-forming die set used for experimental verification.

5.1.3 Experimental procedures

(i) For uniaxial compression test

The flow stress data of aluminium alloy 6063 and stainless steel AISI 316L were acquired by the uniaxial compression test. The test had to be conducted without less barrelling at the strain value ≤ 0.5 for both the materials. Aluminium alloy 6063 was tested at 20, 100, 200, 300, 400, and 500 °C, covering strain rates of 0.1, and 1 /s. Stainless steel AISI 316L was tested at same strain rates at 400, 500, 600, 700, 800 and 900 °C. The displacement limits of the Instron material testing machine and the MTS machine were set to 4.5 mm. And the output loads were restricted to 9.5 kN and 75 kN for safety consideration in the tests of aluminium alloy 6063 and stainless steel AISI 316L respectively. The graphite-based lubricant was applied to the contact surfaces of the specimens. It was essential to limit or minimise the barrelling effect.

(ii) For ring compression test

The ring compression test developed by Male and Cockcroft [128] is probably the most widely used method to determine friction factors in metal forming. By compressing a hollow ring, the change in the internal diameter with decreasing height is determined. The method involves measuring the variation of diameter with height, which depends on the friction between the ring and the die surface, and provides a sensitive response to friction effects [129].

Two tests with five incremental steps for each condition, dry or without lubrication, were carried out with up to about 50 % of reduction in height at 300 °C. In the cases with lubrication, the lubricant W-400 was used. This is a water-soluble-based made by Korea Lube Tech Co., Ltd. It is a non-polluting, liquid lubricant that overcomes the environmental disadvantages of graphite lubricant.

(iii) For welding dissimilar metals

It was expected that the hot pressure welding and forge welding would be suitable for welding the dissimilar metals and the forming bimetallic components. Nevertheless, information about both processes for dissimilar metals is quite rare, as most studies focus on welding similar metals [126,130-134]. The selection and control of process parameters must be explored. In addition, the diffusion of elements between two metals has to be significant to ensure a successful weld. This is one critical criterion for evaluating the effectiveness and weld quality of the solid-state welding processes. Therefore this study used a diffusion analysis of forming bimetallic components under hot pressure welding and forge welding processes, which were performed at various welding temperatures T_w and depth of deformation H_w. The strengths of their welds were evaluated by uniaxial tensile tests. The metallography of diffusion zones was observed by scanning electron microscopy (SEM). Energy dispersive X-ray spectroscopy (EDX) and X-ray diffraction (XRD) were used to investigate the element composition and intermetallic compounds respectively. To examine the reliability of these two solid-state welding processes, statistical

experimental methods were used. This methodology enables interpretation of the variation in findings, and the determination of the process parameters that have the more significant effects on the process centering and spread. From these results, it is possible to gain a better knowledge about how to produce good-quality bimetallic components as well as the selection of appropriate process parameters in the numerical simulation.

The preformed bimetallic specimen was then inserted in a specimen holder that restricted the deformation of upset made near the weld interface. The specimen was heated by an induction coil connected with the radio-frequency power supply while an infra-red thermal imaging camera was recording and monitoring the change of temperature. The induction heat was interrupted when the welding temperature was reached. The specimen was then compressed by either the mechanical press or the hydraulic press.

The fundamental elements influencing the hot pressure welding and forge welding are heat and pressure, because sufficient energy and plasticity (plastic deformation) are necessary to generate the intermetallic bond at the weld interface. However, the pressure could not be adjusted by the test equipment directly. It was substituted by forming deformation H_w as illustrated in Fig. 5.16, whereas another process parameter, welding temperature T_w, was controlled by using the radio-frequency power supply. The test conditions for the two experiments were nearly similar. Both of them were conducted at T_w = 350, 400 and 450 °C and H_w = 4, 6, and 8 mm (i.e., nine trials of combinations). The main differences in the two processes

were the ram speeds of the presses and the 60-second holding time applied in hot pressure welding.

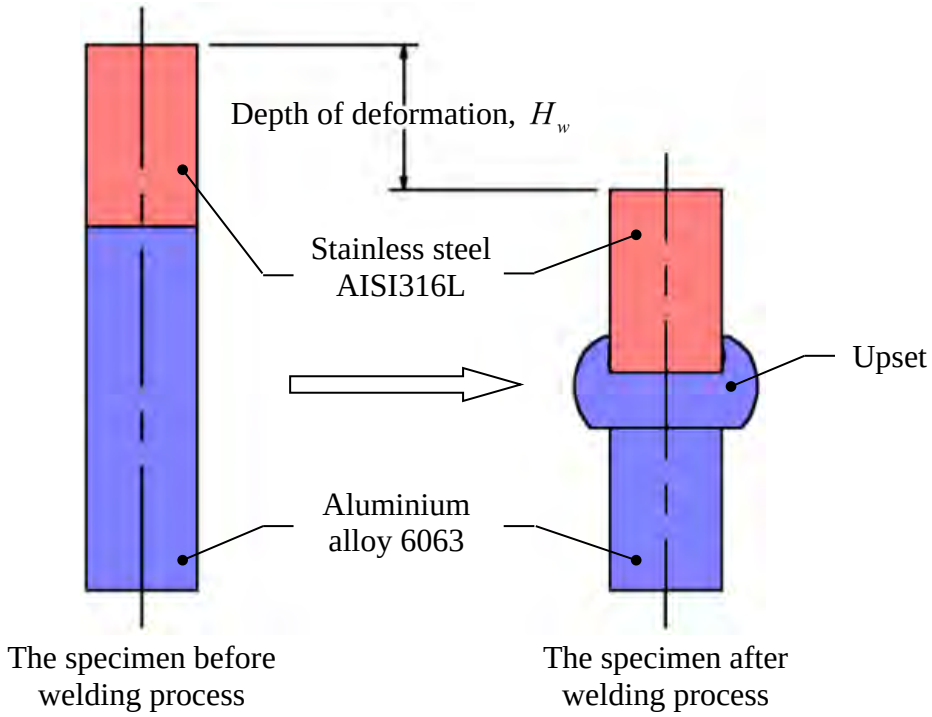

Fig. 5.16 Explanation of depth of deformation H_w.

The welds were evaluated by carrying out the tensile tests and metallographic observation. The uniaxial tensile tests were performed by the MTS machine at room temperature with a constant actuator speed of 0.1 mm/s. The upsets of bimetallic components resulting from both welding processes were removed by turning prior to the tensile tests, which prevented them from influencing the results. Metallographic specimens were cut longitudinally from the weld interfaces. The cross-sections of the interfaces were mounted in epoxy resin. Their surfaces were ground by abrasive papers and polished by cotton cloths. These polished specimens were then observed by SEM so that the diffusion zones and weld continuity could be identified. The EDX was

employed to obtain the compositions of the common elements of two dissimilar metals including silicon (Si), manganese (Mn), chromium (Cr), iron (Fe), and aluminium (Al) across the diffusion zone. The presence of the Fe and Al intermetallic compounds was confirmed by XRD analysis.

(iv) For warm forming bimetallic components

During the bimetal bulk-forming process, the discrepancy of flow stress of two different materials might cause the heterogeneous material flow, which should be minimised by the control of process parameters. At the same strain rates, the flow stress of austenite stainless steel, at 900 to 1100 °C, is close to that of aluminium alloy at 20 to 300 °C [121,135,136]. It was supposed that the heat transfer occurred at the contact surface between the two specimen materials. Hence, in this study, the experiments were conducted with the forming temperatures of stainless steel AISI 316L of 400, 500, 600, 700, 800, and 900 ºC and punch speed of 20, 40, and 70 mm/s when the temperature of aluminium alloy was 20 ºC.

A series of bimetal bulk-forming process simulations were modelled using the commercial finite-element simulation software DEFORM-3D version 6.1 [121]. The program was able to perform the non-isothermal three-dimensional rigid-plastic/viscoplastic analysis of massive deformation. The von-Mises flow criterion was employed. The models for the bimetallic system were created by two separated rigid-plastic objects. A penalty-based contact constraint was added between those two specimen materials. All tool components were assumed as rigid-body objects. In order

to improve the accuracy of material-flow prediction, all geometric models had been halved so as to speed up computations and increase the number of tetrahedral meshes for each volume. Table 5.4 is the summary of the simulation conditions.

Table 5.4 The summary of the process conditions for simulation of warm-forming bimetallic components.

Simulation parameter	Value/setting
Number of mesh of stainless steel	10850
Number of mesh of aluminium alloy	38855
Thickness of stainless steel preform [mm]	3
Thickness of aluminium alloy preform [mm]	6
Iteration method	Direct method
Deformation solver	Sparse
Temperature solver	Sparse
Preform/tool shear friction factor	0.2
Heat-transfer coefficient between each object [$MW/m^2 \cdot K$]	11
Forming stroke [mm]	11
Temperature of main punch and inner punch [°C]	20
Temperature of lower die and ejector [°C]	300
Initial temperature of stainless steel [°C]	400/500/600/700/800/900
Initial temperature of aluminium alloy [°C]	20
Punch speed [mm/s]	20/40/60

Corresponding simulations were run to their conclusions. The die-filling analysis at the end of forming stroke was based on the minimum distance between the formed component and the die cavity, which could be measured in the postprocessor of DEFORM-3D. The die-filling completion as well as the predicted forming loads of each trial were compared with those of the actual experiments as direct verification.

(v) For verification of reverse simulation

The modelling of the warm-forming bimetallic components by the reverse simulation approach required the material data and determined suitable processing conditions, which were obtained by the tests and experiments as mentioned. Therefore, the experimental verification could be carried out according to the simulation results that all the settings and conditions should have been compatible with or equivalent to those of the simulation.

5.2 Process modelling

The plastic deformation problem considers the kinematical velocity field in a continuous domain, in which most bulk-forming problems are difficult or even impossible to be solved. Thus the discretisation of the velocity field is required. The finite-element procedure is applied for this purpose.

The velocity field in the workpiece is distributed within each finite-element in terms of the values at nodal points using interpolation functions (i.e., shape functions).

The functions can be linear or nonlinear and depend upon the type of element. For increase the computing accuracy, four-node quadrilateral (rectangular) elements are used to model the bulk-forming problem in a discrete domain. The components of the velocity at each node become variables to define a bulk-forming problem with the boundary conditions.

In order to minimise the dissipation energy for plastic deformation, a set of non-linear equations are obtained. Since the equations are solved by the Newton-Raphson method, the formulations of the first and second derivatives with respect to each velocity component are required. These formulations which are based on a finite-element procedure are described in this chapter, which make a clear and complete presentation of the finite-element formulation for the plastic deformation problem.

5.2.1 Finite-element procedure

Finite-element discretisation with a quadrilateral element is using the cylindrical coordinate system (r, θ, z) instead of the rectangular coordinate system for a three-node triangular element. The element is a ring element with a quadrilateral cross-section, as shown in Fig. 5.17.

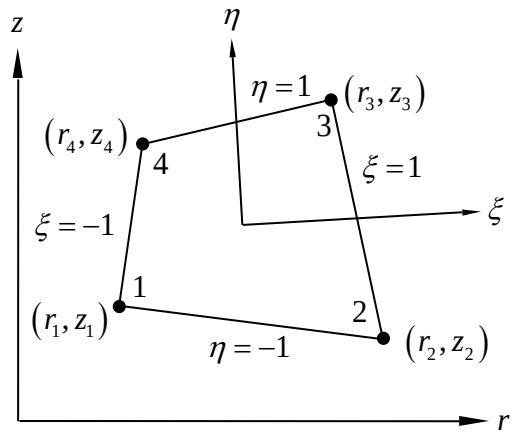

Fig. 5.17 Quadrilateral element and natural coordinate system.

The ξ and η of the natural coordinate system vary from – 1 to 1 within each element. An arbitrary point (r, z) inside the element can be expressed in terms of the natural coordinate (r, z) and the coordinate transformation is expressed by:

$$r(\xi,\eta)=\sum_{n=1}^{4} q_n r_n \tag{5.1}$$

and

$$z(\xi,\eta)=\sum_{n=1}^{4} q_n z_n \tag{5.2}$$

where r_n, z_n (n = 1, …, 4) are the positions of the four surrounding nodal points of an element in the global coordinate system. For an iso-parametric element of Fig. 5.1, transformation functions q_n, in equation (5.1) are the same as shape functions:

$$\mathbf{u}=\begin{Bmatrix} u_r \\ u_z \end{Bmatrix}=\mathbf{N}^{\mathrm{T}}\mathbf{v} \tag{5.3}$$

where T superscript represents transposition. The use of the transposition is only to facilitate the expression of formulations in matrix forms. The vector **u** and **v** are defined by their components according to:

$$\mathbf{u}^{\mathrm{T}} = \left\{ u_r\left(\xi,\eta\right), u_z\left(\xi,\eta\right) \right\} \tag{5.4}$$

$$\mathbf{v}^{\mathrm{T}} = \left\{ u_r^{(1)}, u_z^{(1)}, u_r^{(2)}, u_z^{(2)}, u_r^{(3)}, u_z^{(3)}, u_r^{(4)}, u_z^{(4)} \right\} = \left\{ v_1, v_2, v_3, v_4 \right\} \tag{5.5}$$

respectively, for the case of two-dimensional in-plane deformation. The shape functions can be expressed in the following simplified matrix form:

$$\mathbf{N}^{\mathrm{T}} = \begin{bmatrix} q_1 & 0 & q_2 & 0 & q_3 & 0 & q_4 & 0 \\ 0 & q_1 & 0 & q_2 & 0 & q_3 & 0 & q_4 \end{bmatrix} \tag{5.6}$$

The strain-rate vector is defined by:

$$\dot{\varepsilon} = \begin{Bmatrix} \dot{\varepsilon}_r \\ \dot{\varepsilon}_z \\ \dot{\varepsilon}_\theta \\ \dot{\gamma}_{rz} \end{Bmatrix} = \begin{bmatrix} \dfrac{\partial}{\partial r} & 0 \\ 0 & \dfrac{\partial}{\partial z} \\ \dfrac{1}{r} & 0 \\ \dfrac{\partial}{\partial z} & \dfrac{\partial}{\partial r} \end{bmatrix} \begin{Bmatrix} u_r \\ u_z \end{Bmatrix} = \mathbf{B}\mathbf{v} \tag{5.7}$$

The strain-rate matrix $\mathbf{B}$ in equation (5.7) is given by:

$$\mathbf{B} = \begin{bmatrix} X_1 & 0 & X_2 & 0 & X_3 & 0 & X_4 & 0 \\ 0 & Y_1 & 0 & Y_2 & 0 & Y_3 & 0 & Y_4 \\ P_1 & 0 & P_2 & 0 & P_3 & 0 & P_4 & 0 \\ Y_1 & X_1 & Y & X_2 & Y_3 & X_3 & Y_4 & X_4 \end{bmatrix} \tag{5.8}$$

where

$$\begin{Bmatrix} X_1 \\ X_2 \\ X_3 \\ X_4 \end{Bmatrix} = \frac{1}{8\left|\mathbf{J}\right|} \begin{Bmatrix} z_{24} - z_{34}\xi - z_{23}\eta \\ -z_{13} + z_{34}\xi + z_{14}\eta \\ -z_{24} + z_{12}\xi - z_{14}\eta \\ z_{13} - z_{12}\xi + z_{23}\eta \end{Bmatrix} \tag{5.9}$$

and

$$\begin{Bmatrix} Y_1 \\ Y_2 \\ Y_3 \\ Y_4 \end{Bmatrix} = \frac{1}{8|\mathbf{J}|} \begin{Bmatrix} -r_{24} + r_{34}\xi + r_{23}\eta \\ r_{13} - r_{34}\xi - r_{14}\eta \\ r_{24} - r_{12}\xi + r_{14}\eta \\ -r_{13} + r_{12}\xi - r_{23}\eta \end{Bmatrix} \tag{5.10}$$

and

$$P_i = \frac{q_i}{r} = \frac{q_i}{\sum_n q_n r_n} \tag{5.11}$$

The determinant of the Jacobian of transformation $|\mathbf{J}|$ is expressed by:

$$|\mathbf{J}| = \frac{1}{8}\left[\left(r_{13} \cdot z_{24} - r_{24} \cdot z_{13}\right) + \left(r_{34} \cdot z_{12} - r_{12} \cdot z_{34}\right)\xi + \left(r_{23} \cdot z_{14} - r_{14} \cdot z_{23}\right)\eta\right] \tag{5.12}$$

Volumetric strain-rate $\dot{\varepsilon}_V$ is expressed by:

$$\dot{\varepsilon}_V = \dot{\varepsilon}_r + \dot{\varepsilon}_z + \dot{\varepsilon}_\theta = \mathbf{C}^{\mathrm{T}}\mathbf{v} \tag{5.13}$$

where

$$\mathbf{C}^{\mathrm{T}} = \{1,1,1,0\}\,\mathbf{B} \tag{5.14}$$

The effective strain-rate $\dot{\bar{\varepsilon}}$, in a discrete form is defined by:

$$\dot{\bar{\varepsilon}} = \left(\dot{\bar{\varepsilon}}^{\mathrm{T}}\mathbf{D}\dot{\varepsilon}\right)^{\frac{1}{2}} = \left(\mathbf{v}^{\mathrm{T}}\mathbf{B}^{\mathrm{T}}\mathbf{D}\mathbf{B}\mathbf{v}\right)^{\frac{1}{2}} = \left(\mathbf{v}^{\mathrm{T}}\mathbf{P}\mathbf{v}\right)^{\frac{1}{2}} \tag{5.15}$$

where

$$\mathbf{D} = \begin{bmatrix} 2/3 & & & 0 \\ & 2/3 & & \\ 0 & & 2/3 & \\ & & & 1/3 \end{bmatrix} \tag{5.16}$$

The stiffness equations are expressed as:

$$\frac{\partial \pi}{\partial \mathbf{v}} = \sum_{j}^{M} \left[\int_{V_j} \frac{\bar{\sigma}}{\dot{\bar{\varepsilon}}} \mathbf{P}\mathbf{v} dV + \int_{V_j} \lambda \mathbf{C} dV - \int_{S_{F_j}} \mathbf{N}\mathbf{F} dS \right] = 0 \tag{5.17}$$

and

$$\frac{\partial \pi}{\partial \lambda_j} = \int_{V_j} \mathbf{C}^{\mathrm{T}} \mathbf{v} dV = 0, \quad j = 1, ..., M \tag{5.18}$$

where the subscript j indicates the element number and M is the total number of elements.

5.2.2 Numerical treatment

The Newton-Raphson method with a line search technique is an iterative procedure for finding a suitable approximation to a root of mathematical equation (e.g., $f(x) = 0$). It has been widely applied in most FEM simulation package such as DEFORM for solving the system equations. In the convergence process of Newton-Raphson iterations, the initial assumed velocity should be close to the actual solution. When the deformation process is relatively simple, the initial assumed velocity can be provided. However, if the process is complex and the good initial assumed solution is difficult to obtain, then the direct iteration method is used, in which the constitutive equation is assumed to be liner during each iteration. The non-linear friction term is also approximated by a linear relationship between the frictional stress and the relative sliding velocity. Then the stiffness equation resulting from $\delta\pi = 0$ becomes linear. This solution strategy is adopted in this study also.

The finite-element technique is used to model the bulk-forming problem in a discrete domain using a set of non-linear equations (5.55) of the form:

$$\mathbf{F}(\mathbf{v}) = 0 \tag{5.56}$$

or

$$F_i(v_1, v_2, v_3, \ldots, v_\omega) = 0 \qquad i = 1, 2, \ldots, \omega \tag{5.57}$$

where $\mathbf{v}$ denotes the entire vector of velocities v_i, and $\mathbf{F}$ denotes the entire vector of functions F_i, containing the derivatives of the energy with respect to each velocity component in vector $\mathbf{v}$. ω is the number of variables (i.e., the number of unknown velocity components). These equations are non-linear and thus a multidimensional root-finding method is required. The Newton-Raphson method of solving non-linear equations from an initial guess is commonly used for metal forming problems due to its large convergence range and relatively fast convergence rate [70,107,137-139].

In the neighbourhood of $\mathbf{v}$ (i.e., $\mathbf{v}$ is increased by a small increment $\delta\mathbf{v}$, each of the functions F_i, can be expanded in a Taylor series:

$$F_i(\mathbf{v} + \delta\mathbf{v}) = F_i(\mathbf{v}) + \sum_{j=1}^{\omega} \frac{\partial F_i}{\partial v_j} \delta v_j + O(\delta\mathbf{v}^2) \tag{5.58}$$

where O is a big "O" notation [70]. The matrix of partial derivatives in equation (5.58) is the Jacobian matrix $\mathbf{J}$ (i.e., $J_{ij} = \partial F_i / \partial v_j$). Therefore equation (5.58) in matrix notation becomes:

$$\mathbf{F}(\mathbf{v} + \delta\mathbf{v}) = \mathbf{F}(\mathbf{v}) + \mathbf{J} \cdot \delta\mathbf{v} + O(\delta\mathbf{v}^2) \tag{5.59}$$

By neglecting the terms with order $\delta\mathbf{v}^2$ and higher, as well as setting $\mathbf{F}(\mathbf{v} + \delta\mathbf{v}) = 0$, a set of linear equations for the $\delta\mathbf{v}$ that move each function F_i, closer to zero is obtained by:

$$\mathbf{J} \cdot \delta \mathbf{v} = -\mathbf{F} \tag{5.60}$$

Matrix equation (5.60) can then be solved by a linear equation solver, such as **LU** decomposition [119,140] (where $\mathbf{L}$ and $\mathbf{U}$ denote lower and upper triangular matrices respectively), which is adopted to solve systems of linear equations or calculate the determinant in numerical analysis. Therefore,

$$\delta \mathbf{v} = -\mathbf{J}^{-1} \cdot \mathbf{F} \tag{5.61}$$

$\delta \mathbf{v}$ is called the Newton step. Indeed the **LU** decomposition can factorise a matrix that is the product of **LU** of a lower triangular matrix $\mathbf{L}$, in which the leading diagonal elements are unity, and a upper triangular matrix $\mathbf{U}$. The application of Newton-Raphson method to equation (5.56) leads to the iterative procedure with respect to $\mathbf{v}$,

$$\mathbf{v}_{i+1} = \mathbf{v}_i + \lambda_s \delta \mathbf{v}_i \tag{5.62}$$

where λ_s is called the step length. The value of the step length λ_s may be determined by a strategy which requires that the step decreases $|\mathbf{F}|^2 \left(|\mathbf{F}|^2 = \mathbf{F} \cdot \mathbf{F} \right)$. This is the same requirement for minimising.

$$f = \frac{1}{2} \mathbf{F} \cdot \mathbf{F} \tag{5.63}$$

Note that the Newton step (i.e., $\delta \mathbf{v}$) is a descent direction for f :

$$\nabla f \cdot \delta \mathbf{v} = \left(\mathbf{F} \cdot \mathbf{J} \right) \cdot \left(-\mathbf{J}^{-1} \cdot \mathbf{F} \right) = -\mathbf{F} \cdot \mathbf{F} < 0 \tag{5.64}$$

However, a full Newton step (i.e., $\lambda_s = 1$) may not reduce f. An evaluation is carried out at each iteration to ensure that the proposed step reduces f. If the step is too large, the value of λ is reduced by backtracking along the Newton direction until an acceptable value is found. A line search technique [119,141] which determines the minimum point on a given line may be used to find an approximate value of λ_s. The technique described as follows.

The new value of f may be defined by a function g with the variable λ_s:

$$g(\lambda_s) \equiv f(v_{i+1}) = f(\mathbf{v}_i + \lambda_s \delta \mathbf{v}) \tag{5.65}$$

so that

$$g'(\lambda_s) = \nabla f \cdot \delta \mathbf{v} \tag{5.66}$$

If the backtrack is needed, the λ_s is chosen by minimising the function g with the most current information. If the first step which always starts the full Newton step ($\lambda_s = 1$) is not acceptable, three values $g(0)$, $g'(0)$ and $g(1)$, are available to model $g(\lambda_s)$ as a quadratic curve. The curve can then be used to find a minimum of λ_s. On the second and subsequent backtracks, the function $g(\lambda_s)$ is modelled as a cubic curve and thus a new minimum of λ_s can be determined for the current information. This technique for choosing the step length is called line search.

The Newton step is a descent direction for f as shown is equation (5.64), and it is guaranteed by using line search to find an acceptable step length. Finally, the Newton-Raphson method with the line search technique can minimise f by taking

Newton steps designed to bring $\mathbf{F}$ to zero (i.e., to solve velocity $\mathbf{v}$ for $\mathbf{F}$). The iteration is terminated when

$$\left\|\mathbf{F}\left(\mathbf{v}_i, \lambda_s\right)\right\| < e_e \tag{5.67}$$

where e_e is set to 1×10^{-3}.

5.2.3 Structure of reverse simulation

A commercial two-dimensional finite-element package DEFORM-2D (version v9.1.1) was mainly employed in this study to carry out the finite-element simulation. This software was developed and sold by Scientific Forming Technologies Corporation (SFTC) in USA [142]. It was designed specifically to simulate the axisymmetric and plane strain bulk-forming processes. DEFORM-2D makes use of the finite-element analysis to model the mechanics of material flow as well as thermal effects or heat transfer. The package provides a pre-processor for importing the workpiece geometry and the die geometry, defining the process conditions and boundary conditions, and outputting this information in the format required by the solver. A post-processor is applied to visualise and analyse the result of the simulation. DEFORM-2D also incorporates automatic re-meshing which avoids excessive element distortion when analyzing large deformations. However, this automatic re-meshing engine should be used in the forward simulation only.

The geometry of the final shape of the formed component and the die profile was constructed by the commercial CAD software, AutoCAD [143]. However, this was

not able to generate the mesh of the geometry. The mesh generation, as well as inputting the process parameter, material properties, and boundary conditions, could be treated by the pre-processor of DEFORM-2D. After processing a forward step of the reverse simulation, the finite-element data were exported in ASCII format including the information about the coordinates of nodes and the connectivity of elements. The exported computer file was called the keyword file (in KEY format), which was able to be opened and edited by a simple text editor such as Microsoft Notepad. Based on the backward tracing method, the reverse shape was then determined. The keyword file was modified accordingly. The updated keyword file was read by the pre-processor of DEFORM-2D again, and the re-meshing procedure might be implemented that identified element distortions in many instances of large deformation. After this, the simulation of the bulk-forming process was run in forward mode as the shape verification. The decision regarding the re-mesh was made by checking the quality of elements or, alternatively, re-meshing after each reverse increment. However, the automatic re-meshing procedure could not be used during the forward step of the backward tracing method because the number of elements, the coordinates of nodes and the connectivity of elements were re-arranged after re-meshing. Furthermore, the distance between nodes constructing the boundary of the deformed workpiece might be too small, which results in numerous elements after the re-meshing task was carried out. In such cases, the geometry of the workpiece needed to be re-constructed manually according to the exported information. The above procedure was repeated until the simulation for this bulk-forming stage was finished.

In the process of shape verification, the shape comparisons (i.e., $\mathbf{x}_0^{(n)} - \mathbf{x}_0$ and $\mathbf{x}_0 - \mathbf{x}_0^{(n)}$) were performed by the Booleans function of AutoCAD , which is able to calculate the volume of the whole, protrusion, and indentation, as well as measuring the critical dimensions of the reverse geometry (i.e., D , d , and h). While the predicted reverse shape did not conform with the requirements in terms of constant volume, and allowances of the protrusion and indentation, the shape-reconstruction procedures using SLR, BEM, NDPR, and PO methods were carried out by using AutoCAD manually. Nevertheless the exported geometrical data by DEFORM-2D was in initial graphics exchange specification (IGES) file format, which cannot be opened by AutoCAD. Generally AutoCAD is only able to open the drawing exchange format (DXF) file format. The conversion between the IGES and DXF file formats was done by another CAD software, Rhinoceros [144], which supports all file formats of geometry used in both DEFORM-2D and AutoCAD. The entire transport of data and files between DEFORM-2D, AutoCAD, and Rhinoceros is illustrated by a flowchart in Fig. 5.18.

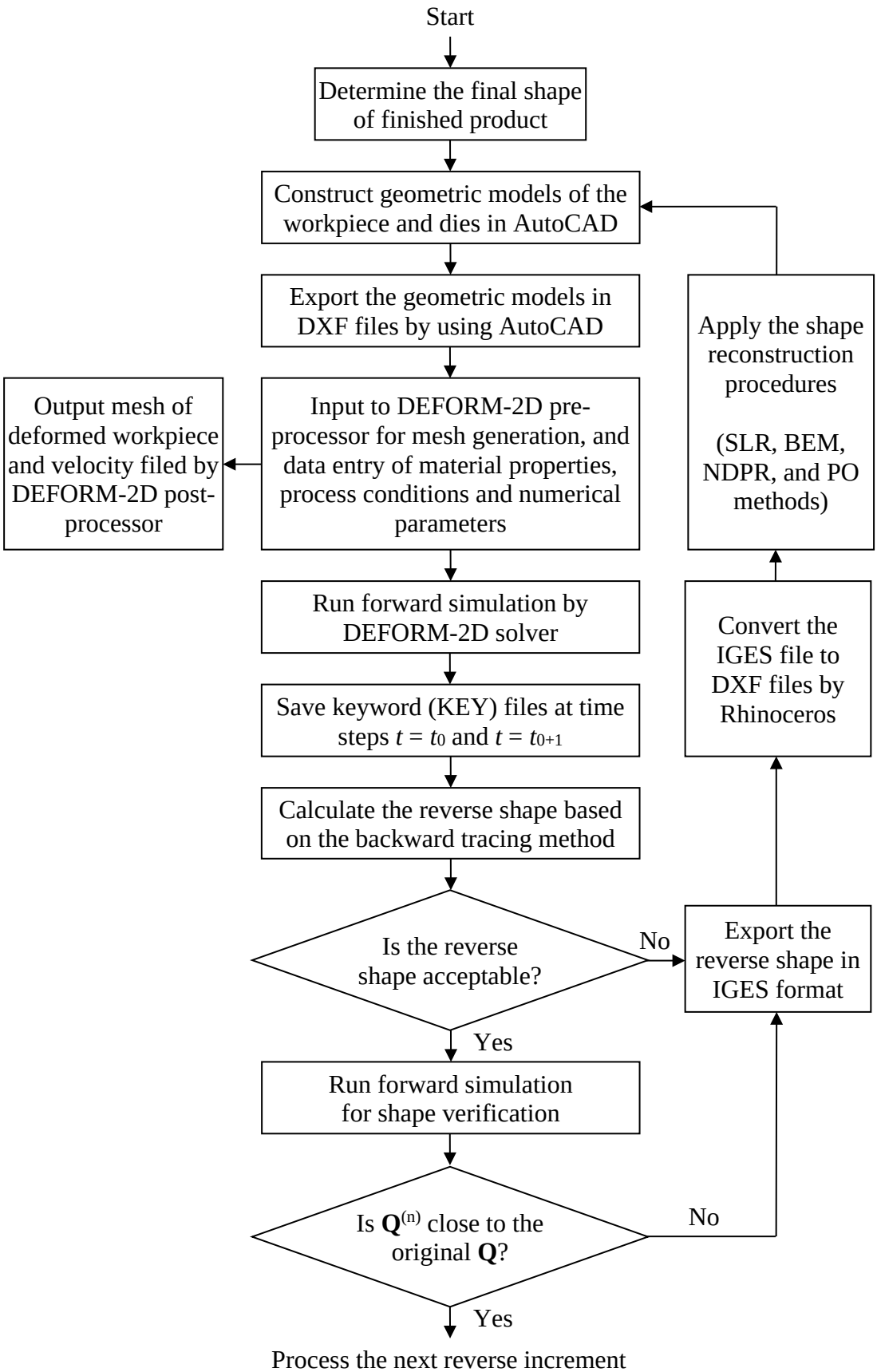

Fig. 5.18 The flow chart of data transport in the process of reverse simulation.

The flowchart of the simulation procedure (i.e., the operation in DEFORM-2D) is presented in Fig. 5.19. In this study, after the finite-element model of the workpiece was generated by the mesh generator in the pre-processor of DEFORM-2D, it was necessary to set the flow stress data (i.e., the material properties of the specimen material), the friction factor, process conditions (e.g., punch speed, die temperature, and initial temperature of workpiece). The deforming workpiece and dies were updated in a small time step according to the solved velocity field until the required target distance was reached. The results of each step of the simulation were recorded for further analysis.

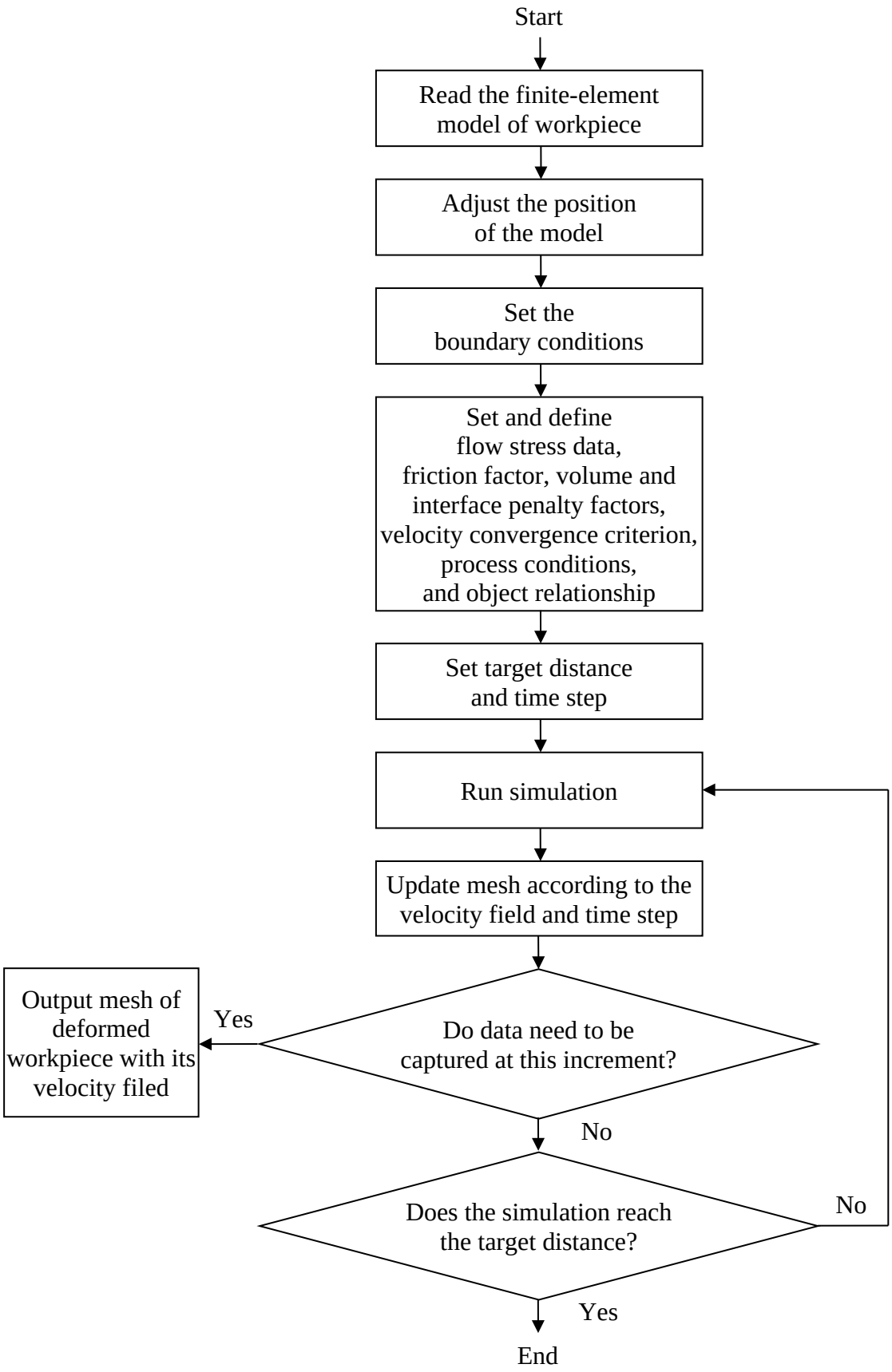

Fig. 5.19 The flow chart of the simulation procedure of DEFORM-2D.

The plastic deformation energy was calculated by the direct solver for the first iteration in each increment. The following iterations were then solved by the Newton-Raphson solver until the velocity field converged. The convergence error limit of velocity was set to 1×10^{-3}. When the solutions failed to converge with this method, the direct method was used as an alternative. This is more likely to converge than Newton-Raphson, but generally requires more iterations to do so. The compressibility of the volume was checked in each iteration. If the incompressibility was not held, the value of the incompressibility penalty (i.e., volume penalty) α was increased. In order to avoid instability in the calculations occurring when the value is too high after several adjustments, the maximum value was set to 1×10^{6}. A similar procedure was also carried out for the value of the normal penalty β (or interface penalty), which controls the penetration of the node into the die. It needed to be at least two to three orders higher than the volume penalty (i.e., 1×10^{8} to 1×10^{9}). Table 5.5 shows the default numerical parameters for preparing the simulation by DEFORM-2D.

Table 5.5 Numerical parameters for preparing the simulation.

Parameter	Value
Incompressibility penalty (volume penalty) factor α	1×10^{6}
Normal penalty (interface penalty) factor β	1×10^{9}
Convergence error limit of velocity	1×10^{-3}
Maximum iteration per time step	200
Maximum strain in workpiece per step	0.1
Time integrating factor	0.75

6. Results and Discussions

6.1 Experimental results used for reverse simulation

The main objective of the warm-forming process is the complete filling of die cavity. This is also the primary aim of the reverse simulation approach proposed in this study. The approach should be able to predict the billets for axisymmetric bulk-forming processes, in which the components are made of single-base metals or bimetals (i.e, dissimilar metals). A comparison of the material flow between predicted deformations and experimental results was the main concern. In addition, the forming load provided a figure of the dissipation of energy that was investigated. The assessment of the reverse simulation was carried out with three axisymmetric cases, which included a non-hollow component and a hollow component made of aluminium alloy, and a hollow bimetallic component composed of aluminium alloy 6063 and stainless steel AISI 316L. Actually, their final shapes were simplified from a watch-case-like component, which was manufactured typically by warm forming.

The billet shapes predicted by reverse simulation from the final shapes of the finished products were also formed in corresponding physical experiments for the process verification. In addition, DEFORM-2D was used to run the forward simulation as compared to the outcomes obtained by reverse simulation. These results were analyzed in order to understand the difference between the real process and the simulations including reverse and forward cases. The analysis aimed to evaluate the possibility of using the commercial software as a virtual forming press (or a forming

system) for carrying out experiments with the warm forming instead of using a real forming press or machine.

6.1.1 Material model and flow stress data

The description of the material behaviour in the bulk-forming process is expressed as a function of temperature T, effective plastic strain $\bar{\varepsilon}$, and effective strain rate $\dot{\bar{\varepsilon}}$ (i.e., the flow stress σ). Flow stress is important because the forming loads and stresses depend mainly on geometry, friction and the flow stress of the deforming material in the metal forming processes. DEFORM-2D provides different methods of defining the flow stress. The tabular data format was used in this study due to its ability to follow the true behaviour of a material. This method was required to enter the values of T, $\bar{\varepsilon}$, and $\dot{\bar{\varepsilon}}$. If simulation conditions of the material exceed the bounds of T, $\bar{\varepsilon}$, and $\dot{\bar{\varepsilon}}$ defined in the tabular data, DEFORM-2D will extrapolate the flow stress data automatically based on the last two data-points, which might lead to loss of accuracy.

It is supposed that if the friction is neglected, the true compressive stress required to produce yielding during the compression tests is:

$$\bar{\sigma} = \frac{F_c}{A_s} = \frac{4F_c}{\pi D_c^{\,2}} \tag{6.1}$$

where F_c is the uniaxial compressive force, A_s is the area of cylinder section, D_c is the diameter of the specimen. According to the assumption of constant volume,

$$D_0^{\,2} h_0 = D_c^{\,2} h_c \tag{6.2}$$

Where h_c is the instantaneous height, and D_0 and h_0 are the initial diameter and height of the specimen, respectively. The compressive stress is:

$$\bar{\sigma} = \frac{4F_c h_c}{\pi D_0^{\,2} h_0} \tag{6.3}$$

Tables 6.1 and 6.2 show the experimental flow stress data aluminium alloy 6063 and stainless steel AISI 316L respectively after the data consolidation, with the true strain given by:

$$\bar{\varepsilon} = \ln \frac{h_0}{h_c} \tag{6.4}$$

Table 6.1 Experimental flow stress data of aluminium alloy 6063.

Strain rate	True strain	True stress (Flow stress) [MPa]					
[/s]		20 °C	100 °C	200 °C	300 °C	400 °C	500 °C
0.1	0.1	215	206	188	169	56	32
0.1	0.2	219	209	191	173	58	33
0.1	0.3	224	215	197	179	61	34
0.1	0.4	223	214	197	179	61	34
0.1	0.5	221	213	196	179	62	34
	Average	221	212	194	176	60	33
1	0.1	296	288	271	255	77	46
1	0.2	309	299	280	262	80	47
1	0.3	309	299	279	260	84	48
1	0.4	309	299	279	259	84	48
1	0.5	305	295	275	255	85	48
	Average	306	296	277	258	82	47

Table 6.2 Experimental flow stress data of stainless steel AISI 316L.

Strain rate	True strain	True stress (Flow stress) [MPa]					
[/s]		400 °C	500 °C	600 °C	700 °C	800 °C	900 °C
0.1	0.1	530	442	390	360	352	245
0.1	0.2	610	533	511	444	383	261
0.1	0.3	655	572	561	485	386	269
0.1	0.4	700	601	592	509	405	272
0.1	0.5	715	617	626	536	420	284
	Average	642	553	536	467	389	266
1	0.1	533	443	389	363	325	280
1	0.2	613	532	506	445	391	315
1	0.3	658	568	550	488	420	328
1	0.4	703	593	573	499	428	325
1	0.5	718	601	588	511	435	327
	Average	645	547	521	461	400	315

In the reverse simulation, both aluminium alloy 6063 and stainless steel AISI 316L are rigid-perfectly plastic. Also, the strain hardening and softening effects are neglected in the model. Therefore, only the average values of the flow stress at various strain rates and temperatures needed to be entered into the DEFORM-2D.

The data presented in Tables 6.1 and 6.2 above conform to the expectation. The discrepancy of average flow stress between the two materials was very large. In order to minimise the heterogeneous material flow during the warm-forming process, the forming temperature of 900 °C was selected for stainless steel AISI 316L. This

temperature is the highest warm-forming temperature of stainless steel. Since the quality of bimetallic weld was required, the forming temperature was determined by the results of experiments of welding dissimilar metals and warm forming bimetallic components discussed in subsequent sections.

6.1.2 Friction factors acquired by ring compression test

When the ring compression test is being used to determine the friction factor for a particular set of experimental data, a set of calibration curves is required. The curves assume that the material follows a rigid-perfectly plastic model without barrelling so that the deformation is completely homogeneous with uniform states of stress and strain. These curves used in this study were plotted according to the simulation results of the ring compression by DEFORM-2D. Process conditions and specimen geometry were the same as or compatible with those of the practical experiments. The curves could act properly as the calibration curves for evaluating the friction of warm forming aluminium alloy 6063 at 300 °C with and without the lubricant W-400.

Figure 6.1 shows the original specimen and the deformed rings. The values of the shear friction factor m were then obtained by the point matching the recorded data into the calibration curves as shown in Fig. 6.2. The m was determined as 0.5 for the case without lubrication (i.e., the contact between aluminium alloy and stainless steel), and 0.2 for the case of applied lubricant.

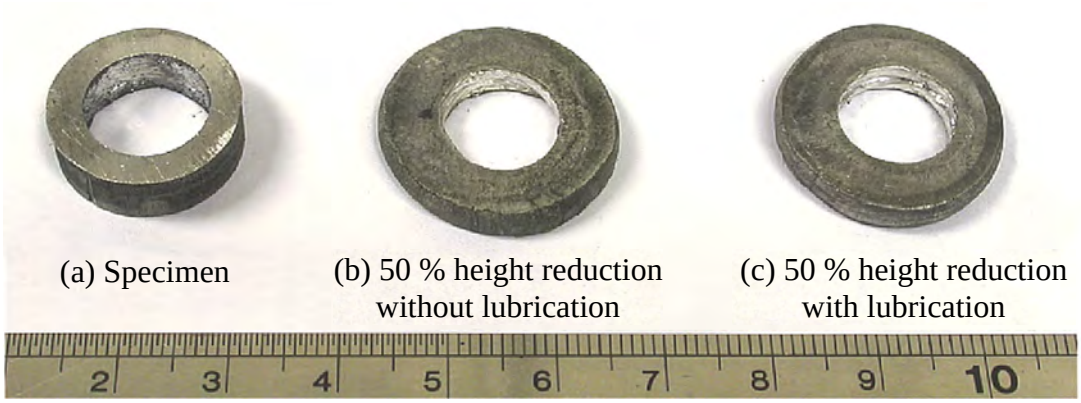

Fig. 6.1 Ring specimen and experimental results from the ring compression test.

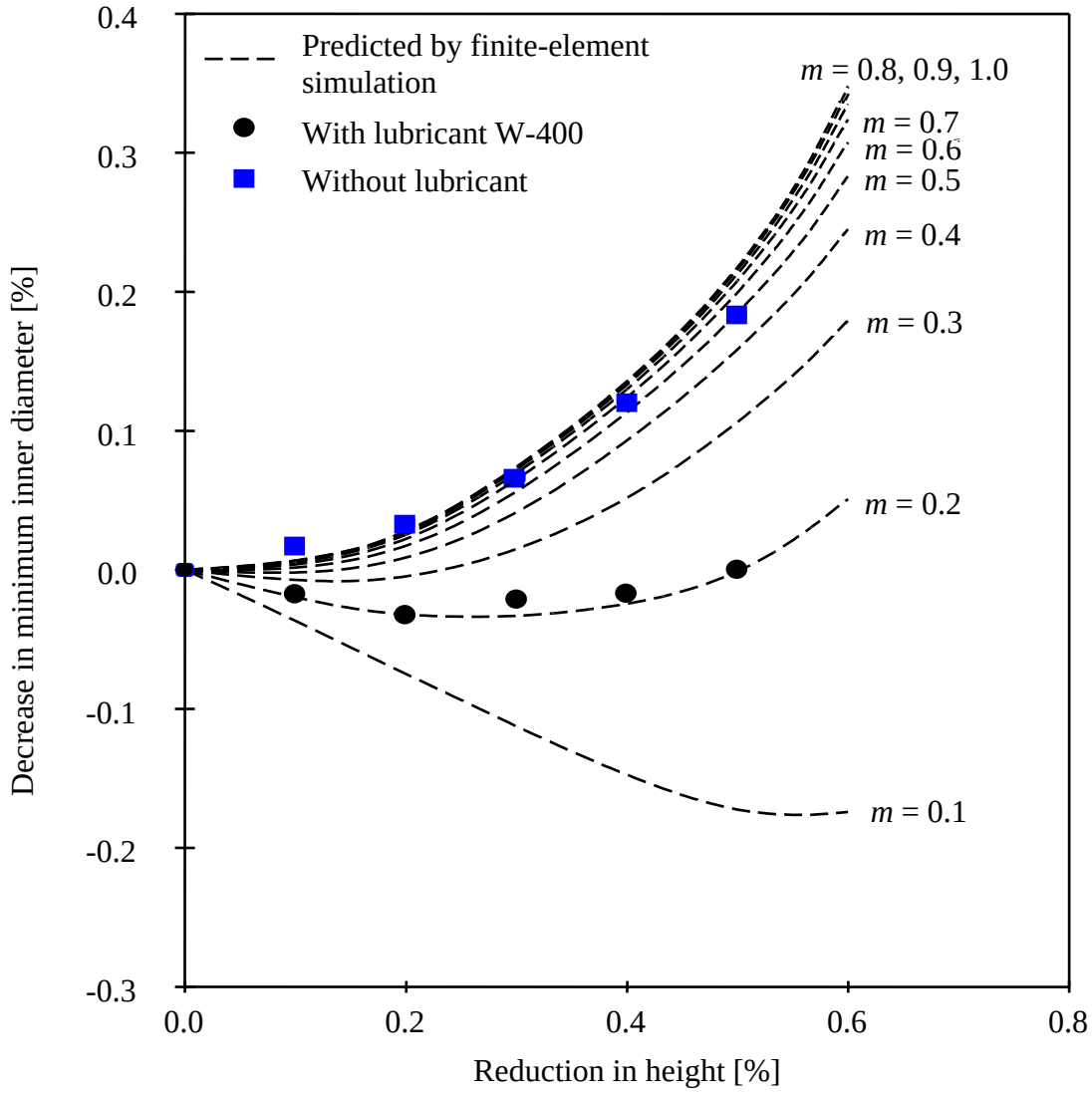

Fig. 6.2 The calibration curves for evaluating the friction of warm forming aluminium alloy 6063 at 300 °C with and without the lubricant W-400.

A constant factor used in the Tresca friction model (i.e., shear friction model) gives the degree of friction [128,129]. The value of m measured by the ring compression test is generally between 0.1 and 0.3 for warm forming with lubricant. This section investigates whether the Tresca friction model can approximate the variation of forming load and deformation as the m is varied. An accurate modelling of friction, however, requires a more complex modelling technique. An investigation of accuracy is not the intention of this approximate modelling approach.

Numerical tests with different m were carried out for an axisymmetric upsetting at 300 °C isothermal condition, which was constructed of 990 elements for a cylindrical billet with a diameter of 6 mm and height of 9 mm. The specimen material was aluminium alloy 6063 incorporated into the flow stress data presented in the previous section. Figure 6.3 shows that the barrelling effect became more significant as the friction factor increased. On the other hand, the forming load shown in Fig. 6.4 had no considerable change as the m increased from 0.1 to 0.9. This phenomenon can result from the fact that the velocity in contacting interfaces is lower in the cases with higher friction.

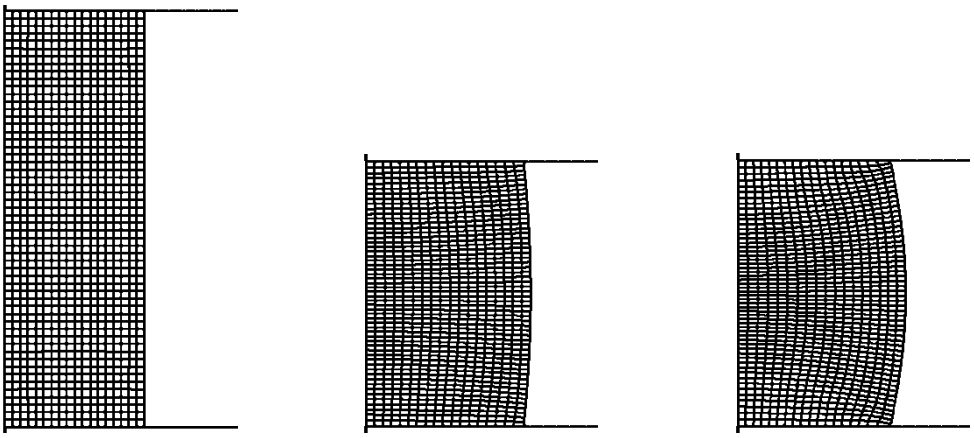

(a) Cylindrical billet (b) Friction factor = 0.1 (c) Friction factor = 0.3

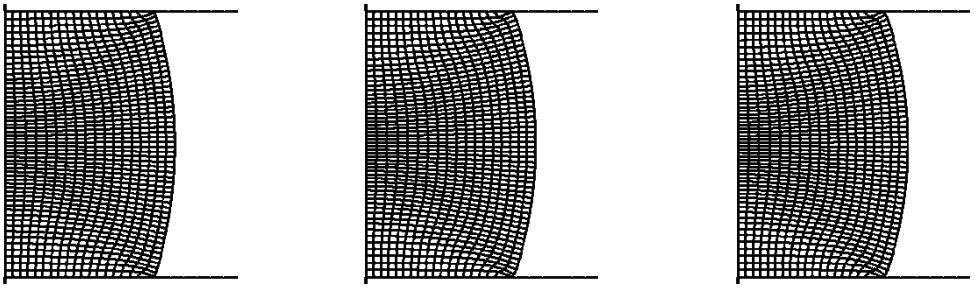

(d) Friction factor = 0.5 (e) Friction factor = 0.7 (f) Friction factor = 0.9

Fig. 6.3 Upsetting deformation with 1/3 high reduction resulting from different shear friction factors in cases with 990 elements.

This simple upsetting process was also constructed with different numbers of elements (192, 990, and 1474) to investigate the effects on the modelling of shear friction. The forming loads induced by the friction in these cases are shown in Figs. 6.4 to 6.8. As the number of elements increased, the results of the forming load had no major difference. This implied that number of elements has no significant influence on the simulation result when using various m in DEFORM-2D.

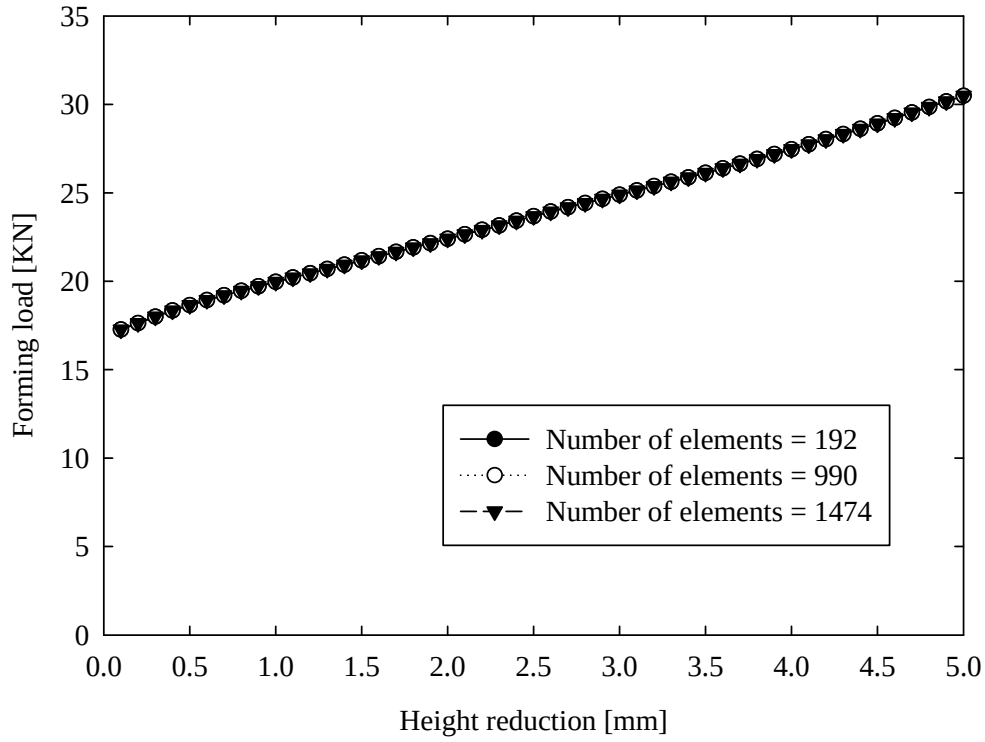

Fig. 6.4 Forming load resulting from shear friction factor 0.1 in comparison with different number of elements.

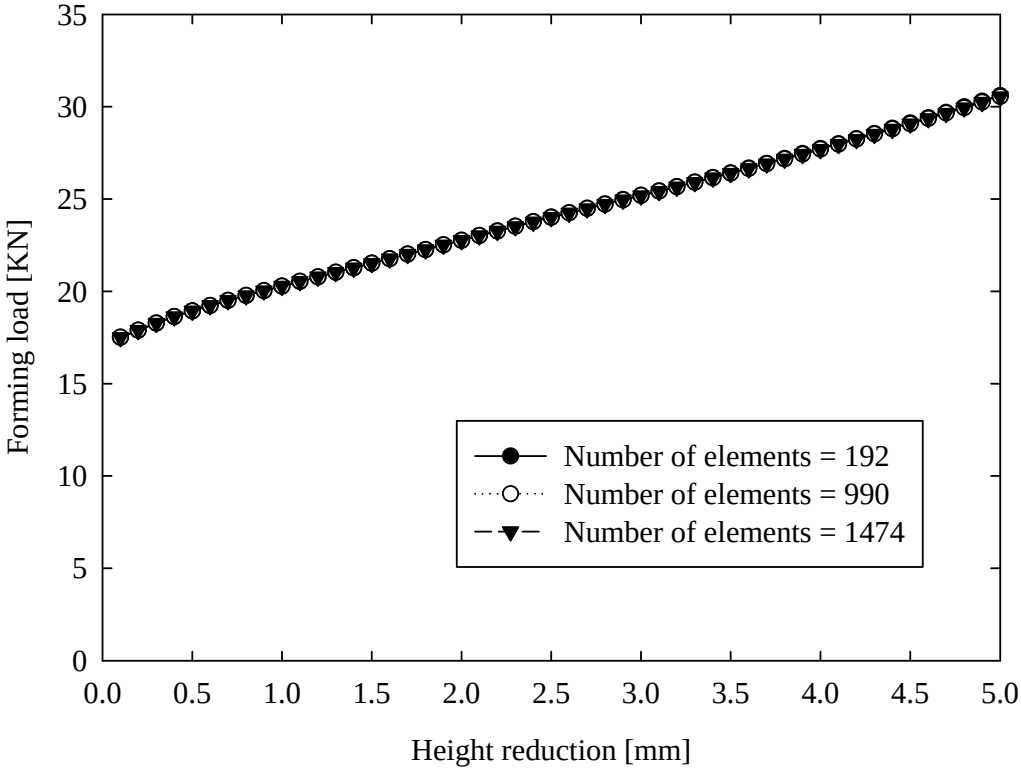

Fig. 6.5 Forming load resulting from shear friction factor 0.3 in comparison with different number of elements.

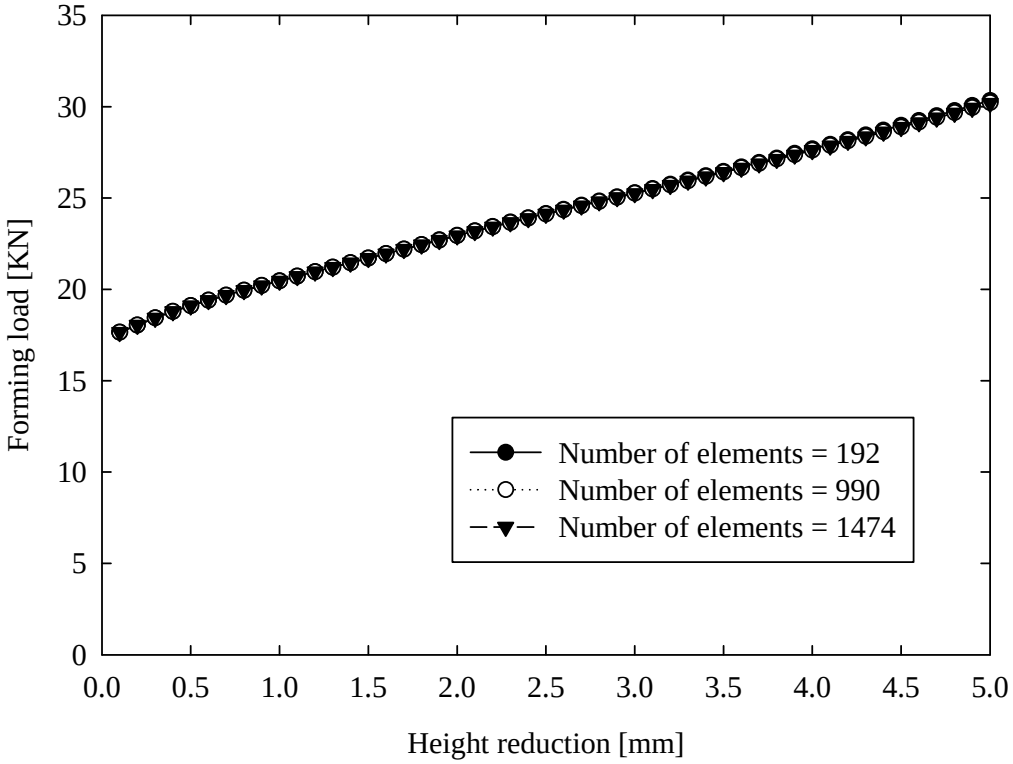

Fig. 6.6 Forming load resulting from shear friction factor 0.5 in comparison with different number of elements.

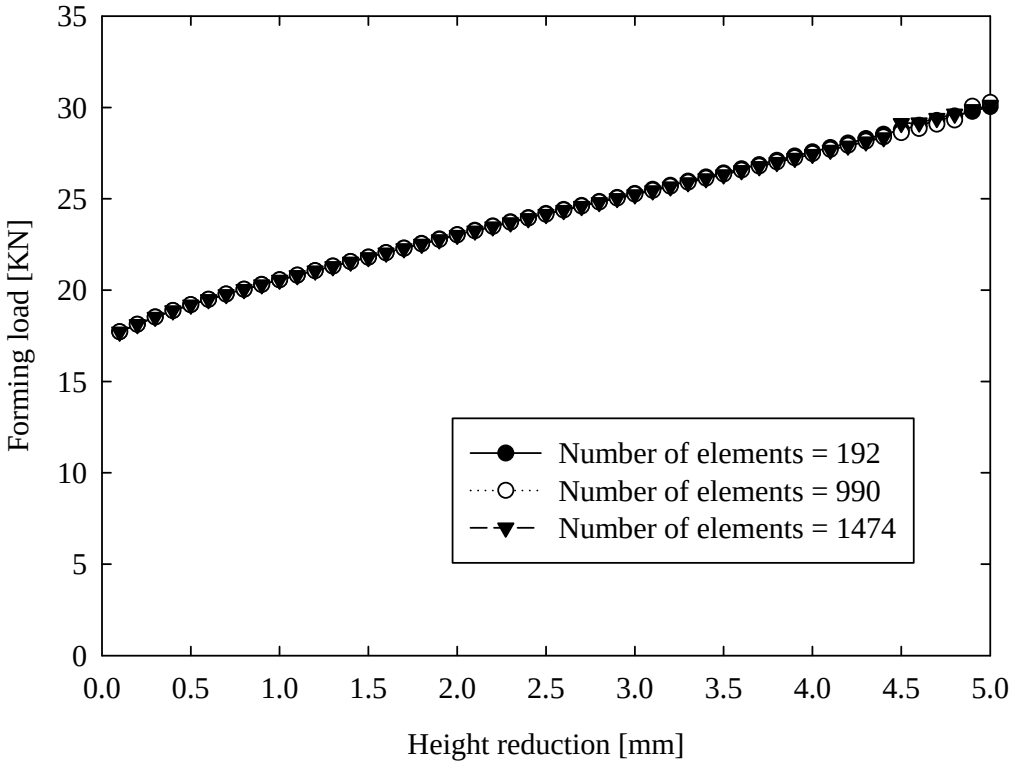

Fig. 6.7 Forming load resulting from shear friction factor 0.7 in comparison with different number of elements.

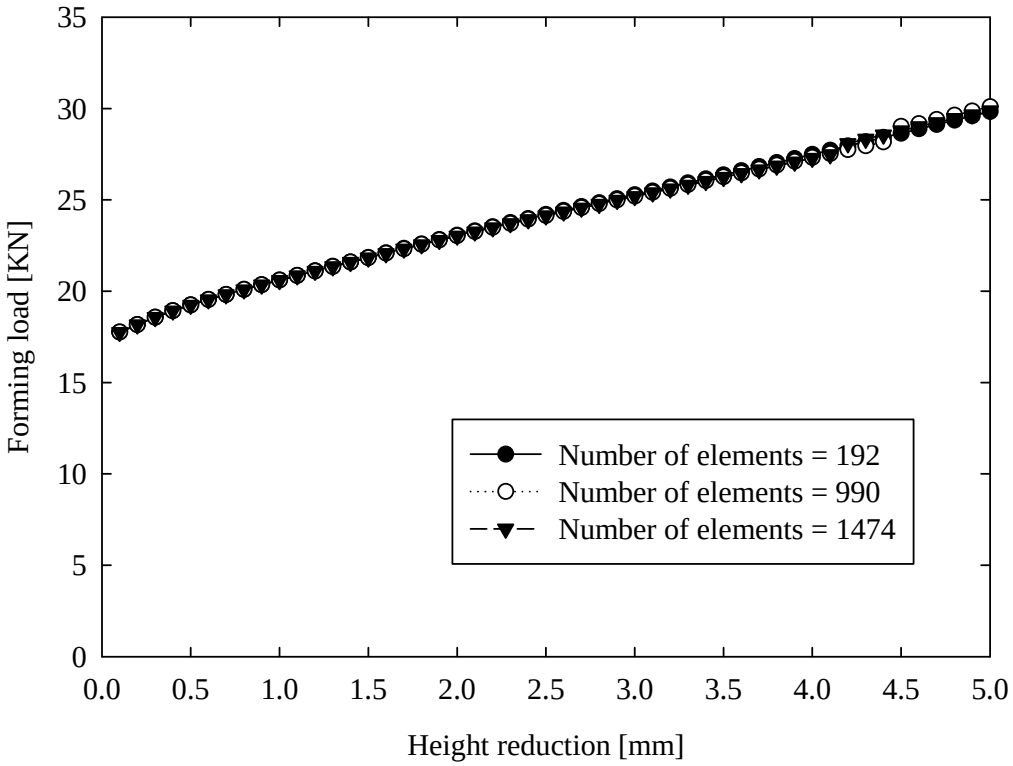

Fig. 6.8 Forming load resulting from shear friction factor 0.9 in comparison with different number of elements.

6.1.3 Welds of dissimilar metals

Previous studies have demonstrated the success of coalescence between aluminium alloy and stainless steel using friction welding and diffusion welding. Sundaresan et al. optimised the process parameters of friction welding to produce quality welds with tensile strengths higher than that of the parent aluminium alloy [145]. Bhanumurthy et al. investigated diffusion welding to weld such dissimilar metals [146]. They found that a satisfactory weld with tensile strength of 91 MPa was welded at 315 °C for 4 hours. A few intermetallic compounds were indicated in its reaction zone (i.e. the diffusion zone). In this study, the welds produced by hot-

pressure welding and forge welding should be stronger than those of previous studies so that process improvement can be achieved.

A series of hot-pressure welding and forge welding experiments was conducted using the concept of statistical experimental methods, which can assess the reliability of the results, particularly for the tensile strengths of bimetallic welds σ_t obtained by the uniaxial tensile tests. These methods can also provide useful visual information that can help provide some understanding of variation in the findings correlated with different process parameters as well as confirming the consistent and repeatable processes. In this study, the control charts were used as the statistical experimental method. These could indicate the stable or consistent variations of the outcomes of the experiments, which were acquired at different T_w and F_w and types of presses. Each trial of these experiments was repeated four times, and the time interval between the trials was ten minutes. Thus, in total, thirty-six bimetallic components were formed in each welding process. The R (range) and *X*-bar (average) charts were used together to analyze the central tendency and spread on σ_t. The R chart illustrated the variation of the weld quality of different processes, while the *X*-bar chart showed the mean of σ_t affected by various T_w and F_w.

For constructing the R chart, the number of subgroups m_{sub} = 9. This was the number of trials. The subgroup size n_{sub} = 4, that was the samples taken for each trial. The equations pertinent to the R chart are given as follows:

$$R_i = \sigma_{i\max} - \sigma_{i\min} \tag{6.10}$$

where R_i is the data point of the R chart, and $\sigma_{i\max}$ and $\sigma_{i\min}$ are the maximum and minimum tensile strengths in a subgroup respectively.

$$\bar{R} = \frac{\sum_{i=1}^{m} R_i}{m_{sub}} \tag{6.11}$$

where $\bar{R}$ is the center line on the R chart which is the average range for the experimental trials.

$$\mathrm{UCL}_R = D_4 \bar{R} \tag{6.12}$$

$$\mathrm{LCL}_R = D_3 \bar{R} \tag{6.13}$$

where UCL_R and LCL_R are the upper and lower control limits of the R chart respectively. When n_{sub} = 4, the multiplying factors for these two probability limits are given as D_4 = 2.284 and D_3 = 0 [147,148]. If only common causes are present or the findings are in statistical control, the probability of data points falling outside the limits is very small. In other words, all data points are disturbed within the control limits. This means that the subgroup range is consistent over time (i.e., stable variations). On the other hand, if there are data points beyond the control limits, the unexpected causes or special causes excluding the T_w and F_w for the out-of-control situation have to be determined.

The control limits of the *X*-bar chart depended on the $\bar{R}$. They were set as the lines equivalent to three standard deviations of subgroup average above and below the center line because the *X*-bar chart assumed an underlying normal distribution

according to the central limit theorem. The equations for the *X*-bar chart are given below.

$$\bar{X}_i = \frac{\sum_{i=1}^{n} \sigma_i}{n_{sub}} \tag{6.14}$$

where $\bar{X}_i$ is the data point of the *X*-bar chart, and σ_i is a tensile strength of a subgroup.

$$\bar{\bar{X}} = \frac{\sum_{i=1}^{m} \bar{X}_i}{m_{sub}} \tag{6.15}$$

where $\bar{\bar{X}}$ is the average of the $\bar{X}_i$ (i.e. the center line on the *X*-bar chart).

$$\mathrm{UCL}_{\bar{\bar{X}}} = \bar{\bar{X}} + A_2 \bar{R} \tag{6.16}$$

$$\mathrm{LCL}_{\bar{\bar{X}}} = \bar{\bar{X}} - A_2 \bar{R} \tag{6.17}$$

where $\mathrm{UCL}_{\bar{\bar{X}}}$ and $\mathrm{LCL}_{\bar{\bar{X}}}$ are the upper and lower control limits of the *X*-bar chart respectively. The value of multiplying factor A_2 for n_{sub} = 4 is 0.729 [147,148], which takes account of the relationship between the range, the result variance, the subgroup average variance, and the control limits based on common-causes, process parameters T_w and F_w, and within the variation of subgroups. The present interpretation of the *X*-bar chart is slightly different from the typical definition, since T_w and F_w have been treated as the special causes. Therefore if the data points greatly exceed the control limits, it is understood that the σ_t is influenced more by these two process parameters, and the process can be controlled with precision.

The hot-pressure welding and forge welding for bimetallic components were conducted under various values of T_w and F_w. The corresponding uniaxial tensile tests, metallographic observation, and diffusion analysis were carried out to evaluate

their welds. However, the tensile-strength data acquired in the hot-pressure welding varied greatly compared with those of the forge welding, as shown in Table 6.3. These findings might not be able to fully represent the effects of process parameters on σ_t in those solid-state welding processes. The reasons are discussed in the later section on the reliability of both welding processes.

Table 6.3 Effects of welding temperature and forming deformation on the tensile strengths of bimetallic welds in hot-pressure welding and forge welding processes.

i	T_w [°C]	F_w [mm]	Tensile strength of bimetallic weld, σ_t [MPa]									
			Hot-pressure welding					Forge welding				
			σ_1	σ_2	σ_3	σ_4	$\bar{X}$	σ_1	σ_2	σ_3	σ_4	$\bar{X}$
1	350	4	3.6	4.1	4.9	16.5	7.3	68.2	69.2	73.8	74	71.3
2	350	6	7.0	11.5	14.7	17.6	12.7	70.0	71.7	72.7	73.7	72.0
3	350	8	12.6	30.6	45.5	65.1	38.4	81.6	81.8	86.7	87.1	84.3
4	400	4	27.6	30.4	26.8	63.4	37.0	70.9	72.2	75.2	76.4	73.7
5	400	6	16.5	38.2	39.8	61.3	38.9	74.7	75.3	77.0	78.2	76.3
6	400	8	13.1	54.5	62.3	68.1	49.5	85.6	85.8	86.1	88.8	86.6
7	450	4	45.1	45.6	46.1	67.5	51.1	100.4	103.2	103.4	104.7	102.9
8	450	6	48.1	73.5	81.5	86.7	72.5	102.8	104.1	105	106.9	104.7
9	450	8	62.3	77.2	85.4	89.2	78.5	109.3	110.8	110.9	114.1	111.3

In the forge welding experiments, the σ_t of the twelve bimetallic components produced at T_w = 450 °C could exceed 100 MPa (over 100 % joint efficiency), much stronger than the results obtained by Bhanumurthy et al. [146]. The fractures all occurred in aluminium alloy regions rather than the weld interfaces, since the tensile strengths of these successful welds were higher than those of the parent aluminium alloy. Figure 6.9 shows the stress-strain curves for aluminium alloy 6063, stainless steel AISI 316L, and their bimetallic components forged welded at T_w = 450 °C and F_w = 8 mm, these examples being used to facilitate the comparison between their tensile strengths. This evidence shows that the capability of forge welding was comparable to friction welding and diffusion welding used in previous studies [145,147] and that forge welding was effective in welding the stainless steel and aluminium alloy within several seconds. Regarding the overall effects of T_w and F_w on the σ_t (mean value, *X*-bar of the subgroups), the σ_t had no great improvement when the T_w was increased from 350 to 400 °C because the heat energy was insufficient to activate the diffusion fully between particles inside the two dissimilar metals, and hence the intermetallic bond was incomplete. On the other hand, at T_w = 450 °C, regardless of whether the F_w = 4, 6, or 8 mm, successful welds could be produced. The increases of F_w from 4 to 6 mm and 6 to 8 mm improved σ_t by 5 and 6 %, respectively. It is well known that a larger deformation at the mating surfaces requires a higher applied pressure. The present result agreed with the findings of other researchers who have studied cold welding [149], friction welding [150-152], and friction-stir welding [153], that joint efficiency can be increased by a provision of higher forge pressure or axial pressure.

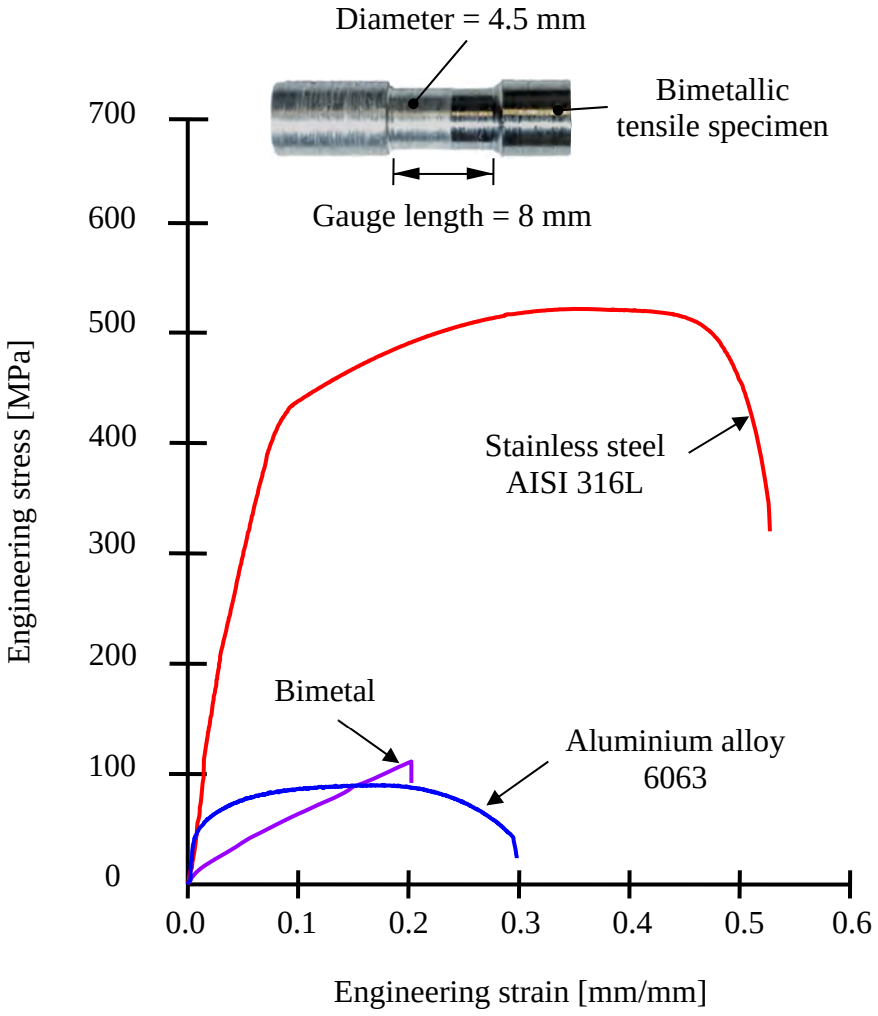

Fig. 6.9 Engineering stress-strain curves for the base-metal and the bimetal produced by forge welding at T_w = 450 °C and F_w = 8 mm.

The stainless steel AISI 316L is an austenitic stainless steel. Its phase transformation and recrystallisation do not occur within the test range of T_w from 350 to 450 °C. In contrast, the Mg_2Si particles inside the aluminium alloy 6063 can be precipitated in the temperature range between 200 and 450 °C, and the recrystallisation temperature of aluminium alloy 6063 is around 450 to 550 °C [154,155]. In particular, during the welding process, the recrystallisation can help to eliminate the micro-void defects existing in the weld interface as well as activating diffusion between the

particles inside two dissimilar metals. Thus the bimetallic components produced at T_w = 450 °C can attain a much higher σ_t. Figure 6.10 shows the good-quality specimens obtained in trial 9 by forge welding. The two dissimilar metals were welded successfully without any aids such as mechanical fastening or fillers. The satisfactory components could be machined by the lathe so that they would not be broken by the cutting force. Nevertheless, the specimens should not be overheated in either of these welding processes. In additional trials, if the T_w exceeded 450 °C, the aluminium alloy 6063 would be damaged seriously, and the two materials were separated after the impulsive force or isostatic pressure was applied. This was because the aluminium alloy 6063 became unstable and became near-liquid while the T_w was close to its melting range of around 616 to 656 °C.

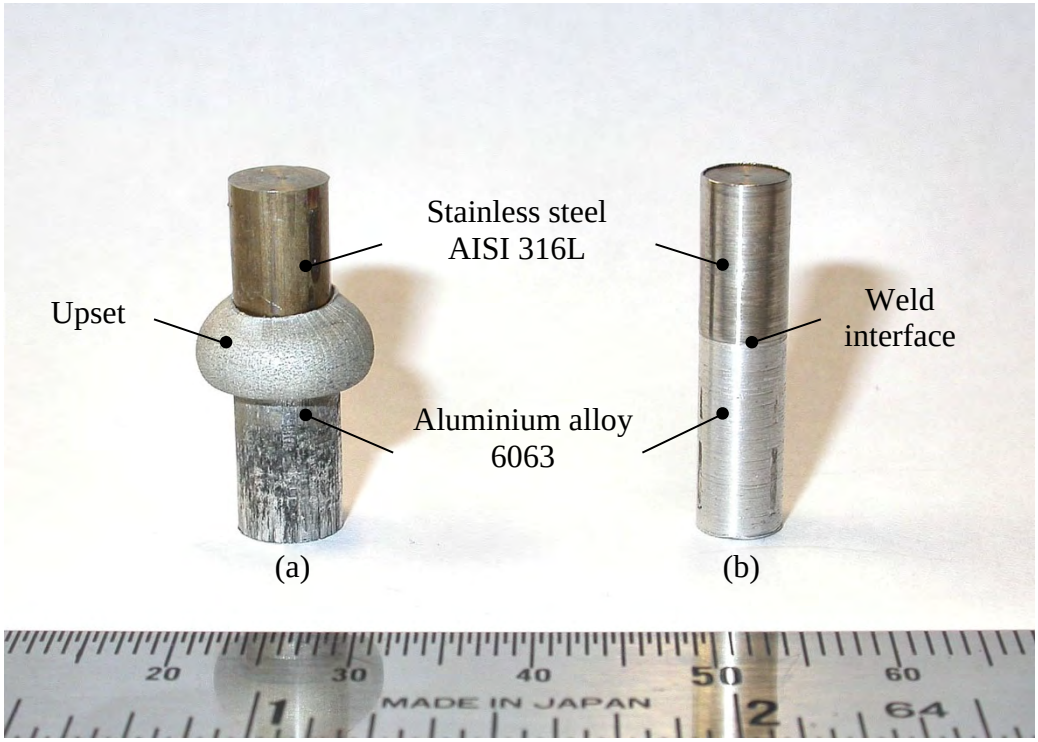

Fig. 6.10 Successful bimetallic components formed by forge welding at T_w = 450 °C and F_w = 8 mm that (a) the upset is present, and (b) the upset is removed.

The metallography of weld interfaces can be used to evaluate the weld quality so as to determine the success of both welding processes. The SEM metallographies of the weld interfaces between aluminium alloy 6063 and stainless steel AISI 316L are presented in Fig. 6.11.

Figure 6.11a shows that the aluminium alloy 6063 and stainless steel AISI 316L are forge-welded properly at T_w = 450 °C and F_w = 8 mm, where the weld interface is devoid of any cracks, voids, pores or discontinuity. Three distinct regions, the aluminium alloy 6063, stainless steel AISI 316L, and diffusion zone can be identified. In fact, the diffusion zone should be kept as narrow as possible because this zone contains intermetallic compounds, which are harder and more brittle than the parent metals. If the brittle diffusion zone is too thick, it may fracture in a random manner, and deteriorate the weld quality as well. Therefore, for the best welds produced by forge welding in this study, the thicknesses of their diffusion zones were restrained to around 4 μm. This was slightly thicker than those produced by Sundaresan et al. (0.15 μm) [145], but narrower than those produced by Bhanumurthy et al. (10 μm) [146]. This was the reason why these forge-welded bimetallic specimens had a tensile strength over 100 MPa.

Some hot-pressure welding and forge welding failed. This could be attributed to flawed diffusion at the weld interfaces. If the T_w and the process were determined inappropriately, the diffusion could not be completed fully. For example, the discontinuous weld with the average σ_t of 84.29 MPa was obtained by forge welding conducted at T_w = 350 °C and F_w = 8 mm. It shows clearly from Fig. 6.11b that the

diffusion at the weld interface was deficient. The weld was relatively weak because the closure of the micro-voids was incomplete, and weld discontinuities occurred. When a tensile load was applied to this bimetallic component, cracks developed from those defects.

Likewise, a cold shut was found in the weld interface of the unsuccessful weld obtained by hot-pressure welding at T_w = 450 °C and F_w = 8 mm, as shown in Fig. 6.11c. This defect was caused by the interruption of coalescence, in which the two dissimilar metals were being diffused. The punch speed used in the hot-pressure welding was much slower (approximately 20 mm/s) than that used in the forge welding even though their process parameters were the same. In the hot-pressure welding, the pressure could not be applied punctually on the mating surfaces during the diffusion of the two metals. Therefore a portion of the surface of the weld was separated after the diffusion period.

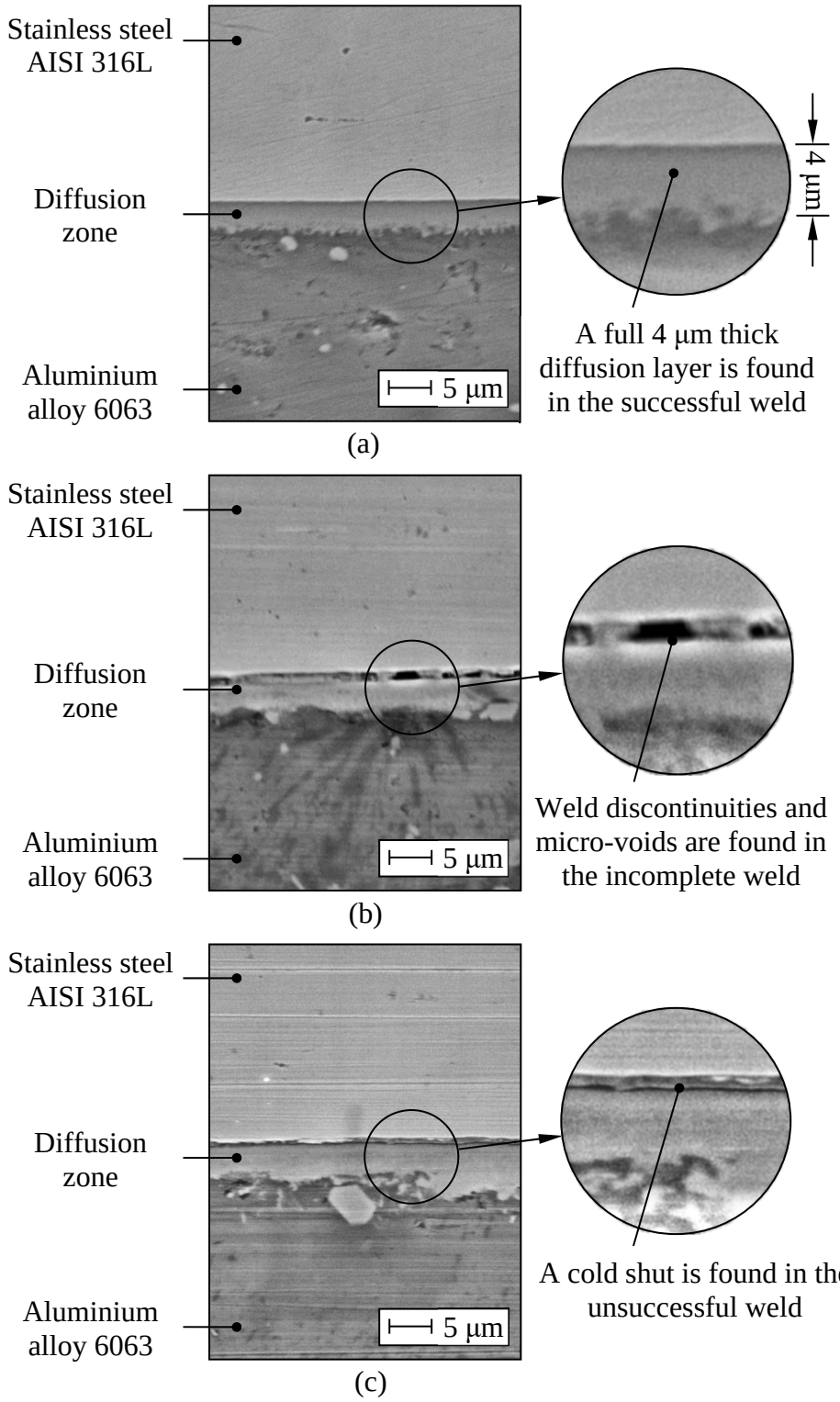

Fig. 6.11 SEM metallography of weld interfaces: (a) successful weld obtained by forge welding at T_w = 450 °C, F_w = 8 mm, (b) discontinuous weld without fully diffusion obtained by forge welding at T_w = 350 °C, F_w = 8 mm, and (c) unsuccessful weld obtained by hot-pressure welding at T_w = 450 °C, F_w = 8 mm.

The composition across the diffusion zone was obtained using EDX. The profiles for Cr, Mn, Si, Fe, and Al across the diffusion zone of the successful weld produced by forge welding at T_w = 450 °C and F_w = 8 mm are shown in Fig. 6.12. The diffusion zone in the middle of the range contained around 40 to 50 weight % of Fe and 30 to 40 weight % of Al. According to the XRD analysis shown in Fig. 6.13, these are expected to be the intermetallic compounds: $FeAl_3$, Fe_2Al_5, Fe_3Al, and Al_5Fe_2, while the other two zones might correspond to $Al_{13}Fe_4$ near the aluminium alloy 6063 region and AlFe near the stainless steel AISI 316L region. Thus, these results provide critical evidence that the two dissimilar metals were welded properly.

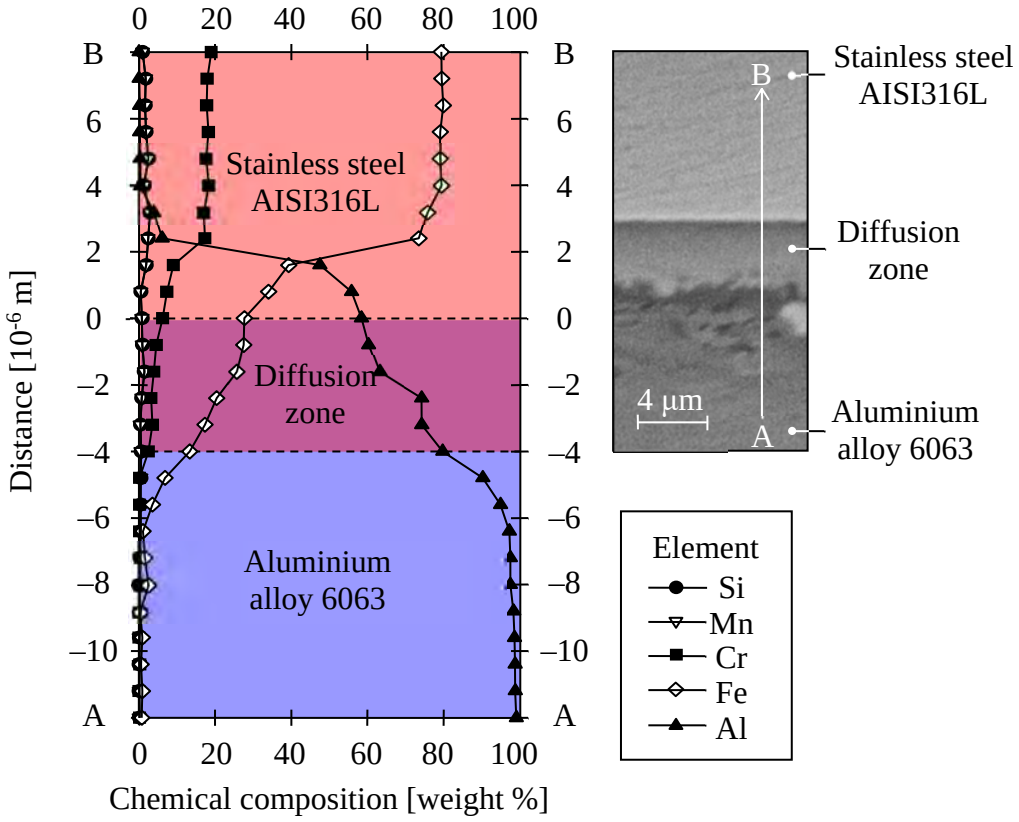

Fig. 6.12 The composition for various elements across the diffusion zone of the specimen produced by forge welding at T_w = 450 °C and F_w = 8 mm.

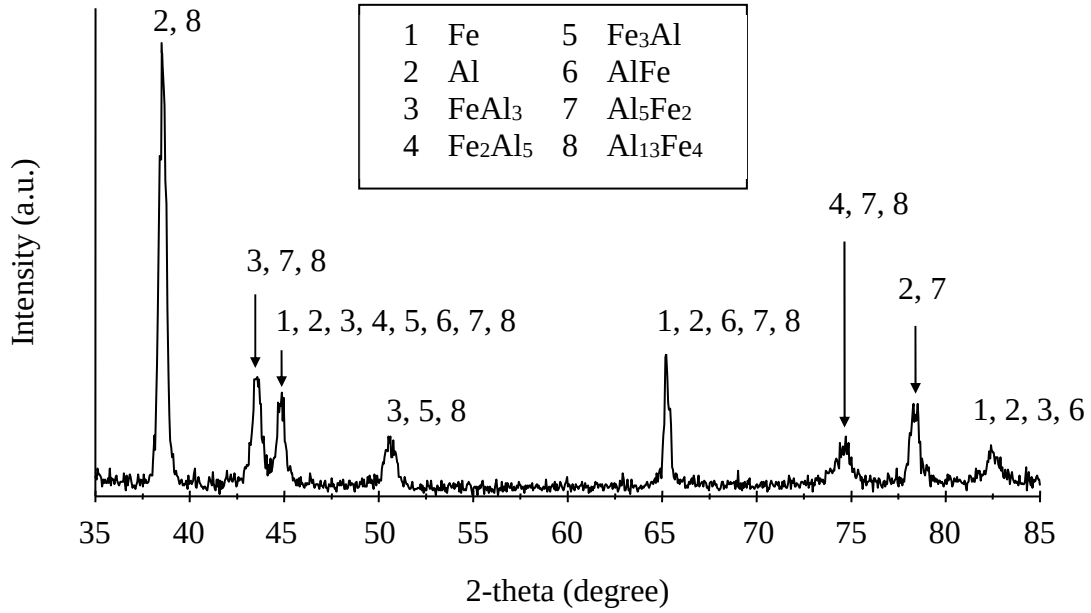

Fig. 6.13 XRD analysis shows the intermetallic compounds of iron (Fe) and aluminium (Al) within the diffusion zone.

The reliability of the hot-pressure welding and forge welding can be demonstrated by the control charts (R charts and X-bar charts) as shown in Figs. 6.14 and 6.15. The x-axes of the charts were the subgroups (i.e., nine trials with different combinations of T_w and F_w). The y-axes of the charts were the range (in R charts) or the mean of the σ_t (in X-bar charts) that acted as the qualitative indexes of bimetallic components.

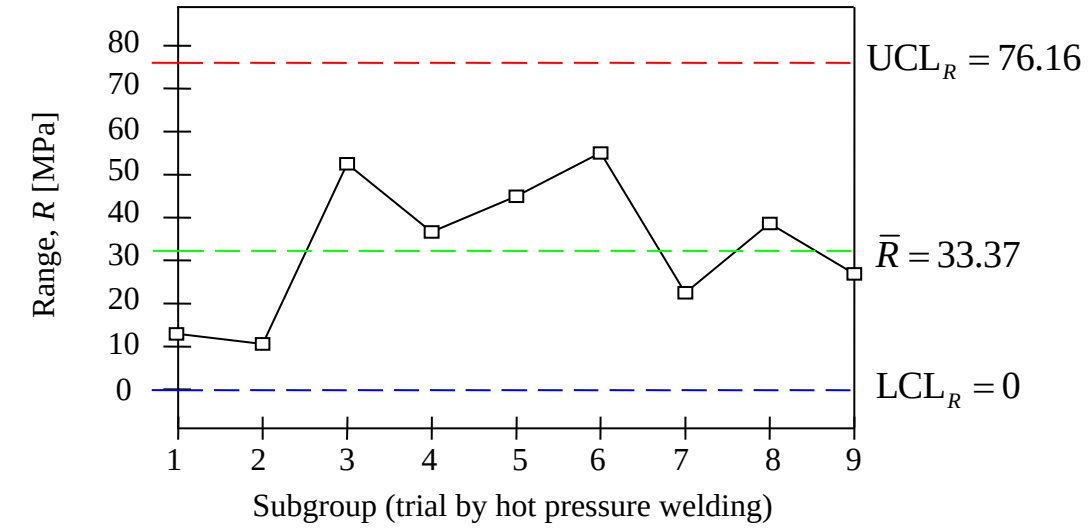

(a) *R* chart of hot-pressure welding

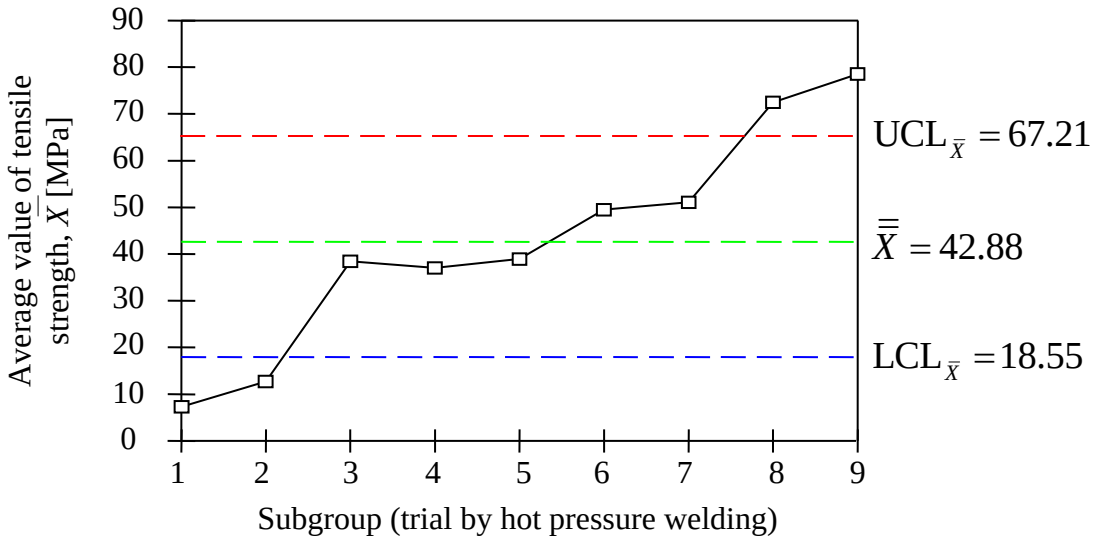

(b) *X*-bar chart of hot-pressure welding

Fig. 6.14 (a) *R* chart and (b) *X*-bar chart for the tensile-strength data of bimetallic welds produced by hot-pressure welding.

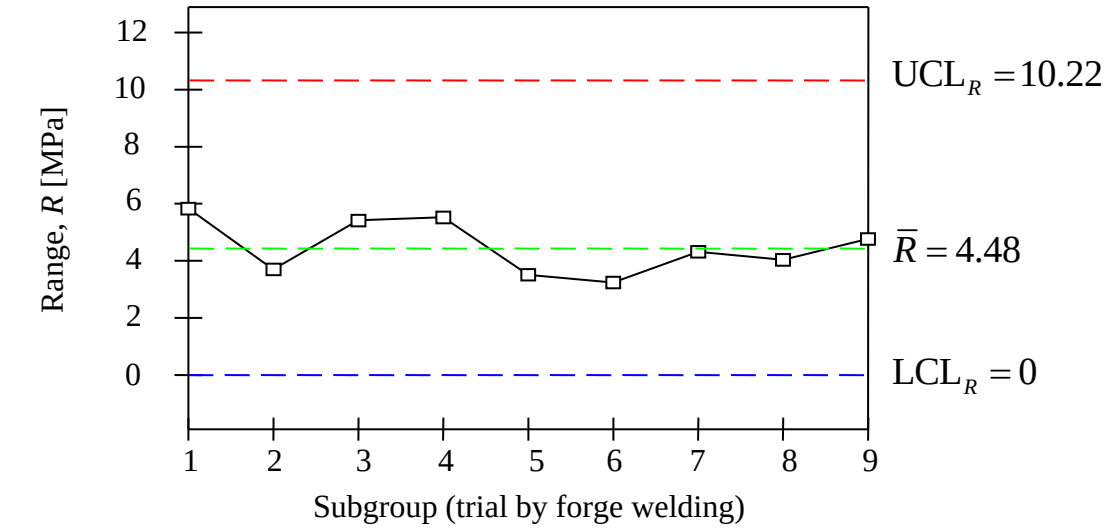

(a) *R* chart of forge welding

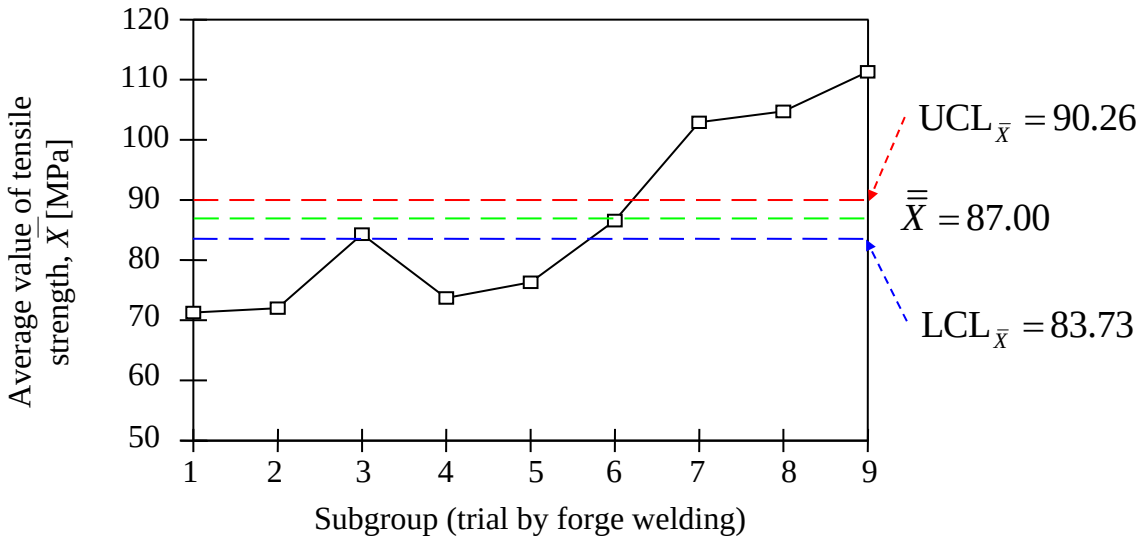

(b) *X*-bar chart of forge welding

Fig. 6.15 (a) *R* chart and (b) *X*-bar chart for the tensile-strength data of bimetallic welds produced by forge welding.

The *R* charts illustrate that both welding processes were in the state of statistical control, since no data point falls outside the 3-sigma control limits. The hot-pressure welding was more unstable than the forge welding because of its larger *R*-bar (average

range). Especially in trials 3 and 6, the differences between the σ_t of their best and worst specimens were greater than 50 MPa, which was nearly the half strength of the good-quality bimetallic components obtained in forge welding. In both processes, the T_w and F_w were monitored carefully by using the infra-red thermal imaging camera and the slide heights of presses. They should be compatible, except for the use of presses and holding time. The tensile-test conditions were the same. In other words, the major factor (i.e., the special cause) causing the unreliable hot-pressure welding and its weld-quality problems was neither the T_w and F_w nor the tensile test. It was in fact the punch speed of the hydraulic press. The mechanical press used in reliable forge welding can provide a punch speed approximately three times higher than that given by the hydraulic press, although it is not a constant speed. The higher punch speed in forge welding actually provides an impulsive force that can avoid losing heat from the center of the weld. Since the thermal imaging camera could only measure the surface temperatures of specimens, the temperatures of their cores were neglected and assumed to be isothermal. In the metallography of unsuccessful welds produced by hot-pressure welding, many cold shuts and partial weld discontinuities were found near the center of the weld interface. The diffusion of certain zones was incomplete since the temperature could not be kept even during the slower deformation process. This is the reason why the reliability of hot-pressure welding is lower.

From the R charts the points on the *X*-bar charts can be interpreted. Even though 7 of the 9 data points in the *X*-bar chart of forge welding fall outside the control limits, this does not mean that the forge welding is out of control. In view of the fact that the

T_w and F_w in each trial are different, the *X*-bar chart just gives the picture that the weld quality of forge welding is influenced highly by them. Comparing the two welding processes, the tendencies of their curves in the *X*-bar charts are similar in that the increment of σ becomes severe by increasing the T_w and F_w. However, the quality of the welds produced by forge welding is better. This is because the impulsive force applied on the weld interface is faster than the isostatic pressure. According to the fundamentals of material flow-stress, the effect of strain rate on flow stress is more significant at elevated temperatures. For the same amount of deformation, the required flow stress (or applied pressure) is greater at a higher strain rate. The ram speed is proportional to the strain rate whereas the applied pressure on the weld interface can be varied by adjusting the ram speed. The faster ram speed and impulsive force used in forge welding not only improve the quality of bimetallic welds, but also reduce the processing time.

The above study investigated the quality of aluminium alloy 6063 and stainless steel AISI 316L bimetallic welds produced by hot-pressure welding and forge welding. The best-quality weld with average σ_t around 111.3 MPa was produced by forge welding successfully at T_w = 450 °C and F_w = 8 mm. The flawless diffusion zones were identified at the joint interface, which provided critical evidence for validating the process capability. Indeed the overall weld quality of hot-pressure welding was satisfactory because its highest average σ_t was 78.5 MPa that already reached over 87 % of joint efficiency. Even though the intermetallic bond produced by hot-pressure welding was imperfect, such provided σ_t could totally achieve the requirements of

most bimetallic products or components such as casings, heads of golf club, and shields. Furthermore the weld quality was not significant in the aspect of workpiece, billet, or preform design using either forward or reverse simulation approaches. The predicted billets or preforms should be applicable for warm-forming processes employing mechanical presses or hydraulic presses with the ram speed higher than 40 mm/s, as completing the best-quality bimetallic components.

6.1.4 Suitable process conditions for warm-forming bimetallic components

All eighteen simulations and corresponding experiments of warm forming bimetallic watch-case-like components with various combinations of forming temperature T_f (i.e., the forming temperature of stainless steel AISI 316L) of 400, 500, 600, 700, 800, and 900 ºC and ram speed S_r of 20, 40, and 60 mm/s were performed. As a satisfactory bimetallic component, a diffusion zone between two dissimilar metals should be able to be found in its joint interface. This was one critical factor among others providing evidence of which of the metals had been cohered properly. Figure 6.16 shows the micrograph of the bimetallic joint interface obtained from the sample taken in the experimental trial carried out at T_f = 900 ºC and S_r = 40 mm. Three distinct regions were demonstrated. The upper side was the stainless steel AISI 316L, the lower side was the aluminium alloy 6063, and the middle was the diffusion zone. The thickness of this diffusion zone was around 4 µm, which was generated in this successful bimetallic component without any macro-defects. The joint of the dissimilar

metals was sufficiently reliable that the bimetal would not be broken and separated under the destructive test with the hack saw and files.

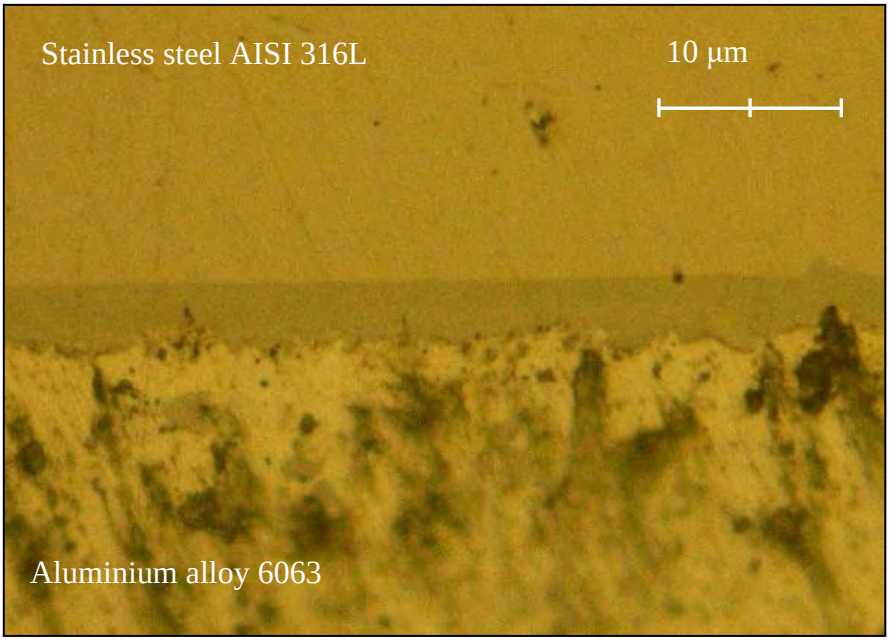

Fig. 6.16 The micrograph of the bimetallic joint interface shows good cohesion of the sample (T_f = 900 °C and S_r = 40 mm/s).

Nevertheless, in some simulation and experimental results, the stainless steel AISI 316L could not completely fill up the die cavities, in particular the 0.3 mm thick circular protrusion of the top face of the component. Figure 6.17 is an example obtained in the process simulated with T_f = 400 ºC and S_r = 20 mm/s. It illustrates that there were two major unfilled areas. The unfilled area A (UA) was located on the top circular protrusion and the unfilled area B (UB) was near the lateral portion of the lug. These two defects could also be found in most unsuccessful components.

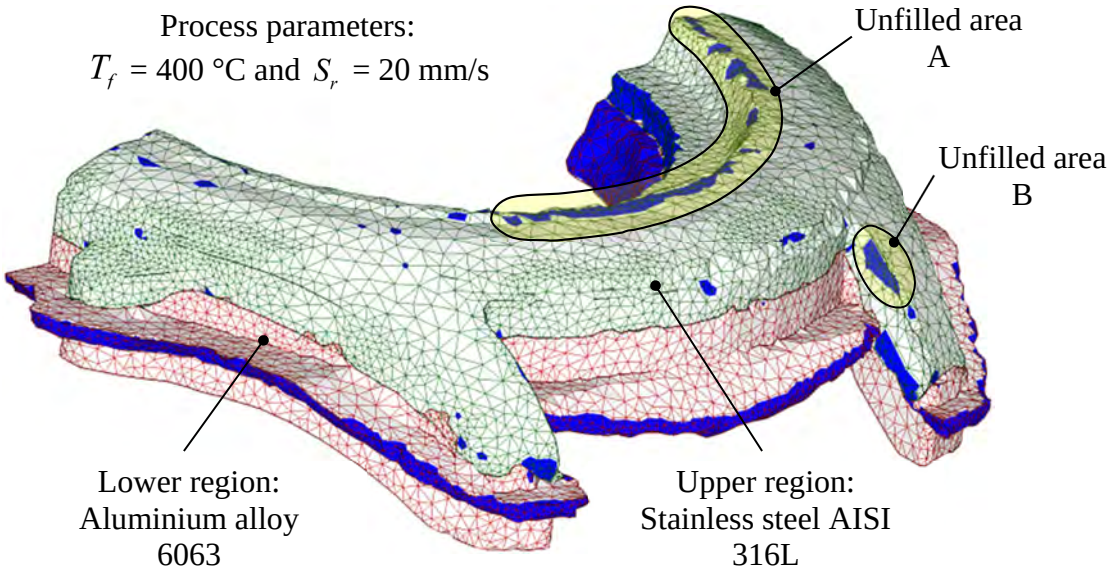

Fig. 6.17 The unfilled areas of the unsuccessful formed component after simulation.

Figure 6.18 shows the completion of die filling in each trial. The y-axis of the graph was labelled the die-filling percentage, which was based on the ratio of the minimum height of UA (measured at the end of the forming stroke) to the full height of UA (i.e., 0.3 mm). A lower percentage meant that a larger cavity of the die had not been filled whereas the complete die filling was achieved in the hundred-percent completion. As shown by both simulation results and experimental measurement, the increases of T_f and S_r were able to improve the die filling.

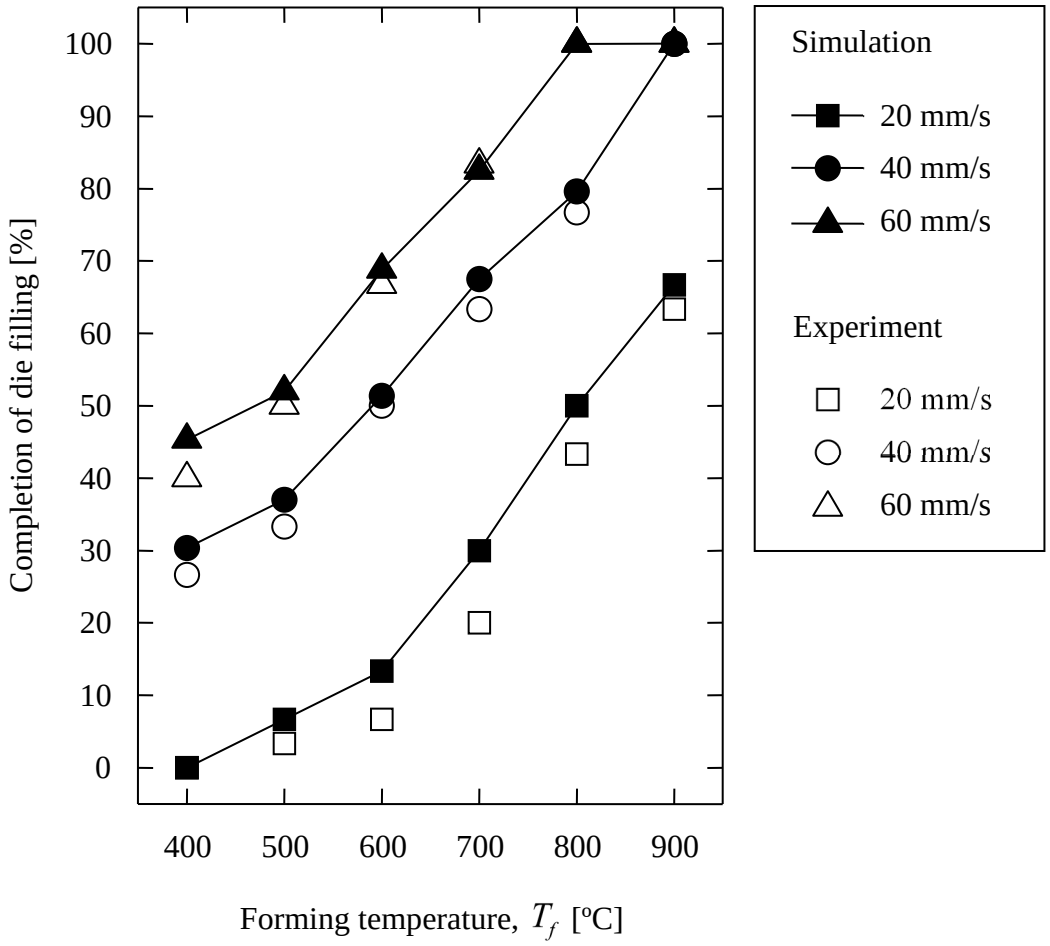

Fig. 6.18 The completion of die filling for each trial.

(i) Effects of forming temperature

The bulk-forming simulations and experiments were carried out under non-isothermal conditions. The initial temperatures of the two separated preforms and the die components were different, as given in Table 5.4. Heat transfer between their contact surfaces occurred during the process. According to the fundamental of material deformation behaviour, changes of temperature of the preforms highly influenced the material flow as well as the die filling, and hence this had to be discussed additionally. Both stainless steel AISI 316L and aluminium alloy 6063 softened when their

temperatures were increased. Consequently the temperature discrepancy between these two materials at the identical time step T_{di} should be kept to a certain amount. In other words, the stainless steel AISI 316L should be much hotter than the aluminium alloy 6063. This could compensate for the extreme difference of their plasticity so that the die filling is improved considerably. Figure 6.19 shows the average temperatures T_{av} of stainless steel AISI 316L and aluminium alloy 6063 entire workpieces at the stroke of 11 mm (i.e., the end of forming stroke) in each simulation trial. Three trials that achieved the complete die filling were the processes carried out at T_f = 900 ºC and S_r = 40 mm/s, T_f = 800 ºC and S_r = 60 mm/s, and T_f = 900 ºC and S_r = 60 mm/s, their T_{di} being 582, 583, and 640 ºC respectively. On the other hand, the T_{di} of the slightly failed trial (T_f = 800 ºC and S_r = 40 mm/s) was just 521 ºC. It showed that the T_{di} had a great effect on the die filling in bulk-forming bimetallic components and the T_{di} higher than 580 ºC was significant in this present case.

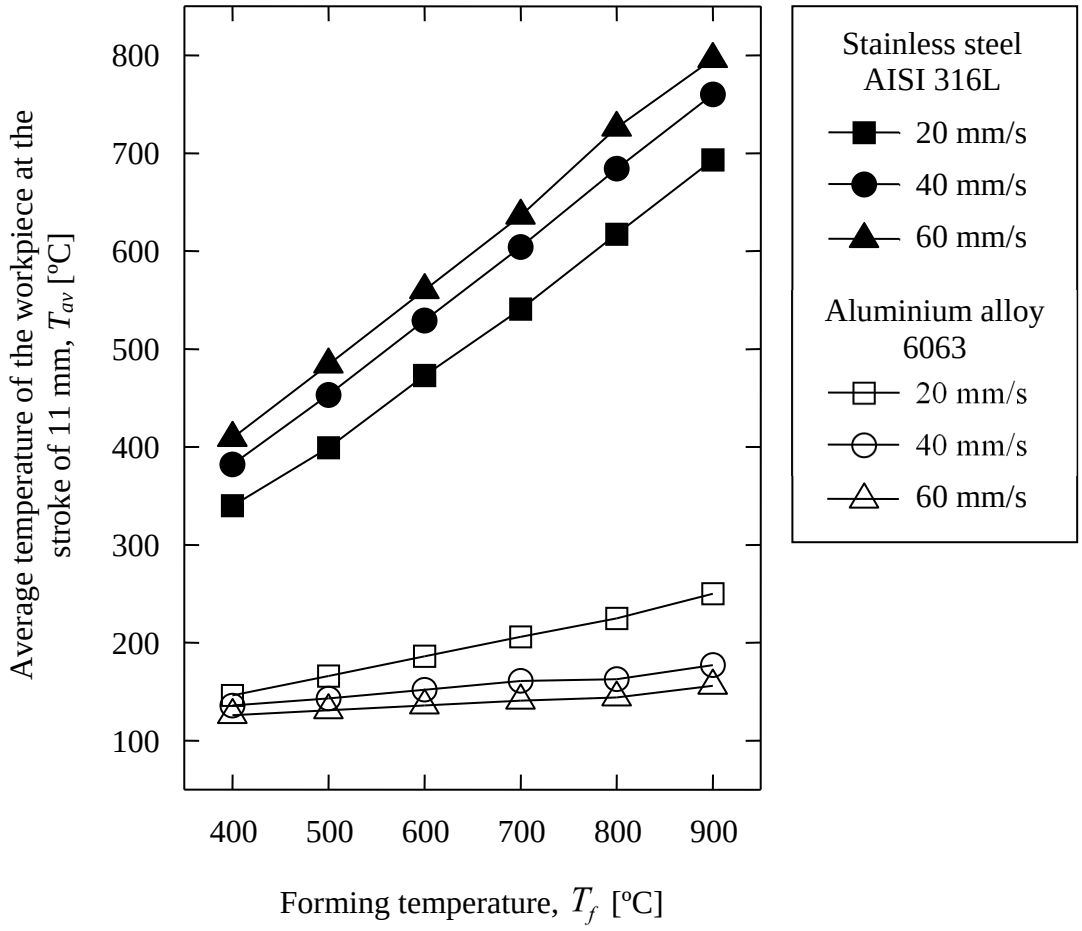

Fig. 6.19 The simulated average temperatures of stainless steel AISI 316L and aluminium alloy 6063 at the stroke of 11 mm for each trial.

The curves plotted in Fig. 6.19 were nearly linear within the test range of T_f, which indicated that the T_{av} drops of stainless steel AISI 316L and the T_{av} raises of aluminium alloy 6063 were uniform. The average percentages of T_{av} drops of stainless steel AISI 316L for S_r of 20, 40, and 60 mm/s were 26.5, 13.3, and 6.9 % respectively. When the faster S_r was used, the T_{av} drops of stainless steel AISI 316L were reduced that could increase the T_{di} and get the better die filling. Indeed the T_{av} of stainless steel AISI 316L had increased slightly at the forming stroke of around 1 mm since that position was starting deformation of the stainless steel AISI 316L and

the heat was generated by the compression of material. Therefore, the average percentage of its T_{av} drop was not an exact inverse proportion to the S_r . To the contrary, the T_{av} of aluminium alloy 6063 was raised much higher at the S_r of 20 mm/s, because the heat from the stainless steel AISI 316L could take a longer time to transfer to the aluminium alloy 6063. Since the thermal conductivity of aluminium alloy 6063 was higher than that of stainless steel AISI 316L, the degree of change of temperature of aluminium alloy 6063 was larger than that of stainless steel AISI 316L.

(ii) Effects of ram speed

The S_r not only affected the T_{av} of specimen materials, but also extended the effect on material flow. The flow patterns of two different materials during the bulk-forming process were investigated using velocity fields of the simulation. Since the discrepancy of the flow directions was not very noticeable between all eighteen trials, the simulation of the processes carried out with the combinations of T_f of 400, and 900 ºC and S_r of 20, 40, and 60 mm/s were selected particularly to demonstrate the changing of their velocity fields at the strokes of 10 and 11 mm, as shown in Fig. 6.20. Except for the unfilled areas of the unsuccessful components, the geometries and bimetallic structure of all the formed components were quite similar. Only the influence of S_r on the magnitudes of velocity was more consequential and had indicated a linear proportional relationship. For instance, the velocities of material flow in the processes taking place at S_r = 60 mm/s were almost three times those of the processes taking place at 20 mm/s. In considering the material flow at different

forming strokes, the materials of the lower region (aluminium alloy 6063) and the materials of the upper region (stainless steel AISI 316L) of the components flowed simultaneously at the stroke of 10 mm. However, at the stroke of 10.5 mm, the aluminium alloy 6063 started flowing faster than the stainless steel AISI 316L. At the end of the stroke, the stainless steel AISI 316L nearly stopped with less deformation and material flow while the aluminium alloy 6063 flowed rapidly. The reason for this was that the flow properties of aluminium alloy 6063 at the initial forming stage were close to those of stainless steel AISI 316L, hence the heterogeneous material flow was minimised and both materials could flow together with parallel velocity fields. Due to the rapid increasing of T_{av} of aluminium alloy 6063, from the stroke of around 11.5 mm, the aluminium alloy 6063 became softer than the stainless steel AISI 316L such that the material flow mainly occurred in the region of aluminium alloy 6063. Therefore, in warm forming aluminium alloy 6063 and stainless steel AISI 316L bimetallic components, particularly at the lower S_r (i.e., equal or below 20 mm/s), the T_f must be sufficient or higher (i.e., over 900 ºC) to led the completed die filling in the region of stainless steel AISI 316L before the softening of aluminium alloy 6063.

T_f	S_r	Stroke			Velocity scale
[°C]	[mm/s]	10 mm	10.5 mm	11 mm	[mm/s]
400	20	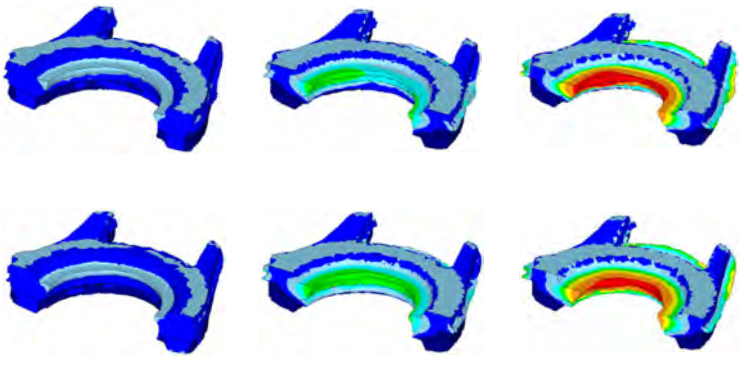			
900	20				
400	40	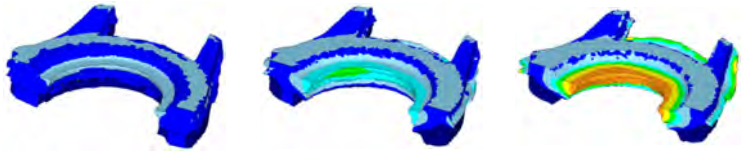			
900	40	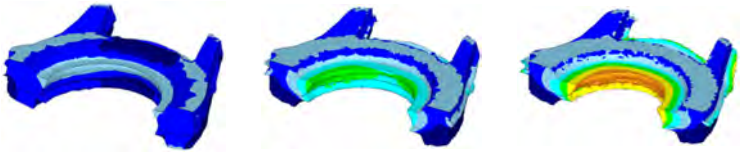			
400	60	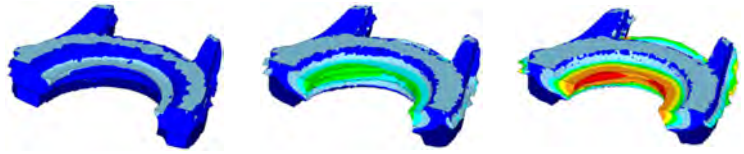			
900	60	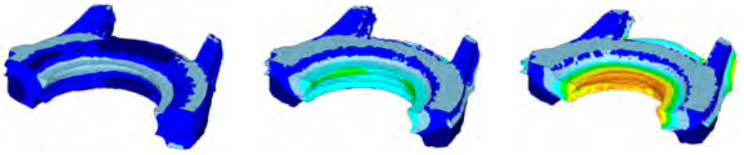			

Fig. 6.20 The simulated velocity field at the stroke of 10, 10.5, and 11 mm for the trials of the process carried out at the combinations of forming temperature (400 and 900 °C) and ram speed (20, 40, and 60 mm/s) respectively.

The forming load F_l required for the bulk forming could be predicted by the simulation software as well as recorded in the experiments. Figure 6.21 shows the peak values of the F_l in each trial. There was a relatively large error between simulations and experiments at 400 and 500 ºC. However, this 3.7 to 4.4 % error was acceptable since the main purpose of this graph was to reflect the natural phenomenon of T_f and S_r to F_l. The F_l was influenced significantly by T_f and S_r. The F_l was reduced overall when the T_f was increased. Although the T_{av} drop of stainless steel AISI 316L at the S_r of 20 mm/s was larger than that at 60 mm/s, the F_l was higher at the faster S_r. Consequently the impact of S_r on F_l was more considerable than that of T_f on F_l. As die life increased with decreasing F_l, if the T_f could be increased, it was recommended to reduce the S_r of the machine for warm forming the aluminium alloy 6063 and stainless steel AISI 316L bimetallic components.

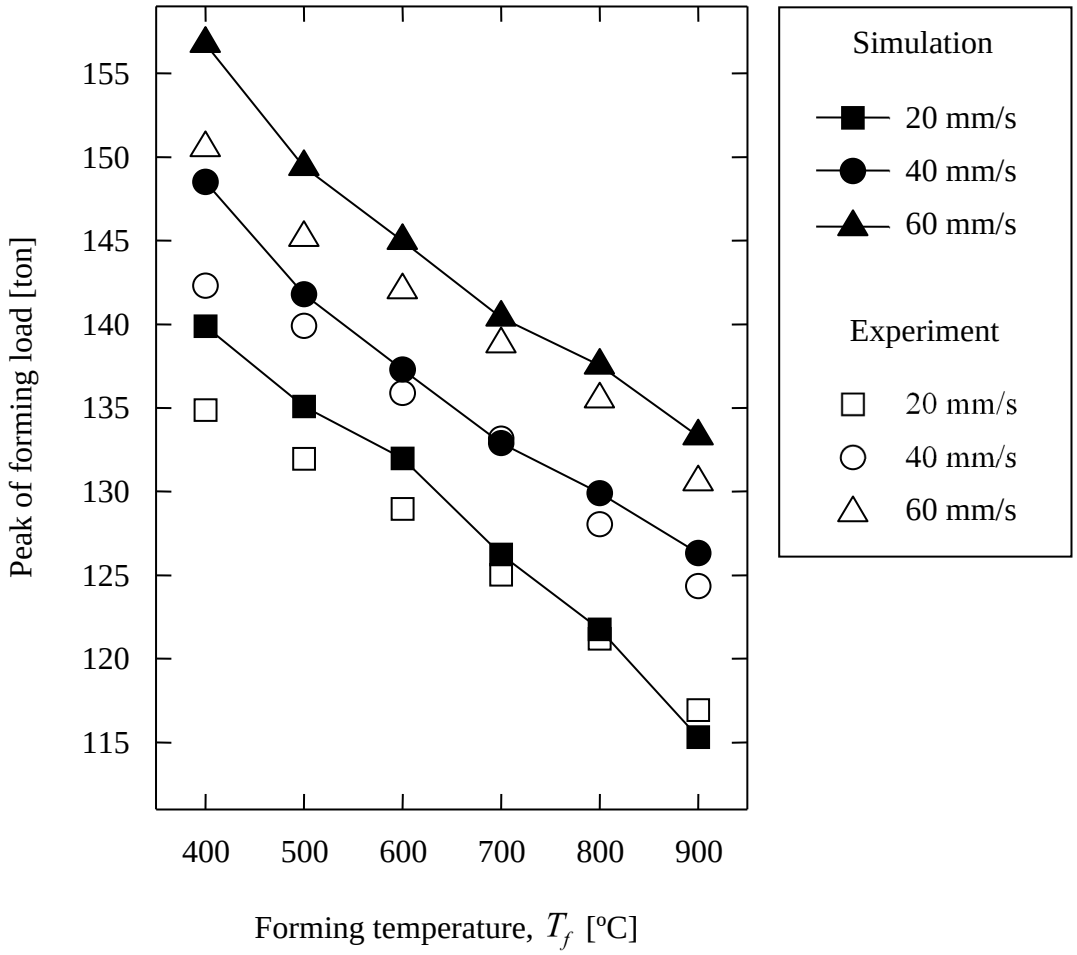

Fig. 6.21 The forming loads required for warm forming the bimetallic components.

In order to verify the proposed methodology and the results obtained from the computer simulation, physical experiments were conducted using the tailor-made die and a mechanical press specially modified for bimetal bulk forming. The process conditions were controlled to nearly match the setting of the simulation, with only the T_f having possible variations of ± 15 ºC and the S_r was adjusted as around 20, 40, and 60 mm/s within the range of forming load. The bimetallic component obtained by the process with T_f = 900 ºC and S_r = 40 mm/s was selected as the most successful example because it was able to completely fill up the die cavity with a minimum F_l, the peaks of F_l of this trial in simulation and experiment were 126 and 124 tons

respectively. On the other hand, the unsuccessful example was taken from the process with T_f = 400 ºC and S_r = 40 mm/s. These two examples of bimetallic components produced by bulk forming are presented in Fig. 6.22. Almost no major forming defect was found on the successful formed component, and the accuracy of critical dimensions such as the total width, length, height, and flash thickness was within a tolerance of ± 0.08 mm. For the unsuccessful component, the unfilled areas were located nearly the same as the simulation result. Those shapes were close to the results acquired in the simulation that thus confirmed the accuracy and reliability of the software.

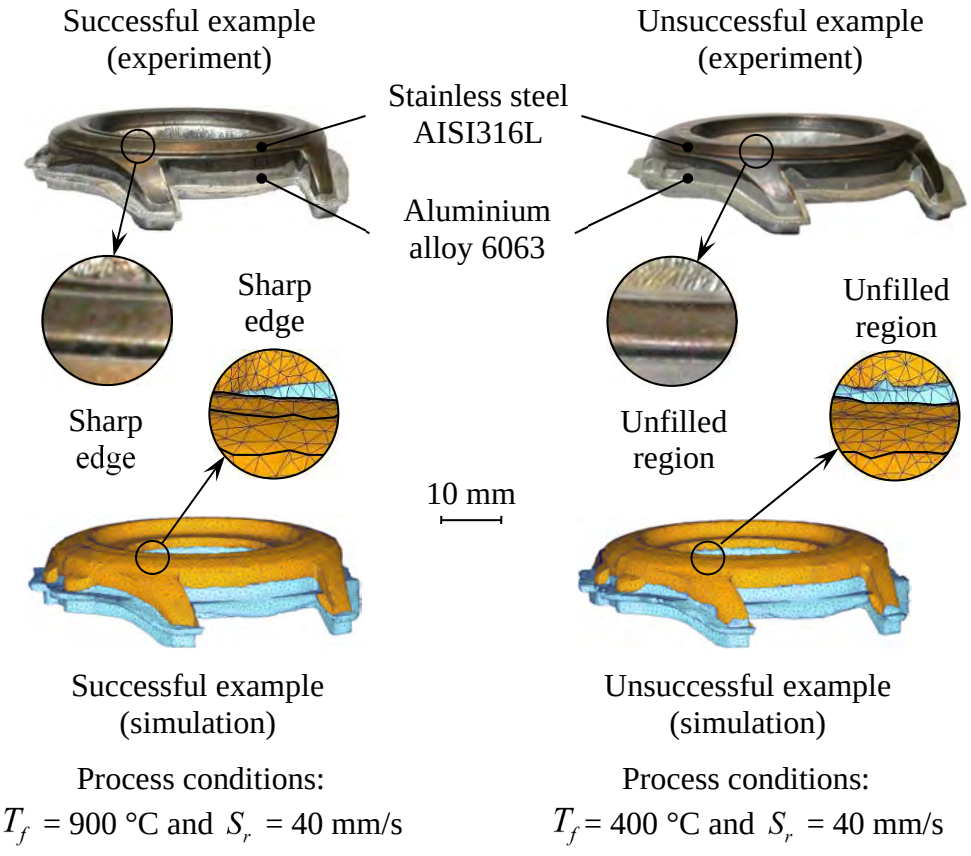

Fig. 6.22 Comparison of component shapes between simulation and experiment for T_f = 400 and 900 °C, and S_r = 40 mm/s.

Figure 6.23 gives another example of warm-forming bimetallic component (it is a watch-case-like component also) using mechanical presses with the aid of computer simulation. Those simulations were carried out by using a commercial three-dimensional FEM package, DEFORM-3D [121]. It was apparent that the results acquired from the simulation agreed with those of the experiments.

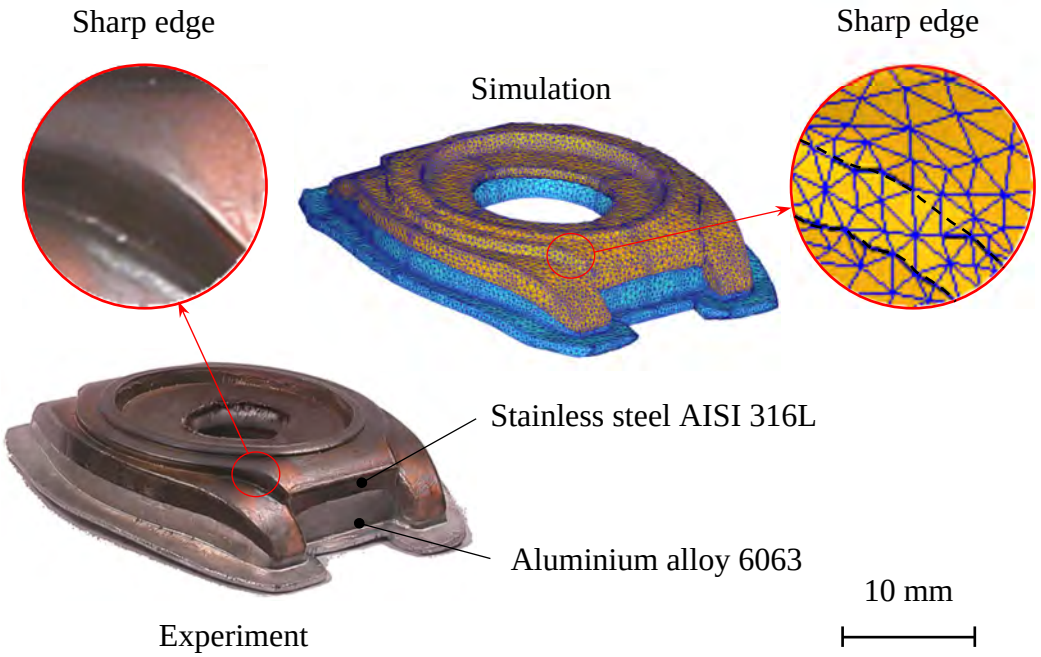

Fig. 6.23 Another successful example of warm-forming bimetallic components with the aid of computer simulation.

Therefore, for modelling the warm-forming process of bimetallic components by the reverse simulation approach, a virtual forming press with the compatible ram speed of the hydraulic press used for typical warm-forming (i.e., 40 mm/s) can be applied, since the constant die velocity is more appropriate for the calculation of reverse velocity fields as well as time increments. In addition, according to the

metallography of the bimetallic interface, the thickness of the diffusion zone was extremely small (i.e., 4 μm as shown in Figs. 6.11 and 6.12) compared to both base metals, and hence this zone or layer would be disregarded when preparing the simulation in DEFORM-2D.

6.2 Evaluation of reverse simulation approach

The rigid-perfectly plastic model with flow stress data was valid for warm-forming the aluminium alloy 6063 and stainless steel AISI 316L. In order to have an accurate verification of reverse simulation, the physical experiments and the forward simulation were performed using the same materials with the compatible forming temperature as well as ram speed (i.e., die velocity). Since the final shapes of three case studies (Fig. 5.8) were similar, the forming die used in the practical work (Fig. 5.15) was able to be as different configurations of die cavities.

6.2.1 Process conditions for simulation

The process conditions for both reverse and forward simulations are summarised in Table 6.4. They were all compatible with the practical experiments. In case studies 1 and 2, the selected forming temperature was 300 °C that was the typical warm-forming temperature for aluminium alloy [2,3]. On the other hand, for the warm forming of bimetallic component in case study 3, the critical temperature of 450 °C should be adopted preferentially as the temperature of the aluminium alloy 6063

section, when the temperature of stainless steel AISI 316L section was set to 900 °C, as mentioned in the previous sections. The shear-friction factor of 0.2 was defined as interface between the specimen materials and die surface since the lubricant W-400 was understood to be applied on the die surface. Nevertheless, the contact of the faying surface of the joint of aluminium alloy 6063 and stainless stress AISI 316L should be dry, and thus the shear friction factors of 0.5 and 0.9 were selected as the sliding condition and sticking condition respectively.

Table 6.4 Process conditions for both reverse and forward simulations.

Process conditions	Case study			
	1	2	3	
Material	Aluminium alloy 6063		Aluminium alloy 6063	Stainless steel AISI 316L
Forming temperature (isothermal condition) [°C]	300	300	450	900
Die velocity (constant speed) [mm/s]	40	40	40	
Shear friction factor (die/workpiece interface)	0.2	0.2	0.2	
Shear friction factor (interface of two specimen materials)	N/A	N/A	sticking condition (m = 0.9) sliding condition (m = 0.5)	

6.2.2 Case study 1 – axisymmetric component

The overall process of reverse simulation started form the final shape of case study 1 as shown in Fig. 6.24. While the top die was being moved upwards, the

material flowed gradually backwards into the desired shape, which was determined by the material distribution with the minimum height of the workpiece subject to the assumption of constant volume. During the backward deformation, the height of the desired shape decreased, consistent with the corresponding reverse shape. The complexity of the workpiece was reduced as well. In other words, the reverse shape progressed towards a simple geometry. The simulation was able to predict the initial billet close to a cylindrical plate successfully. This was then regarded as the billet for this one-stage forming in both forward simulation and practical experiment. The size of the predicted billet was determined as Ø44.98 × 5.87 mm.

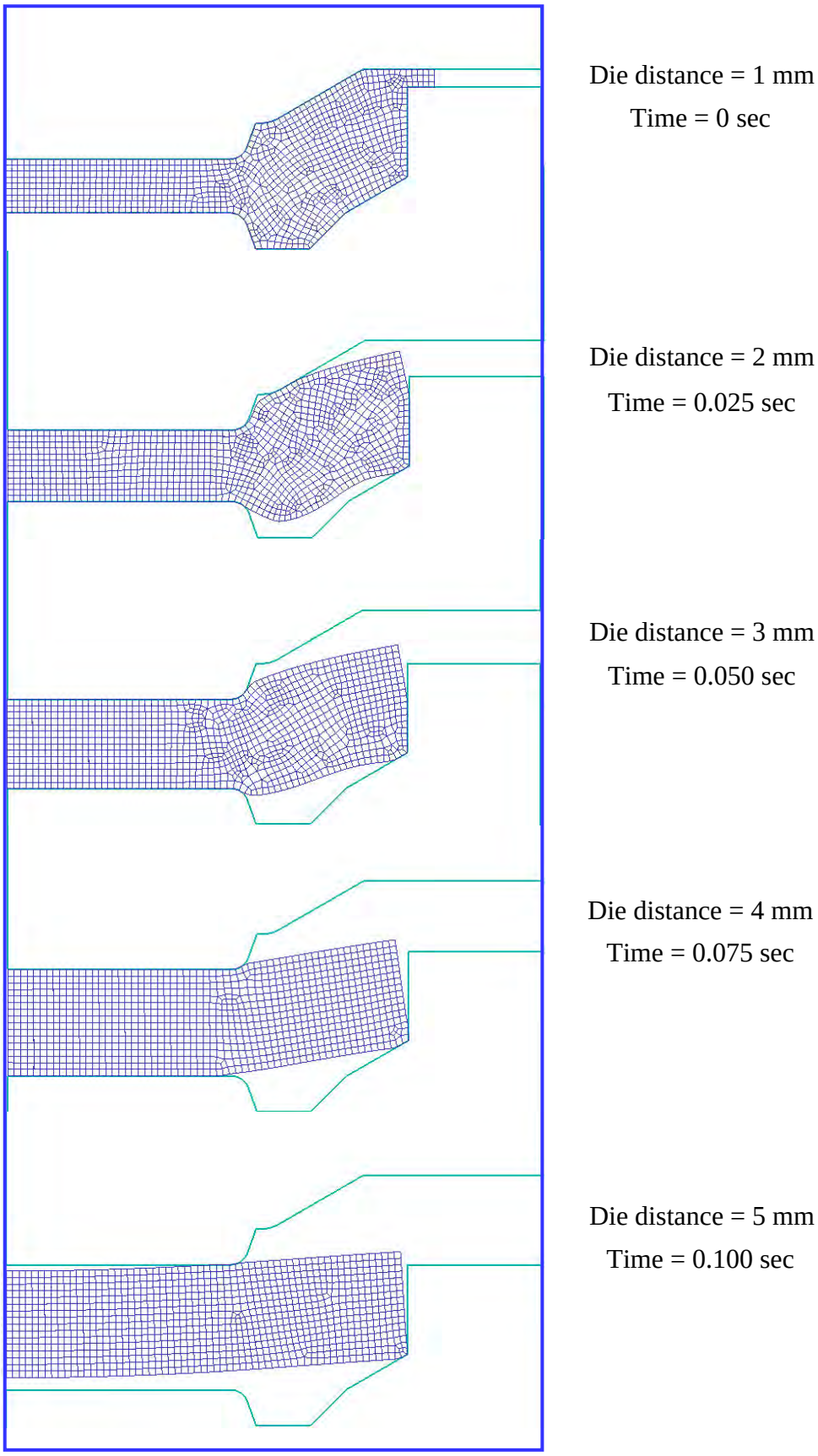

Fig. 6.24 Reverse simulation of warm forming axisymmetric component.

The predicted billet was taken to process the forward simulation by using DEFORM-2D with the same process conditions. The trend of the deformation as shown in Fig. 6.25 is nearly exactly the same as that predicted by the reverse simulation. This outcome was to be expected, since these two billets had no significant difference. According to the procedures of the reverse simulation, the reverse shape predicted at each reverse increment was verified by the forward simulation at the corresponding time increment. Once the shape verification failed, the shape could be reconstructed by the PO method that compensated the lacking volume and eliminated the excess volume in particular regions of the reverse shape. Furthermore, many jagged and concave boundaries found in the unacceptable reverse shape have been treated by the methods of shape reconstruction described in Chapter 4. Therefore the proposed reverse simulation approach could ensure that the material flowed into the die cavity completely as achieving the final shape.

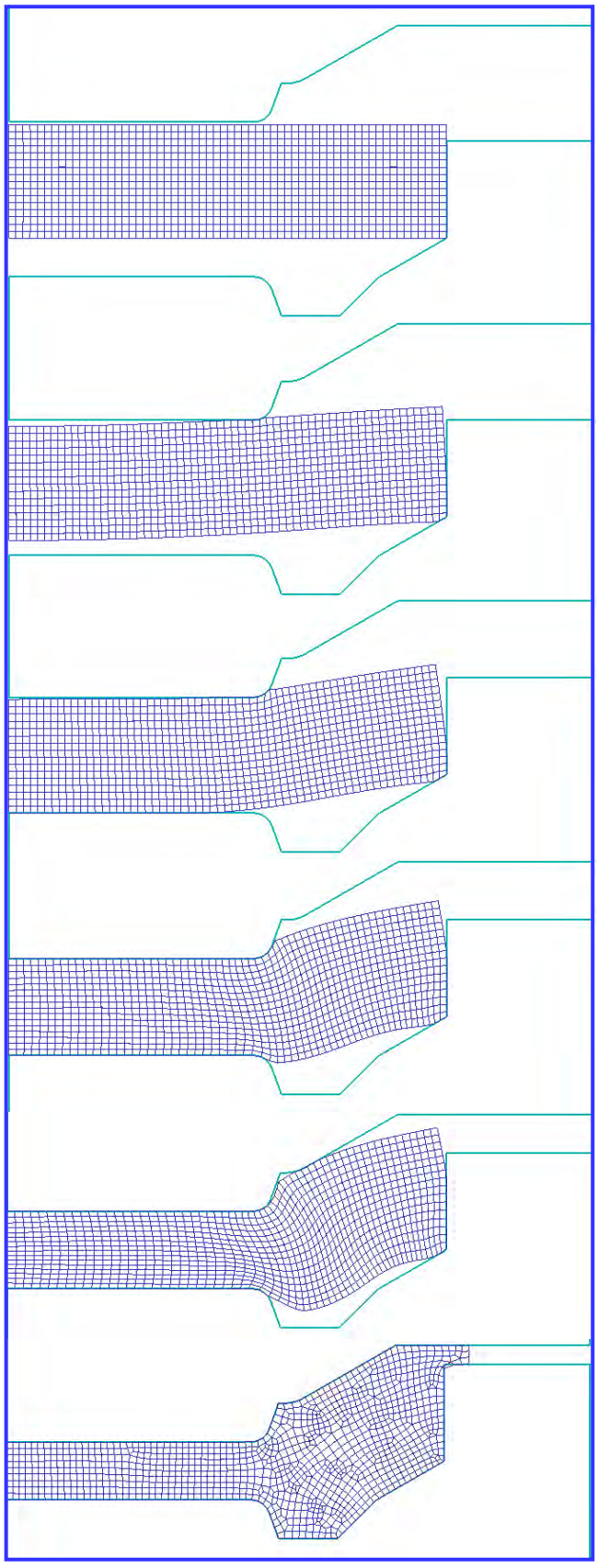

Fig. 6.25 Forward simulation of warm forming axisymmetric component.

Figure 6.26 presents the experimental results from the billet to the final shape. It should be noted that the diameter and height of the billet had to be reduced to Ø44.6 mm or smaller and increased to 6.0 mm, respectively. The diameter of the predicted billet was very close to the size of the cavity of the bottom die. In the actual warm-forming condition, the billet could not be placed into the bottom die due to the thermal expansion of material. In comparison with the experimental result of the cross-section of the formed component as shown in Fig. 6.27, likewise it was almost the same as the predicted profiles from both reverse simulation and forward simulations.

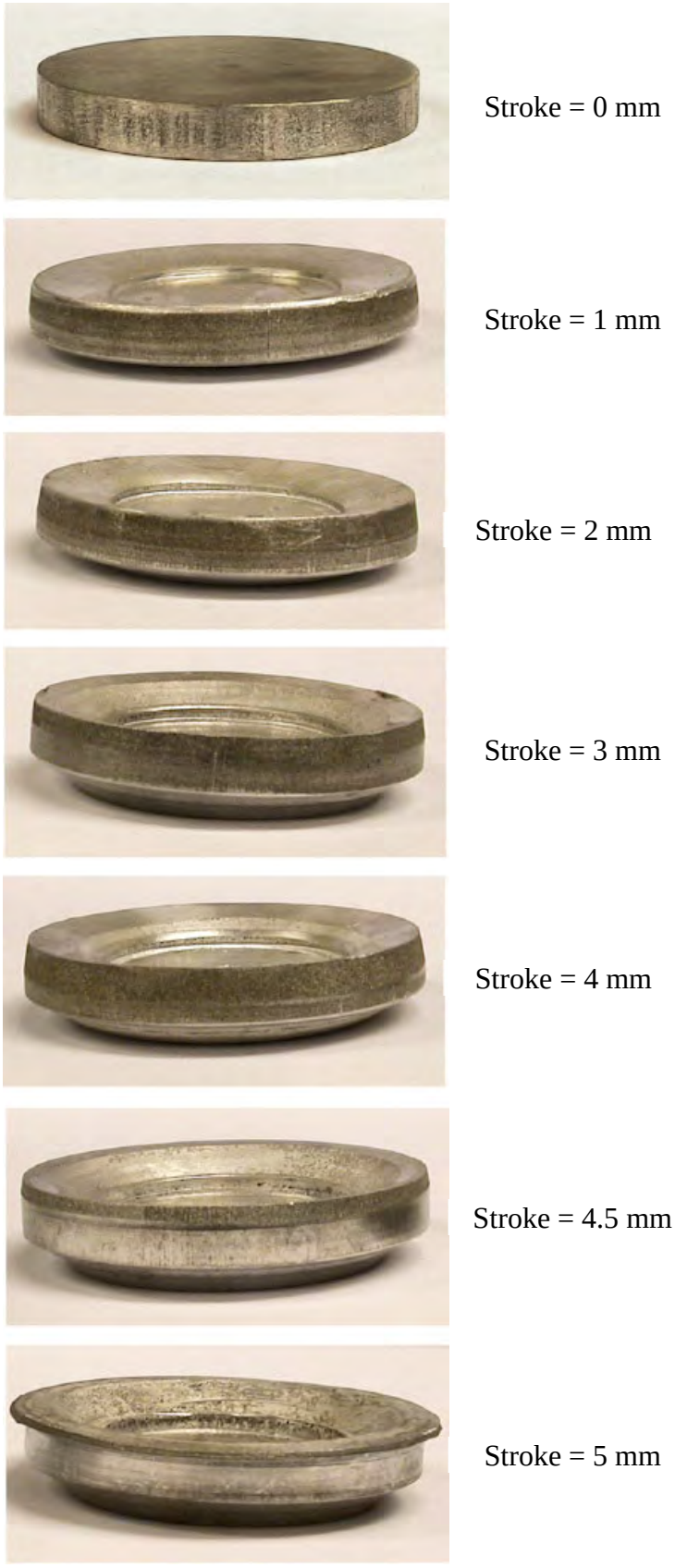

Fig. 6.26 The axisymmetric component produced by warm forming.

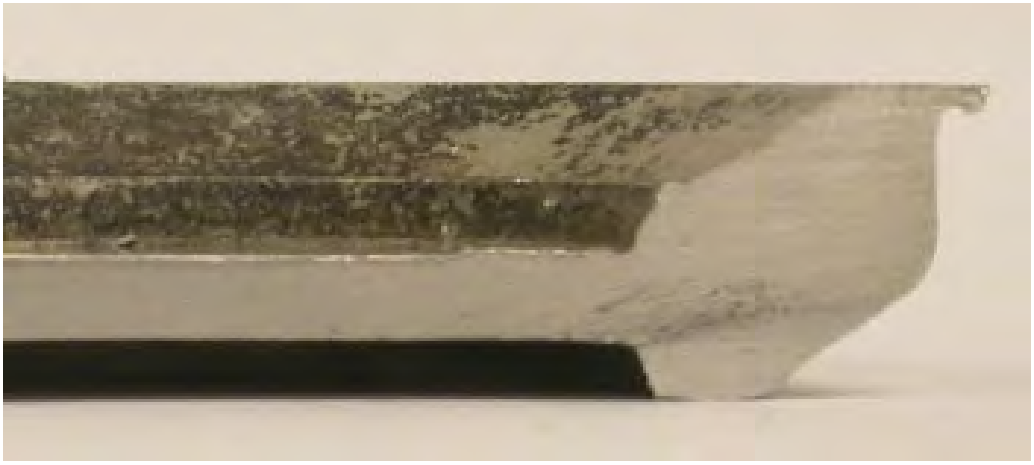

Fig. 6.27 The cross section of the formed axisymmetric component.

The predicted velocity field was based mainly on the material model as well as the die velocity. However, the material used in the reverse simulation was assumed to have a negligible strain-hardening effect, and hence the magnitudes of strain or velocity fields might not be meaningful for analysis. It would be expected to focus on the directions of velocity field as the presentation of material flow. The arrows displayed in Fig. 6.28 represent the directions of material flow. Indeed the billet shapes, numerical parameters, and process conditions of both reverse and forward simulations were essentially the same. Although their scale of velocity was different, the overall predicted directions of material flow in both simulations were also similar.

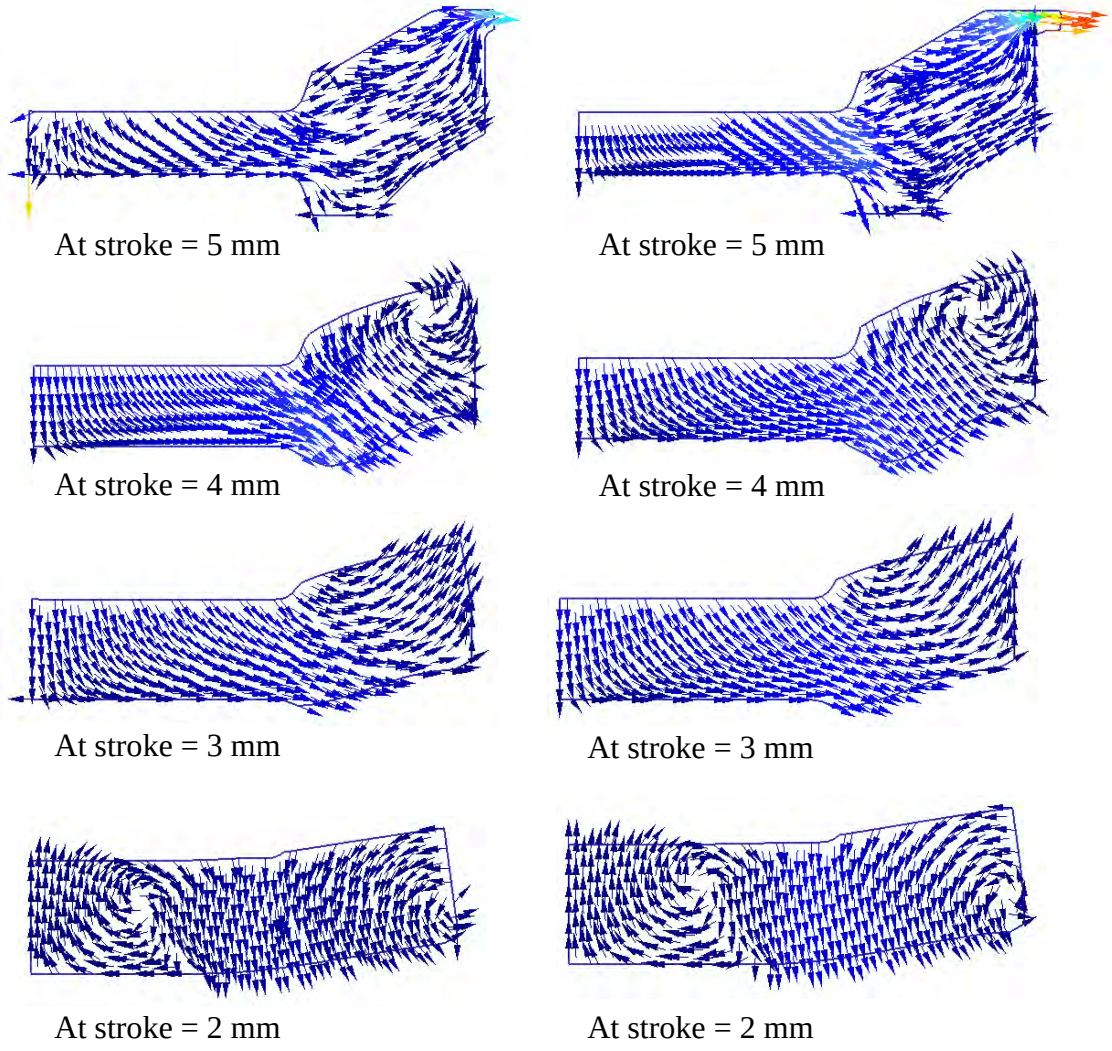

(a) Reverse simulation (b) Forward simulation

Fig. 6.28 Velocity fields of the axisymmetric component.

Moreover the velocity field could illustrate whether material flows were in balance, which was significant for reducing the forming load as well as producing high-quality formed components. It also provided the information about where the material flow, in contact with die surfaces, was at a high speed, and hence the areas in which potentially high die wear could be identified. The velocity field predicted by the numerical simulation showed that the material flowed faster at the bottom region

against those to the top cavity, especially near the corner of the die ejector. The die wear on the surface of the ejector should be more serious than that of the top die because of a higher velocity field on the contact surface. If fillets had not been applied to that corner, the ejector would be broken soon.

Forming loads predicted by forward simulation and acquired from experiments are represented by the corresponding forming stroke (i.e., the displacement of the top die) as shown in Fig. 6.29. The forming load increased as the forming stroke increased. This phenomenon resulted from the increase of the required energy for deformation. The forming load at the finished stroke (i.e., 5 mm) predicted by the forward simulation was much higher than that obtained by the experiments. This could be expected that the warm-forming process modelled by the numerical simulation was performed under an ideal isothermal condition without considering the change of the workpiece temperature. In practical case, the compression of the material would generate heat, as reducing the flow stress at an elevated temperature. This was the reason why the peak forming load of the experiment was much lower than that predicted by the computer simulation. In addition, the forward simulation also predicted a higher overall forming load, except at the early stroke (0 to 2 mm). Such a difference in forming loads between the simulation and the experiment could result from other approximate modelling, particularly from the modelling of plastic deformation since the friction effect was small in this axisymmetric case.

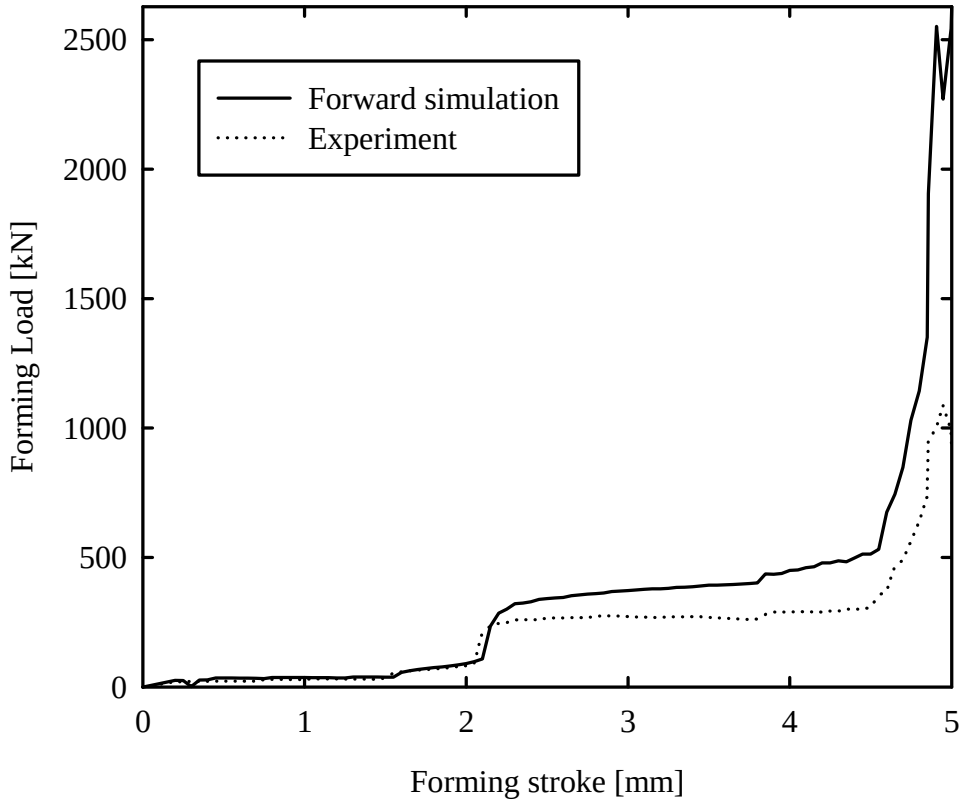

Fig. 6.29 The load-stroke curve of warm forming axisymmetric component.

6.2.3 Case study 2 – hollow axisymmetric component

The case study 2 considered a hollow axisymmetric component, as shown in Fig. 5.8b. Numerical experiments of reverse and forward simulations were carried out to evaluate the proposed methodology for the warm-forming process design. The material model of aluminium alloy 6063 and other process conditions were the same as that applied in case study 1. For forming the hollow component, a ring-shape (i.e., hollow) billet was often preferable, because the forming load could be reduced greatly as the material underwent relatively less deformation compared with the non-hollow cylindrical billet. Furthermore the scraps taken from the center hole of the blank or billet might be used to form other products or components. Such ideas and strategies

were disseminated widely to the metalwork industry. Therefore the case study was valuable as it recognised the hollow billet or preform design.

In the reverse simulation, the material flowed gradually into the desired shape by starting from the final shape as shown in Fig. 6.30. Until the top die nearly separated from the workpiece, a hollow billet was obtained. Its outer diameter, inner diameter, and height were 44.86, 27, and 7.77 mm, respectively. Likewise, during the reverse procedures, shape reconstruction for the concave boundary as well as the die penetration was carried out manually using AutoCAD or Rhinoceros, to keep the constant volume as the final shape. Figures 6.31 and 6.32 demonstrate that the predicted billet was able to fill up the die cavity completely with acceptable flash, resulting in both forward simulation and practical experiment, respectively. Compared with the experimental result of the cross-section of the formed component, as shown in Fig. 6.33, the shape is almost exactly the same as the predicted profile, and thus provides evidence that the proposed reverse simulation approach is reliable.

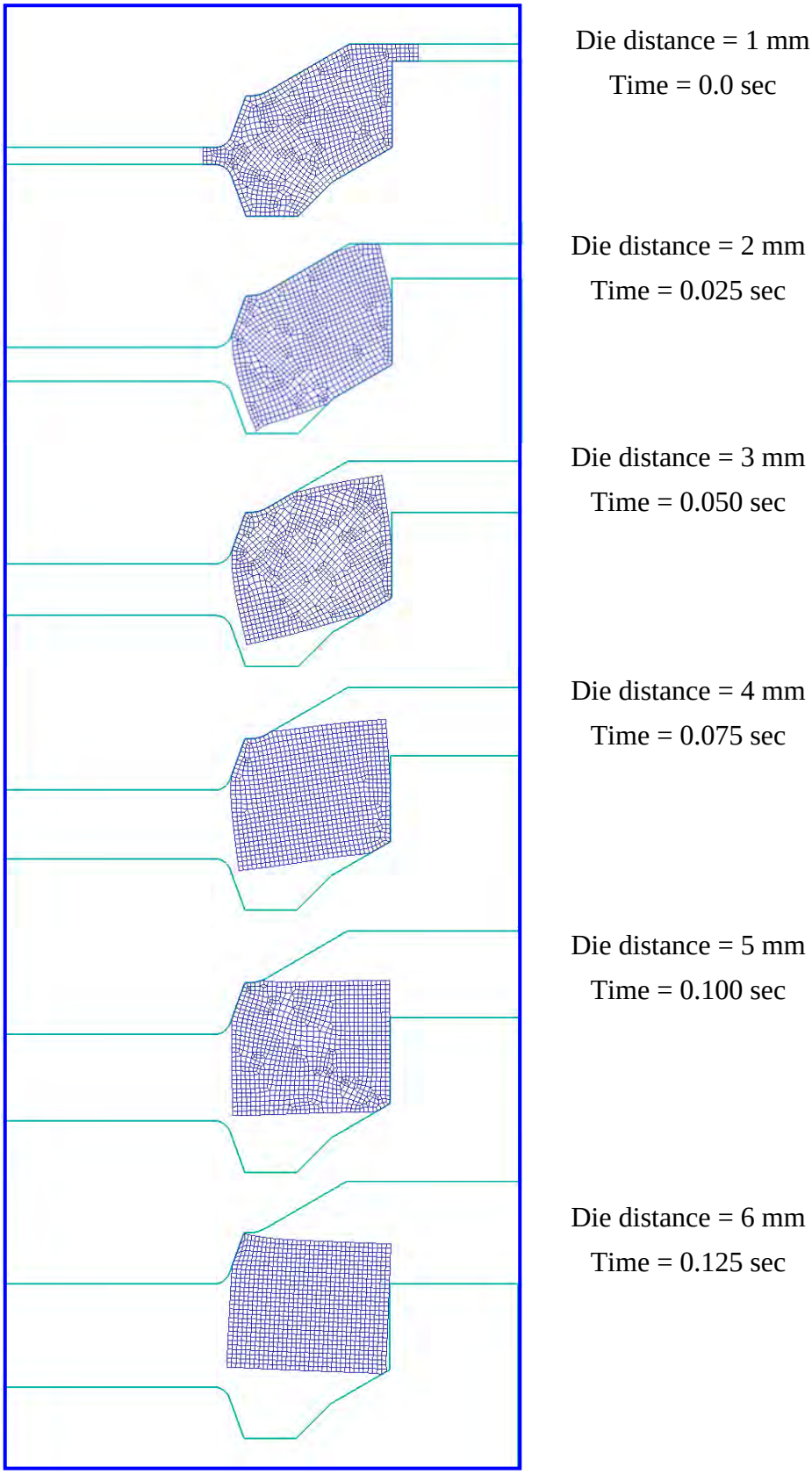

Fig. 6.30 Reverse simulation of warm forming hollow axisymmetric component.

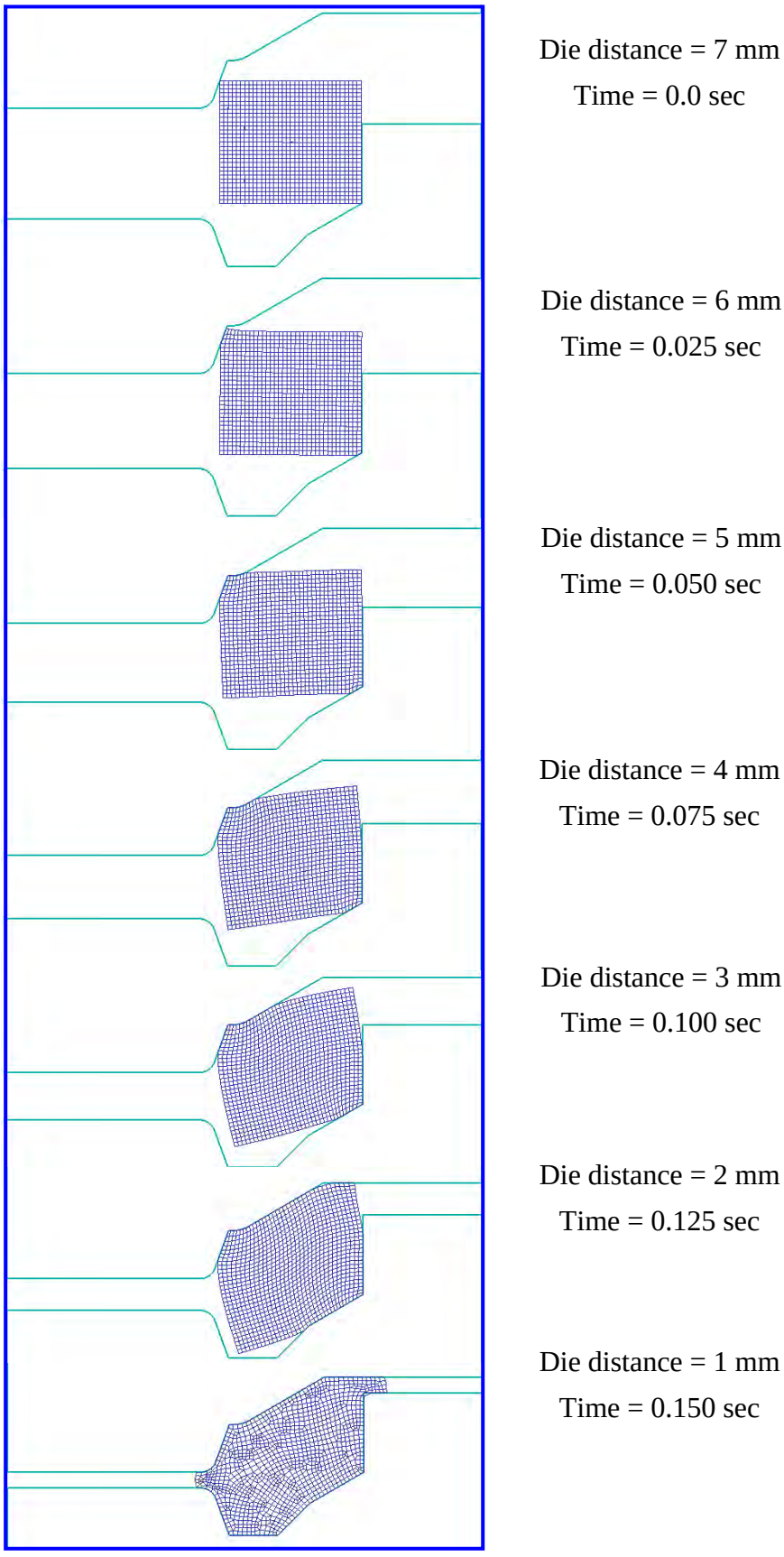

Fig. 6.31 Forward simulation of warm forming hollow axisymmetric component.

Fig. 6.32 The hollow axisymmetric component produced by warm forming.

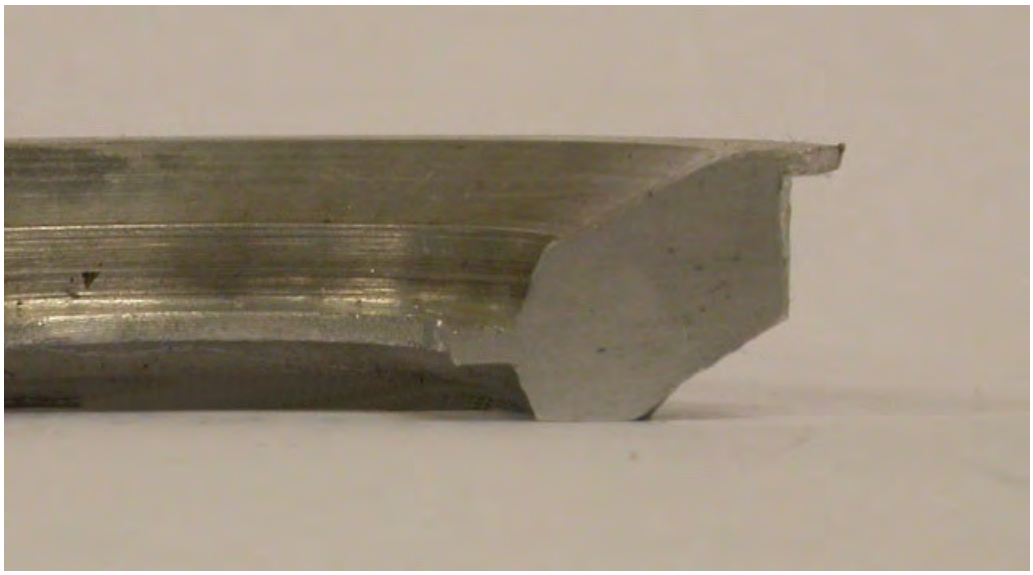

Fig. 6.33 The cross section of the formed hollow axisymmetric component.

The velocity field predicted by the simulation in Fig. 6.34 shows that the speed of the material flow in the bottom-die cavity was relatively high at the end of the process, similar to case study 1. However, in the rest of the reverse increments, the velocity in the same area is relatively small. This result may explain a rapid increase in the forming load from a stroke of 5 to 6 mm in Fig. 6.35, because a higher velocity field requires more plastic deformation power at the end of the process.

In the early deformation, velocity fields shown in Figure 6.34, predicted by the reverse simulation, are slightly different from those predicted by the forward simulation. This could be caused by different contact conditions as the bottom die approaches the major finish position. The overall flow patterns were similar in both simulations. At the end of the forming stroke, velocity fields in the reverse simulation were generally in accord with those in the forward simulation.

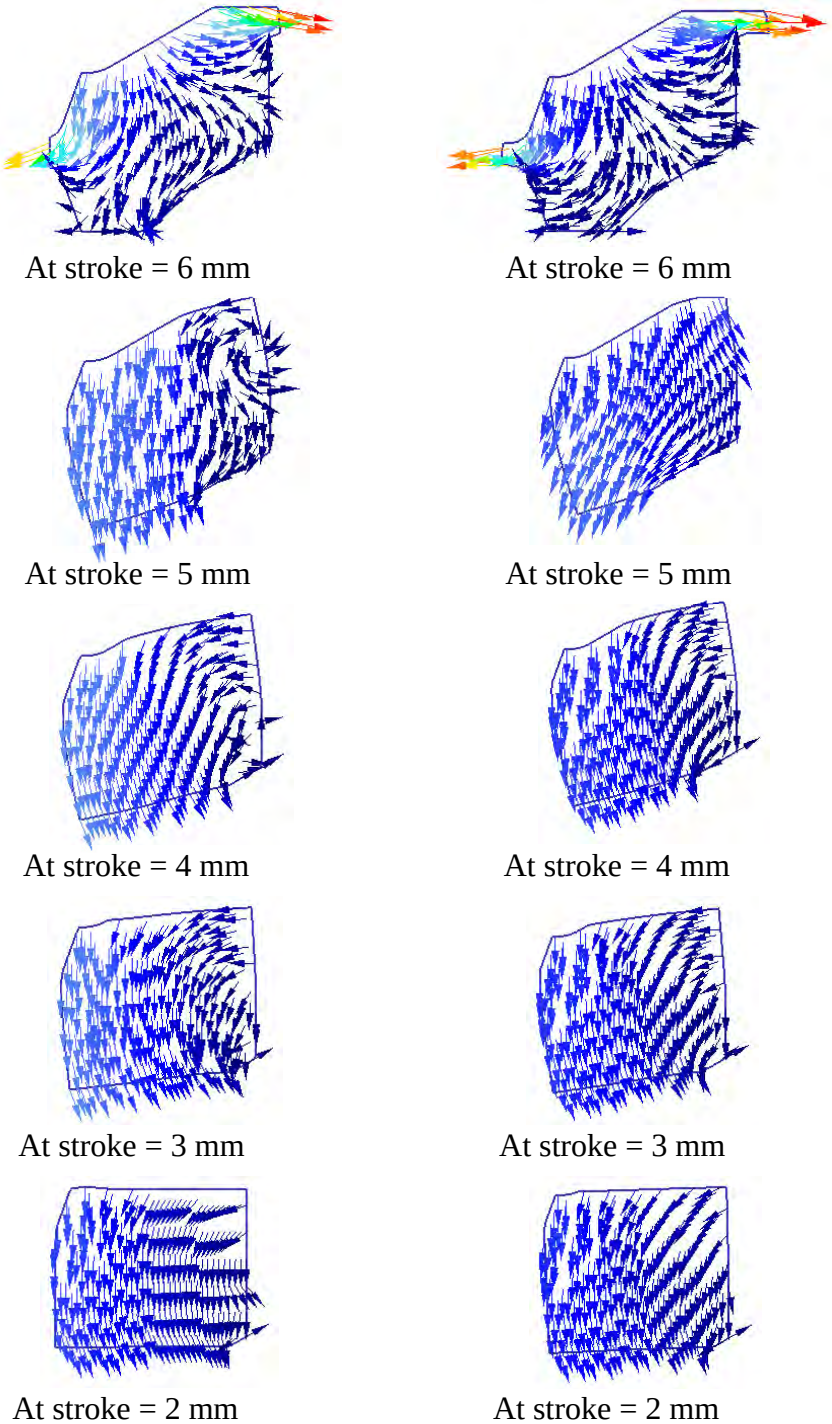

(a) Reverse simulation (b) Forward simulation

Fig. 6.34 Velocity fields of the hollow axisymmetric component.

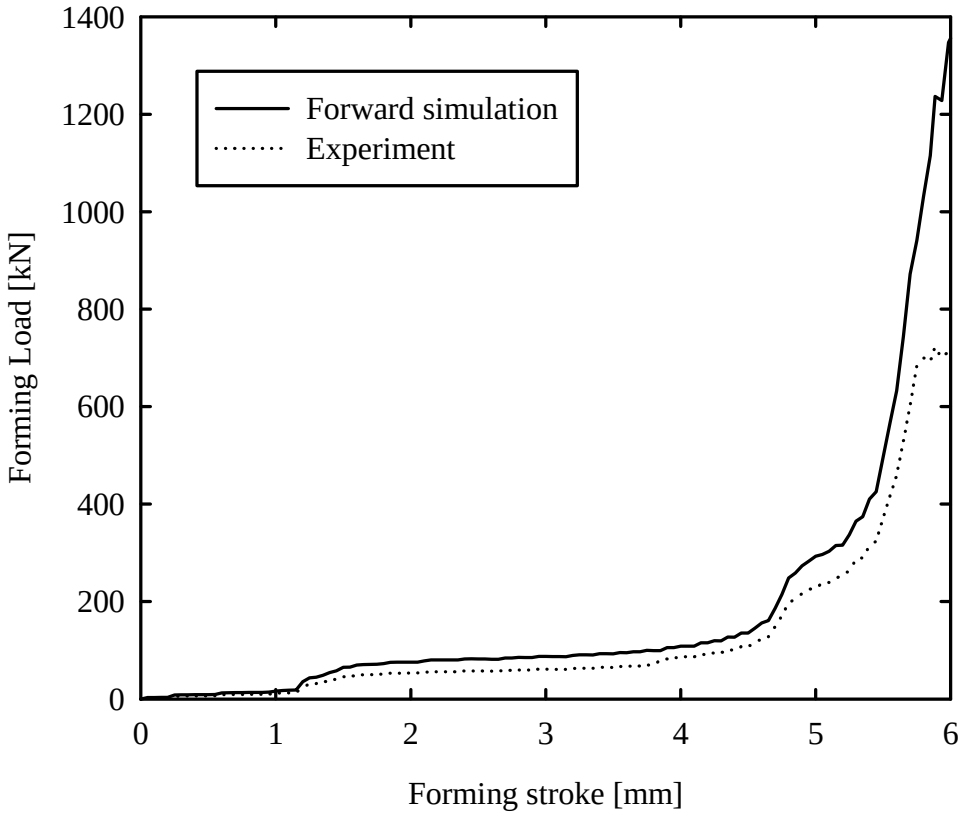

Fig. 6.35 The load-stroke curve of warm forming hollow axisymmetric component.

The contact conditions and the velocity at the interface between the workpiece and the die were used to determine the boundary conditions for predicting the velocity field of the deforming workpiece which represents the minimum energy dissipation required for the bulk-forming process. The energy dissipation is expressed in terms of force (i.e., forming load, according to the known velocity of the die). A higher value of the velocity field should represent higher energy dissipation, and therefore a higher forming load is required.

From the results of this case study, the reverse simulation could predict the initial hollow billet in one single stage and the preform was not required. This was regarding

to the reversibility of material flow, the releasing node strategy, and the method used for shape reconstruction.

6.2.4 Case study 3 – bimetallic component

A considerable amount of theoretical and experimental investigations has been done on the warm-forming single-base metals. However, warm-forming bimetals are very different and more complicated. Since each material has its own flow properties and mechanical behaviour, heterogeneous material flows occur during the process. It is well know that the forming loads and the material flow patterns are influenced highly by workpiece geometries. For this reason, the proposed reverse simulation approach should be a good solution, which predicts the initial billet or preform directly by starting from the final shape of the bimetallic component. Therefore, the cost and time spent on implementing experimental trials and investigations can be greatly reduced.

The configuration of the component used in case study 3 was the same as that used in case study 2. The main difference is that the component of case study 3 is made of aluminium alloy 6063 and stainless steel AISI 316L. In other words, this demonstrated example is a bimetallic hollow axisymmetric component.

The reverse simulation started from the final shape, as shown in Fig. 6.36, until the top die nearly separated from the workpiece. The bimetallic interface was being changed from a sticking condition to a sliding condition during the reverse increments. The predicted shapes were sufficiently simple as the hollow billets or blanks, and

therefore intermediate preforms were not necessary. The two separated hollow billets had been reconstructed by using AutoCAD manually, since the faying surface of both billets should be in close contact to assure the intermetallic bond would be generated under a high pressure and elevated temperatures. Figure 6.36 illustrates that two dissimilar metals flow gradually towards their desired shape as the dies move backwards in the reverse simulation. This movement could also be verified in terms of decreasing shape complexity. However, the predicted deformation has concave profiles on the free surface instead of convex profiles which are expected in bulk-forming processes. The SRL and BEM methods were used to solve this problem. Since the smooth boundaries of the workpiece were difficult to predict, the shape reconstruction procedures proposed in this study has become the significant techniques of the reverse simulation.

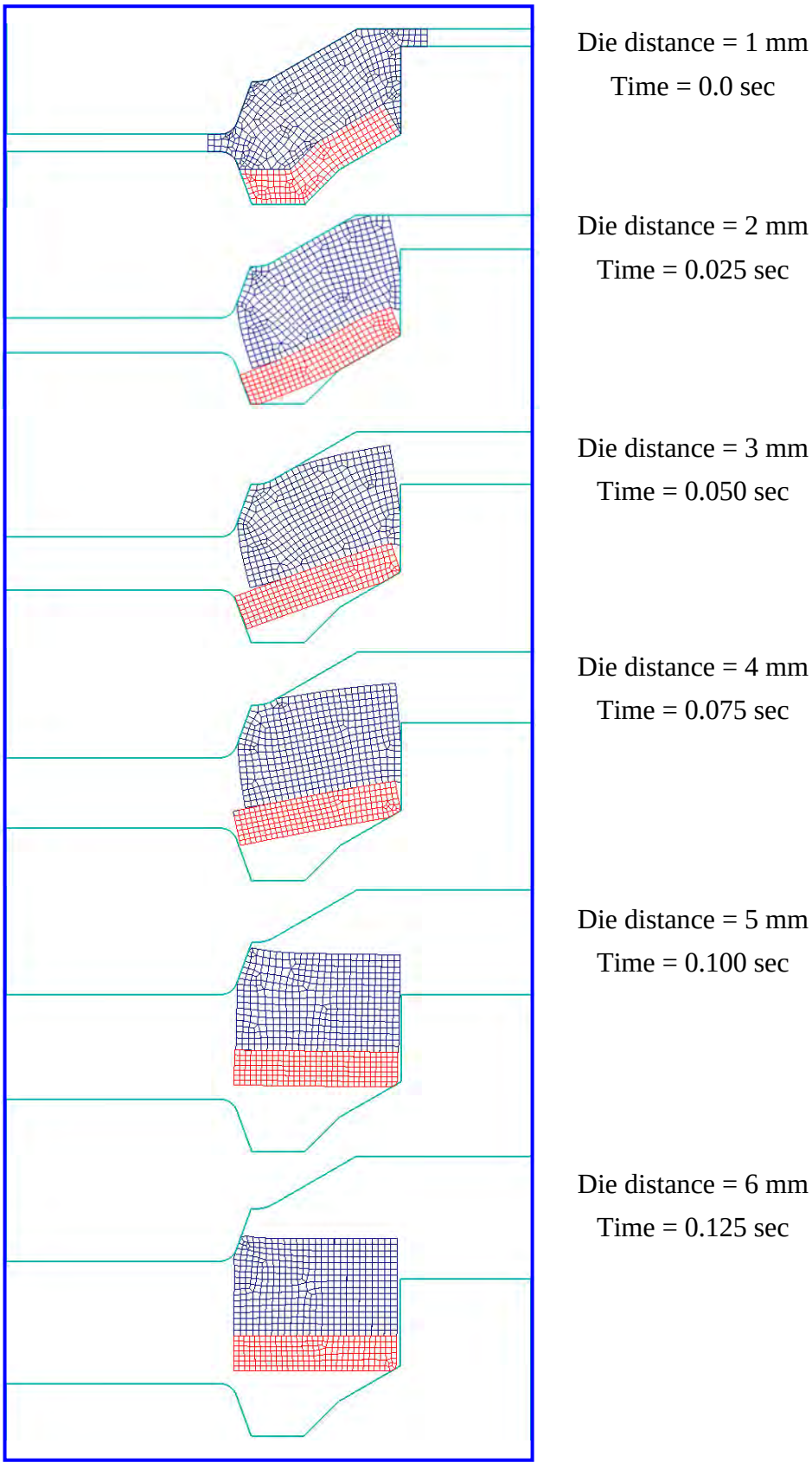

Fig. 6.36 Reverse simulation of warm forming bimetallic component.

The outer diameters and the inner diameters of the predicted aluminium alloy 6063 and stainless steel AISI 316L billets were nearly the same, 44.6 and 26 mm. Heights of the aluminium alloy 6063 and stainless steel AISI 316L were 5.6 and 2 mm, respectively. The forward simulation and practical experiment started from the predicted billets are shown in Figs. 6.37, and 6.38-6.39 respectively. All the results were impressive, that the bimetallic components could be formed successfully by the predicted billets with the determined process conditions. The resulting profiles were nearly the same as the original design illustrated in Fig. 6.40. These findings provide clear evidence that the proposed methodology for predicting the approximate geometry of a billet has considerable potential to be used efficiently in the industry.

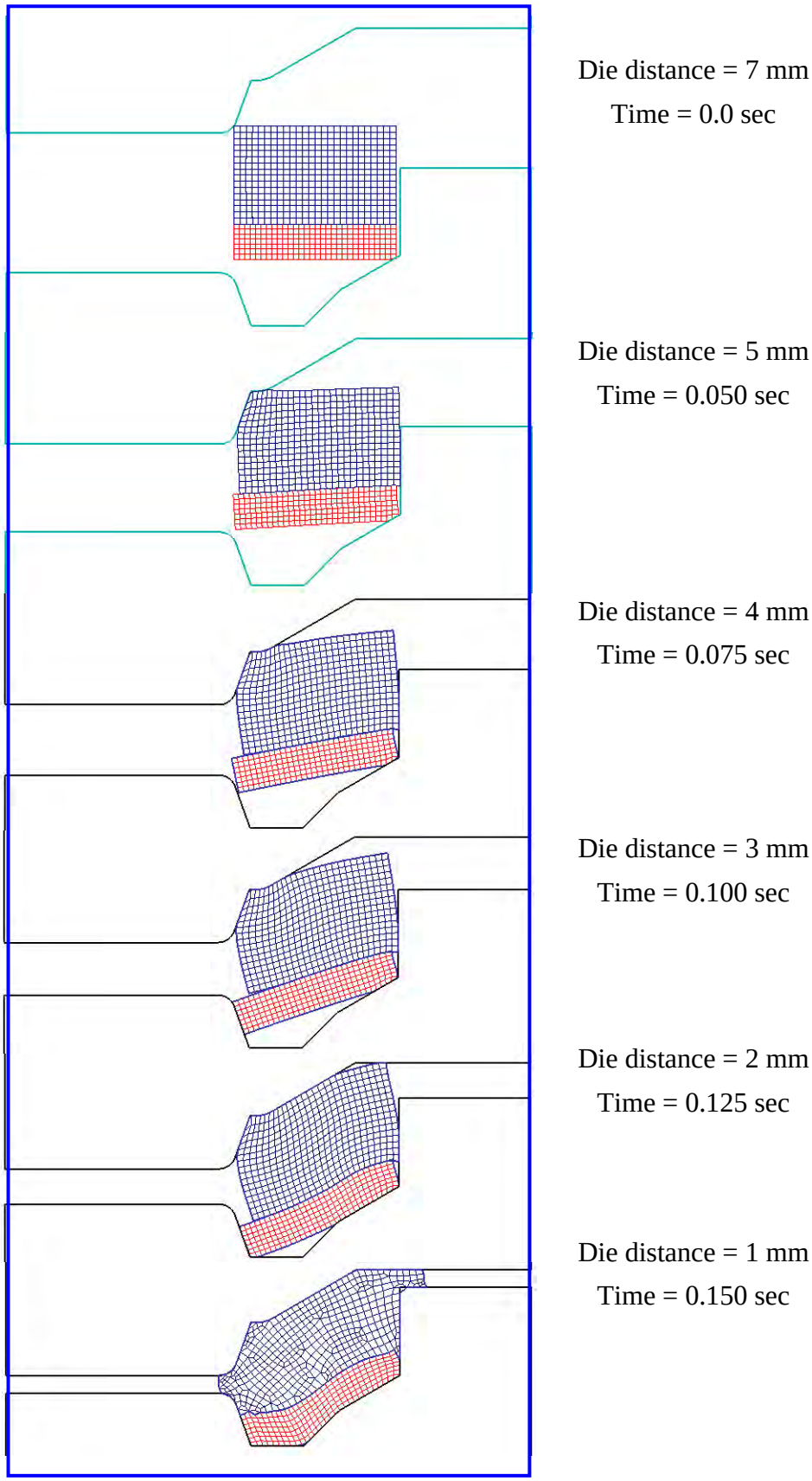

Fig. 6.37 Forward simulation of warm forming bimetallic component.

Stroke = 0 mm
(Two materials were separated)

Stroke = 2 mm
(Two materials were separated)

Stroke = 3 mm
(Two materials were joined)

Stroke = 4 mm
(Two materials were joined)

Stroke = 5 mm
(Two materials were joined)

Stroke = 6 mm
(Two materials were joined)

Fig. 6.38 The bimetallic component produced by warm forming.

Fig. 6.39 The forming sequence of the bimetallic component.

Fig. 6.40 The cross section of the bimetallic component.

The velocity of material flow decreases gradually from the beginning to the end of the forming process, as presented in Fig. 6.41. The predicted velocity field corresponded to the forging process. Since the die velocity was constant, the velocity of material flow increased as the amount of free surface or flash area decreased. Besides, the results of the reverse simulations revealed some deformed zones with low velocity and were generally in accord with those of the forward simulations.

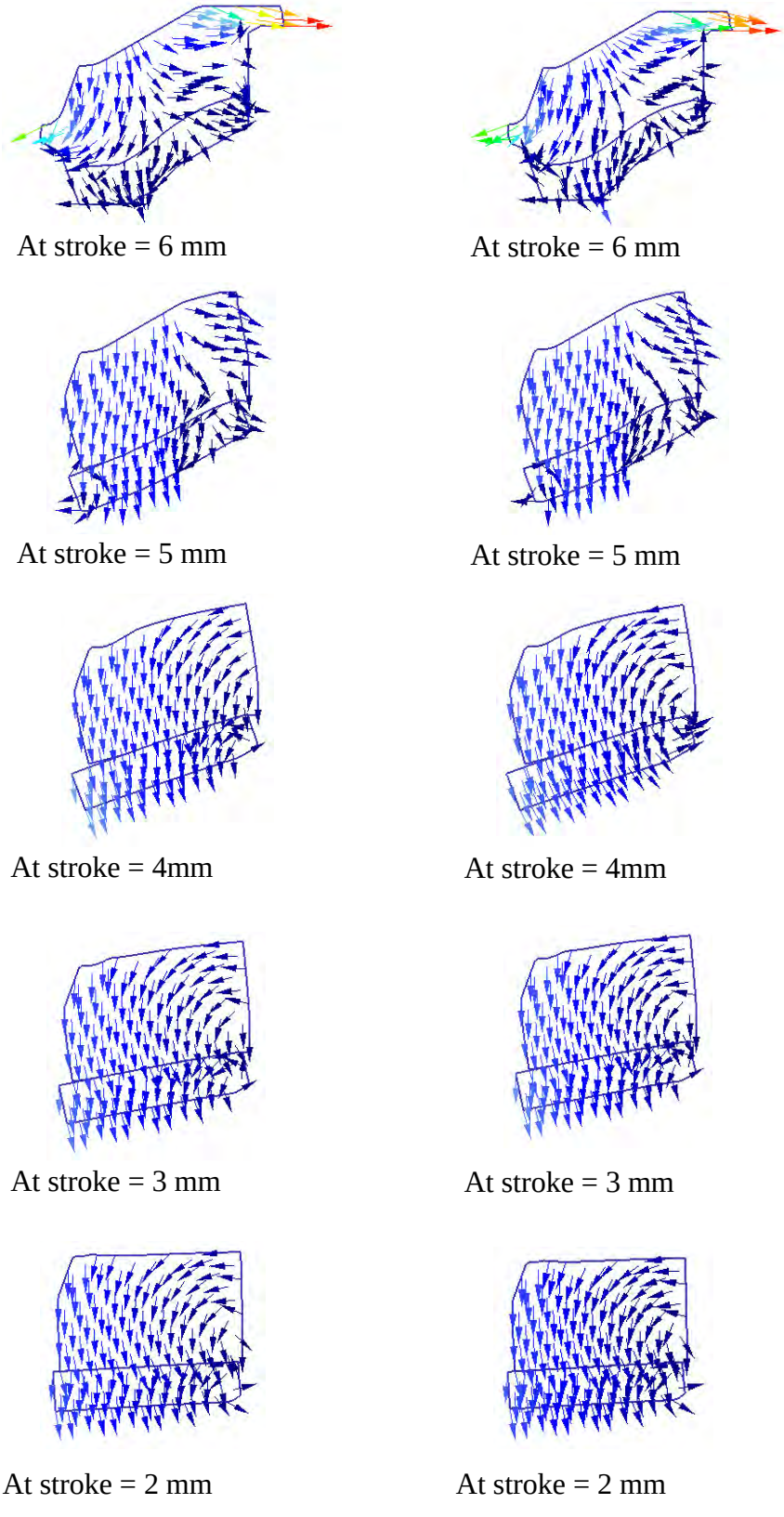

Fig. 6.41 Velocity fields of the bimetallic component.

Forming loads shown in Fig. 6.42 increased as the respective forming strokes increased in both the simulation and the experiment. This phenomenon corresponds to the required power of the deformation in the velocity fields from a high value of flow speed to a low value. In comparison with the maximum forming load between the forward simulation and the experiment, the simulation predicted higher values at the whole forming stroke, especially at the end of the forming. Since the heat transfer and heat generation of the compressed material were not taken into account in the simulation, the predicted peak load might be slightly higher than the actual process.

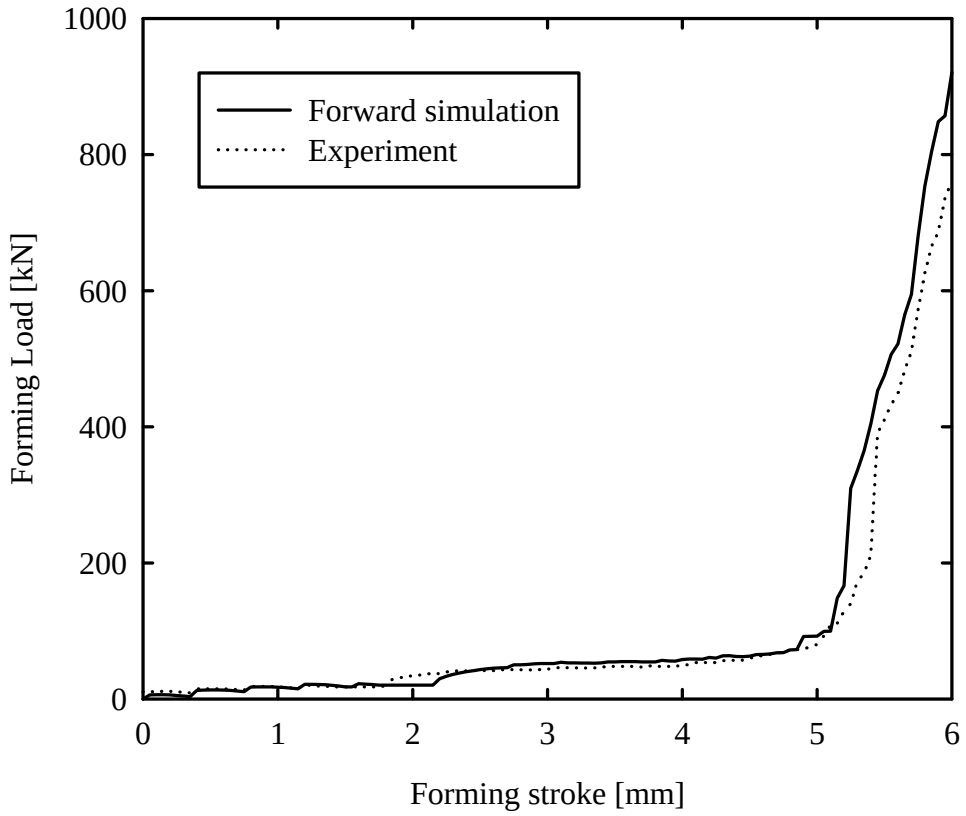

Fig. 6.42 The load-stroke curve of warm forming bimetallic component.

7. Conclusions and Recommendations for Future Work

7.1 Conclusions

An efficient methodology for the warm-forming process design of bimetallic components was developed successfully using the modified reverse simulation approach, directly starting from the final shapes of the formed components to restore the simplest shapes of the initial billets. This study demonstrated the implementation of the proposed idea to control the material flow and distribution of hollow formed components as well as the newly developed methods for shape reconstruction and determination of interface-conditions between two dissimilar metals in the reverse simulation, so as to predict the primary workpiece or billet shapes in the axisymmetric bulk-forming applications, also the warm-forming bimetallic components. It is believed that the methodology is capable of providing a pronounced strength advantage over the traditional trial-and-error or/and systematic approaches of the workpiece and preform design by practical trials or/and forward computer simulation; even the optimisation techniques are used. The outcomes also help the development and manufacture of innovative bimetallic components and the exploration of their potential advanced applications.

Several essential tasks were completed to achieve the objective during the study. (i) The special tooling and equipment were designed and manufactured properly for performing the isothermal uniaxial compression test, ring-compression test, welding experiments of dissimilar metals, and warm-forming experiments; (ii) the flow stress

data were acquired for the aluminium alloy 6063 and stainless steel AISI 316L at evaluated temperatures and different strain rates, as well as the values of friction factors at the interface between formed workpiece and die materials, to be used for process modelling and numerical simulation; (iii) the mechanical properties were obtained for the different base metals and even their bimetals, especially the tensile strengths of the bimetallic joints and interfaces (i.e., the joint efficiency); (iv) the intermetallic bond of diffusion zone in the bimetallic joint and the most suitable process conditions that influenced the modelling of warm-forming bimetallic components significantly was found; (v) the algorithm for determining the reverse shape of the workpiece or preform based on the backward tracking method and finite element formulation of the rigid-plastic materials was developed; (vi) the procedure for defining the desired shape and contact boundary conditions, shape reconstruction, and determination of the condition of bimetallic interface in the reverse simulation was established; (vii) the reverse simulations were carried out for the warm-forming two axisymmetric components and one bimetallic component with various final shapes of finished products; (viii) The predicted results of the billet shapes by the reverse simulation were verified with acceptable agreement by both forward simulation and physical experiments.

The overall review of the reverse simulation approach was accomplished. The algorithm was established with a significant modification based on the backward tracing method for starting the reverse deformation step, and the adaptive strategies for determination of the contact boundary conditions, which were combined with the

original developed methods and techniques throughout the workpiece and preform design of bulk forming. These methods and techniques were deducted from various empirical and physical rules including (i) nearly same outer profiles or cross sections of workpiece and final component, (ii) compensation of material for incomplete die filling, (iii) elimination of excessive material flowing into improper regions of die cavity, (iv) reasonable assumptions about the constancy of the volume of non-porous solid metal, (v) convex expansion of the lateral deformation surfaces, and (vi) material flowing with a higher velocity at the lowest resistant region of die cavity. The key advantage was that the developed methods could provide efficient resolutions for the inevitable problems such as concave and inwards deformation surfaces and die penetration, which were found in the former reverse simulation approach, so that a more realistic and practical reverse shape could be obtained. Also, it was possible to extend the approach for the applications of warm forming bimetallic components, in which the new procedure regarding the interface frictions for determining the sliding and sticking conditions between two dissimilar metals has been worked out successfully.

The hollow geometry (i.e., the profile with a center hole) has been popular in most metalwork manufacture. In order to enhance the industrial viability and reliability of the reverse simulation, an original idea of a billet-height minimization routine was incorporated into the commercial finite-element package for predicting the hollow cylindrical billet, which was defined as the desired shape of the initial billet for two-dimensional axisymmetric cases. The geometric variables of the hollow billet,

including its height, inner diameter, and outer diameter, were expressed as the function of the workpiece volume. The contact region of reverse shape, which was located outside and has the furthest distance to the boundary of the desired shape, was regarded as the most complex region to be released first. After the desired shape and its location were defined, the new contact boundary conditions could be subsequently determined.

The previous studies of reverse simulation have not addressed the problem of concave deformation of reverse shapes. Therefore, in this study, the developed reverse simulation approach was incorporated with the original effective methods. These were the straight-line-repair (SLR), boundary-edge-mirror (BEM), nearest-die-profile-repair (NDPR), and profile-offset (PO) methods established by the empirical and physical rules governing the bulk-forming process. These methods could help to reconstruct the reverse shape exhaustively, while at the same time, avoiding the concave-shape problem and compensating for both excessive and insufficient volume of material. These procedures were adopted sequentially under specified conditions in order to maintain the desired volume of the suitable reverse shape. This is ensure that the predicted shape is a simple and reasonable geometry and provides a workpiece which is able to achieve the primary geometric requirement of the complete die filling.

With the additional procedures for the determination of material temperatures, as well as the change in the condition of the bimetallic interface from a sticking condition to a sliding condition, the developed reverse simulation approach was implemented for warm-forming bimetallic components. The main concern was to identify a larger shear-friction factor as a nearly sticking condition at the weld interface

of the final shape of the finished component. During the reverse increment, this shear-friction factor was being reduced to the sliding condition in stages, which depended on the forming loads required for forming the first reverse shape into the final shape that were obtained from that increment of forward simulation.

The flow stress data of two specimen materials, aluminium alloy 6063 and stainless steel AISI 316L, were obtained by the uniaxial compression tests. The tests were conducted at elevated temperatures ranging from 20 to 900 °C with intervals of 100 °C, except for the larger interval between 20 and 200 °C. These material data, as well as the shear-friction factor evaluated by the ring compression tests, were identified as significant information for process modelling. The values of shear-friction factors were determined as 0.5 for the case without lubrication (i.e., dry condition) and 0.2 for the case of applied lubricant.

The bimetallic welds of aluminium alloy 6063 and stainless steel AISI 316L produced by the hot pressure welding and forge welding were investigated. The best-quality joint, with a tensile strength of around 111.3 MPa (better than the softer base metal), was produced successfully by forge welding at the welding temperature of 450 °C and depth of deformation of 8 mm. The flawless diffusion zones were identified at the joint interface, providing critical evidence for validating the process capability as well as reference process conditions needed by numerical modeling.

The material flow in warm forming bimetallic non-axisymmetric components at forming temperatures T_f of 400, 500, 600, 700, 800, and 900 ºC and ram speeds S_f of 20, 40, and 60 mm/s has been studied successfully. The results show that the most

suitable process parameters were T_f = 900 ºC and S_f = 40 mm/s. The experiments were conducted under compatible process conditions to verify the simulation results. The data and the shapes acquired from the experiments, on average, agreed strongly with those predicted by the simulations.

According to the material data and determined process conditions obtained from the mechanical tests and physical experiments, the modelling of the warm-forming process of bimetallic components by the reverse simulation approach could be carried out. Three case studies of axisymmetric bulk forming were used to evaluate its effectiveness. The components used in these three case studies were an axisymmetric component, a hollow axisymmetric component and a hollow bimetallic component. The results show that reverse simulation was capable of predicting their initial billet shapes. By using the predicted billet, a complete die filling was achieved in the physical experiments.

The developed reverse simulation approach has been applied successfully to the single-stage bulk-forming process for predicting not only the billet shapes of the single-based metal formed components, but also the bimetallic components. With the verification, especially in terms of deformation trends, by the physical experiments and numerical simulations carried out using commercial FEM simulation software, the results have shown that the proposed methodology for predicting the approximate geometry of a workpiece in bulk forming has considerable potential to be used efficiently in industry.

7.2 Recommendations for future work

The developed methods such as SLR, BEM, NDPR, and PO methods for shape reconstruction in this study had to be processed manually, using commercial CAD software such as AutoCAD and Rhinoceros. Since the smooth boundaries of the reverse shape are unusual, the shape reconstruction has become the significant procedure of the reverse simulation. In order to make the approach more efficient, computer programming with artificial intelligence for these reverse-shape-reconstruction methods should be investigated, and hence the bad-quality or abnormal reverse shape can be reconstructed automatically during each reverse increment.

The shear-friction factor and the forming load are empirically confirmed variables and make sense for describing the sticking/sliding conditions between two dissimilar metals. In addition, many other possible key factors or criteria can also be considered conceptually for this purpose such as the mechanical strength of joint interface, plastic flow resistance, and deformation behaviour of softer metals. This area can be studied further by varying simulations and experiments, while imperfect or localised welds or friction at the joint interface may occur during the early or/and intermediate stages of the actual forming process.

Apart from the aluminium alloy and stainless steel, there are many combinations of bimetal to be selected. The manufacture of such bimetallic components should involve knowledge of materials science. Therefore, the scope of study of forming bimetal or bimetallic components can be very large, and it would take great deal of literature to cover the details. Specifically, researchers can focus on combined

functions of strong and light metals, even thermal-deflection nature, which should contribute the highest benefit of using bimetals.

References

[1] Sheljaskvo, S. (1996) Warm forging a technology for manufacturing of precision components, *In: Advanced Technology of Plasticity 1996. Proceedings of the 5th International Conference on Technology of Plasticity, Columbus, Ohio, USA, October 1996 (T. Altan ed.)*, 1, 485-490.

[2] Kayali, E.S., Sunada, H., Oyama, T., Wadsworth, J., and Sherby, O.D. (1979) The development of fine structure superplasticity in cast ultrahigh carbon steels through thermal cycling, *Journal of Materials Science*, 14(11), 2688-2692.

[3] Yu, K., Li, S., and Li, W. (2000) Effect of trace Sc and Zr on the mechanical properties and microstructure of Al alloy 2618, *Journal of Materials Science and Technology*, 16(4), 416-420.

[4] Schuler GmbH. (1998) *Metal forming handbook*, Springer Berlin Heidelberg.

[5] Dallas, D.B. (1976) *Tool and Manufacturing Engineers Handbook, 3rd edition*, New York, McGraw-Hill Book Company.

[6] Smith, E.H. (1994) *Mechanical Engineer's Reference Book, 12th edition*, Oxford, Butterworth-Heinemann Ltd.

[7] Madsen, D.A., (1994) *Print Reading for Engineering and Manufacturing Technology*, New York, Delmar Learning.

[8] Altan, T., Oh, S.I., and Gegel, H.L. (1983) *Metal Forming: Fundamental and Applications*, Ohio, American Society for Metals.

[9] Sapozhnikov, S.Z., Perezhogin, L.A., and Kipriyanova, V.N. (1982) Use of bimetallic parts in hydraulic drive pumps, *Metal Science and Heat Treatment*, 24(10), 734-737.

[10] Dunketrton, S.B. (1986) *Welding Dissimilar Metals*, (N. Bailey ed.), Cambridge, The Welding Institute.

[11] Messler, R.W. (1993) *Joining of Advanced Materials*, Boston, Butterworth Heinemann.

[12] Eager, T.W., Baeslack W.A., and Kapoor R. (1994) *The Encyclopedia of Advanced Materials*, (D. Boolr ed.), Oxford, Pergamon Press.

[13] Nikitina, L.A. (1998) Status and prospects for the manufacture of multilayered and bimetallic metal products, *Metallurgist*, 42(8), 297-301.

[14] Taylor, D., and Pan J. (2001) Modelling and testing for design and durability of tapered bimetallic joints, *International Journal of Materials and Product Technology*, 16(4-5), 430-445.

[15] Dieter, G.E. (1988) *Mechanical Metallurgy*, London, McGraw-Hill Book Company.

[16] Kim, Y.H., Ryou, T.K., Choi, H.J., and Hwang, B.B. (2002) An analysis of the forging processes for 6061 aluminum-alloy wheels, *Journal of Materials Processing Technology*, 123, 270-276.

[17] Sheljaskow, S. (2001) Tool lubricating systems in warm forging, *Journal of Materials Processing Technology*, 113(1-3), 16-21.

[18] DEFORM, Scientific Forming Technologies Corporation, 700 Ackerman Rd., Suite 255, Columbus Ohio 42302-1559, USA.

[19] QForm, Quantor Ltd. P.O.Box 39. 117049 Moscow, Russia.

[20] MSC.SuperForge, MSC.Software Corporation, 2 MacArthur Place, Santa Ana, California 92707, USA.

[21] Park, J.J., Rebelo, N., and Kobayashi, S. (1983) A new approach to preform design in metal forming with the finite element method, *International Journal of Machine Tools and Manufacture*, 23(1), 71-79.

[22] Hwang, S.M., and Kobayashi, S. (1984) Preform design in plane strain rolling by the finite element method, *International Journal of Machine Tool Design and Research*, 24(4), 253-266.

[23] Zhao, G.Q., Wright, E., and Grandhi, R.V. (1995) Forging preform design with shape complexity control in simulating backward deformation, *International Journal of Machine Tools and Manufacture*, 35(9), 1225-1239.

[24] Chang, C.C., and Bramley, A.N. (1998) A new preform design approach using reverse simulation, *Annals of the CIRP*, 47, 193-196.

[25] Chang, C.C., and Bramley, A.N. (2000) Forging preform design using a reverse simulation approach with the upper bound finite element procedure, *Proceedings of the Institution of Mechanical Engineers, Part C: Journal of Mechanical Engineering Science*, 214(1), 127-136.

[26] Bramley, A.N. (2001) UBET and TEUBA: fast methods for forging simulation and preform design, *Journal of Materials Processing Technology*, 116(1), 62-66.

[27] Caporalli, Â., Gileno, L.A., and Button, S.T. (1998) Expert system for hot forging design, *Journal of Materials Processing Technology*, 80, 131-135.

[28] Li, D., and Ghosh, A.K. (2004) Biaxial warm forming behavior of aluminum sheet alloys, *Journal of Materials Processing Technology*, 145(3), 281-293.

[29] Ngaile, G., and Botz, F. (2008) Performance of graphite and boron-nitride-silicone based lubricants and associated lubrication mechanisms in warm forging of aluminum, *Journal of Tribology*, 130(2).

[30] McHugh, K.M., Lin, Y., Zhou, Y., and Lavernia, E.J. (2008) Influence of cooling rate on phase formation in spray-formed H13 tool steel, *Materials Science and Engineering: A*, 477(1-2), 50-57.

[31] Harrison, N.R., Friedman, P.A., and Pan, J. (2015) Warm forming die design, Part III: Design and validation of a warm forming die, *Journal of Manufacturing Processes*, 20, 356-366.

[32] Kong, T.F., Chan, L.C., and Lee, T.C., (2005) Numerical determination of blank shapes for warm forming of non-axisymmetric components, *Journal of Materials Processing Technology*, 167, 472-479.

[33] Sheridan, S.A. (1972) *Forging Design Handbook*, Ohio, American Society for Metals.

[34] Aritzur, B. (1983) *Handbook of Metal-Forming Processes*, United States

[35] Byrer, T.G., Semiatin, S.L., and Vollmer, D.C. eds. (1985) *Forging Handbook*, Ohio, Forging Industry Association and American Society for Metals.

[36] Kalpakjian, S. (1997) *Manufacturing Processes for Engineering Materials*, Harlow, England: Addison-Wesley Publishing Company.

[37] Altan, T., Ngaile, G., and Shen, G. eds. (2004) *Cold and Hot Forging: Fundamentals and Applications*, Materials Park, Ohio, ASM International.

[38] Cho, N.C., Lee, S.H., Hong, S.S., and Lee, J.S. (1994) Experimental-verification of preform design for axisymmetrical heavy forging on a model hammer, *Journal of Materials Processing Technology*, 47(1-2), 103-110.

[39] Duggirala, R., and Badawy, A. (1988) Finite element method approach to forging process design, *Journal of Materials Shaping Technology*, 6(2), 81-89.

[40] Vazquez, V., and Altan, T. (2000) Die design for flashless forging of complex parts, *Journal of Materials Processing Technology*, 98(1), 81-89.

[41] Sheu, J.J., and Yu, C.H. (2009) Preform and forging process designs based on geometrical features using 2D and 3D FEM simulations, *The International Journal of Advanced Manufacturing Technology*, 44(3), 244-254.

[42] Qu, H., and Balendra, R. (1998) Preform design for forging of aerofoil sections using FE simulation, *Journal of Materials Processing Technology*, 80-81, 144-148.

[43] Glynn, D., Lyons, G., and Monaghan, J. (1995) Forging sequence design using an expert system, *Journal of Materials Processing Technology*, 55(2), 95-102.

[44] Kim, D.Y., Park, J.J. (2000) Development of an expert system for the process design of axisymmetric hot steel forging, *Journal of Materials Processing Technology*, 101(1-3), 223-230.

[45] Bettendorf, W., and Davis, R.H. (1990) Knowledge-based support for process planning in a forging environment, *Applied Mathematical Modelling*, 14(3), 140-154.

[46] Tisza, M. (1995) Expert systems for metal forming, *Journal of Materials Processing Technology*, 53(1-2), 423-432.

[47] Esche, S.K., Fidan, I., Chassapis, C., and Manoochehri, S. (1999) Knowledge-based part and process design for metal forging, *SAE Transactions*, 92-99.

[48] Bakhshi-Jooybari, M., Pillinger, I., Hartley, P., and Dean, T.A. (1996) Finite element simulation and experimental study of hot closed-die upsetting. *International Journal of Machine Tools and Manufacture*, 36(9), 1021-1032.

[49] Vemuri, K.R., Oh, S.I., and Altan, T. (1989). BID: a knowledge-based system to automate blocker design, *International Journal of Machine Tools and Manufacture*, 29(4), 505-518.

[50] Lee, R.S., and Hsu, Q.C. (1992). Development of an integrated process planning-based CAE system for cold forging, *Proceedings of the Institution of Mechanical Engineers, Part B: Journal of Engineering Manufacture*, 206(3), 215-225.

[51] Hsu, Q.C., and Lee, R.S. (1997) Cold forging process design based on the induction of analytical knowledge, *Journal of Materials Processing Technology*, 69(1-3), 264-272.

[52] Hassoun, M. H. (1995) *Fundamentals of artificial neural networks*, MIT Press.

[53] Jain, A. K., Mao, J., and Mohiuddin, K. M. (1996) Artificial neural networks: A tutorial, *Computer*, 29(3), 31-44.

[54] Kim, D.J., Kim, B.M. and Choi, J.C. (1997) Determination of the initial billet geometry for a forged product using neural networks, *Journal of Materials Processing Technology*, 72(1), 86-93.

[55] Roy, R., Chodnikiewicz, K., and Balendra, R. (1994) Interpolation of forging preform shapes using neural networks. *Journal of Materials Processing Technology*, 45(1-4), 695-702.

[56] Ko, D.C., Kim, D.H., and Kim, B.M. (1999) Application of artificial neural network and Taguchi method to preform design in metal forming considering workability, *International Journal of Machine Tools and Manufacture*, 39(5), 771-785.

[57] Hsu, Q.C., and Lee, R.S. (1997) Cold forging process design based on the induction of analytical knowledge, *Journal of Materials Processing Technology*, 69(1-3), 264-272.

[58] Zhang, H. C., and Huang, S. H. (1995) Applications of neural networks in manufacturing: a state-of-the-art survey, *The International Journal of Production Research*, 33(3), 705-728.

[59] Poursina, M., Antonio, C. A. C., Castro, C. F., Parvizian, J., and Sousa, L. C. (2004), *Preform optimal design in metal forging using genetic algorithms*, Engineering Computations, 21(6), 631-650.

[60] Yan, H., and Xia, J. (2006) An approach to the optimal design of technological parameters in the profile extrusion process, *Science and Technology Of Advanced Materials*, 7(1), 127.

[61] Fourment, L., and Chenot, J.L. (1996) Optimal design for non-steady-state metal forming processes I, Shape optimization method. *International Journal for Numerical Methods in Engineering*, 39, 33-50.

[62] Fourment, L., BaJan, T., and Chenot, J.L. (1996) Optimal design for non-steady-state metal forming processes II, Application of shape optimization in forging. *International Journal for Numerical Methods in Engineering*, 39, 51-65.

[63] Zhao, G.Q., Wright, E., and Grandhi, R.V. (1997) Preform die shape design in metal forming using an optimization method, *International Journal for Numerical Methods in Engineer*, 40, 1213-1230.

[64] Zhao, G.Q., Wright, E., and Grandhi, R.V. (1997) Sensitivity analysis based preform die shape design for net-shape forging, *International Journal of Machine Tools and Manufacture*, 37(9), 1251-1271.

[65] Zhao, G.Q., Huff R., Hutter, A., and Grandhi, R.V. (1997) Sensitivity analysis based preform die shape design using the finite element method, *Journal of Materials Engineering and Performance*, 6(3), 303-310.

[66] Kusiak, J. (1996) A technique of tool-shape optimization in large scale problems of metal forming. *Journal of Materials Professing Technology*, 57, 79-84.

[67] Oh, J.Y., Yang, J.B., Wu, W.T., and Delgado, H. (2004) Finite element method applied to 2D and 3D forging design optimization, *In American Institute of Physics (AIP) Conference Proceedings*, 712(1), 2108-2113.

[68] Satish, G.D., Singh, N.K., and Ohdar, R.K. (2008). Preform optimization of pad section of front axle beam using DEFORM, *Journal of materials processing technology*, *203*(1-3), 102-106.

[69] Lapovok, R. (1998) Improvement of die life by minimisation of damage accumulation and optimisation of preform design, *Journal of Materials Processing Technology*, 80-81, 608-612.

[70] Kobayashi, S., Oh, S.I., and Altan, T. (1989) *Metal Forming and the Finite-Element Method*, Oxford: Oxford University Press.

[71] Hwang, S.M., and Kobayashi, S. (1986) Preform design in disk forging, *International Journal of Machine Tool Design and Research*, *26*(3), 231-243.

[72] Hwang, S.M., and Kobayashi, S. (1987) Preform design in shell nosing at elevated temperatures, *International Journal of Machine Tools and Manufacture*, *27*(1), 1-14.

[73] Kang, B.S., Kim, N., and Kobayashi, S. (1990) Computer aided preform design in forging of an airfoil section blade, *International Journal of Machine Tools and Manufacture*, 30(1), 43-52.

[74] Kang, B.S., Kim, B.M., and Choi, J.C. (1994) Prefrom design in extrusion by the FEM and its experimental confirmation, *Journal of Materials Processing Technology*, 41, 237-248.

[75] Kang, B.S., Lee, J.H., and Kim, S.Y. (1997) Development of a methodology to form net-shape nosing shells by the backwards tracing scheme of the rigid-plastic FEM, *International Journal of Machine Tools and Manufacture*, 37(6), 737-750.

[76] Kang, B.S., Lee, J.H., and Choi, H.H. (1997) Extension of the backward tracing scheme of the rigid-plastic FEM in three-dimensional deformation, *Transaction of the ASME: Journal of Manufacturing Science and Engineering*, 119, 556-562.

[77] Han, C.S., Grandhi, R.V., and Srinivasan, R. (1993) Optimum design of forging die shapes using nonlinear finite element analysis, *AIAA Journal*, 31(4), 774-781.

[78] Srinivasan, R., Reddy G.H.K., Kumar, S.S., and Grandhi, R.V. (1994) Intermediate shapes in closed-die forging by the backward deformation optimisation method (BDOM), *Journal of Materials Engineering and Performance*, 3(4), 501-513.

[79] Zimmermann, H.J. (1994) *Fuzzy set theory and its Applications. 2nd. Ed.*, Boston, Kluwer Academic Publishers.

[80] Tsoukalas, L.H., and Uhring, R.E. (1997) *Fuzzy and Neural Approaches in Engineering*, New York, John Wiley and Sons, Inc.

[81] Biglari, F.R., O'Dowd, N.P., and Fenner, R.T. (1998) Optimum design of forging dies using fuzzy logic in conjunction with the backward deformation method, *International Journal of Machine Tools and Manufacture*, 38(8), 981-1000.

[82] Zhao, G.Q., Wright, E., and Grandhi, R.V. (1996) Computer aided preform design in forging using the inverse die contact tracking method. *International Journal of Machine Tools and Manufacture*, 38(7), 755-769.

[83] Zhao, G.Q., Wright, E., and Grandhi, R.V. (1996) Preform design in bulk forging processes. *Advanced Technology of Plasticity 1996. Proceedings of the 5th International Conference on Technology of Plasticity, Columbus, Ohio, USA, October 1996 (T. Altan ed.)*, 1, 453-456.

[84] McDermott, R.P., and Bramley, A.N. (1974) Forging analysis – a new approach, *Metallurgia Metal Forming*, 40, 127.

[85] McDermott, R.P., and Bramley, A.N. (1975) An elemental upper-bound technique for general use in forging analysis, *Proceedings of the Fifteenth International Machine Tool Design and Research Conference*, Palgrave, London, 437-443.

[86] McDermott, R.P., Bramley, A.N., and Cramphorn, A.S. (1976) UBET Related Developments in forging analysis, *Proceedings of the Fourth North American Metalworking Research Conference*, 80.

[87] Cramphorn, A.S., and Bramley, A.N. (1977) Computer aided forging design with UBET, *Proceedings of the 18th International MTDR Conference*, 717.

[88] Bramley, A.N. (1987) Computer aided forging design, *Annals of CIRP*, 36(1), 135-138.

[89] Kim, H.Y., and Kim, D.W. (1994) Computer-aided preform design in the closed-die forging process, *Journal of Materials Processing Technology*, 41(1), 83-104.

[90] Liu, Q.B., Wu, S.C., and Sun, S. (1998) Preform design in axisymmetric forging by a new FEM-UBET method, *Journal of Materials Processing Technology*, 74(1-3), 218-222.

[91] Pitt-Francis, J.M., Bowyer, A., and Bromley, A.N. (1996) TEUBA a simple 3D formulation for modelling forging using the upper bound method, *Annals of the CIPR*, 45, 245-248.

[92] Hill, R. (1950) *The Mathematical Theory of Plasticity*, London, Oxford University Press.

[93] Mendelson, A. (1968) *Plasticity: Theory and Application*, New York, MacMillan.

[94] Szczepinski, W. (1979) *Introduction to the Mechanic of Plastic Forming of Metals*, Netherlands, Sijthoff & Noordhoff International Publishers.

[95] Lubliner, J. (1900) *Plasticity Theory*, New York, Macmillan Publishing Pub. Co.

[96] Dieter, G.E., Kuhn, H.A., and Semiatin, S.L. (2003) *Handbook of Workability and Process Design*, Ohio, ASM International.

[97] Munjiza, A. (2004) *The Combined Finite-Discrete Element Method*, John Wiley & Sons Ltd.

[98] Huber, M.T. (1904) Die spezifische Formänderungsarbeit als Maß der Anstrengung eines Materials, *Czasopismo Techniczne, Lemberg (Lwow)*, 20, 81-83.

[99] von Mises, R. (1913) Mechanik der Festen Korper im plastisch deformablen Zustand, *Göttin. Nachr. Math. Phys.*, 1, 582-592.

[100] Timoshenko, S.P. (1953) *History of strength of materials*, Dover Publication, New York.

[101] McMeeking, R.M., and Rice, J.R. (1975) Finite-element formulations for problems of large elastic-plastic deformation, *International Journal of Solids and Structures*, 11, 601-616.

[102] Nagtegaal, J.C., and Veldpaus, F.E. (1984) On the implementation of finite strain plasticity equations is a numerical model, *Numerical Analysis of Forming Processes* (J.F.T. Pittman, O.C. Zienkiewicz, R.D. Wood and J.M. Alexander eds.), Chichester: John Wiley & Sons Ltd., 351-371.

[103] Zienkiewicz, O.C., and Taylor R.L. (1994) *The Finite Element Method, Volume I, 4th. ed*, London: McGraw-Hill Book Company.

[104] Shimazaki, Y., and Thompson E.G. (1981) Elasto visco-plastic flow with special attention to boundary conditions, *International Journal for Numerical Methods in Engineering*, 17, 97-112.

[105] Slater, R.A.C. (1977) *Engineering Plasticity: Theory and Application to Metal Forming Processes*, New York: John Wiley and Sons Inc.

[106] Edwards, L., and Endean, M. (1995) *Manufacturing with Materials*, London: Butterworth-Heinemann Ltd.

[107] Chenot, J.L., and Bellet, M. (1992) The viscoplaatic approach for the finite element modelling of metal-forming process, *Numerical Modelling of Material Deformation Processes* (P. Hartley, I. Pillinger and C. Sturgess eds.), London: Spring-Verlag, 179-224.

[108] Zienkiewicz, O.C., and Godbole P.N. (1975) A penalty function approach to problems of plastic flow of metals with large surface deformations, *Journal of Strain Analysis, 10(3)*, 180-183.

[109] Wagoner, R.H., and Chenot, J. (1997) *Fundamentals of Metal Forming*, New York: John Wiley St Sons Inc.

[110] Luan, Y., and Sun, S. (1997) Reverse simulation using the simulation block technique and its application in the precision forging process, *Journal of Materials Processing Technology*, 63(1-3), 244-247.

[111] Liu, Q., Wu, S., and Sun, S. (1998) Preform design in axisymmetric forging by a new FEM–UBET method, *Journal of Materials Processing Technology*, 74(1-3), 218-222.

[112] Zhao, G.Q., Wang, G., and Grandhi, R.V. (2002) Die cavity design of near flashless forging process using FEM-based backward simulation, *Journal of Materials Processing Technology*, 121(2-3), 173-181.

[113] Alfozan, A., and Gunasekera, J.S. (2002) Design of profile ring rolling by backward simulation using upper bound element technique (UBET), *Journal of Manufacturing Processes*, 4(2), 97-108.

[114] Wright,R.T. (1990) *Processes of Manufacturing*, Goodheart Willcox Company, Inc., South Holland.

[115] Lindbeck, J.R., Williams, M.W., and Wygant, R.M. (1990) *Manufacturing Technology*, Prentice Hall, Englewood Cliffs.

[116] Schey, J.A. (2000) *Introduction to Manufacturing Processes*, Third ed., McGraw-Hill: Boston.

[117] Groover, M.P. (2002) *Fundamentals of Modern Manufacturing*, Second ed., John Wilery and Sons, Inc.: New York.

[118] Tylecote, R.F. (1968) *The Solid Phase Welding of Metals*, Edward Arnold (Publisher) Ltd.: London.

[119] Press, W.H., Teukolsky, S.A., Vetterling, W.T., and Flannery B.P. (1992) *Numerical Recipes in C: The Art of Scientific Computing, 2nd ed*. Cambridge: Cambridge University Press.

[120] Semiatin, S. L. (Ed.). (2005) *Metalworking: bulk forming (Vol. 14)*, Materials Park, Ohio, ASM International.

[121] Prasad, Y.V.R.K., and Sasidhara S. (1997) *Hot Working Guide: A Compendium of Processing Maps, 1997*, Materials Park, Ohio, ASM International.

[122] Lange, K. (1985) *Handbook of Metal Forming*, New York, McGraw-Hill Book Company.

[123] Bartle, P.M. (1979), *Welding Institute: Albington*, Cambridge, 1979.

[124] Nicholas, M.G. (1998) *Joining Processes: Introduction to Brazing and Diffusion Bonding*, Kluwer Academic Publishers: Dordrecht, 16-21.

[125] O'Brien, A. (2007) (ed.) *Welding Handbook, Part 2*, Vol.3, Ninth ed., American Welding Society: Miami, 184-592.

[126] McEwan, K.J.B., and Milner, D.R. (1962) Pressure welding of dissimilar metals, *British Welding Journal, 9*, 406-420.

[127] Olson, D.L., Siewert, T.A., Liu, S., and Edwards, G.R. (1993) (eds.) *ASM handbook*, Vol.6, Tenth ed., ASM International, Materials Park, 481-557.

[128] Male, A.T., and Cockcroft, M.G. (1964) A method for determination of the coefficient of friction of metals under conditions of bulk plastic deformation, *Journal of the Institute of Metals*, 93, 38-46.

[129] Hawkyard, J.B. and Johnson, W. (1967) An analysis of the changes in geometry of a short hollow cylinder during axial compression, *International Journal of Mechanical Sciences*, 9, 163-182.

[130] Hastings, D.C. (1955) Sn application of pressure welding to fabricate continuous welded rails, *Welding Journal*, 34 (11), 1065-1069.

[131] Lage, A.P. (1956) Application of pressure welding to the aircraft industry, *Welding Journal*, 35 (11), 1103-1109.

[132] Guy, A.G., and Eiss, A.L. (1957) Diffusion phenomena in pressure welding, *Welding Journal*, 36 (11), 473-480.

[133] McKittrick, E.S., and Donalds, W.E. (1959) Oxyacetylene pressure welding of high-speed rocket test track, *Welding Journal*, 38 (5), 469-474.

[134] Metzger, G.E. (1978) Hot pressure welding of aluminium alloys, *Welding Journal*, 57 (1), 37-43.

[135] Fluhrer J (2007) *DEFORM-3D Version 6.1 User's Manual*, Scientific Forming Technologies Corporation, Columbus

[136]Suzuki H, Hashizume S, Yabuki Y, Ichihara Y, Nakajima S (1968) *Studies on the flow stress of metals and alloys*, The Institute of Industrial Science, University of Tokyo, Tokyo

[137] Pascoe, S.K. (1997) Finite elements in contact problems, *Lecture note: Nonlinear Finite Element Analysis of Geometric Nonlinearities and Contact*, University of Nottingham, 3-4 July 1997.

[138] Pittman, J.F.T., Zienkiewicz O.C., Wood R.D., and Alexander, J.M. eds. (1984) *Numerical Analysis of Forming Processes*, Chichester: John Wiley and Sons Ltd.

[139] Lam, Y.C., and Zhang, X.Q. (1994) Evaluation of relaxation schemes for Newton-Raphson iteration in rigid-plastic finite-element analysis, *Journal of Materials Processing Technology*, 41(4), 361-373.

[140] Golub, G.H., and Van Loan, C.F. (1996) *Matrix Computations, 3rd ed.* Baltimore: The Johns Hopkins University Press.

[141] Luenberger, D.G. (1984) *Linear and Nonlinear Programming*, Reading, Massachusetts: Addison-Wesley Publishing Company.

[142] SFTC (2006), *DEFORM-2D V9.0 User Manual*, Columbus, Ohio, USA.

[143] AutoCAD, Autodesk Inc., 111 McInnis Parkway, San Rafael, CA 94903, USA.

[144] Rhinoceros, McNeel North America 3670 Woodland Park Ave N Seattle, WA 98103 USA.

[145] Sundaresan, S., and Murti, K.G.K. (1993) Friction welding of aluminium to austenitic stainless steel, *International Journal for the Joining of Materials*, 5, 66-70.

[146] Bhanumurthy, K., Fotedar, R.K., Joyson, D., Kale, G.B., Pappachan, A.L., Grover, A.K., and Krishnan, J. (2006) Development of tubular transition joints of aluminium/stainless steel by deformation diffusion bonding, *Material Science and Technology*, 22, 321-330.

[147] Turner, W.C., Mize, J.H., Case, K.E., and Nazemetz, J.W. (1993) *Introduction to Industrial and Systems Engineering*, Prentice Hall: Englewood Cliffs, 234-247.

[148] Murdoch, J. (1979) *Control Charts*, Macmillan Press Ltd.: London, 36-48.

[149] Iordachescu, M., Iordachescu, D., Scutelnicu, E., and Ocaña, J. (2007) FEM model of butt cold welding, *Science and Technology of Welding and Joining*, 12 (5), 402-409.

[150] Kimura, M., Choji, M., Kusaka, M., Seo, K., and Fuji, A. (2005) Effect of friction welding conditions and aging treatment on mechanical properties of A7075-T6 aluminium alloy friction joints. *Science and Technology of Welding and Joining*, 10 (4), 406-412.

[151] Kimura, M., Nakamura S., Kusaka, M., Seo, K., and Fuji, A. (2005) Mechanical properties of friction welded joint between Ti-6Al-4V alloy and Al-Mg alloy (AA5052), *Science and Technology of Welding and Joining*, 10 (6), 666-672.

[152] Kimura, M., Choji, M., Kusaka, M., Seo, K., and Fuji, A. (2006) Effect of friction welding conditions on mechanical properties of A5052 aluminium alloy friction welded joint, *Science and Technology of Welding and Joining*, 11 (2), 209-215.

[153] Zhang, Z., and Zhang, H.W. (2007) Numerical studies on effect of axial pressure in friction stir welding, *Science and Technology of Welding and Joining*, 12 (3), 226-248.

[154]Gehanno, H., Brechet, Y., Louchet, F., and Bechet, D. (1994) Microstructure and mechanical properties of a 6063 aluminium alloy at high temperature, *Key Engineering Materials*, 97-98, 347-352.

[155] Karamış, M.B., and Halıcı, İ., (2007) The effects of homogenization and recrystallization heat treatments on low-grade cold deformation properties of AA 6063 aluminum alloy, *Material Letters*, 61, 944-948.